

# **Development and characterization of thermochemical materials based on salt hydrates and salt alcoholates**

Von der Fakultät Nachhaltigkeit  
der Leuphana Universität Lüneburg zur Erlangung des Grades

Doktorin der Naturwissenschaften  
(Dr. rer. nat.)

genehmigte Dissertation von  
Dipl.-Ing. Kathrin Korhammer

geboren am 04.03.1984 in Altötting

November 2018



Eingereicht am: 29.11.2018

Mündliche Verteidigung (Disputation) am: 24.02.2020

Erstbetreuer und Erstgutachter: Prof. Dr.-Ing. Wolfgang K. L. Ruck

Zweitgutachter: Prof. Dr. Oliver Opel

Drittgutachter: Prof. Dr. Frédéric Kuznik

Die einzelnen Beiträge des kumulativen Dissertationsvorhabens sind oder werden wie folgt veröffentlicht:

- I Fopah Lele A, Korhammer K, Wegscheider N, Rammelberg HU, Osterland T, Ruck W. Thermal conductivity measurement of salt hydrate as porous material using calorimetric (DSC) method. 8th World Conference on Experimental Heat Transfer, Fluid Mechanics and Thermodynamics (ExHFT), Lisboa, Portugal: A. Faria - Edicao Electronica Lda.; 2013.
- II Druske M-M, Fopah-Lele A, Korhammer K, Rammelberg HU, Wegscheider N, Ruck W, et al. Developed materials for thermal energy storage: Synthesis and characterization. Energy Procedia 2014;61:96–9.
- III Korhammer K, Druske M-M, Fopah-Lele A, Rammelberg HU, Wegscheider N, Opel O, et al. Sorption and thermal characterization of composite materials based on chlorides for thermal energy storage. Applied Energy 2016;162:1462–72.
- IV Korhammer K, Apel C, Osterland T, Ruck WKL. Reaction of calcium chloride and magnesium chloride and their mixed salts with ethanol for thermal energy storage. Energy Procedia 2016;91:161–71.
- V Korhammer K, Mihály J, Bálint S, Trif L, Vass Á, Tompos A, et al. Reversible formation of alcohol solvates and their potential use for heat storage. Journal of Thermal Analysis and Calorimetry 2019;138:11–33.
- VI Korhammer K, Neumann K, Opel O, Ruck WKL. Micro-scale thermodynamic and kinetic analysis of a calcium chloride methanol system for process cooling. Energy Procedia 2017;105:4363–9.
- VII Korhammer K, Neumann K, Opel O, Ruck WKL. Thermodynamic and kinetic study of  $\text{CaCl}_2\text{-CH}_3\text{OH}$  adducts for solid sorption refrigeration by TGA/DSC. Applied Energy 2018;230:1255–78.
- VIII Korhammer K, Opel O, Ruck WKL. Energy storage and adsorption cooling efficiency of novel composite adsorbents. To be submitted to *Thermochimica Acta*.





# Contents

Nomenclature	iii
Abstract	v
Zusammenfassung	vii
1. Heat storage in hydrates and alcoholates	1
1.1. General introduction	1
1.1.1. Background and motivation	1
1.1.2. Classification and evolution of thermal energy storage technologies	2
1.1.3. Current state of knowledge of thermochemical energy storage	5
1.2. General approaches and main results	9
1.2.1. Selection and assessment of appropriate salt hydrates and salt alcoholates	9
1.2.2. Design of two-component composite adsorbents	11
1.2.3. Thermal energy storage characteristics of the composite adsorbents designed and their parent salts	13
1.2.4. Transport and kinetic phenomena observed in the composite adsorbents designed and their parent salts	15
1.2.5. Prediction of discharge/charge cycling effects on the thermal stability of the TCMs tested	17
1.3. General discussion	18
2. Paper overview	21
3. Paper I	25
4. Paper II	31
5. Paper III	37
6. Paper IV	49
7. Paper V	61

8. Paper VI	85
9. Paper VII	93
10. Paper VIII	119
Appendices	154
A. Final energy consumption statistics	155
B. Selective literature review on composite materials	157
C. List of materials and devices used in this study	163
D. Supplementary data on paper II and paper III	167
E. Supplementary data on paper IV	171
Bibliography	198
Acknowledgements	199
Curriculum vitae	201
Declaration of authorship	207

# Nomenclature

## Latin symbols

symbol	description	unit
$D$	diameter	m
$d_{pore}$	pore diameter	m
$p$	vapor pressure	Pa
$S_{BET}$	specific surface area	$m^2 g^{-1}$
$T_b$	boiling point	$^{\circ}C$
$T_m$	melting point	$^{\circ}C$
$V_{pore}$	pore volume	$m^3 kg^{-1}$
$w$	salt content	wt%

## Greek symbols

symbol	description	unit
$\lambda$	thermal conductivity	$W m^{-1} K^{-1}$
$\rho_b$	bulk density	$kg m^{-3}$
$\rho_a$	area density	$g m^{-2}$
$\rho_s$	density	$kg m^{-3}$

## Abbreviations

ACF	activated carbon foam
BC	biochar
DSC	differential scanning calorimetry
ENG	expanded natural graphite compacted
ENGP	expanded natural graphite powder
EV	expanded vermiculite
EV2	expanded vermiculite
PCM	phase change material
SG	silica gel
TCM	thermochemical material
TES	thermal energy storage
TGA	thermogravimetric analysis
TG-MS	thermogravimetry-mass spectrometry
XRD	X-ray diffraction
Z13X	binderless zeolite 13X
ZNC	zeolite natural clinoptilolite





# Abstract

The geographical situation of Germany considerably affects the final energy consumption of the country. Thermally intensive processes are the largest consumer of energy. In contrary, the level of energy consumed by air conditioning systems and utilized on process cooling is relatively low. Thermal energy storage systems have a high potential for a sustainable energy management, as they provide an efficient integration of thermal energy from renewables and heat recovery processes through spatial and temporal decoupling.

Low temperature thermochemical energy stores based on gas-solid reactions represent appealing alternative options to sensible and latent storage technologies, in particular for heating and cooling purposes. They convert heat energy provided from renewable energy and waste heat sources into chemical energy and can effectively contribute to load balancing and CO<sub>2</sub> mitigation. Reasonable material intrinsic energy storage density and cooling power are demanded. At present, several obstacles are associated with the implementation in full-scale reactors. Notably, the mass and heat transfer must be optimized. Limitations in the heat transport and diffusions resistances are mainly related to physical stability issues, adsorption/desorption hysteresis and volume expansion and can impact the reversibility of gas-solid reactions.

The aim of this thesis was to examine the energy storage and cooling efficiency of CaCl<sub>2</sub>, MgCl<sub>2</sub>, and their physical salt mixtures as adsorbents paired with water, ethanol and methanol as adsorbates for utilization in a closed, low level energy store. Two-component composite adsorbents were engineered using a representative set of different host matrices (activated carbon, binderless zeolite NaX, expanded natural graphite, expanded vermiculite, natural clinoptilolite, and silica gel). The energetic characteristics and sorption behavior of the parent salts and modified thermochemical materials were analyzed employing TGA/DSC, TG-MS, Raman spectroscopy, and XRD. Successive discharging/charging cycles were conducted to determine the cycle stability of the storage materials.

The overall performance was strongly dependent on the material combination. Increase in the partial pressure of the adsorbate accelerated the overall adsorbate uptake. From energetic perspectives the CaCl<sub>2</sub>-H<sub>2</sub>O system exhibited higher energy storage densities than the CaCl<sub>2</sub> and MgCl<sub>2</sub> alcoholates studied. The latter were prone to irreversible decomposition. Ethyl chloride formation was observed for MgCl<sub>2</sub> at room and elevated temperatures. TG-MS measurements confirmed the evolution of alkyl

chloride from  $\text{MgCl}_2$  ethanulates and methanulates upon heating. However,  $\text{CaCl}_2$  and its ethanulates and methanulates proved reversible and cyclable in the temperature range between 25 °C and 500 °C.

All composite adsorbents achieved intermediate energy storage densities between the salt and the matrix. The use of carbonaceous matrices had a heat and mass transfer promoting effect on the reaction system  $\text{CaCl}_2\text{-H}_2\text{O}$ . Expanded graphite affected only moderately the adsorption/desorption of methanol onto  $\text{CaCl}_2$ .  $\text{CaCl}_2$  dispersed inside zeolite 13X showed excellent adsorption kinetics towards ethanol. However, main drawback of the molecular sieve used as supporting structure was the apparent high charging temperature. Despite variations in the reactivity over thermal cycling caused by structural deterioration, composite adsorbents based on  $\text{CaCl}_2$  have a good potential as thermochemical energy storage materials for heating and cooling applications. Further research is required so that the storage media tested can meet all necessary technical requirements.

# Zusammenfassung

Die geografische Lage Deutschlands bestimmt wesentlich den Endenergieverbrauch des Landes. Wärmeintensive Prozesse stellen den größten Anteil am Energieverbrauch dar. Im Vergleich dazu ist der Energiebedarf von Klimaanlage und Kälteanwendungen verhältnismäßig niedrig. Wärmespeicher haben ein großes Potential für eine nachhaltige Energiewirtschaft, indem sie eine effiziente Integration von thermischer Energie aus erneuerbaren Energien oder Wärmerückgewinnungsprozessen durch eine räumliche und zeitliche Trennung ermöglichen.

Thermochemische Niedertemperaturspeicher, die auf Gas-Feststoff Reaktionen basieren, sind eine attraktive Alternative zu sensiblen und latenten Speichertechnologien, insbesondere für Kühlungs- und Heizungszwecke. Sie wandeln Wärmeenergie, welche von erneuerbaren Energien oder Abwärmequellen stammt, in chemische Energie um und können somit effektiv zum Lastenausgleich und zur Reduktion von CO<sub>2</sub> beitragen. Anforderungen sind eine angemessene materialspezifische Energiespeicherdichte und Kühlleistung. Bei der Implementierung in Pilotanlagen bestehen derzeit noch erhebliche Hindernisse. Zu optimierende Größen sind vor allem der Stoff- und Wärmetransport. Limitierungen im Wärmetransfer und Diffusionswiderstände stehen ferner mit Problemen der physikalischen Stabilität, dem Phänomenen der Hysterese bei der Adsorption und Desorption und der Volumenvergrößerung im Zusammenhang und können die Reversibilität von Gas-Feststoff Reaktionen beeinträchtigen.

Diese Arbeit untersuchte die Energiespeicherdichte und Kälteleistung von CaCl<sub>2</sub>, MgCl<sub>2</sub> und deren physikalischen Mischungen als Adsorbentien in Kombination mit Wasser, Ethanol und Methanol als Adsorbate für den Einsatz in einem geschlossenen Niedertemperaturniveau-Energiespeicher. Zwei-Komponenten Kompositmaterialien wurden unter Verwendung einer repräsentativen Auswahl von Trägerstrukturen (Aktivkohle, bindemittelfreier NaX Zeolith, expandierter natürlicher Graphit, expandiertes Vermiculit, natürlicher Klinoptilolith und Silikagel) hergestellt. Die energetischen Eigenschaften und das Sorptionsverhalten der Muttersubstanzen und modifizierten thermochemischen Materialien wurden mittels TGA/DSC, TG-MS, Raman Spektroskopie und XRD untersucht. Sukzessive Entlade- und Beladezyklen wurden durchgeführt, um die Zyklenfestigkeit der Speichermaterialien zu messen.

Die Gesamtleistung hing stark von der Materialkombination ab. Eine Zunahme des Partialdrucks des Adsorbats beschleunigte insgesamt die Adsorbataufnahme. Das CaCl<sub>2</sub>-H<sub>2</sub>O System zeigte eine höhere Energiespeicherdichte als die untersuchten CaCl<sub>2</sub>

und  $\text{MgCl}_2$  Alkoholate. Letztere neigten zu irreversibler Zersetzung. Die Bildung von Ethylchlorid wurde für  $\text{MgCl}_2$  bei Raumtemperatur und erhöhten Temperaturen beobachtet. TG-MS Messungen bestätigten die Freisetzung von Alkylchlorid aus  $\text{MgCl}_2$  Ethanolaten und Methanolaten bei Erwärmung.  $\text{CaCl}_2$  und seine Ethanolate und Methanolate erwiesen sich allerdings über den Temperaturbereich von  $25\text{ }^\circ\text{C}$  bis  $500\text{ }^\circ\text{C}$  als reversibel und zyklenstabil.

Alle Kompositadsorbentien erzielten Energiespeicherdichten, welche zwischen denen des Salzes und der Trägermatrizen lagen. Das Verwenden von kohlenstoffhaltigen Matrizen hatte einen wärme- und stofftransportfördernden Einfluss auf das Reaktionssystem  $\text{CaCl}_2\text{-H}_2\text{O}$ . Expandierter Graphit beeinflusste nur in mäßiger Weise die Adsorption/Desorption von Methanol an  $\text{CaCl}_2$ . In Zeolith 13X dispergiertes  $\text{CaCl}_2$  zeichnete sich, gegenüber Ethanol, durch eine exzellente Sorptionskinetik aus. Hauptnachteil des als Trägerstruktur verwendeten Molekularsiebes war allerdings die augenscheinlich hohe Beladungstemperatur. Trotz Variationen in der Reaktivität im Verlauf der thermischen Zyklisierung, welche durch strukturelle Veränderungen verursacht wurden, sind Komposite basierend auf  $\text{CaCl}_2$  als thermochemische Wärmespeichermaterialien für Wärme- und Kälteanwendungen potentiell gut geeignet. Damit die getesteten Speichermedien alle gestellten technischen Anforderungen erfüllen können, bedarf es jedoch weiterer Forschung.

# 1. Heat storage in hydrates and alcoholates

## 1.1. General introduction

### 1.1.1. Background and motivation

On 30 November 2016, the European Commission presented a new Energy Winter Package in Brussels [1]. The renewable energy directive proposal contains policy instruments that aim at increasing the share of renewable energies in the future European energy landscape and advancing energy efficiency, energy performance, and energy cleanliness. The substitution of fossil fuels by climate friendly alternatives is a continuous process and influenced by multiple factors. Among member states, the transition towards a socio-economic and sustainable energy supply and decarbonized society cannot solely be accomplished by generating 50% of electricity from renewables by 2030 [2]. Energy efficiency can be either improved through implementation of new and emerging technologies or through investigation of energy saving potentials of available techniques. In the context of energy policies, strong focus needs to be given to waste heat recovery. The recovery of excess heat from electricity generation in building applications and waste heat produced as by-product in industrial processes, for instance from municipal sewage treatment works and solid waste plants, or industrial and domestic cooling can contribute towards the mitigation of CO<sub>2</sub> emissions and foster the economic development. Waste heat energy can be harnessed to supply a broad range of energy demands, from process heating, space heating, and hot water production to cold energy supply and heat-to-power solutions [3]. The geographical situation of Germany considerably affects the country's final energy consumption. From an energy point of view, thermally intensive processes have been the largest consumer of energy in the last decades (Figure 1.1).

In 2015, a considerable amount of the residential and commercial final energy was consumed for space heating. The industrial sector contributed towards the final energy consumption primarily through process heating. In the transport sector, mechanical energy dominated the total final energy consumption. An overview of the total energy consumption by energy-end-use sectors and application is provided in Figure A.1 in Appendix A. Key challenge is the mismatch between supply and demand of heat energy. Heat generation from waste heat and renewable energy sources is subjected to periodic fluctuations and seasonal variations. As a result, heat is provided intermittently. This challenge can be addressed through spatial and temporal decoupling of heat energy

using integrated thermal energy storage (TES) systems.

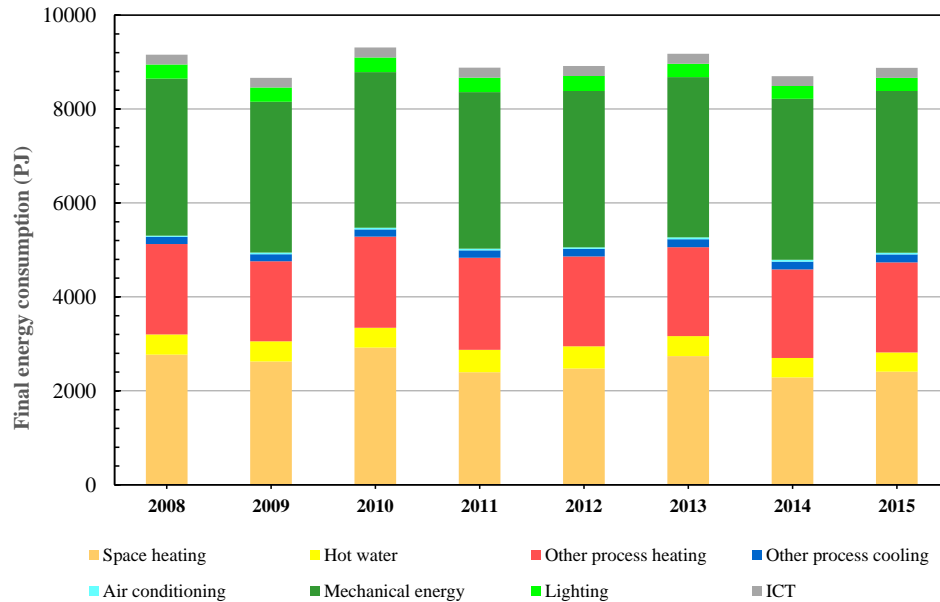


Figure 1.1.: Total final energy consumption by different applications in Germany from 2008 to 2015. Data extracted from [4].

### 1.1.2. Classification and evolution of thermal energy storage technologies

TES systems are environmentally benign and flexible solutions, and play a pivotal role in smart and sustainable energy management. They can operate in load levelling and peak shaving strategy, and effectively increase the energy efficiency balance through energy conservation. By storing and extracting waste heat for heating and cooling purposes as needed, the use of nuclear power and fossil fuel resources as primary energy supply sources and related greenhouse gases, which substantially contribute to global warming, can be reduced. At legislative level, political decisions and the adoption of new legislation are the basis for societal acceptance. However, implementation of new technologies is still a significant driving force. Different TES systems exist in terms of (i) application spectrum, (ii) storage purpose, (iii) storage duration, (iv) source/end-use temperature, and (v) storage mechanism. According to the operating temperature of the application, TES can be classified as low temperature, medium temperature, and high temperature TES. High temperature heat is mainly required in technical and industrial processes. Medium temperature applications encompass automotive catalyst heating, whereas low temperature TES covers the thermal energy demand of residential building applications,

## 1. Heat storage in hydrates and alcoholates

---

for example space and water heating, air conditioning, and refrigeration [3]. In the low temperature regime, end-use temperatures range roughly from 20 °C to less than 200 °C. According to the storage mechanism, TES can be categorized into (i) sensible, (ii) latent, and (iii) thermochemical energy storage [5].

The oldest form of low temperature thermal energy storage is the sensible storage of heat in water for food preservation, space cooling, and other cooling needs [6]. Sensible heat storage media, so-called capacity heat storage media, store and release heat while changing their temperature without phase transition when heated or cooled. Sensible heat storage systems are well developed, clearly understood, and widely used [7]. Water is abundantly available and has a remarkably high heat capacity compared to other sensible heat storage liquids and solids and accordingly a high energy density. Consequently, it is the most commonly employed sensible heat storage material in centralized solar thermal and geothermal storage systems.

Latent heat storage is associated with a phase change from one state of aggregation to another over a narrow temperature interval allowing large quantities of heat energy to be stored in small volumes for long-term operations [8]. Solid-liquid systems have been the most intensively investigated phase change materials (PCMs) [9]. PCMs can be divided into organic, inorganic, and eutectic materials [10]. Latent heat storage materials are popular for conventional energy conversion and storage [11]. Unlike sensible storage materials, PCMs absorb and release heat at a nearly constant temperature and have volumetric storage capacities 5-14 times higher than sensible storage materials [12].

The desirability of high energy densities has aroused notable interest in thermochemical energy storage [13]. Thermochemical energy storage can be subclassified into two categories, sorption heat storage and chemical reaction heat storage. The term sorption designates all processes in which a sorbate (e.g. gas, vapor, liquid) is captured in an interfacial layer (adsorption) or attached to the solid surface of a solid sorbent (absorption) by physical forces [10]. Key factors are the specific surface area, the porosity of the sorbent, and the molecular polarity between sorbent and sorbate. Some widespread materials used in sorption heat stores, heat pumps, and refrigerators are silica gels [14–28], aluminophosphates [29–31], aluminosilicates [16, 30, 32], zeolites [14, 18, 30, 31, 33–42], metal-organic frameworks [43–49], activated carbons or activated carbon fibers [34, 50–61], and salt solutions [62–66]. In building applications, the sorbate involved in heat storage is predominantly water [10]. Water is normally employed in pair with silicates, zeolites or metal-organic frameworks. For refrigeration, alcohol (ethanol, methanol) [26, 34, 36, 43, 46–48, 50, 51, 54–57, 67] or ammonia [52, 53, 58, 59] are the refrigerants of choice.

Thermochemical energy storage based on reversible chemical reactions has the highest theoretical energy density per volume material (Figure 1.2). Since heat energy is converted into chemical energy, chemisorption involves energy of higher quality.



According to the First Law of thermodynamics, the internal energy of a closed system is expressed in terms of heat energy and work, and can be infinitesimally changed from an initial to a final state by applying work on the system or by heating. In thermochemical energy storage, heat is transferred under isobaric conditions, no work is done. Therefore, the heat energy equals the enthalpy of the involved reaction. The chemical reaction induces a change in the molecular configuration of the compound. Cyclic reversibility of the chemical reaction applied is a relevant criterion. The heat to be stored shall be completely recoverable. The performance of the chemisorption store is strongly dependent on the thermodynamics and kinetics of the reaction type applied. Numerous types of gas-solid reactions are available for thermal energy storage as stated in published literature [68]. They occur within a specific temperature regime. In the low temperature range, halides, nitrates, and sulfates of alkali and alkaline earth metal salts are the most suitable substances. To achieve high energy densities, the utilization of easily condensable reaction partners is favored, encompassing alcohols, ammonia, and water [69]. These reactants combine with the respective salts to form alcoholates, ammoniates, and hydrates of different stoichiometry, which are termed metal coordination complexes [70]. In coordination compounds, the neutral ligands alcohol, ammonia, and water are coordinated to the central metallic cation through a coordinate bond and constitute the coordination sphere. Reversible gas-solid reactions are heat energy consuming in one direction and heat energy yielding in the reverse direction. A detailed description of the generic principle of reversible gas-solid reactions is given in the following chapter.

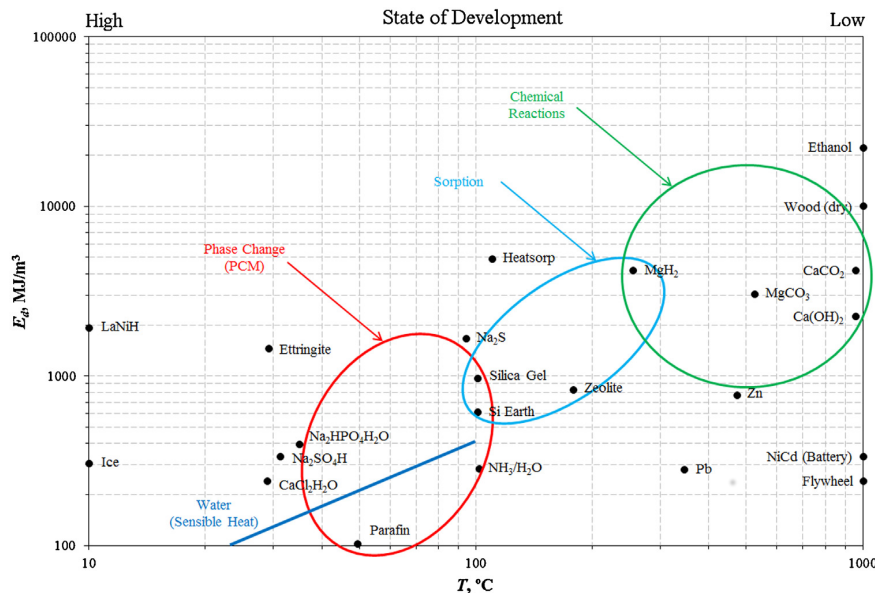
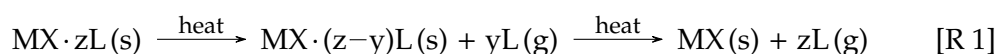


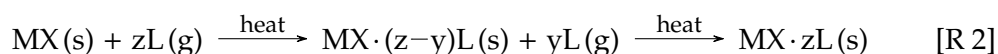
Figure 1.2.: Energy storage densities of different classes of materials. Adapted from [71].

### 1.1.3. Current state of knowledge of thermochemical energy storage

In general, thermochemical energy stores are operated either in open or closed operating mode [72]. A basic chemical reaction heat storage unit comprises a semi-batch reactor containing the solid reactant and a condenser/evaporator for the condensable working fluid. Safety issues arising from non-condensable working fluids or high fluid pressure can be approached through substitution of the condenser/evaporator unit by a second reactor containing another solid reactant chemically different from the other one. Thermally driven chemical heat pumps, heat transformers, and chillers are typically designed with two reactors [73], a high temperature and a low temperature heat reactor. Major advantage of the dual reactor configuration is the continuous heat and cold energy output. The reactors operate in counter-phase, which means that heat is evolved in the high temperature heat reactor while heat is absorbed in the low temperature heat reactor [74]. The underlying basic thermodynamic cycle is illustrated in Cot-Gores et al. [73]. Considering thermochemical materials (TCMs) as gas-solid reactions, the dissociation reaction can be described via the following reaction scheme:



During heat exposure, the solid reactant  $\text{MX} \cdot z\text{L}$ , i.e. salt ethanolate, salt hydrate or salt methanolate, is dissociated completely or stepwise via intermediates  $\text{MX} \cdot (z-y)\text{L}$  into an anhydrous salt  $\text{MX}$  and the gas  $\text{L}$ . The associated change in enthalpy  $\Delta_r H^\circ$ s called enthalpy of reaction. The endothermic dissociation reaction corresponds to the charging process in which heat introduced into the reaction is stored over a finite time period at ambient temperature. The volatile product can be condensed or used to discharge another solid reactant. In the discharging process the reverse reaction takes place. The ionic salt anhydride and the working fluid in gas state are combined in an exothermic reaction regenerating the starting compound as follows:



Gas-solid reactions are heterogeneous monovariant reactions, according to Gibbs phase rule. Reactants and products are in different physical states; the change of the state is induced by physical or chemical transformations. The position of the chemical equilibrium and the spontaneity of the reaction are highly contingent upon the partial pressure of the gaseous reactant and the temperature applied. Pressure and temperature are fundamental thermodynamic state properties. The van't Hoff plot depicts the region of thermodynamic stability of reaction systems. At equilibrium the partial pressure of the gaseous reactant is proportional to the inverse of the reaction temperature  $1/T$ . A straight line indicates that the reaction enthalpy is temperature independent within the

specified temperature range. Separation of the working pair and storage of the TCM at ambient temperature facilitates long-term storage with negligible sensible thermal losses [69, 75]. Compared to sensible heat and PCM stores, chemical heat stores exhibit several remarkable features. Due to their compactness and modular construction, they are well suited for distributed solutions in building and transportation applications.

A selective literature review on chemical reaction and compound adsorbent TES has been conducted and the results are reported in the following paragraphs. To date, a variety of low temperature TCMs for heating and cooling purposes, with a focus on pure salt hydrates, have been studied analytically, numerically, at laboratory scale, and sporadically at prototype scale [75–103]. Another class of TCMs that has been extensively researched are pure salt ammoniates [74, 75, 90, 104–115]. With regard to chemical energy storage, salt alcoholates have excited little interest. Very few publications exist on the reaction of pure metal salts and aliphatic primary alcohols such as ethanol [116, 117] and methanol [109, 110, 116–119].

Among the various inorganic salts investigated, chloride- and bromide-based metal halides and metal sulfates have been most frequently chosen to be characterized in more in-depth lab-scale studies. Metal sulfates and their hydrates display high energy densities compared to metal halides, but to be fully decomposed high regeneration temperatures must be applied [100]. Kinetic constraints profoundly impact the dehydration/rehydration reactions of sulfate-based salts and their hydrates. The high energy density of salt hydrates is the result of the ability to incorporate significant amounts of water into their crystal lattice. Owing to their hygroscopic character, chlorides of calcium, magnesium, and lithium, for example, can easily adsorb moisture from the surrounding. Anhydrous  $\text{CaCl}_2$  is primarily used as desiccant in various industrial applications for fluid dehumidification.

Van Essen et al. [77] performed hydration experiments under low pressure conditions in a small laboratory fixed bed reactor with sample loadings of 0 g to 40 g. They recognized agglomeration during hydration when chlorides of calcium and magnesium were used. The formation of a gel-like structure reduced the bed porosity of the material and decelerated rehydration reactions. The authors clearly emphasized that the salt hydrates examined are problematic for large-scale TES applications. The formation of a skin of hydrated salt with low porosity on the surface of bulk  $\text{MgSO}_4$  powder was observed by Hongois et al. [120]. Further gas exchange was impaired and the rates of the rehydration/dehydration reactions considerably diminished. Furthermore, pressure drop problems in the reactor and a continuous decrease in the energy storage density of the TCM can occur when pure metal salts with small particle sizes are used [68]. Internal diffusion resistances relating to physical stability issues, sorption/desorption hysteresis, salt swelling, along with deliquescence and disintegration pose severe obstacles to the implementation of chemical reactions in TES. Low reaction rates and slow heat transfers, due to low thermal conductivities of the inorganic salts and their complexes in powder

form, are other important considerations for assessing the potential use in full-scale plants. These material intrinsic disadvantages can be eliminated through optimization measures at material and reactor scale. Attempts at material modification have been carried out by many researchers in recent years.

Physical mixing and recrystallization from solution of single metal salts are simple approaches to prevent deliquescence and liquefaction. Vaccarino et al. [121] pioneered the utilization of salt hydrate mixtures for storing solar thermal energy. They mixed magnesium salt hydrates ( $\text{MgSO}_4\text{-MgNO}_3$ ) with anhydrous  $\text{NH}_4\text{NO}_3$ , which showed excellent reversible capacity over 700 cycles. Rammelberg et al. [122] prepared various binary salt mixtures of different ratios using  $\text{CaCl}_2$ ,  $\text{MgBr}_2$ ,  $\text{MgCl}_2$ ,  $\text{MgSO}_4$ , and  $\text{FeSO}_4$ . They tested the suitability of these binary salt pairs for domestic heat storage at milligram scale by TGA/DSC. In particular, the mixture of  $\text{CaCl}_2$  and  $\text{MgCl}_2$  hydrates exhibited improved kinetics and thermal cyclability without reaction control up to dehydration temperatures of  $150^\circ\text{C}$ . The good cycle stability of the salt mixture  $\text{CaCl}_2\text{-MgCl}_2$  even under stressed dehydration/hydration conditions was verified in a more detailed study by Rammelberg et al. [123]. The cycling efficiency of the mixture remained almost constant over 55 cycles at maximum dehydration temperatures of  $120^\circ\text{C}$ , indicating that a stabilized mixture was obtained after repeated forced overhydration. The formation of a chemical mixture (tachyhydrite) during the dehydration/hydration reaction was confirmed by XRD. In a recent publication, Pathak et al. [124, 125] demonstrated numerically that appropriate chemical mixing of  $\text{CaCl}_2$  and  $\text{MgCl}_2$  hydrates can enhance the resistance to hydrolysis in the operating range of solar thermal TES systems. The hydrolysis temperature of the double salt is significantly higher when compared with the elementary salt hydrates leading to improved durability of the TCM.

The confinement of hygroscopic salts into host matrices with open pore structure and large surface area for improved structural integrity and mass transfer has received considerable attention over the last years. Since diverse combinations of salts and matrices are applicable, composite adsorbents with varying characteristics can be designed to meet specific operational requirements. The use of thermally conductive carrier materials can have an enhancing effect on the heat transfer performance of pure salts [126–131]. The latest research on innovative composite adsorbents alias Composite Salt inside Porous Matrix (CSPM) [132] or Salt In Matrix (SIM) [71] as TCM for low temperature TES has prevalently focused on Selective Water Sorbents (SWS). This term has been introduced in the 1990s by Aristov et al. [133, 134] and refers to hybrid sorbents consisting of an ionic compound and a physical adsorbent paired with water as reaction partner. Experimental investigations range from grain to pilot plant scale, the former appearing to be predominant. Some researchers combined numerical simulations and experimental studies to accurately predict the sorption and kinetic behavior of CSPMs. A variety of hygroscopic salts ( $\text{CaCl}_2$ ,  $\text{LiBr}$ ,  $\text{LiCl}$ ,  $\text{MgCl}_2$ ,  $\text{MgSO}_4$ ,  $\text{SrBr}_2$ , etc.) are

considered as conceivable impregnating agents. Salt-silica [71, 131, 133–168], salt-clay [31, 71, 152, 166, 169–178], and salt-zeolite [71, 120, 152, 153, 171, 179–182] composites are the subject of many research studies. In the last few years, a growing number of materials with hierarchical pore structure has been identified as appropriate host matrix candidates such as aluminosilicates [18, 183–185], activated carbons [71, 135, 152, 158, 186–189], expanded graphites [85, 190], carbon nanotubes [191, 192], and metal-organic frameworks [193]. For adsorption cooling and air conditioning applications, the working pairs CSPM- $C_2H_5OH$  [194–196] and CSPM- $CH_3OH$  [130, 162, 165, 191, 197–205] have elicited special interest among a handful of researchers.

The first attempt to combine salt hydrate mixtures with supportive structures was performed by Posern and Kaps. In a first trial, they deposited salt hydrate mixtures of  $MgSO_4$ - $MgCl_2$  and  $MgSO_4$ - $LiCl$  in certain mixing ratios within the pore network of glass pellets with different pore sizes and pellet diameters [206]. Partial substitution of  $MgSO_4$  by salt hydrates with lower relative deliquescence humidity resulted in increased enthalpies of sorption. They observed that small pore sizes favored high sorption heats. In a second trial, they dispersed a salt hydrate mixture of  $MgSO_4$ - $MgCl_2$  inside attapulgite granulates [173]. Higher heat releases and higher temperature lifts were measured as a result of increased water absorption in the concentrated salt solution compared to the energy density, temperature lift, and water loading of single  $MgSO_4$ . Gordeeva et al. [162, 199] synthesized CSPMs comprising binary salt systems ( $LiCl$ - $LiBr$ ,  $CaCl_2$ - $CaBr_2$ ) as active components and mesoporous silica gel or macroporous expanded vermiculite as host matrices. They experimentally studied the phase composition and sorption equilibrium with methanol and water at various salt contents. Mixing and dispersion of the salts inside the porous matrices changed the equilibrium temperature of the solid salt solution formed. Casey et al. [176] impregnated macroporous vermiculite with a mixture of  $CaCl_2$  and  $LiNO_3$ , and experimentally investigated its potential for domestic building thermal energy provision. The hygrothermal performance of the binary salt system confined to the matrix pores was unexpectedly poor when compared with zeolite 13X and composite  $CaCl_2$ -vermiculite. Recently, Jamiri et al. [166] have determined the heat storage capacity of composite adsorbents containing the salt pairs  $MgSO_4$ - $CaCl_2$ ,  $CaCl_2$ - $LiCl$ , and  $MgSO_4$ - $MgCl_2$  and porous vermiculite. The researchers accentuated the good thermal energy storage performance of the mixture-based composites. The energy densities of the compound composites with binary salt hydrate pairs were in general  $20 \text{ kJ kg}^{-1}$  higher than that of the composite materials with individual salt hydrates.

A representative summary of existing published literature on compound adsorbents and ethanol (Table B.1), methanol (Table B.2), and water (Table B.3) as sorbate for application in heat storage and adsorption cooling is given in Appendix B.

### 1.2. General approaches and main results

A considerable range of conventional TES technologies, including in particular sensible and latent heat storage solutions, is already deployed and commercially available. In contrast, advanced, highly efficient TES technologies based on chemical reactions are still at low Technology Readiness Levels [207], as reviewed in the previous chapter. To contribute to the scale-up of heat powered thermochemical energy stores and to enhance their market access, comprehensive research has to be executed. In this thesis, sustained emphasis is placed on the investigation of appropriate reaction pairs and tailored composite adsorbents taking into account the predetermined operating conditions of the targeted application. The PhD thesis aims at analyzing the energy storage and cooling efficiency and corresponding heat transfer and mass diffusion constraints of pure and modified inorganic salts for utilization in a closed TES system driven by low grade thermal energy sources. The following research questions were addressed:

1. What salt hydrates and salt alcoholates are suitable to be used in a closed TES system?
2. What are the thermal energy storage and reactivity characteristics of the salt hydrates and salt alcoholates selected?
3. Which optimization techniques can be applied to design thermochemical materials with tuned properties, i.e. enhanced heat and mass transfer, cyclic ability?
4. How are the association/dissociation reaction behavior and thermal performance of pure salts affected by material modification?

#### 1.2.1. Selection and assessment of appropriate salt hydrates and salt alcoholates

In **paper I**, **paper III**, **paper IV**, **paper VI**, and **paper VII**, the material selection process is briefly explained, as addressed in research question 1. For the assessment of inorganic metal salts as promising TCM candidates for heat and cold production a selection criteria matrix was defined. According to information provided from suppliers, published literature, and theoretical calculations based on energy binding theory several substances were preselected. The following criteria were considered: (i) human toxicity, (ii) environmental benignity, (iii) economic procurement, (iv) manufacturing costs, (v) technical requirements, (vi) adsorbent-adsorbate interaction, (vii) low dissociation (regeneration) temperature, (viii) theoretical sorption capacity, and (ix) hygrothermal and chemical stability. Three inorganic metal salts were finally chosen:  $\text{CaCl}_2$ ,  $\text{MgCl}_2$ , and  $\text{KCl}$ . The latter was used as stabilizing agent. The sorbate materials selected were  $\text{H}_2\text{O}$ ,  $\text{C}_2\text{H}_5\text{OH}$ , and  $\text{CH}_3\text{OH}$ .  $\text{H}_2\text{O}$  is a natural, safe, and non-toxic reagent. It has a high latent

heat of vaporization when compared to  $C_2H_5OH$  and  $CH_3OH$ . The interesting feature of  $C_2H_5OH$  and  $CH_3OH$  is that they can be deployed as refrigerants in refrigeration systems operating below the freezing point of  $H_2O$ .  $CaCl_2$  reacts with  $H_2O$  to form stable hydrates of different stoichiometry, in fact mono-, di-, tetra-, and hexahydrate [208–212]. High reaction enthalpies and accordingly high energy densities characterize the reaction pair  $CaCl_2-H_2O$ . The theoretical standard enthalpies of reaction of the mono-, di-, tetra-, and hexahydrate are  $-71.6 \text{ kJ mol}^{-1}$ ,  $-123.5 \text{ kJ mol}^{-1}$ ,  $-246.5 \text{ kJ mol}^{-1}$ , and  $-361.2 \text{ kJ mol}^{-1}$ , respectively [213]. The corresponding theoretical energy densities are  $644.8 \text{ kJ kg}^{-1}$ ,  $1112.5 \text{ kJ kg}^{-1}$ ,  $2221.2 \text{ kJ kg}^{-1}$ , and  $3254.5 \text{ kJ kg}^{-1}$ , respectively.  $MgCl_2$  also exists in anhydrous form as well as in the four hydrated forms mono-, di-, tetra-, and hexahydrate [211, 214–217]. Hydrates of  $MgCl_2$  are susceptible to hydrolysis and irreversible decomposition over the temperature range of interest [218–221]. The removal of the last two  $H_2O$  molecules is accompanied by the evolution of hydrogen chloride gas and the production of hydroxychloride. Consequently, the reaction system  $MgCl_2-H_2O$  was discarded from further investigations.

A systematic literature review revealed that the reaction of inorganic salts and  $C_2H_5OH$  or  $CH_3OH$  has scarcely been studied in terms of its application in TES. There is a limited amount of thermodynamic data available for the reaction systems  $CaCl_2-C_2H_5OH$ ,  $CaCl_2-CH_3OH$ ,  $MgCl_2-C_2H_5OH$ , and  $MgCl_2-CH_3OH$ . Most of the data available is inadequate and inconsistent. Due to the variety of synthesis procedures and conditions, an apparent discrepancy of the stoichiometry is found in the literature (see **paper V**). The synthesis method plays a crucial role, with regard to the nature of the reactants [222]. Common preparation methods for (crystalline) salt alcoholates are direct synthesis, recrystallization, solution crystallization, and efflorescence crystallization. Therefore, a major objective of this study was to synthesize and analyze salt-alcohol addition compounds of different stoichiometry based on anhydrous  $CaCl_2$  and  $MgCl_2$ . **Paper VI** describes in detail the synthesis method, which is based on the operating principle of a chemical heat store.  $CaCl_2$  ethanulates,  $CaCl_2$  methanulates,  $MgCl_2$  ethanulates, and  $MgCl_2$  methanulates were prepared by adding a stoichiometric amount of liquid  $C_2H_5OH$  or  $CH_3OH$  to the respective salt while agitating under inert atmosphere. The theoretical alcohol/salt molar ratios varied between two and eight. Changes in temperature, textural and optical properties were monitored. The chemical composition, the dissociation reaction pattern, and temperature range, the standard reaction enthalpy, and the standard dissociation enthalpy of the samples were determined by simultaneous thermogravimetric analysis (TGA) and differential scanning calorimetry (DSC). Thermogravimetry and microcalorimetry are versatile thermal analysis techniques and serve as key tools in the investigation of TCMs. A qualitative analysis of the chemical composition, the structure, and the morphology of the synthesized salt alcoholates was carried out by the cooperation partner at the Institute of Materials and Environmental Chemistry at the

Research Center for Natural Sciences, Budapest, using coupled thermogravimetry-mass spectrometry (TG-MS), Raman spectroscopy, and X-ray diffraction (XRD) analysis. Correlations between the obtained thermochemical, structural, and crystallographic data were conducted.

Evidence for the strong chemical stability of the  $\text{CaCl}_2\text{-C}_2\text{H}_5\text{OH}$  system yielded from TGA/DSC measurements. The highest level of ethanolation measured is two moles of  $\text{C}_2\text{H}_5\text{OH}$  per mole  $\text{CaCl}_2$ , irrespective of the initial amount of  $\text{C}_2\text{H}_5\text{OH}$  added.  $\text{CaCl}_2\text{-C}_2\text{H}_5\text{OH}$  solvates of higher or lower ethanolated states, as identified by Parker et al. [213], Carling [90], and Iyimen-Schwarz [117], could not be synthesized under the experimental conditions applied. Results imply that  $\text{CaCl}_2$  binds with two molecules of  $\text{CH}_3\text{OH}$ . Formation of the  $\text{CaCl}_2$  trimethanolate and  $\text{CaCl}_2$  tetramethanolate is substantiated by the inclusion of  $\text{CH}_3\text{OH}$  molecules into the crystal lattice. Increase in the coordination number is associated with a linear increase in the standard enthalpy of dissociation. Conversely, a non-linear relationship was observed between the coordination number and the standard enthalpy of reaction. At methanolation levels higher than two, the reaction enthalpies per mole  $\text{CH}_3\text{OH}$  ranged from  $30.7 \text{ kJ mol}^{-1}$  to  $37.6 \text{ kJ mol}^{-1}$ . These values are fairly close to the standard enthalpy of vaporization of liquid  $\text{CH}_3\text{OH}$ , connoting the presence of physically adsorbed  $\text{CH}_3\text{OH}$ . Intrinsic chemical instability is encountered in  $\text{MgCl}_2$  alcoholates. Experimental stoichiometric numbers of alcohol molecules attached to  $\text{MgCl}_2$  significantly deviated from theoretical values.  $\text{MgCl}_2$  forms a homologous series of ethanolates with coordination numbers of approximately one, two, three, and four. However,  $\text{CH}_3\text{OH}$  coordinates to  $\text{MgCl}_2$  to form non-integer solvates with  $\text{CH}_3\text{OH}/\text{MgCl}_2$  ratios of 1.9, 2.3, 4.6, and 3.5 under the experimental conditions studied. Besides well-defined compounds, adducts of non-integer stoichiometry were also reported in some fundamental studies, as mentioned in **paper V**. Findings are supported by complementary analysis.

### 1.2.2. Design of two-component composite adsorbents

The adsorbent material is the core component of a TES system. Central issues of pure salts are their volume expansion and contraction during consecutive discharging/charging cycles impeding heat and mass transfer. To improve the sorbate diffusion and thermal transport of salt hydrates and salt alcoholates, novel composite materials were engineered (**paper I, paper II, paper III, paper VIII**), as addressed in research question 3.  $\text{CaCl}_2$  was embedded into diverse porous matrices. Different families of matrices exist, they are distinguished by their internal pore width. A generic classification of the internal pore width is given by the International Union of Pure and Applied Chemistry (IUPAC) [223].

By selecting a representative set of host matrices, the effect of the varying morphological, structural, and physico-chemical properties of the host matrices on the energy storage efficiency of pure  $\text{CaCl}_2$  was examined. Silica gel (**paper I**), expanded vermiculite



(**paper I, paper VIII**), activated carbon foam (**paper II, paper III**), expanded graphite (**paper II, paper III, paper VIII**), natural and synthetic zeolites (**paper VIII**) as well as biochar (**paper VIII**) were selected. These supports were chosen on the basis of their surface chemistry, pore size distribution, porosity, surface area, and thermal conductivity. The material specific physico-chemical properties of the host matrices are given in Table C.3 in Appendix C. Although considerable research has been devoted to the synthesis of salt-silica, salt-clay and salt-zeolite compound adsorbents, rather less attention has been paid to couple inorganic salts and carbonaceous matrices.

The composite adsorbents were synthesized by impregnation. Impregnation is a well-established method in heterogeneous catalysts synthesis. It consists in contacting a solid with a solvent containing the components to be deposited on the surface of the solid [224]. Successful impregnation is mainly contingent on the chemical nature of both the host and the hygroscopic salt, and the synthesis conditions (e.g. pretreatment, impregnation temperature, solvent pH, salt concentration). Different impregnation methods are described in the literature. In this study, wet impregnation, also referred to as soaking, was applied to make the composites SG-CaCl<sub>2</sub> (**paper I**), EV-CaCl<sub>2</sub> (**paper I**), CaCl<sub>2</sub>-ENGP-S-4, CaCl<sub>2</sub>-ENGP-S-2, CaCl<sub>2</sub>-ENGP-S-1 (**paper II, paper III**), CaCl<sub>2</sub>-Z13X, CaCl<sub>2</sub>-ZNC (**paper VIII**), and CaCl<sub>2</sub>-BC (**paper VIII**). In wet impregnation, the volume of the salt solution exceeds the pore volume of the support and excess solvent is eliminated by evaporation or by filtration. The composites CaCl<sub>2</sub>-ENG-VI, CaCl<sub>2</sub>-MSH-ENG-VI, CaCl<sub>2</sub>-ENG (**paper II, paper III, paper VIII**), CaCl<sub>2</sub>-ACF-VI, CaCl<sub>2</sub>-MSH-ACF-VI (**paper II, paper III**), and CaCl<sub>2</sub>-EV2 (**paper VIII**) were prepared by wet impregnation at subatmospheric pressure, designated vacuum impregnation. The composite materials synthesized are listed in Table C.4 in Appendix C. A parametric study on the variation in the salt concentration of the salt solution implied that a good degree of impregnation can be achieved with saturated salt solutions. The salt content of the composite adsorbents prepared was determined by weighting the dry sample before and after impregnation. The content of the confined CaCl<sub>2</sub> varied between 16 wt% and 90 wt% depending on impregnation method, synthesis condition, and support material. It was observed that very high CaCl<sub>2</sub> loadings have no beneficial effect on the sorption and energy storage properties of composite adsorbents. Deposition of CaCl<sub>2</sub> inside the porous structure led to decreased surface area and total pore volume. It is assumed that at high CaCl<sub>2</sub> concentrations the salt particles agglomerate and the clusters formed narrow or even block the diffusion pathways reducing the sorption capacity. Furthermore, deliquescence and leakage are likely to occur at high sorbate levels, as experienced in other studies carried out at the institute.

The confinement of CaCl<sub>2</sub> in silica gel, expanded vermiculite, expanded natural graphite, and activated carbon foam increased the effective thermal conductivity, as reported in **paper I**. The nature of the host matrix and the overall CaCl<sub>2</sub> content had a

substantial influence on the effective thermal conductivity. Composite samples with high  $\text{CaCl}_2$  content showed reduced heat transfer when compared with composite adsorbents with lower degree of impregnation. Due to its high thermal conductivity, expanded natural graphite is a remarkable heat diffusion enhancer. Expanded vermiculite, silica gel, and activated carbon foam have high porosities and are less conductive than powder and compacted expanded natural graphite. The effective thermal conductivity was measured by DSC. The measurements were performed by Armand Fopah-Lele.

### 1.2.3. Thermal energy storage characteristics of the composite adsorbents designed and their parent salts

The thermal characteristics of the reaction systems selected and the composite adsorbents designed for heating and cooling applications that operate at low level temperature were evaluated with simultaneous TGA/DSC, as addressed in research question 2 and 4. Some samples were subjected to multiple repeated discharging/charging cycles to determine changes in the sorption ability, the energy storage and cooling performance, and the uptake/release behavior of the respective sorbate over cycling. Schematics of the experimental setups for the in-situ experiments are illustrated in **paper III** (salt- $\text{H}_2\text{O}$  and composite- $\text{H}_2\text{O}$  systems), **paper IV** (salt- $\text{C}_2\text{H}_5\text{OH}$  systems), **paper VII** (salt- $\text{CH}_3\text{OH}$  systems) and **paper VIII** (salt- $\text{C}_2\text{H}_5\text{OH}$  system, composite- $\text{C}_2\text{H}_5\text{OH}$  systems, salt- $\text{CH}_3\text{OH}$  system and composite- $\text{CH}_3\text{OH}$  systems). The specific experimental procedures are described in the respective paper. Hydration, ethanolation, and methanolation were run at different  $\text{H}_2\text{O}$  vapor pressures (1.0 kPa, 1.7 kPa, and 2.0 kPa),  $\text{C}_2\text{H}_5\text{OH}$  vapor pressures (3.1 kPa, 3.7 kPa, and 4.1 kPa), and  $\text{CH}_3\text{OH}$  vapor pressures (6.8 kPa, 8.2 kPa, and 9.1 kPa). The values were chosen to prevent condensation and to ensure appropriate sorption rates. All sorption experiments were performed at a temperature of 25 °C. The regeneration temperature varied from 25 °C to 180 °C and corresponds to the operating temperature range of low grade heat sources. Data collected on the association/dissociation reaction behavior and thermal performance of the salt in matrix samples were compared with that of the parent salt. The enthalpy of reaction, the formation/dissociation enthalpy, respectively, and the gravimetric energy density, which is an important key performance indicator of TES systems, were obtained from microcalorimetry results.

The calculated enthalpies of reaction of all  $\text{CaCl}_2 \cdot 2 \text{C}_2\text{H}_5\text{OH}$  analyzed in **paper V** were in the range of 91.5  $\text{kJ mol}^{-1}$  to 130.1  $\text{kJ mol}^{-1}$ , which were consistent with literature values [116, 225], resulting in an energy density normalized to the ethanolated  $\text{CaCl}_2$  between 475  $\text{kJ kg}^{-1}$  and 642  $\text{kJ kg}^{-1}$ . In **paper IV**, the sorption characteristics of  $\text{CaCl}_2$  towards  $\text{C}_2\text{H}_5\text{OH}$  was tested under different  $\text{C}_2\text{H}_5\text{OH}$  vapor pressure conditions. Under the experimental conditions studied, the only stable ethanolate formed was the  $\text{CaCl}_2 \cdot 1 \text{C}_2\text{H}_5\text{OH}$ . The dissociation reaction enthalpies roughly varied from 57  $\text{kJ mol}^{-1}$  to 63  $\text{kJ mol}^{-1}$  and the corresponding energy densities were between 346  $\text{kJ kg}^{-1}$  and 394  $\text{kJ kg}^{-1}$ . As

presented in **paper V**, the reaction enthalpy of  $\text{CaCl}_2 \cdot 2 \text{CH}_3\text{OH}$  ( $101.1 \text{ kJ mol}^{-1}$  and  $116.0 \text{ kJ mol}^{-1}$ ) slightly deviated from data published by Aristov et al. [226], Carling et al. [116], Iyimen-Schwarz [117], and Offenhartz et al. [118]. Accordingly, the associated energy storage densities ranged from  $518 \text{ kJ kg}^{-1}$  to  $649 \text{ kJ kg}^{-1}$ . In **paper XIII**, the energy storage densities for the  $\text{CaCl}_2\text{-CH}_3\text{OH}$  system, measured under various conditions, reached values between  $541 \text{ kJ kg}^{-1}$  and  $760 \text{ kJ kg}^{-1}$ . The results are equivalent to the previously reported ones.

Reference data on  $\text{MgCl}_2$  ethanolates and  $\text{MgCl}_2$  methanolates are rarely available. A significant difference appeared between enthalpy values for  $\text{MgCl}_2 \cdot 1 \text{ C}_2\text{H}_5\text{OH}$ ,  $\text{MgCl}_2 \cdot 1 \text{ CH}_3\text{OH}$ , and  $\text{MgCl}_2 \cdot 3 \text{ CH}_3\text{OH}$  determined by Iyimen-Schwarz [117] using vacuum DSC and values experimentally obtained in this thesis. This can be explained by comparing the evaluation procedure. The values given by Iyimen-Schwarz are values averaged over several cycles. However, the maximum reaction enthalpies are of the same order of magnitude. In **paper V**, the enthalpies of reaction of all  $\text{MgCl}_2$  ethanolates and  $\text{MgCl}_2$  methanolates varied from  $64.7 \text{ kJ mol}^{-1}$  to  $158 \text{ kJ mol}^{-1}$  and from  $68.9 \text{ kJ mol}^{-1}$  to  $183.4 \text{ kJ mol}^{-1}$ , respectively. The corresponding energy storage densities ranged from  $354 \text{ kJ kg}^{-1}$  to  $616 \text{ kJ kg}^{-1}$  for  $\text{MgCl}_2$  ethanolates. For about 0.6 mol to 1.1 mol of  $\text{C}_2\text{H}_5\text{OH}$  exchanged by one mole of  $\text{MgCl}_2$ , the energy storage densities, determined in **paper IV**, were between  $265 \text{ kJ kg}^{-1}$  and  $313 \text{ kJ kg}^{-1}$ .  $\text{MgCl}_2$  methanolates exhibited higher energy densities ( $555 \text{ kJ kg}^{-1}$  to  $943 \text{ kJ kg}^{-1}$ ) than  $\text{MgCl}_2$  ethanolates.

In an optimization approach  $\text{MgCl}_2$  and  $\text{CaCl}_2$  were physically mixed in a molar fraction of 1:2 to improve the thermal performance (**paper IV**). The binary mixture showed advanced sorption capabilities and energy storage densities compared to the individual salts. The uptake of around three moles of  $\text{C}_2\text{H}_5\text{OH}$  per mole dry mixture resulted in reaction enthalpies of  $145 \text{ kJ mol}^{-1}$  to  $159 \text{ kJ mol}^{-1}$  and energy storage densities of  $334 \text{ kJ kg}^{-1}$  to  $366 \text{ kJ kg}^{-1}$  per unit mass of ethanolated mixture.

The incorporation of  $\text{CaCl}_2$  into silica gel resulted in a composite adsorbent that contained 32 wt%  $\text{CaCl}_2$  and yielded a  $\text{H}_2\text{O}$  uptake  $0.17 \text{ g g}^{-1}$  (**paper I**). The composite achieved an energy density of  $321 \text{ kJ kg}^{-1}$ . The composite material EV- $\text{CaCl}_2$ , containing 22 wt% of  $\text{CaCl}_2$ , took up  $0.20 \text{ g g}^{-1}$  and hence the energy density amounted to  $602 \text{ kJ kg}^{-1}$  (**paper I**). The composites based on ACF,  $\text{CaCl}_2\text{-ACF-VI}$  and  $\text{CaCl}_2\text{-MSH-ACF-VI}$ , adsorbed merely  $0.12 \text{ g g}^{-1}$  and  $0.20 \text{ g g}^{-1}$ . Consequently, the energy densities were comparatively low ( $235 \text{ kJ kg}^{-1}$  and  $298 \text{ kJ kg}^{-1}$ ), as stated in **paper III**. The expanded graphite supported  $\text{CaCl}_2$  composites,  $\text{CaCl}_2\text{-ENG-VI}$  and  $\text{CaCl}_2\text{-MSH-ENG-VI}$ , featured good  $\text{H}_2\text{O}$  uptake capabilities with values of  $0.67 \text{ g g}^{-1}$  and  $0.72 \text{ g g}^{-1}$  (**paper III**). The associated high energy storage densities of  $1642 \text{ kJ kg}^{-1}$  and  $1905 \text{ kJ kg}^{-1}$ , respectively, make them an appealing option for thermal energy storage applications.

The  $\text{CaCl}_2$  in expanded graphite composite  $\text{CaCl}_2\text{-ENG}$ , which had a  $\text{CaCl}_2$  loading of 64 wt%, displayed a  $\text{C}_2\text{H}_5\text{OH}$  uptake of  $0.41 \text{ g g}^{-1}$  and exhibited an energy storage

density of  $323 \text{ kJ kg}^{-1}$  averaged over five ethanolation/deethanolation cycles. The value was normalized to the mass of dry composite, as presented in **paper VIII**. The composite adsorbent  $\text{CaCl}_2\text{-ZNC}$ , containing 30 wt%  $\text{CaCl}_2$ , adsorbed an amount of  $\text{C}_2\text{H}_5\text{OH}$  of  $0.18 \text{ g g}^{-1}$  and thus the energy density was  $234 \text{ kJ kg}^{-1}$  (**paper VIII**). A poor  $\text{C}_2\text{H}_5\text{OH}$  adsorption was observed for the composite compound  $\text{CaCl}_2\text{-Z13X}$ , as described in **paper VIII**. The  $\text{C}_2\text{H}_5\text{OH}$  adsorption capacity did not exceed a value of  $0.10 \text{ g g}^{-1}$ . For this composite, which possessed the lowest  $\text{CaCl}_2$  loading, an energy storage density of  $195 \text{ kJ kg}^{-1}$  was attained.

Regarding the  $\text{CH}_3\text{OH}$  sorption ability of  $\text{CaCl}_2$  supported by expanded vermiculite, introduced in **paper VIII**, the  $\text{CaCl}_2\text{-EV2}$  composite, which had a  $\text{CaCl}_2$  content of 69 wt%, exhibited a good affinity towards  $\text{CH}_3\text{OH}$ . The  $\text{CH}_3\text{OH}$  adsorption and the energy storage density yielded  $0.41 \text{ g g}^{-1}$  and  $631 \text{ kJ kg}^{-1}$ , respectively. The values were averaged over twenty-nine methanolation/demethanolation cycles. The composite  $\text{CaCl}_2\text{-BC}$ , which was based on biochar and 83 wt%  $\text{CaCl}_2$ , achieved a  $\text{CH}_3\text{OH}$  uptake of  $0.48 \text{ g g}^{-1}$ , as given in **paper VIII**. The corresponding energy storage density reached a value of  $681 \text{ kJ kg}^{-1}$ , averaged over sixteen methanolation/demethanolation runs.

### 1.2.4. Transport and kinetic phenomena observed in the composite adsorbents designed and their parent salts

Profound understanding of mass transfer phenomena and reaction kinetics of the reaction systems investigated are of great practical importance. Comparison of the formation/decomposition behavior was done by calculating the time required to reach an extent of conversion of 50 % and 90 %. Sorption/desorption rates were determined by using the first derivative of the TGA curve (DTG curve). The inflexion point of the DTG curve indicates the point of the greatest rate of mass change.

Improved mass transfer was observed for the composite adsorbents  $\text{CaCl}_2\text{-ACF-VI}$ ,  $\text{CaCl}_2\text{-MSH-ACF-VI}$ ,  $\text{CaCl}_2\text{-ENG-VI}$ , and  $\text{CaCl}_2\text{-MSH-ENG-VI}$ , which were in research focus in **paper III**. By using ENG and ACF as matrices, the dehydration reaction was enhanced over the whole temperature range on account of the increased dehydration rate, in particular at lower temperatures. The supports ENG and ACF functioned as both mass and heat promoter. The decomposition temperatures of the hydrated  $\text{CaCl}_2$  were shifted towards lower temperatures. The findings give answer to question 4.

The effect of the vapor pressure on the formation reaction of  $\text{CaCl}_2$  ethanolates,  $\text{MgCl}_2$  ethanolates,  $\text{CaCl}_2\text{-MgCl}_2$  ethanolates (**paper IV**), and  $\text{CaCl}_2$  methanolates (**paper VI**, **paper VII**) was analyzed by exposing the respective single and binary salts to different sorbate vapor partial pressures, as addressed in research question 2. The sorption rate (aka ethanolation/methanolation rate) varied with partial pressure at constant temperature. Increase in the partial pressure accelerated the sorption rate.  $\text{CaCl}_2$  was methanolated at a moderate rate. The ethanolation of  $\text{CaCl}_2$  proceeded the fastest, moreover, exhibiting

the highest maximum ethanolation rate among the ethanolates evaluated. The binary salt possessed sorption properties which were between the ones of its elementary components. In general, the ethanolation of  $\text{CaCl}_2$ ,  $\text{MgCl}_2$ , and  $\text{CaCl}_2\text{-MgCl}_2$  are slow processes. For instance, the thermodynamically stable  $\text{CaCl}_2 \cdot 2\text{C}_2\text{H}_5\text{OH}$  could not be reached under the pressure and temperature conditions studied. Improvement measures include the increase of the  $\text{C}_2\text{H}_5\text{OH}$  vapor pressure and the elongation of the exposure time.

As shown in **paper VIII**, the dispersion of  $\text{CaCl}_2$  inside binderless zeolite 13X was observed to have a pronounced impact on the  $\text{C}_2\text{H}_5\text{OH}$  adsorption. The  $\text{CaCl}_2\text{-Z13X}$  possessed excellent adsorption energetics and kinetics. The thermally conductive matrix expanded graphite is well known for its enhancement effect on the heat transfer and was used as support matrix. However, expanded graphite had minimal effect on the overall adsorbent characteristics. Variations in the reactivity caused by structural deterioration were experienced with increasing operating cycles. The composite adsorbent  $\text{CaCl}_2\text{-ZNC}$  showed an increase in the  $\text{C}_2\text{H}_5\text{OH}$  loading and speed of the ethanolation reaction over cycling, which are assignable to structural changes. To prevent the intrinsic physical instability problem of  $\text{CaCl}_2$  and its methanolates, the salt was dispersed within a biochar matrix. No significant improvement of the  $\text{CH}_3\text{OH}$  transport was realized by using biochar. The  $\text{CaCl}_2\text{-EV2}$  composite exhibited an accelerated methanolation reaction, but the reaction rate gradually declined with increasing number of cycles. The  $\text{CH}_3\text{OH}$  was released at slightly lower temperatures compared to single  $\text{CaCl}_2$ .

Knowledge on the reaction kinetics taking into account the various characteristics of the reactant/product system is essential for a proper design of chemical heat stores. There is a fairly extensive literature on the formation and dissociation mechanism of salt hydrates, while the reaction of inorganic salts and primary chain alcohols has not been deeply studied. **Paper V** focuses on the  $\text{C}_2\text{H}_5\text{OH}$  vapor partial pressure dependence of the ethanolation reaction and the deethanolation kinetics of the reaction pairs  $\text{CaCl}_2\text{-C}_2\text{H}_5\text{OH}$ ,  $\text{MgCl}_2\text{-C}_2\text{H}_5\text{OH}$ , and  $\text{CaCl}_2\text{-MgCl}_2\text{-C}_2\text{H}_5\text{OH}$ . Kinetic information were obtained from non-isothermal DSC measurements, which were carried out at multiple heating rates, as addressed in question 2. For the interpretation of kinetic data of solid-state reactions from thermogravimetric measurements, different approaches can be employed. They are classified into two different types, model-fitting and model-free. Model-free methods are based on the empirical Arrhenius equation. The Arrhenius equation represents the dependence of the rate constant on the temperature. Pre-exponential factors and activation energies, the so-called Arrhenius parameters, were derived from the model-free Kissinger method. Kissinger proposed that the peak temperature of the maximum weight loss rate changes with a change in the heating rate. A first-order behavior, which can also be described by the Avrami-Erofeev equation, was assumed. The decomposition of fine powders has been reported as being satisfactorily represented by the first-order rate equation [227].

### 1.2.5. Prediction of discharge/charge cycling effects on the thermal stability of the TCMs tested

Cycle stability of salt hydrates and salt alcoholates is of utmost interest for the application in thermochemical heat stores. Successive discharging/charging cycle tests were conducted to assess the cycle performance of selected pure and hybrid materials. The cycle performance was examined via simultaneous TGA/DSC using controlled temperature programs. The experimental procedures used are outlined in the respective papers.

The  $\text{CaCl}_2\text{-C}_2\text{H}_5\text{OH}$  system showed a good operational stability over 35 cycles under the conditions studied, as reported in **paper IV**. Despite overstoichiometric  $\text{C}_2\text{H}_5\text{OH}$  uptake resulting in  $\text{CaCl}_2$  ethanolates with 1.1 to 1.6 moles of  $\text{C}_2\text{H}_5\text{OH}$  per mole  $\text{CaCl}_2$ , the ethanolation level only slightly declined. The ethanolation and deethanolation enthalpies increased in the first cycles and stabilized in the consecutive ones. Note that the deethanolation enthalpies were higher than the ethanolation enthalpies. Irreversible decomposition of the  $\text{MgCl}_2$  ethanolates strongly depressed the cycle efficiency. A continuous degradation was observed over 15 cycles resulting in a substantial decrease in the ethanolation level and ethanolation/deethanolation enthalpy. Addition of  $\text{CaCl}_2$  to  $\text{MgCl}_2$  in the mixing ratio of 2:1 resulted in an eminent cyclability when compared to the ingredient  $\text{MgCl}_2$ . A stable ethanolation/deethanolation behavior with only a marginal decrease of the ethanolation level with increasing operating cycles was observed. The enthalpies of ethanolation and deethanolation followed the same trend. Considering the constant methanolation levels and associated enthalpies of methanolation and demethanolation over 18 cycles, the  $\text{CaCl}_2\text{-CH}_3\text{OH}$  system exhibited a good cycle stability (**paper VII, paper VIII**). However, thermal cycling influenced the methanolation reaction kinetics. With increasing number of cycles, the reaction time was prolonged by 30% to 35%, referred to the 2<sup>nd</sup> methanolation reaction, was needed to attain an extent of conversion of 50%. Thermal analysis results disclosed that heat absorption and release remained constant for the composite adsorbents  $\text{CaCl}_2\text{-BC}$  and  $\text{CaCl}_2\text{-EV2}$  over cyclic methanolation/demethanolation under dynamic conditions, but the  $\text{CH}_3\text{OH}$  diffusion and thermal transfer were impaired (**paper VIII**). Thermal and mechanical stress disrupted the structure of the  $\text{CaCl}_2\text{-EV2}$  sample during the cycling test resulting in physical instability. Deformations in the material structure were also optically examined for  $\text{CaCl}_2\text{-ZNC}$  and  $\text{CaCl}_2\text{-ENG}$ . As a result, the  $\text{C}_2\text{H}_5\text{OH}$  adsorption behavior changed over cycling. The composite adsorbent  $\text{CaCl}_2\text{-Z13X}$  possessed good cyclic reproducibility (**paper VIII**). The  $\text{C}_2\text{H}_5\text{OH}$  adsorption and desorption curves resembled the sorption profiles of pure zeolite 13X. This characteristic is attributed to the low  $\text{CaCl}_2$  content of the material. Main drawback of the molecular sieve used as supporting structure is the apparent high charging temperature and slow mass transport in the charging mode, which make  $\text{CaCl}_2\text{-Z13X}$  unfavorable for low temperature applications.

### 1.3. General discussion

This thesis investigates the energy efficiency and thermal performance of selected pure salt hydrates and salt alcoholates as well as engineered composite materials to be used in closed low temperature TES systems for heating and cooling. I studied the thermodynamic and kinetic properties of  $\text{CaCl}_2$  hydrates,  $\text{CaCl}_2$  ethanolates,  $\text{CaCl}_2$  methanolates,  $\text{MgCl}_2$  ethanolates,  $\text{MgCl}_2$  methanolates,  $\text{CaCl}_2$ - $\text{MgCl}_2$  ethanolates, and 14 different composite adsorbents by TGA/DSC. Since data on the energy density and performance reliability of the respective salt-alcohol systems are scarcely available, a comprehensive study was carried out employing different analytical techniques.

From the energetic viewpoint,  $\text{CaCl}_2$  hydrates are superior to  $\text{CaCl}_2$  alcoholates and  $\text{MgCl}_2$  alcoholates. I found that  $\text{CaCl}_2$  hydrates possess the highest gravimetric energy density, followed by  $\text{MgCl}_2$  methanolates,  $\text{CaCl}_2$  methanolates,  $\text{CaCl}_2$  ethanolates, and  $\text{MgCl}_2$  ethanolates. The salt alcoholates showed an association/dissociation reaction manner similar to that of salt hydrates. The results clearly reflect the influence of the affinity of the ligands towards the various metal salts. The hydrophilicity decreases with increase in the length of the non-polar carbon chain along the homologous series of primary alcohols. I confirmed the hypothesis given by Iyimen-Schwarz [117] that  $\text{MgCl}_2$  is more ethanolated and methanolated than  $\text{CaCl}_2$ . The magnesium ion and the calcium ion have the same ionic charge, but the magnesium ion has a smaller ionic radius and thus binds more alcohol molecules than the calcium ion. The temperature lift that is also an important criterion for the characterization of adsorbents in thermal applications was measured during the alcoholation reaction of  $\text{CaCl}_2$  and  $\text{MgCl}_2$  at gram scale in a laboratory test rig. The  $\text{CaCl}_2$  alcoholates showed a temperature lift of 20 °C to 25 °C, which is sufficient for the targeted application, but lower than achieved with  $\text{CaCl}_2$  hydrates [100].

The inconsistent reaction enthalpies and cyclic irreversibility of the  $\text{MgCl}_2$ -alcohol solvates are ascribed to hydrolysis processes occurring during storage and thermal cycling. The formation of ethyl chloride from  $\text{MgCl}_2$  ethanolates at room temperature was proven by Raman spectroscopic analysis. TG-MS measurements validated the evolution of alkyl chloride from  $\text{MgCl}_2$  ethanolates and  $\text{MgCl}_2$  methanolates upon heating. The alkyl chloride ion current slightly increased from the beginning of the heating process and strengthened above 140 °C. XRD patterns supported the decomposition of all  $\text{MgCl}_2$  alcoholate samples with alkyl chloride evolution. Although traces of salt hydrates were present in all samples analyzed by the cooperation partner, which could induce the hydrolytic decomposition, a direct hydrolysis pathway (alcoholysis) is assumed. Since ethyl chloride was detected without heating, it was considered more likely that the interaction between the chloride anion in the coordination sphere of the magnesium cation and the hydroxyl group of the alcohol catalyzes the alcoholysis reaction. The findings confirm the thermal degradation of  $\text{MgCl}_2$  alcoholates proposed by Iyimen-Schwarz

[117]. Olmer and Quinet [228] observed that the addition compound  $\text{MgCl}_2 \cdot 6 \text{CH}_3\text{OH}$  decomposed with the formation of  $\text{HCl}$ ,  $\text{CH}_3\text{Cl}$ ,  $\text{MgO}$ , and  $\text{MgCO}_3$  when rapidly heated to  $100\text{ }^\circ\text{C}$  to  $300\text{ }^\circ\text{C}$  under vacuum. A similar decomposition mechanism was reported for  $\text{MgCl}_2 \cdot 6 \text{C}_2\text{H}_5\text{OH}$  by Olmer and Quinet [228]. Upon heating,  $\text{HCl}$  and  $\text{C}_2\text{H}_5\text{Cl}$  were released and the residue  $\text{MgCl}_2$  contained  $\text{MgO}$  [229]. According to published literature, the decomposition reaction appears to proceed at temperatures similar to the temperature of  $\text{MgCl}_2$  hydrate hydrolysis [215–221]. Lloyd et al. [230] stressed that there occur in many cases more profound reactions between alcohols and salts. The reactions of  $\text{AlCl}_3$ ,  $\text{FeCl}_3$  or  $\text{CuCl}_2$  and  $\text{C}_2\text{H}_5\text{OH}$  or  $\text{CH}_3\text{OH}$  are also marked by a difficultly reversible character. In this study,  $\text{CaCl}_2$  and its ethanolates and methanolates proved reversible and cyclable in the temperature domain from  $25\text{ }^\circ\text{C}$  to  $500\text{ }^\circ\text{C}$ .

All composite adsorbents studied achieved intermediate energy storage densities between the salt and the matrix. Chemisorption was considered the major sorption mechanism. The sorbate uptake was principally dependent on the porosity of the matrix and the impregnation success. This is best exemplified by the heat storage ability of natural zeolite clinoptilolite and synthetic zeolite NaX impregnated with  $\text{CaCl}_2$  and the reaction partner  $\text{C}_2\text{H}_5\text{OH}$ , as presented in **Paper VIII**. The zeolites studied by multi-cycle TGA/DSC measurements provided unsatisfying sorption abilities and energy densities. This observation is attributed to pore blocking phenomena. The zeolite 13X belongs to the class of microporous materials and possesses well-defined frameworks with cross-linked channels. By depositing  $\text{CaCl}_2$  inside the narrow pores and channels, the accessibility to sorption sites is obstructed. Moreover, strong adsorbent-adsorbate interactions resulted in high desorption temperatures. Therefore, the  $\text{CaCl}_2$ -zeolite composites tested were considered unsuitable in combination with  $\text{C}_2\text{H}_5\text{OH}$  as sorbate for low temperature heat storage. The utilization of thermally conductive matrices effectively enhanced the thermal conductivity of the salt in matrix composites and shortened the heat transfer path in case of the reaction system  $\text{CaCl}_2\text{-H}_2\text{O}$ . A facilitated thermal transport by addition of supports seems in agreement with other published work. An increase in the thermal conductivity and corresponding heat transfer coefficient of a consolidated bed of the composite material  $\text{CaCl}_2$ -silica gel was observed by Aristov et al. [127], Tanashev and Aristov [147], and Tanashev et al. [131]. Tian et al. [231] studied the correlation between the thermal conductivity and the gas permeability of the adsorption material  $\text{CaCl}_2$ -ENG. They found that gas diffusion and heat transfer are contradictory and are not only related to the fraction of ENG, but also associated to the density of the compacted composite adsorbent. This conclusion indicates that the  $\text{CaCl}_2$  content,  $\text{H}_2\text{O}$  uptake, and porosity of the matrix play a critical role and have to be adjusted carefully. In closed TES systems, precise control of the process variables system temperature and sorbate vapor pressure is important. As aforementioned, composite adsorbents with high  $\text{CaCl}_2$  loading exhibited high sorption abilities, but may be prone to  $\text{CaCl}_2$  leakage. In large scale reactors, leaks



of  $\text{CaCl}_2$  can cause severe corrosion in reactor components and hence impair the function of the TES system. Hydrophilic or alcophilic, so-called active supporting materials such as silica gel, zeolite or expanded vermiculite can contribute to the sorption process and tend to swelling when exposed uncontrollably to  $\text{H}_2\text{O}$  or alcohol. Silica gels possess an inherent disadvantage. In the presence of hydrogen and hydroxyl ions, silica gels can undergo hydrolysis. This reaction is accelerated with decreasing pH of the aqueous  $\text{CaCl}_2$  solution [232].

At milligram scale, the reaction between pure  $\text{CaCl}_2$  and  $\text{C}_2\text{H}_5\text{OH}$  as well between pure  $\text{CaCl}_2$  and  $\text{CH}_3\text{OH}$  is characterized by a high apparent degree of reversibility when the ethanolates/methanolates are being completely deethanolated/demethanolated. Methanolation/demethanolation reaction cycle experiments carried out at alternating regeneration temperatures demonstrated that partial demethanolation of single  $\text{CaCl}_2$  and the formation of lower non-integer  $\text{CaCl}_2$  methanolates affect heat/cold output and reaction kinetics. Kinetic data on the reaction system  $\text{CaCl}_2\text{-C}_2\text{H}_5\text{OH}$  were derived from the model-free Kissinger method. A major disadvantage of the Kissinger method is the fact, that only a single value of the activation energy for the rate-determining step is calculated. The decomposition of addition compounds of  $\text{CaCl}_2$  and  $\text{C}_2\text{H}_5\text{OH}$ , however, is a heterogeneous reaction composed of sequential processes. The consideration of model-fitting approaches was beyond the scope of this thesis. Morphological modifications observed after consecutive discharging/charging runs and variations in the reaction rates endorse the theory of structural changes over cycling. In upscaled reactors in which uniform TCM distribution is difficult to realize, the increased thickness and density of the TCM layer, a fortiori, will negatively influence the speed of the reaction. Evidently, the dispersion of  $\text{CaCl}_2$  inside host matrices improved the discharging/charging reaction behavior and thermal performance. Short-term cycling tests confirmed the good cyclability of expanded vermiculite and biochar supported  $\text{CaCl}_2$  under constant methanolation/demethanolation conditions. Some composite adsorbents displayed enhanced kinetics in comparison to the chemical adsorbents. The host matrices provided an enlarged surface area and increased the ease of the sorbate diffusion to and from the reaction zone. Since the deposition of  $\text{CaCl}_2$  particles within the pores of matrices leads to decreased surface areas and pore volumes when compared to the untreated matrices [233], the  $\text{CaCl}_2$  content is a major controlling factor for the kinetics. I experimentally verified that kinetic characteristics are also sensitive to reaction conditions. Variation in the sorbate vapor pressure, temperature program, and thermal pretreatment altered the speed of the association and dissociation reaction. At the current stage of research, the chemical and composite adsorbents do not fulfill all of the technological requirements of the targeted closed TES system for heating and cooling applications. Future investigations on relevant material characteristics by supplementary analysis are required to validate the applicability of the composite adsorbents and to infer optimization approaches.

## 2. Paper overview

Overview of articles included in this cumulative PhD thesis entitled "Development and characterization of thermochemical materials based on salt hydrates and salt alcoholates"

(in accordance with the guideline for cumulative dissertations in Sustainability Science, January 2012)

Papers included:

- I Fopah Lele A, Korhammer K, Wegscheider N, Rammelberg HU, Osterland T, Ruck W. Thermal conductivity measurement of salt hydrate as porous material using calorimetric (DSC) method. 8th World Conference on Experimental Heat Transfer, Fluid Mechanics and Thermodynamics (ExHFT), Lisboa, Portugal: A. Faria - Edicao Electronica Lda.; 2013.
- II Druske M-M, Fopah-Lele A, Korhammer K, Rammelberg HU, Wegscheider N, Ruck W, et al. Developed materials for thermal energy storage: Synthesis and characterization. *Energy Procedia* 2014;61:96–9.
- III Korhammer K, Druske M-M, Fopah-Lele A, Rammelberg HU, Wegscheider N, Opel O, et al. Sorption and thermal characterization of composite materials based on chlorides for thermal energy storage. *Applied Energy* 2016;162:1462–72.
- IV Korhammer K, Apel C, Osterland T, Ruck WKL. Reaction of calcium chloride and magnesium chloride and their mixed salts with ethanol for thermal energy storage. *Energy Procedia* 2016;91:161–71.
- V Korhammer K, Mihály J, Bálint S, Trif L, Vass Á, Tompos A, et al. Reversible formation of alcohol solvates and their potential use for heat storage. *Journal of Thermal Analysis and Calorimetry* 2019;138:11–33.
- VI Korhammer K, Neumann K, Opel O, Ruck WKL. Micro-scale thermodynamic and kinetic analysis of a calcium chloride methanol system for process cooling. *Energy Procedia* 2017;105:4363–9.
- VII Korhammer K, Neumann K, Opel O, Ruck WKL. Thermodynamic and kinetic study of  $\text{CaCl}_2\text{-CH}_3\text{OH}$  adducts for solid sorption refrigeration by TGA/DSC. *Applied Energy* 2018;230:1255–78.
- VIII Korhammer K, Opel O, Ruck WKL. Energy storage and adsorption cooling efficiency of novel composite adsorbents. To be submitted to *Thermochimica Acta*.

Table 2.1.: Authors' contribution to the articles and articles' publication status according to § 16 of the guideline for cumulative dissertations in Sustainability Science, January 2012. Part a.

Paper No.	Title	Specific contributions of all authors	Author status	WF	Publication status	Conference contributions
I	Thermal conductivity measurement of salt hydrate as porous material using calorimetric (DSC) method	AFL, KK, NW, HUR: sample preparation, measurements, data analysis AFL, KK, HUR: research concept, literature review, paper writing TS, WR: overall research concept, discussions	Co-author with important contribution	0.5	Published in Conference proceedings of the 8th World Conference on Experimental Heat Transfer, Fluid Mechanics and Thermodynamics (ExHFT).	ExHFT 2013
II	Developed materials for thermal energy storage: Synthesis and characterization	MMD, AFL, KK, NW: measurements, data analysis MMD, AFL, KK, HUR: research concept, literature review, paper writing TS, WR: overall research concept, discussions	Co-author with predominant contribution	1.0	Published in Energy Procedia (CS: 1.44)	ICAE 2014
III	Sorption and thermal characterization of composite materials based on chlorides for thermal energy storage	KK, MMD, AFL, NW: measurements, data analysis KK, MMD, AFL, HUR: research concept, literature review, paper writing OO, TO, WR: overall research concept, discussions	Co-author with predominant contribution	1.0	Published in Applied Energy (IF: 7.900, CS: 8.44)	ICAE 2014
IV	Reaction of calcium chloride and magnesium chloride and their mixed salts with ethanol for thermal energy storage	KK, CA: measurements, data analysis, calculations KK, CA: research concept, literature review, paper writing TO, WR: overall research concept, discussions	Co-author with predominant contribution	1.0	Published in Energy Procedia (CS: 1.44)	SHC 2015
			Subtotal:	3.5		

## 2. Paper overview

Table 2.2.: Authors' contribution to the articles and articles' publication status according to § 16 of the guideline for cumulative dissertations in Sustainability Science, January 2012. Part b.

Paper No.	Title	Specific contributions of all authors	Author status	WF	Publication status	Conference contributions
V	Reversible formation of alcohol solvates and their potential use for heat storage	KK, ET: research concept KK, JM, SB, LT, AV, ET: measurements, data analysis, calculations, literature review KK, JM, SB, LT, ET: paper writing AT: topic setting, overall research concept	Co-author with equal contribution	1.0	Published in Journal of Thermal Analysis and Calorimetry (IF: 2.209, CS: 2.10)	KEN 2016, PhD Hallgatók 2. Környezettudományi Konferenciája
VI	Micro-scale thermodynamic and kinetic analysis of a calcium chloride methanol system for process cooling	KK, KN: measurements, data analysis KK: literature review KK, OO: paper writing WR: topic setting, research concept, discussions	Co-author with predominant contribution	1.0	Published in Energy Procedia (CS: 1.44)	IRES 2016, ICAE 2016
VII	Thermodynamic and kinetic study of CaCl <sub>2</sub> -CH <sub>3</sub> OH adducts for solid sorption refrigeration by TGA/DSC	KK, KN: measurements, data analysis KK: literature review KK, OO: paper writing WR: topic setting, research concept, discussions	Co-author with predominant contribution	1.0	Published in Applied Energy (IF: 7.900, CS: 8.44)	IRES 2016, ICAE 2016
VIII	Energy storage and adsorption cooling efficiency of novel composite adsorbents	KK: measurements, data analysis KK: literature review KK, OO: paper writing WR: topic setting, research concept	Co-author with predominant contribution	1.0	To be submitted to Thermochimica Acta (IF: 2.189, CS: 2.41)	
			Subtotal:	4.0		
			Grand total:	7.5		

## Explanations

### *Specific contributions of all authors*

AFL: Armand Fopah-Lele, AT: András Tompos, AV: Ádám Vass, CA: Christina Apel, ET: Emília Tálas, HUR: Holger Urs Rammelberg, JM: Judith Mihály, KK: Kathrin Korhammer, KN: Karsten Neumann, LT: László Trif, MMD: Mona-Maria Druske, NW: Nina Wegscheider, OO: Oliver Opel, SB: Szabolcs Bálint, TO: Thomas Osterland, TS: Thomas Schmidt, WR: Wolfgang Ruck

WF: Weighting factor

### *Publication status*

IF: Thomson Reuters Citation Reports 2017; impact factors 2017

CS: CiteScore 2017

### *Conference contributions (acronym, society, date, venue, website)*

ExHFT 2013, 8th World Conference on Experimental Heat Transfer, Fluid Mechanics and Thermodynamics. June 16-20, 2013, Lisbon, Portugal. <http://www.exhft8.org>. Oral presentation\*

ICAE 2014, 6th International Conference on Applied Energy. May 30 - June 2, 2014, Taipei, Taiwan. [www.applied-energy.org](http://www.applied-energy.org). Oral presentation

ICAE 2016, 8th International Conference on Applied Energy. October 8-11, 2016, Beijing, China. <http://www.applied-energy.org/icae2016/>. Oral presentation

IRES 2016, 10th International Renewable Energy Storage Conference. March 15-17, Düsseldorf, Germany. <https://www.eurosolar.de/de/index.php/archiv-2016/1945-int-konferenz-zur-speicherung-erneuerbarer-energien-ires-2016>. Poster and oral presentation

KEN 2016, XXXIX. KÉMIAI ELŐADÓI NAPOK. October 17-19, 2016, Szeged, Hungary. <http://www.staff.u-szeged.hu/mkecsmcs/ken.htm>. Oral presentation\*

PhD Hallgatók 2. Környezettudományi Konferenciája. April 26, 2016, Budapest, Hungary. Poster presentation\*

SHC 2015, 4th International Conference on Solar Heating and Cooling for Buildings and Industry. December 2-4, 2015, Istanbul, Turkey. <http://www.shc2015.org/home.html>. Oral presentation

\* presented by co-author

### **3. Paper I**

8th World Conference on Experimental Heat  
Transfer, Fluid Mechanics, and Thermodynamics  
June 16-20, 2013, Lisbon, Portugal

## THERMAL CONDUCTIVITY MEASUREMENT OF SALT HYDRATES AS POROUS MATERIAL USING CALORIMETRIC (DSC) METHOD

Armand Fopah Lele\*, Kathrin Korhammer\*, Nina Wegscheider\*, Holger Urs Rammelberg\*,  
Thomas Schmidt\* and Wolfgang K. L. Ruck\*

\* Institute of Sustainable and Environmental Chemistry, Leuphana University of Lueneburg,  
Scharnhorststrasse 1 – 21335 Lueneburg, Germany  
Corresponding e-mail: [tschmid@leuphana.de](mailto:tschmid@leuphana.de) – Tel: 004941316772951

### ABSTRACT

The effective thermal conductivity of calcium chloride was measured and its value was increased by two and around three times when impregnating Expanded Vermiculite and Silica Gel with calcium chloride with standard uncertainty  $\pm 0.004\%$ . The porous matrix was fabricated by taking Silica Gel / Expanded Vermiculite that had been soaked in a bath of calcium chloride solution with a salt concentration of 40 wt% and then heat-treated at 200 °C. The properties of the porous materials were measured using the heat flux DSC for particles size of 0 – 3 mm in the temperature range from 100 °C to 200 °C. These are small samples having a diameter less than 5.0 mm, a height less than 4.25 mm and a low thermal conductivity. In the studied properties, we focus on thermal conductivity, the obtained values were presented as function of the porosity range values. The performance of the salt-composite widely demonstrated nowadays, will be used in a heat storage system for households application. However, some problems related to the heat loss and open system have not allowed to observe the accurate thermal resistance as expected. Some avenues are explored prior to a new and more appropriate design and eventually a new operating mode.

*Keywords* : Thermal conductivity, Porous material, DSC, Porosity, Impregnation

### 1. Introduction

Thermal energy storage system with reversible gas-solid, liquid-solid reactions have been widely studied over the last years, using solid or liquid salts [1;2]. Salt hydrates are very interesting thermal energy storage materials in terms of their high storage density ( $\sim 1 \text{ GJ/m}^3$ ). However, it was noticed that their thermal properties are strongly influenced by particle size and porosity on the outputs [3]. In a reactor for thermochemical storage, hydration reaction rate is strongly linked to the thermal conductivity of the salt bed. Reaction rate increases with the effective thermal conductivity of the salt [4]. Knowing that salts in general have a low thermal conductivity, composites based on salts are generally synthesized in order to enhance thermal properties such as thermal conductivity. These composite materials are based on a porous carrier matrix and a salt. The carrier matrix fulfills different functions: it defines the stability, the shape and the size of the material, which can be specially adapted for the application [5]. It also provides a high inner surface allowing a fine dispersion and uniform distribution of the salt within the carrier matrix. Salts on active carrier matrix as well as salts on honeycomb matrix have been produced as part of the project's collaborative work with the National Institute of Chemistry (NIC) in Slovenia and the Fraunhofer Institute for Solar Energy FhG ISE in Germany [5]. The hygroscopic salt introduced in the porous matrices is  $\text{CaCl}_2$ .

In the literature, there are few data on the measurement of thermal conductivity of salt hydrates using calorimetry methods. Recently, the thermal conductivity of  $\text{FeCl}_3 \cdot 6\text{H}_2\text{O}$  and  $\text{FeSO}_4 \cdot 7\text{H}_2\text{O}$  [6;7] were measured with uncertainties of  $\pm 3\%$  and  $\pm 2\%$ , respectively. The results, obtained by means of a

Differential Scanning Calorimeter (DSC) show good agreement with the literature. Still with DSC method, but on polymer, Camirand [11], with only one sample, measures thermal conductivity with an experimental error of less than 5% by fitting the decreasing part of the thermogram.

Using another method, Wang et al. [8] measured the effective thermal conductivity of pure  $\text{CaCl}_2$  (powder form) and found out a range of 0.3 – 0.4 W/m K.

Knowledge of the effective thermal conductivity is necessary for accurate heat transfer analysis and dynamic simulation of an adsorber. There have been however, very few experimental studies on the effective thermal conductivity of Expanded Vermiculite/Silica Gel- $\text{CaCl}_2$  in the literature. Michel et al. and Aristov et al. [4;9;10] have developed composites by impregnating  $\text{CaCl}_2$  solution into an exfoliated vermiculite and Silica Gel matrix, respectively. The high porosity leads to lower density and low thermal conductivity; and good heat transfer properties are obtained when preparing materials by compaction. But they did not characterize its thermal conductivity although Michel [16] used a range of 0.3 – 0.7 W/m K for sorption simulations (for energy density from 60 to 250  $\text{kW/m}^3$ ).

This paper presents experimental results on the effective thermal conductivity of three types of adsorbent, pure  $\text{CaCl}_2$  powder, Silica Gel impregnated with calcium chloride (SG- $\text{CaCl}_2$ ) (1–3 mm) composite and Expanded Vermiculite impregnated with calcium chloride (EV- $\text{CaCl}_2$ ) (0–1 mm) composite for different porosities, measured by the “DSC method” at fixed pressure and temperature under nitrogen flow.

### 2. Material and Method

### 2.1 Preparation of porous materials

For this work anhydrous calcium chloride (AppliChem Company) was used. The salt-porous-carrier composites were synthesized by Wegscheider [17] by impregnating Silica Gel (SG) and Expanded Vermiculite (EV) matrices with an aqueous solution of calcium chloride with a salt concentration of 40 wt%. The two matrices SG (Roth) and EV (Deutsche Vermiculite Dämmstoff GmbH) with a particle size of 0-3 mm and 0-1 mm were first preheated at 200 °C for 4 hours to remove residual water and then soaked in the calcium chloride solution over night. After filtration, the samples were washed with a few millimeters of ice-cold 70% ethanol to remove impurities and dried at 200 °C for further 4 hours. The composites were stored in a sealed container and placed in a dry area to protect them from moisture.

### 2.2 Thermal conductivity measurements

A TGA/DSC1 (Mettler) was used to analyze the heat flux during the thermal conductivity experiments. The porous and composite materials were measured at a heating rate of 10 °C/min with nitrogen flow rate of 50 mL/min. The amount of materials used was around 100 mg. For the calibration, three (3) sensor materials with known thermal conductivities, which give clear different melting peaks between 29 °C and 229 °C, were used with a standard deviation of 0.6 for heat flow and of 0.03 for temperature. For each sample, four measurements were made in order to find the accurate one to use in the final measurements. Then an adjustment was made in order to scope the apparatus to the calibration sample parameters, and finally a re-calibration is performed to validate the calibration process. The sensor materials are given in Table 1. At the first step of DSC measurements, sensor materials pellets (1 mm diameter) prepared under atmospheric pressure were placed into 5 mm alumina container and then the melting curves were determined. At the second step, the sensor material was placed on top of the salt/composite material which was compacted in the alumina containers with a specific height of 4.24 mm and cross-sectional area of 19.63 mm<sup>2</sup> illustrated in Fig. 1. Subsequently the DSC measurements were carried out again until the sensor material melted.

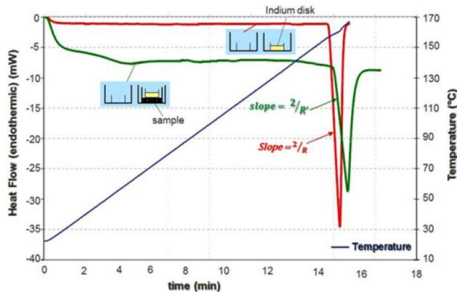


Fig. 1. Sensor and sensor + sample and DSC curves.

Table 1 List of sensor materials and their melting point.

Sensor materials	Melting point (°C)	Thermal conductivity (W/m K)
Gallium	29.7	40.6
Indium	156.6	81.8
Tin (Sn)	229	66.8

The purpose of this measurement is to determine the thermal conductivity values by the method of Camirand [11] which is an improvement of the method presented by Flynn et al. [12]. The method used here utilizes the measurement of rate of heat flow into a sensor material during its first order transition to obtain the thermal resistance of a material placed between the sensor material and the heater in DSC. The sample for which we want to determine the thermal conductivity is placed into the sample furnace of the calorimeter, and a sensor substance (indium) is placed on top of the salt sample. The reference crucible is kept empty. During melting of the calibration substance, the temperature of the calibration substance must be constant. A scan is performed to measure the differential power produced during the melting of the calibration substance. The curve obtained is approximately linear before the melting and decreases exponentially during melting (Fig. 1). Taking up the slopes of the DSC curves at melting stage of the sensor material, the thermal resistance of the sample is determined by Eq.(1).

$$R_s = R - R' \quad (1)$$

where, R is the thermal resistance between calorimeter and sensor material, R' is the thermal resistance between calorimeter and sensor material with sample. Taking into account all the thermal resistances, the slope can be defined from the linear side of the melting peak [13] (see Fig. 2) as:

$$Slope = (q(t) - q_{onset}) / (T(t) - T_{onset}) \quad (2)$$

where  $q_{onset}$  and  $T_{onset}$  are the heat flow and melt temperature of salt at the onset of melting. The thermal conductivity is then determined using the Eq.(3).

$$\lambda_s = L / (A * R_s) = L / \{A * (R - R')\} \quad (3)$$

where, L is the sample height, A is the contact area between sample and sensor material (1 mm<sup>2</sup>).

For the effective thermal conductivity (according to the salt bed in the Alumina container), a relationship commonly used in the case of porous media composed of a single component is the relationship of Archie [14]. This correlation has been validated for porous beds by Olivès [15]:

$$\lambda_{eff} = \lambda_s * (1 - \epsilon)^\xi \quad (4)$$

where  $\lambda_s$  is the thermal conductivity of the salt,  $\epsilon$  the porosity of the porous medium and  $\xi$  the degree of consolidation (cementation factor), which reflects the mechanical strength of



the material. This factor is generally between 1 and 4. For granular (1 – 3 mm) porous media, it is commonly accepted that the degree of consolidation is between 1.3 and 2.0 [16]. The porosity of the dehydrated/hydrated salt bed should be a function of the energy density, the molar density of the material and the reaction enthalpy, so the sample experimental parameters account for the porosity. Since the DSC curves do not show any chemical reaction (see Fig. 4) and no porosimetry has been performed, our results are presented as a function of porosity range.

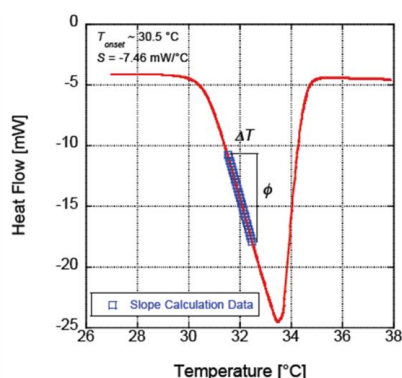


Fig. 2. Example of slope calculation on heat flow vs. temperature curve for salt sample [13].

### 3. RESULTS AND DISCUSSION

#### 3.1 Thermal Conductivity results

First of all thermal conductivity of salt samples was measured in the range of 100 °C to 200 °C with 50 mL/min nitrogen flow and effective thermal conductivity was calculated using the method explained in section 2.2. The effective thermal conductivities of  $\text{CaCl}_2$  powders vary between 0.05-0.81 W/m K according to porosity range and a degree of consolidation of 1.3 (see Fig.3) with a mean value of 0.39 W/m K. These low values of the effective thermal conductivity require high temperature gradients to heat the  $\text{CaCl}_2$  for a complete desorption. At the beginning, the samples are dried (drying process at 200 °C) and the measurements are performed with increasing temperature.

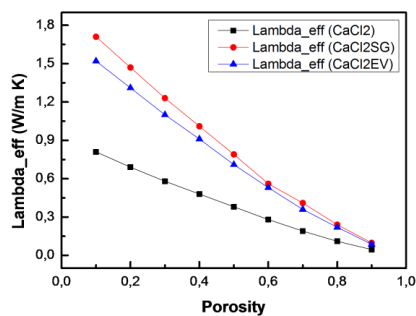
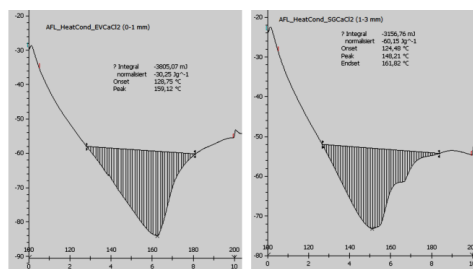


Fig. 3. Temperature dependence of the effective thermal conductivity of  $\text{CaCl}_2$  completely dehydrated under Nitrogen flow.

The results obtained in Fig. 3 show that for a porosity of 0.5, we are in the range of Wang et al. (0.31-0.39 W/m K [8]) results and for a porosity range of (0.2-0.5) we are in the range used by Michel [16] for his simulation. Let us notice that, Wang used a hot wire method under atmosphere with a different sample preparation. Also, the heat losses have not been evaluated, since the crucibles are open (no encapsulation) in the furnace. Nevertheless, it can be seen that  $\text{CaCl}_2$  is a bad thermal conductor of heat, but its exothermic property makes it attractive in chemical engineering.



a) DSC curves of EV- $\text{CaCl}_2$       b) DSC curves of SG- $\text{CaCl}_2$

Fig. 4. DSC (heat flux vs. temperature) curves of SG- $\text{CaCl}_2$  and EV- $\text{CaCl}_2$  used to determine the effective thermal conductivity.

The calculated (mean) effective thermal conductivity of  $\text{CaCl}_2$  by impregnation into Silica Gel and Expanded Vermiculite is 0.83 W/m K and 0.74 W/m K, respectively. These results highlight the fact that Silica Gel matrix enhances the heat transfer slightly more than Expanded Vermiculite, since the effective thermal conductivity of  $\text{CaCl}_2$  is increased about 35% with addition of EV and about 44% with SG. The uncertainties of this measurement are mainly a function of the sample dimensions and the slope, since the latter is a function of the heat flow and the temperature. We cannot talk about error here, since the “true” thermal conductivity of salt hydrate is not really known. The calibrated caliper used for sample dimensions has a resolution of 0.05 mm, and according to the TGA/DSC 1 STAR<sup>®</sup> system manual the resolution of temperature and heat flow measurement are 0.00003 K and 0.1 mW, respectively. This led to a standard uncertainty of 2.5% for the slope and 0.004% for the thermal conductivity. Let’s recall that, small uncertainty may be due to the fact that some important systematic effect was overlooked. Unknowingly, a measurement result can have a very small error and a large associated uncertainty. The reverse is also true: a measurement result may carry with it a very small uncertainty while its (unknown) error is large [18].

These previous measured values cannot be compared or validated. Characterization of these two composites with

emphasis on effective thermal conductivity has not yet been mentioned in the literature. The observed values in the results might be subjected to sources of systematic effects, which are: the one-dimensional model does not take into account the effects due to the other dimensions in the furnace; the sum of the thermal contact resistances vary from one sample to another; some heat is lost from the samples by convection and radiation since the crucible is open; the thermal conductivity varies with range temperature (100 °C to 200 °C); there is dilation of the samples during the process; the width of the discontinuity of the temperature field at the contact surfaces is not nil; the samples do not have exactly the same diameter; the bottom and upper surfaces of the samples are not perfectly flat; the thermal conditions seen by the salt and salt composites before the measurement could influence its thermal conductivity (storage conditions, room humidity); the weight of the samples could influence the thermal contact resistances; in reality the indium mass does not entirely cover the upper surface of the samples; positioning the crucibles in the measuring cell; the bottom surfaces of the indium discs are not perfectly smooth; the 2 used in the slope [11], compacity was not measured, finally, the temperature gradients inside the sensor material may not be negligible compared to the thermal gradients inside the sample.

### 3.2 Future scope

In order to overcome previous limitations and alternatives for thermal conductivity measurement of salt composites, a steady state method is being developed. This method is characterized by the simultaneous measurement of a heat flow passing through the sample and a temperature difference and allows to achieve the thermal resistance of the sample. The apparatus is constituted of a water bath or electrical heater (Fig. 5), a heating layer used as heat exchanger, a cooling system (can be another bath or tap water system), two cylinders made of Teflon, an insulating material, clams and Pt 100 (T1, T2, T3). One cylinder contains a sample and the other a standard material with the same thermal conductivity range as the sample.

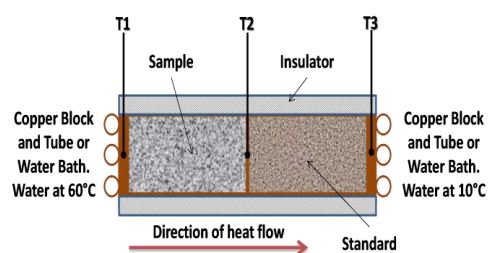


Fig. 5. Absolute Method Apparatus for thermal conductivity measurement.

The standard material (with known conductivity, dimensions) with a cross-sectional area equal to the area of the sample will be placed on a copper block with i.e. 50 °C (this temperature will be below the transition/melting temperature of samples) water

running through copper tubes on the copper block (or power from the electrical heater). The sample will be placed beside the standard block and then beside and very close, a copper block with 10 °C water circulating in the tubes (this system can be replaced by a water bath system). The temperature drop across the sample and standard will be measured using a Pt100, placed at the center of each surface. The apparatus will be insulated to ensure one-dimensional heat transfer and heat layer will be placed (or welded) on each surface to ensure minimal thermal resistance across the interfaces. The results will be presented and compared in a near future.

### 4. CONCLUSIONS

A well known problem of using solid adsorbents in heating and cooling systems is their poor thermal conductivity (0.1-0.5 W/m K). To overcome this problem, heat transfer additives are usually used in a composite adsorbent. Based on the assumptions made, it can be seen that Silica Gel and Expanded Vermiculite matrices can improve the effective thermal conductivity. These matrices have been used as sorption materials and for heat transfer enhancement. Effective thermal conductivity of  $\text{CaCl}_2$  powder, EV- $\text{CaCl}_2$  and SG- $\text{CaCl}_2$  were measured using differential scanning calorimetry (DSC). Despite the above mentioned causes of uncertainties, a substantial increase of effective thermal conductivity was observed with impregnated  $\text{CaCl}_2$ . Based on this paper, the enhancement of heat transfer using impregnation of EV and SG cannot be completely approved now. That is why; another experiment is in development, in order to validate our performed measurement.

### 5. ACKNOWLEDGEMENTS

This work was performed within the research project innovation-inkubator / competence tandem "Thermische Batterie". The authors would like to acknowledge the EU-foerdert Niedersachsen (EFRE) and the Leuphana University of Lüneburg in Germany for their financial support.

### REFERENCES

1. N'Tsoukpoe K. E., Liu H., LE Pierrès N., Luo L., A review on long-term sorption storage, *Renewable and Sustainable Energy Reviews*, 13, pp.2385-2396, 2009.
2. R. Cuypers, C. Finck, E. Henquet, H. Oversloot, A. de Geus, MERITS: More Effective use of Renewables Including compact seasonal Thermal energy Storage, *Proc. Immostock Conference, Lleida-Spain*, pp.123, May 2012.
3. Z. Yang, S. V. Garimella, Thermal analysis of solar thermal energy storage in a molten-salt thermocline, *Solar Energy*, 84, issue 6, pp.974-985, 2010.
4. B. Michel, N. Mazet, S. Mauran, D. Stitou, J. Xu, Thermochemical process for seasonal storage of solar energy: Characterization and modeling of a high density reactive bed, *Energy*, 47, Issue 1, pp.553-563, 2012.
5. Wim Van Helden, Andreas Hauer, Feature article on advances in compact thermal energy storage - material

- development, *SHC (IEA Solar Heating and Cooling programme) 2012 Annual Report*, pp. 166. March 2013.
6. N. Guang-hua, Z. Zhi-ying, Measurement of Thermal Conductivities of Salt Hydrates II.  $\text{FeCl}_3 \cdot 6\text{H}_2\text{O}$ ,  $\text{FeSO}_4 \cdot 7\text{H}_2\text{O}$ , *Journal of Hubei Institute for Nationalities*; China 03, 2002.
  7. N. Guang-hua, L. Yao-hua, ZHANG Zhi-, Measurement of the thermal conductivity of  $\text{Al}(\text{NO}_3)_3 \cdot 9\text{H}_2\text{O}$  and  $\text{Ba}(\text{OH})_2 \cdot 8\text{H}_2\text{O}$  in the temperature range from  $10^\circ\text{C}$  to  $80^\circ\text{C}$ , *Energy Research and Information*, 01, 2004.
  8. K. Wang, J. Y. Wu, R. Z. Wang, L. W. Wang, Effective thermal conductivity of expanded graphite- $\text{CaCl}_2$  composite adsorbent for chemical adsorption chillers. *Energy Conversion and Management*, 47, pp. 1902-1912, 2006.
  9. Y. I. Aristov, G. Restuccia, M. M. Tokarev, H.-D. Buerger, A. Freni, Selective water sorbents for multiple applications:  $\text{CaCl}_2$  confined to Expanded Vermiculite. *Reaction Kinet. Catal. Letters*, 71 (N° 2), pp. 377-384, 2000.
  10. Y. I. Aristov, M. M. Tokarev, G. Cacciola, G. Restuccia, Selective water sorbents for multiple applications:  $\text{CaCl}_2$  confined in mesopores of Silica Gel – Sorption properties. *Reaction Kinet. Catal. Letters*, 59 (N° 2), pp. 325-333, 1996.
  11. C. P. Camirand, Measurement of thermal conductivity by Differential Scanning Calorimetry, *Thermochimica Acta* 417, pp.1-4, 2004.
  12. J. H. Flynn, D. M. Levin, A method for the determination of thermal conductivity of sheet material by differential scanning calorimeter (DSC). *Thermochimica Acta*, 126, pp.93-100, 1988.
  13. B. D. Iverson, J. G. Cordaro, A. M. Kruienza, Thermal property testing of Nitrate thermal storage salts in the solid-phase, *Proc. ASME 5<sup>th</sup> International Conference on Energy Sustainability*, ES2011-54159, Washington, DC, USA, 8 pages, August 2011.
  14. G. E. Archie, The electrical resistivity log as an aid in determining some reservoir characteristics, *T. Am. I. Min. Met. Eng.*, 146, pp. 54-62, 1942.
  15. R. Olivès, S. Mauran, A highly conductive porous medium for solid-gas reactions: Effect of the dispersed phase on thermal tortuosity. *Transport in Porous Media*, 43, pp.377-394, 2001.
  16. Benoît Michel, Procédé thermochimique pour le stockage intersaisonnier de l'énergie solaire : modélisation multi-échelle et expérimentation d'un prototype sous air humide, Ph.D thesis, Ecole Doctorale Energie-Environnement de l'Université Via Domitia Perpignan, France, 2012.
  17. Nina Wegscheider, Synthese und Charakterisierung von Kompositen aus Salzen und mesoporösen Trägermaterialien für eine Thermochemische Batterie, Bachelor thesis, Institute of sustainable and Environmental Chemistry of Leuphana University of Lüneburg, Germany, 2013.
  18. Ignacio Lira, Evaluating the measurement uncertainty: Fundamentals and practical guidance, in Series in Measurement Science and Technology (ed), *Institute of Physics Publishing*, M Afsar, Tufts University, USA, 2002.

## 4. Paper II

Available online at [www.sciencedirect.com](http://www.sciencedirect.com)**ScienceDirect**

Energy Procedia 61 (2014) 96 – 99

---



---

Energy  
**Procedia**


---



---

The 6<sup>th</sup> International Conference on Applied Energy – ICAE2014

## Developed materials for thermal energy storage: synthesis and characterization

Mona-Maria Druske<sup>a</sup>, Armand Fopah-Lele<sup>a</sup>, Kathrin Korhammer<sup>a</sup>, Holger Urs Rammelberg<sup>a,\*</sup>, Nina Wegscheider<sup>a</sup>, Wolfgang Ruck<sup>a</sup>, Thomas Schmidt<sup>a</sup>

<sup>a</sup>*Leuphana University Lüneburg, Scharnhorststr. 1, 21335 Lüneburg, Germany*

### Abstract

Heat storage or thermal energy storage is one of the key technologies towards an efficient use of renewable energy resources, particularly the thermochemical heat storage looks promising, but the progress has not yet been succeeded. Therefore our research group focuses on the development of a heat storage system called “thermal battery” for private households and industry applications. On the one hand especially thermochemical reactions have a high potential for high energy density and long term storage. On the other hand the used materials in particular hygroscopic salts are related to disadvantages such as agglomeration, storage capacity loss over cycling or slow reaction kinetics. Those disadvantages are caused by deliquescence and by the occurrence of side reactions, among other effects. We combined the optimization of mixing of salt hydrates and impregnation of carriers to overcome these disadvantages. This paper reports on synthesis of thermochemical materials and comparison of the material properties energy density and effective thermal conductivity.

© 2014 The Authors. Published by Elsevier Ltd. This is an open access article under the CC BY-NC-ND license (<http://creativecommons.org/licenses/by-nc-nd/3.0/>).

Peer-review under responsibility of the Organizing Committee of ICAE2014

Keywords: thermochemical heat storage, composites, mixtures, impregnation, water vapor pressure, thermal conductivity

### 1. Introduction

Thermal energy storage is one of the key technologies towards an efficient use of renewable energy resources. Hereby thermochemical heat storage promises higher storage density as sensible or phase change heat storage. Based on reversible chemical reactions long term storage becomes possible. Many challenges are associated with potential thermochemical heat storage materials. Hygroscopic salt hydrates have a high kinetic water uptake but tend to agglomeration. This deliquescence reduces the water uptake rate and cycle stability of the storage material. In order to overcome this disadvantage many studies have

\* Thomas Schmidt. Tel.: +49-4131-677-2951; fax: +49-4131-677-2822.

E-mail address: [thomas.schmidt@inkubator.leuphana.de](mailto:thomas.schmidt@inkubator.leuphana.de) – [holger\\_urs.rammelberg@inkubator.leuphana.de](mailto:holger_urs.rammelberg@inkubator.leuphana.de)

been performed.[1] The Impregnation of the salt hydrates into porous matrices prevented deliquescence and improved the diffusion of water vapor into the material.[2] The Controlling of the water vapor access into the material prevents in micro scale the deliquescence, too.[IRES2012] However, this procedure is not manageable in macro scale because of the heterogenic reactions occurring in the storage bulk. Salt mixtures of metal chlorides and sulfates showed high cycle stability beside deliquescence.[1] This paper reports on the synthesis of thermochemical materials and the comparison of the material properties energy density and effective thermal conductivity.

#### Nomenclature

ACF	activated carbon foam
ENGB	compacted expanded natural graphite
ENGP	expanded natural graphite powder

## 2. Experiments

Hydration levels of used pure salts were confirmed by TGA – measurements.

### 2.1. Sample preparation

Salt-porous-carrier composites were synthesized by impregnating host matrices with molten salt (soaking) and a saturated aqueous salt solution (wet impregnation) under vacuum (10 mbar) and at atmospheric pressure. The impregnation time varied between seconds and minutes. For all experiments anhydrous  $\text{CaCl}_2$  (AppliChem Company),  $\text{CaCl}_2 \cdot 6 \text{H}_2\text{O}$  (AppliChem Company) and KCl (Merck) were used. The host matrices activated carbon foam media ACF (Blücher GmbH), compacted expanded natural graphite ENGB (SGL Group) and expanded natural graphite powder ENGP (SGL Group) were first preheated to remove residual water and then impregnated and finally dried. The mixed salts of  $\text{CaCl}_2$  and KCl were crystallized from a solution of their basic salt components in pure water. The mixing ratios depend on the compound expected to form and are calculated by molecular weight of the involved salts.

### 2.2. TGA/DSC –Measurements

Thermogravimetric analysis and heat flux measurement was performed using a simultaneous TGA/DSC 1 device from Mettler Toledo to investigate the water sorption properties and the long-term thermal stability of the host matrices upon modification. The gas flow was controlled by a gas box, providing 2 independent mass flow controllers connected to the TGA/DSC control. We used silica gel-dried nitrogen as purge gas at a flow rate of 50 mL/min. In addition to the purge gas flow, we used a separate nitrogen flow, humidified via a tempered gas bubbler flask as the reaction gas during hydration. The hydration measurements were done at 25 °C at a water vapor pressure of 20 mbar. The dehydration was done with a heating rate of 3 K/min up to 200 °C at atmospheric pressure. Salt mixtures were measured with a heating rate of 5 K/min in two steps up to 200 °C. The mass of samples were 10 - 20 mg. Integration of the hydration heat fluxes over time was done manually using the Mettler Toledo STARE Software 11.00a.

### 2.3. Thermal conductivity measurements

First of all thermal conductivity of salt samples was measured in the range of 100 °C to 200 °C with 50 mL/min nitrogen flow and bed thermal conductivity was calculated using the calorimetric method [3]. The heating rate of 10 °C/min has been chosen because of the results according to the literature or provider data. Heat conductivity enhancement is clearly shown in the following table.

### 3. Results and discussion

The pure calcium chloride shows higher release of water as uptake, caused in the mentioned delinquency behaviour. (Table 1) The mixing of calcium chloride and potassium chloride gave a heterogeneous picture. The salt mixtures showed completeness rehydration depending on the amount of calcium chloride. The measurements of the reaction enthalpies the results of enthalpy were not clear. Results show that the impregnation success is related to the host matrix and the impregnating medium. The composite based on ACF has with 63 wt-% the lowest salt content in comparison to the samples with ENGB and ENGP as host matrices (Table 1). Due to its open pore structure ACF tends to lose calcium chloride during impregnation and drying. Expanded natural graphite impregnated with molten salt (Ca-ENGB-S, Ca-ENGB-S1) have a slightly higher salt content than those impregnated with aqueous salt solutions (Ca-ENGB-W, Ca-ENGP-W). All samples show good water sorption behaviour, Ca-ENGP-W has a more stable water sorption behaviour than the other composites. In general the water uptake is about 30-40 % higher than the water release. Despite a high salt content of 90 wt-%, samples impregnated with molten salts have a lower water sorption than those impregnated with an aqueous salt solution. The more salt is confined to the matrix surface and into the matrix pores the lower is the diffusivity of the water vapour during hydration and dehydration due to partial pore blocking and thus the total energy density of the composite is decreased.

Table 1. Water release and uptake – mass and enthalpy (ACF and ENG showed no sorption properties)

Material	Water release		Water uptake	
	(g/g)	(J/g)	(g/g)	(J/g)
CaCl <sub>2</sub>	0.71	2203	0.62	1375
KCl	0.02	-*	0.01	-*
KCl + 2 CaCl <sub>2</sub>	0.69	1302	0.70	1260
KCl + CaCl <sub>2</sub>	0.45	1111	0.49	1572
2 KCl + CaCl <sub>2</sub>	0.42	838	0.52	969
Ca-ENGB-W	0.35	1038	0.50	1397
Ca-ACF-S	0.16	701	0.24	645
Ca-ENGB-S	0.29	910	0.44	1222
Ca-ENGB-S1	0.27	624	0.44	1160
Ca-ENGP-W	0.45	1268	0.50	613

The impregnation of calcium chloride in ACF or ENG improved the heat conductivity. Different impregnation ratios of calcium chloride and ENG or ACF were synthesized. Impregnated samples with higher amount of calcium chloride showed less heat conductivity as samples with less amount of calcium chloride (Table 2).

Table 2. Thermal conductivity measurements using DSC

Materials	Mass	Bulk	Specific	Thermal	Literature values of thermal conductivity
-----------	------	------	----------	---------	---

	(mg)	density (kg/m <sup>3</sup> )	energy (J/g)	conductivity (W/m·K)	(W/m·K)
ACF	53.7	537	3.8	0.55	0.15 – 0.5 [4]; 0.36 [6]
ENG	2.3	23	93.8	4.78	3 – 10 [5]
CaCl <sub>2</sub>	49.7	497	2.5	0.54	0.1 – 0.5 [3] [7]
ACF-CaCl <sub>2</sub> -V	64.9	649	2.7	1.03	n.a.
ENG-CaCl <sub>2</sub> -1:1	8.5	85	21.1	1.64	1.7 (d=550Kg/m <sup>3</sup> ); 1.66 (d=450Kg/m <sup>3</sup> ) [6]
ENG-CaCl <sub>2</sub> -1:2	4.6	46	35.7	0.74	1.51 (d=550Kg/m <sup>3</sup> ); 1.23 (d=450Kg/m <sup>3</sup> ) [6]

#### 4. Conclusion

We have showed new results of our experiments of mixing calcium chloride with potassium chloride and impregnation of calcium chloride in matrices as ACF or ENG. The synthesized composites showed improved dehydration and hydration behavior, and heat conductivity. We will use the modified salt mixture to impregnate porous materials to obtain a stable thermochemical storage material with high energy density. Further we will focus on the development of better mixing methods to create salt hydrate mixtures of other salt hydrates too.

#### Acknowledgements

We thank Dagmar Schuchardt, who have helped mixture preparation, and Melanie Böhme, who has assisted in evaluation of the data. Rammelberg, H. U. thanks the Friedrich-Ebert-Stiftung for financial support. We gratefully acknowledge the financial support of this project by the European Regional Development Fund (EFRE).

#### References

- [1] Rammelberg, H. U., Myrau, M., Schmidt, T. and Ruck, W., An optimization of salt hydrates for thermochemical heat storage, IMPRES 2013, Fukuoka, 04.-06. September 2013.
- [2] Shkatulov, A., Ryu, J., Kato, J. and Aristov, Y., Composite material "mg(oh)2-vermiculite": a promising new candidate for storage of middle temperature, Heat Powered Cycles 2012: Conference Proceedings, 09.09.-12.09.2012, Alkmaar, Netherlands, 2012.
- [3] Fopah Lele, A., Korhammer, K., Wegscheider, N., Rammelberg, H.U., Schmidt, T., Ruck, W.K.L., 2013. Thermal Conductivity of Salt Hydrates as Porous Material using Calorimetric (DSC) Method, in: 8th World Conference on Experimental Heat Transfer, Fluid Mechanics, and Thermodynamics, 2013. Lisbon, Portugal, ISBN 978-972-8620-23-3.
- [4] D. Meynard; X. Py; N. Mazet. Chem. Eng. Process. (46) 565-572. 2007.
- [5] M. Smale; G. Shives et al. ASME Interpack 05. 2005.
- [6] B. Tian; Z.Q. Jin; L.W. Wang; R. Z. Wang. Int. Journ. H. And M. Transfer. (55) 4453 – 4459. 2001.
- [7] K. Wang. J. Y. Wu. R. Z. Wang. L. W. Wang. Energy Conversion and Management. (47). 1902-1912. 2006.





## 5. Paper III

## ARTICLE IN PRESS

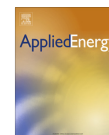
Applied Energy xxx (2015) xxx–xxx



ELSEVIER

Contents lists available at ScienceDirect

Applied Energy

journal homepage: [www.elsevier.com/locate/apenergy](http://www.elsevier.com/locate/apenergy)

## Sorption and thermal characterization of composite materials based on chlorides for thermal energy storage<sup>☆</sup>

Kathrin Korhammer<sup>\*</sup>, Mona-Maria Druske, Armand Fopah-Lele, Holger Urs Rammelberg, Nina Wegscheider, Oliver Opel, Thomas Osterland, Wolfgang Ruck

Innovation Incubator "Competence Tandem Thermal Battery", Leuphana University Lüneburg, Building 16 – Scharnhorststraße 1, 21335 Lüneburg, Germany

### HIGHLIGHTS

- Composite materials design based on CaCl<sub>2</sub> for thermochemical energy storage is presented.
- Thermal and sorption characterizations are performed.
- Hydration levels along with stoichiometry of composites are determined.
- Heat transfer and water sorption enhancement is highlighted.

### ARTICLE INFO

**Article history:**  
Received 13 November 2014  
Received in revised form 25 May 2015  
Accepted 16 August 2015  
Available online xxx

**Keywords:**  
Thermochemical heat storage  
Composites  
Mixtures  
Impregnation  
Sorption  
Thermal conductivity

### ABSTRACT

Thermochemical heat storage is a promising technology towards efficient use of renewable energy resources. Materials based on salts and their hydrates have a high potential for a good energy storage density and the benefit of long-term storage ability. However, the process has not yet been successfully implemented due to limitations in mass and heat transfer. This paper investigates how to improve the less desirable properties of CaCl<sub>2</sub> and its hydrates such as low melting points, agglomeration, low cycle stability and low sorption rates. The optimization of CaCl<sub>2</sub> properties was achieved by mixing with KCl and impregnation in carrier materials to obtain a composite material. The tests show at first that, with the admixtures of KCl, water uptake during hydration is 2 times higher than that of CaCl<sub>2</sub>. Water release during dehydration is 1.3 times higher than that of CaCl<sub>2</sub>. Secondly, the use of compacted expanded natural graphite (ENG) or activated carbon foam (ACF) increases the cycle stability, thermal conductivity and the water sorption performance. Due to their hydrophobic nature those matrices have no influence on the reaction scheme, thus the total amount of water molecules sorbed by the salt-in-matrix is close to the value of CaCl<sub>2</sub>. The degree of impregnation varies from 31 to 90 wt% depending on the host matrix and the impregnating medium used. The water vapour uptake is up to 0.61 g g<sup>-1</sup> and the water released ranges from 0.12 to 0.72 g g<sup>-1</sup>. The thermal conductivity of CaCl<sub>2</sub>-in-matrix is 3 times higher than that of sole CaCl<sub>2</sub>.

© 2015 Elsevier Ltd. All rights reserved.

### 1. Introduction

Thermal energy storage is one of the key technologies towards an efficient use of renewable energy resources. Storing thermal energy and then releasing it to higher extent helps solving

intermittent availability of energy and increases the energy efficiency. Although there are different ways to store thermal energy, the thermal performance of the system strongly depends on the thermodynamic properties of the used energetic media. Among other properties, high energy storage density and reversibility are required for the used materials to store and release thermal energy. Hereby thermochemical heat storage based on reversible chemical reactions, promises higher storage density than sensible or phase change heat storage for which researches and prototypes are well developed [1–3]. Based on reversible gas–solid reactions, long-term storage becomes possible. Many challenges are associated with potential thermochemical heat storage materials. Inorganic salts are used as the storage materials and generally water

<sup>☆</sup> This article is based on a short proceedings paper in Energy Procedia Volume 161 (2014). It has been substantially modified and extended, and has been subject to the normal peer review and revision process of the journal. This paper is included in the Special Issue of ICAE2014 edited by Prof. J Yan, Prof. DJ Lee, Prof. SK Chou, and Prof. U Desideri.

<sup>\*</sup> Corresponding author. Tel.: +49 4131 677 1768; fax: +49 4131 677 2822.  
E-mail address: [korhammer@leuphana.de](mailto:korhammer@leuphana.de) (K. Korhammer).

<http://dx.doi.org/10.1016/j.apenergy.2015.08.037>  
0306-2619/© 2015 Elsevier Ltd. All rights reserved.

Please cite this article in press as: Korhammer K et al. Sorption and thermal characterization of composite materials based on chlorides for thermal energy storage. Appl Energy (2015), <http://dx.doi.org/10.1016/j.apenergy.2015.08.037>



## ARTICLE IN PRESS

K. Korhammer et al. / Applied Energy xxx (2015) xxx–xxx

3

**Table 1**  
Thermo-physical properties of the matrices.

Matrix	ID	Shape	$d_{\text{pore}}$ (nm)	$V_{\text{pore}}$ (cm <sup>3</sup> g <sup>-1</sup> )	$\rho_b$ (kg m <sup>-3</sup> )	$S_{\text{BET}}$ (m <sup>2</sup> g <sup>-1</sup> )	$\rho_a$ (g m <sup>-2</sup> )	$\lambda$ (W m <sup>-1</sup> K <sup>-1</sup> )
Expanded natural graphite powder	ENGP	Powder	–	–	90–130	20	–	–
Expanded natural graphite compacted	ENG	Pellet	–	–	–	–	750	–
Activated carbon foam media	ACF	Foam	0.70–3.00	0.70–1.30	–	1432–1946	4600	0.25–0.30

**Table 2**  
List of synthesized composite materials based on impregnation.

Material	Matrix	Active substance	Synthesis method	Drying temperature
CaCl <sub>2</sub> -ACF-VI	ACF	CaCl <sub>2</sub>	Wet impregnation	200 °C
CaCl <sub>2</sub> -MSH-ACF-VI	ACF	Molten hydrated CaCl <sub>2</sub>	Wet impregnation	RT
CaCl <sub>2</sub> -ENG-VI	ENG	CaCl <sub>2</sub>	Wet impregnation	200 °C
CaCl <sub>2</sub> -MSH-ENG-VI	ENG	Molten hydrated CaCl <sub>2</sub>	Wet impregnation	RT
CaCl <sub>2</sub> -ENGP-S-4	ENGP	CaCl <sub>2</sub>	Soaking	200 °C
CaCl <sub>2</sub> -ENGP-S-2	ENGP	CaCl <sub>2</sub>	Soaking	200 °C
CaCl <sub>2</sub> -ENGP-S-1	ENGP	CaCl <sub>2</sub>	Soaking	200 °C

saturated aqueous salt solution of CaCl<sub>2</sub>, which volume exceeded the pore volume of the matrix, and molten salt hydrate (CaCl<sub>2</sub>-MSH) were used as impregnating media. Prior to impregnation the carriers (ACF and ENG) were dried in an oven at 200 °C and cooled down in a vacuum desiccator to remove any residual moisture. After drying they were immersed into the saturated aqueous solution or molten salt hydrate placed in a vacuum sealed vessel which was evacuated with a membrane vacuum pump to 10 mbar. The impregnation time was set to several minutes. The wet CaCl<sub>2</sub>-based composites were finally dried in an oven at 200 °C until the weight remained constant, whereas the composites made from CaCl<sub>2</sub>-MSH were dried over night at room temperature. All samples were stored in a sealed bottle in a dry area to protect them against moisture and exposure. In the latter method the ENGP was soaked in a saturated aqueous solution of CaCl<sub>2</sub> with a CaCl<sub>2</sub>:ENGP ratio of 4:1, 2:1 and 1:1 while stirring. The excess solvent was removed by evaporation and drying at 200 °C.

The mixed salts of CaCl<sub>2</sub> and KCl were crystallized from a solution of their basic salt components in pure water. The first step is to prepare an under-saturated aqueous solution of CaCl<sub>2</sub> and KCl. In the second step the two solutions were mixed together. The samples were either dried at 70–120 °C in the oven for quick use or stored in a desiccator for slow crystallization and to avoid melting and formation of amorphous phases in the mixture. The mixing ratios depend on the compound expected to form and were calculated by molecular weight of the involved salts.

The bulk density of the materials was calculated by dividing the mass of this latter with the total occupied volume by the material. The void fraction and density of the bed in Table 6, are respectively determined using the following equation:

$$\text{Void fraction (\%)} = \frac{V_s}{V_o} * 100\% = \frac{m_s}{d_c * V_o} * 100\% \quad (1)$$

$$\text{bed density } (\rho_b) = \frac{m_s}{V_o} \quad (2)$$

where  $V_s$  is the volume of the sample,  $V_o$  the volume occupied by the sample in the cylinder,  $m_s$  the sample weight (g),  $d_c$  the theoretical density of the sample and  $\rho_b$  the bulk density of the bed.

### 2.2. TGA/DSC: measurements of change in mass and enthalpy

Thermogravimetric analysis and heat flux measurements were carried out using a simultaneous TGA/DSC 1 device from Mettler Toledo®. This device determines simultaneously the change in sample mass (precision of mass determination is  $\pm 0.1 \mu\text{g}$ ) as a

function of time while the specimen is subjected to a temperature scanning programme in a controlled atmosphere and the heat flux (precision of heat power determination is  $\pm 1 \text{ mW}$ ) into the specimen compared to a reference. The experimental setup is shown in Fig. 1.

A gas box, providing two different mass flow controllers, connected to the TGA/DSC controlled the gas flow rate of the protective purge gas. We used silica gel-dried nitrogen as purge gas at a flow rate of 50 ml min<sup>-1</sup>. During hydration a reactive gas stream, which is humidified via a tempered gas bubbler, is used, in addition to the purge gas stream. By forcing this gas stream through a glass frit filled with glass wool, the containing water droplets are homogenized and the gas is adapted to the ambient temperature in the laboratory.

Samples of 10–20 mg were tested in crucibles made of alumina with a volume of 70  $\mu\text{L}$  under realistic conditions. All experiments were performed under realistic conditions of common closed-type sorption systems. The hydration measurements consisted of three consecutive steps varying in the operating pressure (10 mbar, 17 mbar and 20 mbar) in order to obtain equilibrium data on the pressure dependence of the water sorption behaviour of the samples. The hydration temperature was adjusted to 25 °C to avoid condensation. In dehydration-runs the salt mixtures and composite materials were gradually heated in two steps to 100 °C and 200 °C at a constant heating rate of 5 K min<sup>-1</sup>. A low temperature-ramp rate was chosen to avoid overlapping stages. Previous experiments showed that the salts used can completely be dehydrated below 200 °C. The water amount sorbed and the integration of the hydration heat fluxes over time were done manually with the Mettler Toledo STARE Software 11.00a.

### 2.3. TGA/DSC: measurements of thermal conductivity

The TGA/DSC 1 from Mettler Toledo was also used for the analysis of the heat fluxes and the temperature through a sample in order to evaluate the thermal resistance of the material (Fig. 2a and b). In the DSC cell, both temperature and heat flow are measured at the contact area between sample and sensor [24]. The temperature at the opposite side of the sample cannot be measured directly. By placing a pure metal with a known melting point on top of the sample, this temperature can be measured indirectly by observing its melting behaviour [25]. Thermal conductivity can be determined without modification of the DSC cell, using a method based on the assumption that the bottom side of the sample at the heat source follows an applied temperature modulation [26]. This implies that no thermal resistance between

Please cite this article in press as: Korhammer K et al. Sorption and thermal characterization of composite materials based on chlorides for thermal energy storage. Appl Energy (2015), <http://dx.doi.org/10.1016/j.apenergy.2015.08.037>

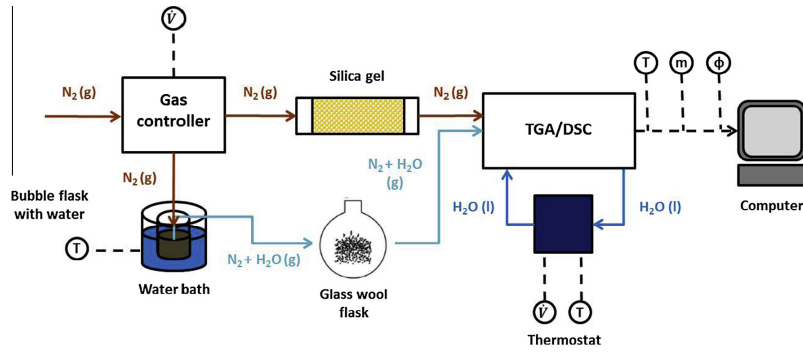


Fig. 1. Schematic illustration of the experimental setup.

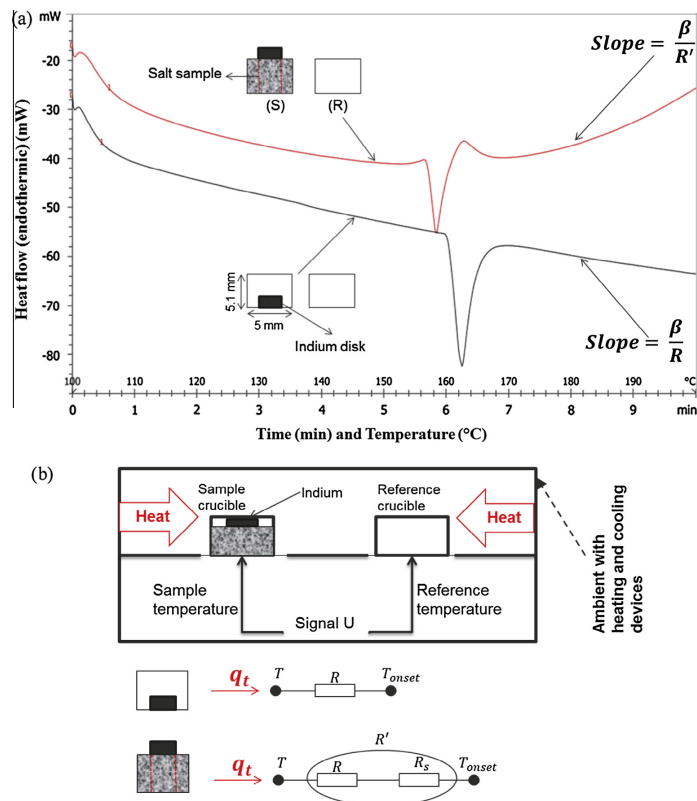


Fig. 2. (a) The schematic description of the measurement, showing aluminium pans, the reference (R) and the sample (S) with the corresponding melting curves, of indium on top of the sample and the indium alone. (b) The physical model of DSC measurements.

Please cite this article in press as: Korhammer K et al. Sorption and thermal characterization of composite materials based on chlorides for thermal energy storage. Appl Energy (2015), <http://dx.doi.org/10.1016/j.apenergy.2015.08.037>

## ARTICLE IN PRESS

K. Korhammer et al. / Applied Energy xxx (2015) xxx–xxx

5

the sample and the furnace exists [27] which has a significant effect on the sample heat capacity, hence on the thermal conductivity. The porous and host materials were measured at different heating rates with nitrogen flow rate of  $50 \text{ ml min}^{-1}$ . The amount of materials used is around  $0.1 \text{ g}$ . For the calibration, two sensor materials (gallium and indium) with known thermal conductivities, which give clear different melting peaks at  $29.7^\circ\text{C}$  and  $156.6^\circ\text{C}$  respectively, were used with a standard deviation of  $0.0006 \text{ W}$  for heat flow and of  $0.03^\circ\text{C}$  for temperature. However, thermal property measurements with high accuracy can be performed using DSC, if the calibration is carefully implemented [28]. In addition to the given resolution on DSC, the results can be meaningfully interpreted with up to four significant digits. For each sensor material, three calibration-measurements were done in order to find the accurate one to be used for the final measurements. Then the apparatus was adjusted to the calibration sample parameters, and finally a re-calibration was performed to validate the calibration process. As the first step of DSC measurements, sensor material pellets (diameter =  $1 \text{ mm}$ ) – prepared under atmospheric pressure – were placed in an aluminium pan with an inner diameter of  $5 \text{ mm}$  and specific height of  $5.1 \text{ mm}$  before the melting curves were determined (Fig. 2a). During the second step, the sensor material was placed on top of the non-compacted specimen in the aluminium pan and subsequently measurements were carried out until the sensor material melted. However, the sample height in the pan is about  $4.9 \text{ mm}$ . The surface area ( $A_s = 7.8 \cdot 10^{-7} \text{ m}^2$ ) of the indium corresponds to the exact surface area of the sample (delimited region on sample pan on Fig. 2a) where the thermal resistance is measured.

Using DSC measurement for thermal conductivity evaluation implies to find a good balance for the heating rate, in other terms, to choose the appropriate heating rate in the slope equation (Eq. (3)). Some hydrated salts may partially or completely melt within the actual temperature range, depending on the heating rate, since their melting points are typically lower than those of anhydrate phases. A slow heating rate allows for the crystal water to escape before the respective melting points of the hydrated salts are reached.

As in the previous configuration heat loss was observed, the satisfying results for thermal resistance may still be inaccurate. In his research, Hakvoort et al. [25] obtained best results when the sensor totally covers the sample, having the same cylindrical diameter as the sample height with a sample height not more than  $3 \text{ mm}$ . Due to technical limitations the measurements were performed with a sensor covering only a fourth of the total material diameter. The purpose of this measurement is to determine the thermal conductivity values from an adaptation to Camirand's method [29]. His method required only one sample and used a constraint equation determined by the slope of the increasing part of the heat flow curve. The method used here utilises the measurement of heat flow rate into a sensor material during its first order transition, obtaining the thermal resistance of a material placed between the sensor material and the heater in DSC. Starting at low temperature, when the indium is solid, sample and reference pans are heated with a constant heating rate ( $1, 5$  and  $10 \text{ K min}^{-1}$ ). Instead of using a fixed heating rate as Camirand, in this study the heating rate was selected individually for each specimen to avoid the melting of the respective sample. The sensor temperature and the DSC signal were recorded against time. During melting of the sensor (indium), the temperature of the sensor remains constant, so that the top of the sample remains at a constant temperature as well, while the temperature on the lower side of the sample continually increases at a constant rate. A scan is performed to measure the difference in heat flow during the melting of the sensor substance. The curve obtained tends to decrease linear before melting and decreases exponentially during melting (Fig. 2a).

The thermal resistance ( $R_{th}$ ) to heat flow ( $q_t$ ) through a sample under temperature difference between the heater and the melted sensor can be expressed as follows:

$$R_{th} = \frac{(T(t) - T_{onset})}{q_t} \quad (3)$$

Taking up the slopes of the DSC curves at melting the stage of the sensor material, the thermal resistance of the sample is determined by the difference between the measurement with the indium on top and without as follows:

$$R_s = R - R' \quad (4)$$

where  $R$  is the thermal resistance between calorimeter and sensor material,  $R'$  is the thermal resistance between calorimeter and sensor material on top of the sample (see Fig. 2b).

Measurement of the slope of the decreasing part of the curve allows determination of the thermal conductivity of the sample. Taking into account all the thermal resistances, the slope can be defined from the linear side of the melting peak [30]. The slope calculation is based on the principle of Fig. 3 with the aid of the STARe software 11.00a from Mettler Toledo. The first derivative of the heating curve (meaning the thermal power against the time) gives a specific slope which is further divided by the heating rate. Therefore we obtained the following expression:

$$\text{Slope} = \beta \cdot \frac{q_t(t) - q_{t,onset}}{T(t) - T_{onset}} = \frac{\beta}{R_{th}} \quad (5)$$

where  $q_{t,onset}$  and  $T_{onset}$  are the heat flow and melting temperature of salt at the onset of melting,  $q_t(t)$  is the thermal power at a given time,  $\beta$  the heating rate and  $R_{th}$  the thermal resistance (can be  $R$  or  $R'$  depending of what is measured). This correlation of temperature in the material to the thermal resistance is in principle similar to the resistance temperature detector (RTD) where only the thermal resistance is measured and correlated to the temperature.

It clearly shows the heating rate dependence. The obtained total (crucible, sample and sensor) thermal resistance in comparison with the thermal resistance of the sensor and the crucible yields directly to the bed sample thermal conductivity as follows:

$$\lambda_s = \frac{L_s}{A * R_s} = \frac{L_s}{A * (R - R')} \quad (6)$$

where  $L_s$  is the sample length,  $A$  is the contact area between sample and sensor material.

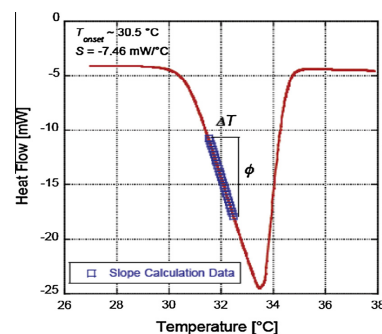


Fig. 3. Example of slope calculation on heat flow vs. temperature curve for salt sample [30].

Please cite this article in press as: Korhammer K et al. Sorption and thermal characterization of composite materials based on chlorides for thermal energy storage. Appl Energy (2015), <http://dx.doi.org/10.1016/j.apenergy.2015.08.037>

The used method requires an accurate measurement of the axial (middle central line of the crucible) temperature gradient to the sensor at the bottom. If not properly accounted for, some uncertainty may lead to inaccurate heat flow measurement. Some possible uncertainty source may come from thermal contact with the bottom of the pan, if it is not good enough. Samples are not thin enough and no lid is used to cover the sample in order to maintain the contact.

### 3. Results and discussion

#### 3.1. Measurements of water sorption and sorption enthalpy

##### 3.1.1. Composites based on mixture

The untreated calcium chloride showed higher release of water than uptake, caused by the mentioned deliquescence and agglomeration behaviour (Table 3). The mixing of calcium chloride and potassium chloride gave a more heterogeneous picture. The salt mixtures showed complete rehydration depending on the ratio of calcium chloride to potassium chloride.

As there is no literature about natural occurring KCl–CaCl<sub>2</sub> minerals, it is unknown whether the sample contains a mixture or a compound. However, even if no new compound of the two educts is formed, replacing up to two thirds of the CaCl<sub>2</sub> with KCl is supposed to increase cycle stability due to the KCl lacking deliquescence and therefore reducing agglomeration and thus improving the water transfer within the sample. Another potential effect is that with a significant higher KCl content the extreme low melting point of CaCl<sub>2</sub> · 6H<sub>2</sub>O ( $T_m = 30\text{ °C}$ ) can be raised (KCl:  $T_m = 770\text{ °C}$ ), especially in case of an eutectic mixture.

In Table 4, the water release and uptake at different temperature steps are calculated from weight loss/gain during the TGA-analysis.

$$N = \frac{n_{\text{H}_2\text{O}}}{n_x} = \frac{m_{\text{H}_2\text{O}}}{m_x} \cdot \frac{M_x}{M_{\text{H}_2\text{O}}} \quad (7)$$

The water sorption  $N$  is expressed as moles of water  $n_{\text{H}_2\text{O}}$  sorbed per mole anhydrous salt  $x$   $n_x$ , where  $x$  is either CaCl<sub>2</sub>, KCl + CaCl<sub>2</sub>, KCl + 2CaCl<sub>2</sub> or 2KCl + CaCl<sub>2</sub> and  $m_{\text{H}_2\text{O}}$  is the water loss,  $m_x$  the mass of the dehydrated salt and  $M_x$  the molar mass of the anhydrous salt. In case of the composites the latter was calculated from the difference of the residual sample mass detected in the TGA/DSC measurements and the mass of the host matrix.

In case of the slight weight increase of the KCl sample during the hydration step, water probably gathered only on the surface of the salt grains without undergoing chemical bonding with KCl. Temperature for the hydration was kept constant with only the influx of water vapour changing.

##### 3.1.2. Composites based on impregnation

The salt content is expressed as the percentage of salt based on the dry mass of the sample. It was calculated from the mass

difference obtained by weighing the support before and after impregnation as follows:

$$w = \frac{m_s}{m_c} \cdot 100 = \frac{m_c - m_M}{m_c} \cdot 100(\text{wt}\%) \quad (8)$$

where  $m_s$  (g) is the mass of the CaCl<sub>2</sub> or molten hydrated CaCl<sub>2</sub>,  $m_M$  (g) is the mass of the host matrix and  $m_c$  (g) is the mass of the dried composite material.

As shown in Table 6 the degree of impregnation varied from 31 to 90 wt% depending on the host matrix and the impregnating medium used. Samples with ENG contain about 87 wt% CaCl<sub>2</sub> and 90 wt% molten hydrated CaCl<sub>2</sub>, the ENG-based composite with molten salt hydrate has a slightly higher salt content than those impregnated with aqueous salt solutions. Composite materials with ACF and either CaCl<sub>2</sub> or molten hydrated CaCl<sub>2</sub> could only incorporate about 31 wt% and 58 wt% of salt. The compacted expanded natural graphite serves as a good carrier for the salt particles due to its honeycomb structure with stacks of parallel planes of carbon atoms between which the salt can be inserted. ACF has a well-defined foam and ordered microporous structure but due to voids in the framework between single ACF beads the salt can easily be washed out during impregnation, drying and in particular while reacting with water vapour. Moreover, the number of salt molecules that can access the micropores is limited. A homogenous and uniform distribution of the CaCl<sub>2</sub> particles inside the pores and internal surface could not be achieved as seen on microscopic images. Formation of salt clusters on the external surface could be observed, in particular in composites with ACF. The preparation method strongly influences the dispersion and fixation of the active substance within the supporting structure. Thus, the effect of varied synthesis parameters on the sorption characteristics of the composite sorbents will be investigated in detail in future studies.

The thermogram of the designed materials is shown in Fig. 4. The TGA curves were blank curve corrected in order to exclude buoyancy terms. The percentage of the mass loss is plotted versus the reaction time. Calcium chloride hydrate undergoes dehydration in three distinct stages. Major mass loss occurs below 100 °C. A similar multi-stage mass loss can be observed in composites containing ENG. The steep steps indicate a large mass loss rate. The curve of composites with ACF is more continuous in shape revealing that water is released more gradually. Desorption is completed slightly above 100 °C. The amount of water desorbed is small compared to the mass loss in the untreated salt and the composites with ENG as support. Samples based on ENG show good sorption behaviour. The addition of ENG, which possesses a high thermal conductivity, seems to enhance the heat transfer inside the sample so that the heat can be transported faster onto the internal surface. Moreover, the water vapour can easily be released through the diffusion channels of the host.

ACF is also a good heat transfer promoter but due to the lower CaCl<sub>2</sub> loading the rate of sorption is likely to be lower in

**Table 3**

Water release and uptake – mass and enthalpy (ACF and ENG showed no sorption properties). Material was first dehydrated at 100 °C and then at 200 °C, hydration enthalpies and weight loss were measured after both dehydrations. The water release and the enthalpy are calculated on the basis of the residual sample mass at the end of the 200 °C dehydration process.

Material	Water release (100 °C) (g g <sup>-1</sup> )	Enthalpy of hydration stage (100 °C) (J g <sup>-1</sup> )	Water release (200 °C) (g g <sup>-1</sup> )	Enthalpy of hydration stage (200 °C) (J g <sup>-1</sup> )
CaCl <sub>2</sub> · nH <sub>2</sub> O	0.96	1190	0.70	1369
CaCl <sub>2</sub> · 6H <sub>2</sub> O [31]	CaCl <sub>2</sub> · 6H <sub>2</sub> O → CaCl <sub>2</sub> · 2H <sub>2</sub> O + 4H <sub>2</sub> O	1295	CaCl <sub>2</sub> · 2H <sub>2</sub> O → CaCl <sub>2</sub> + 2H <sub>2</sub> O	1584
KCl · nH <sub>2</sub> O	0.00	<sup>a</sup>	0.02	<sup>a</sup>
(KCl + 2 CaCl <sub>2</sub> ) · nH <sub>2</sub> O	0.36	1092	0.58	1294
(KCl + CaCl <sub>2</sub> ) · nH <sub>2</sub> O	0.29	433	0.42	536
(2 KCl + CaCl <sub>2</sub> ) · nH <sub>2</sub> O	0.14	564	0.39	758

<sup>a</sup> The enthalpy could not be calculated as the detected DSC signals were too low.

Please cite this article in press as: Korhammer K et al. Sorption and thermal characterization of composite materials based on chlorides for thermal energy storage. Appl Energy (2015), <http://dx.doi.org/10.1016/j.apenergy.2015.08.037>



## ARTICLE IN PRESS

K. Korhammer et al. / Applied Energy xxx (2015) xxx–xxx

7

**Table 4**

Water release and uptake at different temperature steps. As the total water uptake depends on the number of cations in the mixture, a theoretical total is calculated for each compound from the measurements of the untreated salts. Each sample was tested in three dehydration cycles with two hydrations in between.

Material		Stage 1		Stage 2		Stage 3		Stage 4		$n_{H_2O}$ calc total	$n_{H_2O}$ total
		T (°C)	N	T (°C)	N	T (°C)	N	T (°C)	N		
CaCl <sub>2</sub>	Dehyd1	61.07	3.8	96.28	2.1	–	–	–	–	–	5.9
	Dehyd2	47.67	0.1	97.28	1.9	151.83	2.2	–	–	–	4.3
	Hyd1	–	0.2	–	2.2	–	1	–	–	–	3.3
	Hyd2	–	0.3	–	1.5	–	2	–	–	–	3.8
KCl	None										
	KCl + 2CaCl <sub>2</sub>									11.8	
KCl + 2CaCl <sub>2</sub>	Dehyd1	58.28	5.9	–	–	–	–	–	–	–	5.9
	Dehyd2	74.89	3.2	142.79	5	169.02	1.3	190.19	0.8	8.6	10.3
	Dehyd3	72.55	2.8	144.96	4	168.48	1.6	193.29	0.7	8.6	9.2
	Hyd1	–	1	–	4	–	3.9	–	–	6.6	8.9
KCl + CaCl <sub>2</sub>	Dehyd1	–	1.6	–	5	–	5.2	–	–	7.6	11.8
	Dehyd1	64.61	4.4	–	–	–	–	–	–	–	5.9
	Dehyd2	79.83	1.7	141.05	2.4	148.65	2.1	–	–	–	4.3
	Dehyd3	69.06	0.8	142.44	3.3	–	–	–	–	–	4.3
2KCl + CaCl <sub>2</sub>	Hyd1	–	0.2	–	1.4	–	1.5	–	–	–	3.3
	Hyd2	–	0.4	–	1.9	–	2.3	–	–	–	3.8
	Dehyd1	44.46	2	–	–	–	–	–	–	–	5.9
	Dehyd2	62.11	1.3	147.18	4.3	–	–	–	–	–	4.3
2KCl + CaCl <sub>2</sub>	Dehyd3	62	1.1	122.98	0.1	141.06	1.5	147.29	2.2	4.3	5
	Hyd1	–	0.6	–	2.5	–	2.2	–	–	–	3.3
	Hyd2	–	0.7	–	3.3	–	3.4	–	–	–	3.8
	Hyd2	–	0.7	–	3.3	–	3.4	–	–	–	7.4

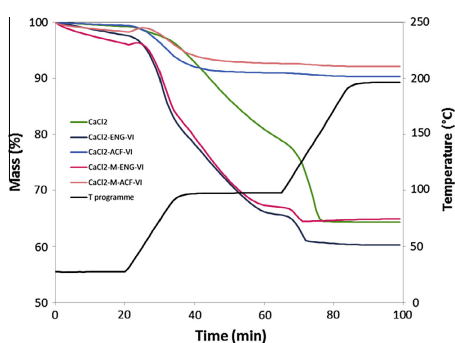


**Fig. 4.** Mass loss in untreated CaCl<sub>2</sub> and CaCl<sub>2</sub>-ENG/ACF-composites as a function of time.

comparison to ENG-based sorbents. According to Fujioka et al. [32] the average sorption rate in composites made from expanded graphite could indeed be increased with increased effective thermal conductivity.

Therefore, the effect of ENG and ACF as heat and mass transfer enhancers on the water sorption has been investigated. According to Zhu et al. [33] the absolute sorption rate  $k$  can be obtained from the differential of the sorption amount ( $dm$ ) to time ( $dt$ ).

$$k = \frac{dm}{dt} \left( \frac{\text{mg}}{\text{min}} \right) \quad (9)$$

The sorption amount  $\Delta m$  is defined as the amount of water in gram sorbed per gram dry composite for the composite materials and per gram anhydrous CaCl<sub>2</sub> for the untreated CaCl<sub>2</sub>, respectively. In order to compare the dehydration behaviour of the different materials, the overall degree of conversion has been normalized and is presented in Fig. 5. The reaction time required for desorbing 50% ( $t_{50}$ ) and 90% ( $t_{90}$ ) of the maximum water

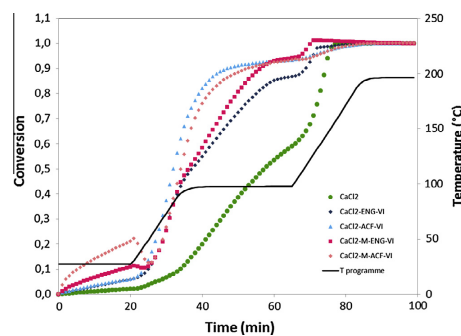


**Fig. 5.** Conversion in untreated CaCl<sub>2</sub> and CaCl<sub>2</sub>-ENG/ACF-composites as a function of time.

**Table 5**

Comparison of the mass loss rates  $k_{50}$  and  $k_{90}$  of untreated and composite sorbents.

Material	$\Delta m$ (g g <sup>-1</sup> )	$t_{50}$ (min)	$k_{50}$ (mg min <sup>-1</sup> )	$t_{90}$ (min)	$k_{90}$ (mg min <sup>-1</sup> )
CaCl <sub>2</sub> hydrate	0.54	57	0.05	74	0.25
CaCl <sub>2</sub> -ACF-VI	0.10	32	0.07	47	0.005
CaCl <sub>2</sub> -MSH-ACF-VI	0.08	34	0.05	53	0.003
CaCl <sub>2</sub> -ENG-VI	0.61	37	0.08	69	0.10
CaCl <sub>2</sub> -MSH-ENG-VI	0.52	36	0.07	56	0.04

content of the initial sample and the obtained sorption rates have been compared in Fig. 6. The results summarized in Table 5 confirm the assumption that among the used supports, ENG has a sorption promoting effect.

By using ENG impregnated with CaCl<sub>2</sub> the water desorption can be accelerated over the whole temperature range on account of the increased sorption rate, particularly at lower temperatures (Fig. 6).

Please cite this article in press as: Korhammer K et al. Sorption and thermal characterization of composite materials based on chlorides for thermal energy storage. Appl Energy (2015), <http://dx.doi.org/10.1016/j.apenergy.2015.08.037>

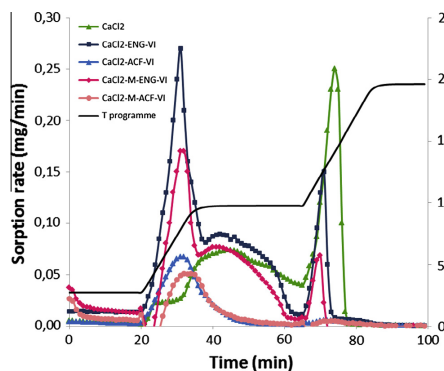


Fig. 6. Sorption rate in untreated  $\text{CaCl}_2$  and  $\text{CaCl}_2$ -ENG/ACF-composite as a function of time.

Towards the end of the dehydration phase, when more than 90% of the water is desorbed, the water sorption is slowed down. Composites with a higher degree of  $\text{CaCl}_2$  impregnation have a higher total mass loss rate compared to the other samples. The water sorption in the ACF-supported  $\text{CaCl}_2$  and molten hydrated  $\text{CaCl}_2$  samples are lower than  $0.2 \text{ mg min}^{-1}$  according to the mass loss rate values.

Table 6 presents the total water uptake  $\Delta m_{\text{sorp}}$  and water release  $\Delta m_{\text{des}}$  of the samples tested over a temperature range of 25–200 °C. The results are related to the dry mass of the material. Samples with ENG as host matrix with high salt content demonstrate the highest water sorption ability comparable to untreated  $\text{CaCl}_2$ . More than 70% of the water sorbed can be released during the dehydration process. The composite with ENG and molten salt hydrate ( $\text{CaCl}_2$ -MSH-ENG-VI) appears to have a higher water uptake than the  $\text{CaCl}_2$ -ENG-VI composite, but less of the water sorbed can be desorbed. The shape of the TGA curves is similar, except in the last part in which a higher mass loss is detected for  $\text{CaCl}_2$ -ENG-VI. The more salt is confined to the matrix surface and into the matrix pores the lower the diffusivity of the water vapour during hydration and dehydration due to partial pore blocking and thus the maximum water amount sorbed is decreased. In addition to the pore blocking effect, the formation of a dry layer on the surface is also considered to lead to a diffusion barrier for the water vapour from inside the material. The water sorption capacity of ACF-supported composites is less than  $0.20 \text{ g g}^{-1}$ . This finding indicates that the sorption behaviour is not only affected by the amount of salt dispersed within the ACF but also its morphology. The steric hindrance of the nonpolar functional groups in the ACF is likely to limit the effective water uptake.

Table 6  
Sorption properties of the synthesized composite materials.

Material	w (wt%)	Dehydration		Hydration	
		$\Delta m_{\text{des}}$ ( $\text{g g}^{-1}$ )	$\Delta H_{\text{des}}$ ( $\text{J g}^{-1}$ )	$\Delta m_{\text{sorp}}$ ( $\text{g g}^{-1}$ )	$\Delta H_{\text{sorp}}$ ( $\text{J g}^{-1}$ )
$\text{CaCl}_2$ -ACF-VI	31	0.10	235	0.12	198
$\text{CaCl}_2$ -MSH-ACF-VI	58	0.08	298	0.20	471
$\text{CaCl}_2$ -ENG-VI	87	0.61	1642	0.67	1451
$\text{CaCl}_2$ -MSH-ENG-VI	90	0.52	1905	0.72	1310
$\text{CaCl}_2$ -ENGP-S-4	87	– <sup>a</sup>	– <sup>a</sup>	– <sup>a</sup>	– <sup>a</sup>
$\text{CaCl}_2$ -ENGP-S-2	66	– <sup>a</sup>	– <sup>a</sup>	– <sup>a</sup>	– <sup>a</sup>
$\text{CaCl}_2$ -ENGP-S-1	51	– <sup>a</sup>	– <sup>a</sup>	– <sup>a</sup>	– <sup>a</sup>

<sup>a</sup> Not analysed via TGA/DSC.

The hydrophobicity of the untreated carbonaceous supports could be confirmed by TGA/DSC measurements. Hence, the contribution of those materials to the sorption is negligible. In addition to possessing a high thermal conductivity, carbonaceous supports do not tend to uncontrolled swelling or variation in volume making them advantageous over other common supporting materials. The beneficial effect of expanded graphite addition has also been reported in other studies. Okada et al. [34] used the dry impregnation technique to prepare  $\text{CaCl}_2$ -impregnated activated carbon composites from solutions with different  $\text{CaCl}_2$  concentrations. The variation in the solution salt concentration resulted in different salt contents (0, 30, 40, 50 and 70 wt%) and water vapour uptake performances ranging from  $0.04$  to  $0.52 \text{ g g}^{-1}$ , respectively. The higher the salt content of the composite the higher the water amount sorbed. Only composite sorbents with active supports such as zeolite or silica gel proved to have higher water sorption capacities as given in Refs. [33,35,36], for instance, combined a microporous zeolite and mesoporous silica gel with  $\text{CaCl}_2$  and obtained superior results in terms of the latter. The impregnated silica gel containing 33 wt% of  $\text{CaCl}_2$  adsorbed around  $0.85 \text{ g g}^{-1}$  at 27 °C at 33.3 bar water vapour pressure. Tokarev et al. [35] presented a novel  $\text{CaCl}_2$ -confined to MCM-41 material that demonstrates a sorption capacity of  $0.75 \text{ g g}^{-1}$ . When comparing those values the different testing conditions must be considered. Zhu et al. [33] obtained similar values ( $0.73 \text{ g g}^{-1}$  at 30 °C and  $p/p_0 = 0.8$ ) in their experimental study on composite silica gel supported  $\text{CaCl}_2$  sorbent. Silica gel and zeolite possess a very high hydrophilic surface and can therefore contribute to the overall water absorptivity.

The associated sorption and desorption enthalpies are also displayed in Table 6. In general, the higher the water sorption capacity of the materials, the higher are both dehydration  $\Delta H_{\text{des}}$  and hydration enthalpy  $\Delta H_{\text{sorp}}$  and the higher the total energy storage density. Two melting events occurred in the DSC diagram which contribute to the high desorption enthalpy of the materials.

The satisfying dehydration achieved below 100 °C and the very high water uptake and energy storage density make composites consisting of ENG and either  $\text{CaCl}_2$  or molten hydrated  $\text{CaCl}_2$  attractive for thermal energy storage in applications that use low-grade heat sources.

Examples of water sorption/desorption cycles are illustrated in Fig. 7 for untreated  $\text{CaCl}_2$ ,  $\text{CaCl}_2$ -MSH-ENG-VI and  $\text{CaCl}_2$ -ENG-VI composite. A hysteresis loop common for gas–solid reactions is observed. The confinement of  $\text{CaCl}_2$  to the compacted expanded graphite leads to a widening of the loop due to larger sorption

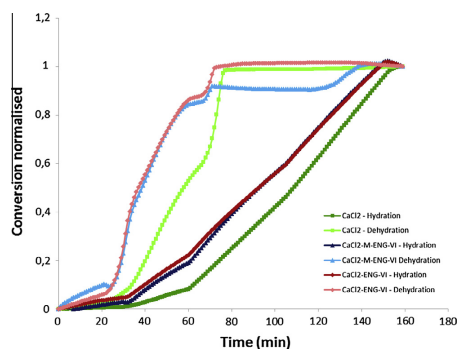


Fig. 7. Water sorption/desorption cycle of  $\text{CaCl}_2$ -MSH-ENG-VI,  $\text{CaCl}_2$ -ENG-VI and untreated  $\text{CaCl}_2$ .

Please cite this article in press as: Korhammer K et al. Sorption and thermal characterization of composite materials based on chlorides for thermal energy storage. Appl Energy (2015), <http://dx.doi.org/10.1016/j.apenergy.2015.08.037>

## ARTICLE IN PRESS

K. Korhammer et al./Applied Energy xxx (2015) xxx–xxx

9

and desorption rates. During hydration water is not only chemically attached but also physisorbed due to over-hydration (overstoichiometric uptake of water molecules) resulting in a moisture loss after the run was finished. The slight gain in mass before the dehydration measurement shows that despite impregnation of the salt into a matrix, its deliquescent behaviour cannot fully be prevented.

The influence of the host matrices on the dehydration process and reaction temperature has been evaluated by calculating the degree of hydration in each dehydration step. The water sorption  $N$  is defined in Eq. (7).

The results are listed in Table 7. As the salt content of the composite sorbents analysed via TGA/DSC differs from the total salt content determined by weighing due to inhomogeneous dispersion of the salt within the porous structure, the accuracy of the given values are affected with considerable uncertainties.

As shown in Table 7 the use of heat promoting additives results in a shift in the reaction temperature to lower temperatures of up to 18 °C in the first reaction stage and up to 52 °C in the second reaction stage, respectively. The composites based on ENG showed a sorption behaviour similar to untreated  $\text{CaCl}_2$ , as a result the total amount of moles sorbed per mole on  $\text{CaCl}_2$ -ENG-VI and  $\text{CaCl}_2$ -MSH-ENG-VI is with 4.4 and 3.6 close to the value for untreated  $\text{CaCl}_2$ . In the first stage around 2 moles of water are released, except for  $\text{CaCl}_2$ -MSH-ACF-VI and  $\text{CaCl}_2$ -MSH-ENG-VI which desorb only 1 mol of water. ACF-based composites could only hold 2 moles of water maximum.

It is well-known that the morphology and the distribution of salt within the sample exert a strong influence on the position of the peak temperature in the DSC signal. The findings are in accordance with the results for the different water sorption rates mentioned above (see Figs. 4 and 6). It was observed that samples with  $N \geq 4$  undergo melting between 40 and 48 °C. This temperature corresponds to the melting point of the  $\text{CaCl}_2$  tetrahydrate

[8]. As a consequence the crystal structure might be changed. A small melting peak could also be seen in the DSC of the  $\text{CaCl}_2$ -MSH-ENG-VI sample. According to the calculations in Table 7 this sample took up only 3.6 moles of water which is lower than  $N = 4$ . It is assumed that the composites comprise of a mixture of salt hydrates of different hydration states.

In case of samples of salt hydrates with a number of water molecules equal or higher than four moles per mole of salt anhydrate, melting occurred but did apparently not affect the reaction reversibility of the material. Long-term thermal stability is an important factor in heat storage applications: fast degradation of the salt limits the operating period of the storage unit. In order to reliably assess the overall lifetime of such a system a cycle stability test consisting of more than twenty cycles is recommended and will be performed in future experiments.

### 3.2. Measurements of thermal conductivity

In order to validate the experimental and developed methods, the thermal conductivity of anhydrous glass is determined and compared with the literature and supplier data. The glass studied here is commercially known as "glass beads – GP", produced by Kuhmichel®. The chosen glass presented as spheroidal beads is in a homogeneous spherical form with the following properties in Table 8.

The thermal conductivity of the glass beads measured under transient heat flow is calculated by using Eq. (6). The results are shown in Table 9. The bulk (effective) thermal conductivity of the bed, as a function of parameters such as the thermal conductivity of the beads, the bed porosity and the dimension of the grains, is not determined here, since it requires some model to be designed or adapted. The average thermal conductivity of glass beads under dry air at 100 kPa is  $\lambda_s = 1.16 \pm 0.02 \text{ W m}^{-1} \text{ K}^{-1}$  ( $m_{\text{glass}} \sim 139 \text{ mg}$ ). The evaluated errors and uncertainties in this

**Table 7**  
Calculation of the hydration level of the composite materials based on impregnation.

Material	Stage 1			Stage 2			Stage 3			Total $N_{\text{total}}$
	$n_{\text{H}_2\text{O}}$ (mmol)	$N_1$	$T$ (°C)	$n_{\text{H}_2\text{O}}$ (mmol)	$N_2$	$T$ (°C)	$n_{\text{H}_2\text{O}}$ (mmol)	$N_3$	$T$ (°C)	
$\text{CaCl}_2$	0.12	2.0	98	0.09	1.4	145				3.4
$\text{CaCl}_2$ -ACF-VI	0.05	1.8	76	<0.00	0.2	111	–	–	–	2.0
$\text{CaCl}_2$ -MSH-ACF-VI	0.04	0.8	93	<0.00	0.1	–	–	–	–	0.9
$\text{CaCl}_2$ -ENG-VI	0.12	2.0	80	0.10	1.8	98	0.03	0.6	128	4.4
$\text{CaCl}_2$ -MSH-ENG-VI	0.06	1.3	88	0.09	2.0	93	0.01	0.3	125	3.6

**Table 8**  
Glass beads physico-chemical properties [37]. The data on thermal conductivity is taken from [38].

Grain shape	Spherical
Melting point	Approx. 730 °C
Bulk density (depending on granular size)	Approx. 1.5–1.6 g cm <sup>3</sup>
Average grain size	200–300 μm
Thermal conductivity according to the chemical analysis and temperature range	0.8–1.2 W m <sup>-1</sup> K <sup>-1</sup> for % SiO <sub>2</sub> < 96 and % Fe <sub>2</sub> O <sub>3</sub> < 1 at $T > 20$ °C
Chemical analysis of the used glass beads	SiO <sub>2</sub> (70–75%) MgO (max. 5%) Na <sub>2</sub> O (12–15%) Al <sub>2</sub> O <sub>3</sub> (max. 2.5%) CaO (7–12%) K <sub>2</sub> O (max. 1.5%) Fe <sub>2</sub> O <sub>3</sub> (max. 0.5%) Others (max. 2%)

**Table 9**  
Experimental results for effective thermal conductivity of anhydrous glass beads using DSC.

Material	Specific energy (J g <sup>-1</sup> )	Bed length (m)	Void fraction (%)	Temperature range (°C)	Thermal resistance (°C W <sup>-1</sup> )	Effective thermal conductivity (W m <sup>-1</sup> K <sup>-1</sup> )	Uncertainty of effective thermal conductivity (W m <sup>-1</sup> K <sup>-1</sup> )
Glass beads	2.21	0.0051	89	100–200	5586	1.29	0.019
	2.62	0.0051	89	100–200	5154	1.12	0.020
	2.9	0.0051	89	100–200	5968	1.07	0.016

Please cite this article in press as: Korhammer K et al. Sorption and thermal characterization of composite materials based on chlorides for thermal energy storage. Appl Energy (2015), <http://dx.doi.org/10.1016/j.apenergy.2015.08.037>

**Table 10**  
Effective thermal conductivity measurement results.

Material	Mass (mg)	Bulk density (kg m <sup>-3</sup> )	Specific energy (J g <sup>-1</sup> )	Effective thermal conductivity (W m <sup>-1</sup> K <sup>-1</sup> )	Uncertainty on effective thermal conductivity (W m <sup>-1</sup> K <sup>-1</sup> )	Literature values of thermal conductivity (W m <sup>-1</sup> K <sup>-1</sup> )
ACF	53.7	537	3.8	0.52	0.17	0.15–0.5 [40]; 0.36 [41]
ENG	2.3	23	93.8	4.78	1.30	3–10 [42]
CaCl <sub>2</sub>	49.7	497	2.5	0.54	0.15	0.1–0.5 [24,43,44]
CaCl <sub>2</sub> -ACF-VI	64.9	649	2.7	1.03	0.30	n.a.
CaCl <sub>2</sub> -ENGP-S-1	8.5	85	21.1	1.64	0.47	1.7 ( <i>d</i> = 550 kg m <sup>-3</sup> ); 1.66 ( <i>d</i> = 450 kg m <sup>-3</sup> ) [41]
CaCl <sub>2</sub> -ENGP-S-2	4.6	46	35.7	0.74	0.20	1.51 ( <i>d</i> = 550 kg m <sup>-3</sup> ); 1.23 ( <i>d</i> = 450 kg m <sup>-3</sup> ) [41]

work are purely systematics and based on the guide to the expression of uncertainty in measurement (GUM) [39] (Appendix A). For DSC measurements, it is calculated from the standard deviation on heat flow and temperature, mentioned in GUM (Section 2.3). However, Gomez et al. [28] affirmed that a DSC can perform thermal property measurements with low uncertainty, if the calibration is carefully performed. In addition to the given resolution of the DSC, the results can be interpreted with up to four significant digits.

The salt inside the composites will partially or completely melt in the applied temperature range, depending on the heating rate. After calibration experiments were completed and validated with glass beads, the calculations showed consistent results for a heating rate of 10 K min<sup>-1</sup>, so it has been adopted for the following measurements. Additionally a blank was included in the method developed for DSC measurements, in order to correct systematic errors from external influences on the possible dehydration or hydration reactions. The results obtained by the DSC are within the range of literature values (Table 8) with a relative uncertainty of less than 10%, as shown in Table 9, which ensures the validation of our measurement procedure.

As a measurement procedure, each sample is run three times under the same conditions and the mean values of the results are used. Table 10 shows the thermal conductivity of matrices and composites based on chlorides with different proportions when the temperature ranges from 100 to 200 °C. Results show that the measurements are in good agreement with the data from literature. It indicates that thermal conductivity increases when the mass ratio of the salt decreases. However, accuracy of obtaining this thermophysical property is around 29% according to the uncertainties in Table 10. The thermal conductivity of composites made of CaCl<sub>2</sub> and ENG at an equal mass ratio is 3 times higher than that of CaCl<sub>2</sub>, highlighting the heat transfer enhancement of the untreated salt.

#### 4. Conclusion

To overcome the disadvantages of sole calcium chloride in thermal energy storage, the material has been mixed with potassium chloride and impregnated into matrices such as ACF or ENG. The synthesized salt mixtures and ENG-supported CaCl<sub>2</sub> and molten hydrated CaCl<sub>2</sub> composites showed remarkable dehydration and hydration behaviour in microscale sorption experiments and enhanced thermal conductivity in comparison to untreated CaCl<sub>2</sub>. Of the KCl–CaCl<sub>2</sub> mixtures the ratio of 2 KCl to 1 CaCl<sub>2</sub> yielded the best results concerning water uptake, with an increase to 5.3 H<sub>2</sub>O molecules into the salt structure after a dehydration at *T* = 100 °C and to 7.4 H<sub>2</sub>O molecules after a dehydration at *T* = 200 °C. Compared to the expected amounts, calculated from the measurements of untreated CaCl<sub>2</sub> and KCl this is an improvement to 160% (100 °C) and 195% (200 °C) efficiency. Due to the higher water uptake, the salt releases an increased amount of water during the next dehydration cycles as well, which

keeps the energy storage density at a stable level. However, concerning the energy storage density, the mixture with the ratio of 1 KCl to 2 CaCl<sub>2</sub> is more effective as the loss of released energy compared to untreated CaCl<sub>2</sub> after dehydration at *T* = 100 °C is only 8.2% and after dehydration at *T* = 200 °C is only 5.5%, while the energy release of the mixture with the 2 KCl to 1 CaCl<sub>2</sub> ratio decreases by 52.6% (*T* = 100 °C) and respectively 44.6% (*T* = 200 °C). Composites consisting of ENG and either CaCl<sub>2</sub> or molten hydrated CaCl<sub>2</sub> possess good water sorption properties below 100 °C. With a water uptake of 0.67 g g<sup>-1</sup> and 0.72 g g<sup>-1</sup>, respectively, and an energy storage density of 1451 J g<sup>-1</sup> and 1310 J g<sup>-1</sup> these materials are very attractive for thermal energy storage applications driven by low-grade heat sources. The high thermal conductivity of the host ENG improves the heat transfer in the composite materials based on CaCl<sub>2</sub>. The overall thermal conductivity was tripled compared to untreated CaCl<sub>2</sub> samples. In future studies, we will use the modified salt mixtures to impregnate porous materials such as ENG, silica gels and zeolites to obtain a stable thermochemical storage material with high energy storage density and improved mass and heat transfer performance. Moreover, we will focus on the development of better mixing methods and impregnation techniques to create composite sorbents comprising of other salt hydrates.

#### Acknowledgements

We thank Dagmar Schuchardt, who has helped us with mixture preparation, and Melanie Böhme, who has assisted in the data evaluation. Rammelberg, H.U. thanks the Friedrich-Ebert-Stiftung for financial support. We gratefully acknowledge the financial support of this project by the European Regional Development Fund (ERDF) in the framework “Thermische Batterie – Project” (application number: CCI N° 2007DE161PR001) of the Innovation Incubator Lüneburg.

#### Appendix A. Uncertainty calculation for the DSC

The determination of the thermal conductivity is based on the measurement of the heat flux through the sample and the corresponding temperature difference with the reference pan. That heat flux or thermal power has a standard deviation or systematic uncertainty of 0.0006 W. The temperature measurement has a standard deviation of 0.03 °C. The height and diameter of the sample is measured using a digital calliper (Powerfix) with the uncertainty of ±0.02 mm.

The error calculation of thermal conductivity under transient state measurement is obtained via Eqs. (5) and (6):

$$\left| \frac{d\text{slope}}{\text{slope}} \right| = \left| \frac{dq_t}{q_t} - \frac{dT}{T} \right| = \left| \frac{dR_s}{R_s} \right| \leq \left| \frac{dq_t}{q_t} \right| + \left| \frac{dT}{T} \right| \quad (\text{A-1})$$

$$\left| \frac{dz}{z} \right| = \left| \frac{dL_s}{L_s} - \frac{dA}{A} - \frac{dR_s}{R_s} \right| \leq \left| \frac{dL_s}{L_s} \right| + \left| \frac{dA}{A} \right| + \left| \frac{dR_s}{R_s} \right| \quad (\text{A-2})$$

Please cite this article in press as: Korhammer K et al. Sorption and thermal characterization of composite materials based on chlorides for thermal energy storage. Appl Energy (2015), <http://dx.doi.org/10.1016/j.apenergy.2015.08.037>

## ARTICLE IN PRESS

K. Korhammer et al./Applied Energy xxx (2015) xxx–xxx

11

## References

- [1] Garg HP, Mullick SC, Bhargava AK. Solar thermal energy storage. In: Sold and distributed in the U.S.A. and Canada by Kluwer Academic Publishers. Dordrecht; Boston; Hingham, MA; D. Reidel; 1985. p. 292.
- [2] Kilius B, Kakac S. *Energy storage systems*. vol. 167. Springer; 1989.
- [3] Kousskou T, Bruel P, Jamil A, El Rhaifki T, Zeraoui Y. Energy storage: applications and challenges. *Sol Energy Mater Sol Cells* 2014;120(Part A):59–80. <http://dx.doi.org/10.1016/j.solmat.2013.08.01>
- [4] Critoph RE, Zhong Y. Review of trends in solid sorption refrigeration and heat pumping technology. *Proc Inst Mech Eng, Part E: J Process Mech Eng* 2005;219:285–300. <http://dx.doi.org/10.1243/095440805X6982>
- [5] Boer R de, Haije WG, Veldhuis JBJ, Smeding SF. Solid-sorption cooling with integrated thermal storage: the SWEAT prototype. In: Third international heat powered cycles conference – HPC 2004, Larnaca, Cyprus, 11–13 oktober 2004, vol. 1, Larnaca, Cyprus: ECN Energy Efficiency in Industry; 2004. p. 10.
- [6] De Boer R, Haije WG, Veldhuis JBJ. Determination of structural, thermodynamic and phase properties in the Na<sub>2</sub>S–H<sub>2</sub>O system for application in a chemical heat pump. *Thermochim Acta* 2002;395:3–19.
- [7] Ferchaud C, Zondag H, De Boer R, Rindt CCM. Characterization of the sorption process in thermochemical materials for seasonal solar heat storage application. In: The 12th international conference on energy storage, Lleida, Spain; 2012. p. 4.
- [8] N'Tsoukpoe KE, Schmidt T, Rammelberg HU, Watts BA, Ruck WKL. A systematic multi-step screening of numerous salt hydrates for low temperature thermochemical energy storage. *Appl Energy* 2014;124:1–16. <http://dx.doi.org/10.1016/j.apenergy.2014.02.053>
- [9] Van Essen VM, Cor Gores J, Bleijendaal LPJ, Zondag HA, Schuitema R, Bakker M, et al. Characterization of salt hydrates for compact seasonal thermochemical storage. In: ASME 2009 third international conference on energy sustainability, vol. 2, San Francisco, California, USA: ASME; 2009. p. 825–30. doi: 10.1115/ES2009-90289.
- [10] Aydin D, Casey SP, Riffat S. The latest advancements on thermochemical heat storage systems. *Renew Sustain Energy Rev* 2015;41:356–67. <http://dx.doi.org/10.1016/j.rser.2014.08.024>
- [11] Tatsidjodjone P, Le Pierres N, Luo L. A review of potential materials for thermal energy storage in building applications. *Renew Sustain Energy Rev* 2013;18:327–49. <http://dx.doi.org/10.1016/j.rser.2012.10.025>
- [12] N'Tsoukpoe KE, Rammelberg HU, Fopah Lele A, Korhammer K, Watts BA, Schmidt T, et al. A review on the use of calcium chloride in applied thermal engineering. *Appl Therm Eng* 2015;75:513–31. <http://dx.doi.org/10.1016/j.applthermaleng.2014.09.047>
- [13] Aristov Y, Restuccia G, Tokarev MM, Cacciola G. Selective water sorbents for multiple applications, 10. Energy storage ability. *React Kinet Catal Lett* 2000;69:345–53. <http://dx.doi.org/10.1023/A:1005616420331>
- [14] Fukai J, Kanou M, Kodama Y, Miyatake O. Thermal conductivity enhancement of energy storage media using carbon fibers. *Energy Convers Manage* 2000;41:1543–56. [http://dx.doi.org/10.1016/S0196-8904\(99\)00166-1](http://dx.doi.org/10.1016/S0196-8904(99)00166-1)
- [15] Guilleminot JJ, Choisier A, Chalferin JB, Nicolas S, Reymoney JL. Heat transfer intensification in fixed bed adsorbers. *Heat Recov Syst CHP* 1993;13:297–300. [http://dx.doi.org/10.1016/0890-4332\(93\)90052-W](http://dx.doi.org/10.1016/0890-4332(93)90052-W)
- [16] Jiang L, Wang LW, Wang RZ. Investigation on thermal conductive consolidated composite CaCl<sub>2</sub> for adsorption refrigeration. *Int J Therm Sci* 2014;81:68–75. <http://dx.doi.org/10.1016/j.ijthermalsci.2014.03.003>
- [17] Tamainot-Telto Z, Critoph RE. Monolithic carbon for sorption refrigeration and heat pump applications. *Appl Therm Eng* 2001;21:37–52. [http://dx.doi.org/10.1016/S1359-4311\(00\)00030-2](http://dx.doi.org/10.1016/S1359-4311(00)00030-2)
- [18] Druske M-M, N'Tsoukpoe KE, Wickenheisser M, Rammelberg HU, Schmidt T, Ruck W. Mineralogical approach on the selection of candidates for thermochemical heat storage. In: Eighth international renewable energy storage conference and exhibition, Berlin, Germany: Eurosolar; 2013. p. 1.
- [19] Rammelberg HU, Myrau M, Schmidt T, Ruck WKL. An optimization of salt hydrates for thermochemical heat storage. IMPRES-2013, vol. 1, Fukuoka, Japan: Chemical Science & Engineering Series: Innovative Materials for Processes in Energy Systems; 2013. p. 6.
- [20] Shkatulov A, Ryu J, Kato Y, Aristov Y. New composite “MG(OH)2-Vermiculite”; as promising candidate for storage of middle temperature heat. heat powered cycles conference, vol. paper N° fhpc380, Alkmaar, The Netherlands: ECN-HPC; 2012. p. 6.
- [21] Kiplagat JK, Wang RZ, Li TX, Oliveira RG. Enhancement of heat and mass transfer in solid–gas sorption systems. *Int J Air-Condition Refrig* 2012;20. <http://dx.doi.org/10.1142/S201013251130001>. 1130001 (1–16).
- [22] Van Essen VM, He Z, Rindt CCM, Zondag HA, Gores JC, Bleijendaal LPJ, et al. Characterization of MgSO<sub>4</sub> hydrate for thermochemical seasonal heat storage. *J Sol Energy Eng* 2009;131:041014-1–7. <http://dx.doi.org/10.1115/1.4009275>
- [23] Mauran S, Prades P, L'Haridon F. Heat and mass transfer in consolidated reacting beds for thermochemical systems. *Heat Recov Syst CHP* 1993;13: 315–9. [http://dx.doi.org/10.1016/0890-4332\(93\)90055-Z](http://dx.doi.org/10.1016/0890-4332(93)90055-Z)
- [24] FopahLele A, Korhammer K, Wegscheider N, Rammelberg HU, Schmidt T, Ruck WKL. Thermal conductivity of salt hydrates as porous material using calorimetric (DSC) method. In: Eighth world conference on experimental heat transfer, fluid mechanics, and thermodynamics, vol. 0424533, Instituto Superior Técnico, Lisbon, Portugal: A. Faria – Edicao Electronica Lda; 2013. p. 5.
- [25] Hakvoort G, van Reijen LL, Aartsen AJ. Measurement of the thermal conductivity of solid substances by DSC. *Thermochim Acta* 1985;93:317–20. [http://dx.doi.org/10.1016/0040-6031\(85\)85081-4](http://dx.doi.org/10.1016/0040-6031(85)85081-4)
- [26] Marcus SM, Blaine RL. Thermal conductivity of polymers, glasses and ceramics by modulated DSC. *Thermochim Acta* 1994;243:231–9. [http://dx.doi.org/10.1016/0040-6031\(94\)85058-5](http://dx.doi.org/10.1016/0040-6031(94)85058-5)
- [27] Merzlyakov M, Schick C. Thermal conductivity from dynamic response of DSC. *Thermochim Acta* 2001;377:183–91. [http://dx.doi.org/10.1016/S0040-6031\(01\)00553-6](http://dx.doi.org/10.1016/S0040-6031(01)00553-6)
- [28] Gomez JC, Glatzmaier GC, Mehos M. Heat capacity uncertainty calculation for the eutectic mixture of biphenyl/diphenyl ether used as heat transfer fluid. *SolarPACES*, vol. NREL/CP-5500-56446, Marrakech, Morocco: NREL (National Renewable Energy Laboratory); 2012. p. 9.
- [29] Camirand CP. Measurement of thermal conductivity by differential scanning calorimetry. *Thermochim Acta* 2004;417:1–4. <http://dx.doi.org/10.1016/j.tca.2003.12.023>
- [30] Iverson BD, Cordaro JG, Kruienza AM. Thermal property testing of nitrate thermal storage salts in the solid-phase. In: ASME 54686-fifth international conference on energy sustainability, Parts A, B, and C; 2011. p. 495–502. doi: 10.1115/ES2011-54159.
- [31] Iyimen-Schwarz Z, Lechner MD. Energiespeicherung durch chemische reaktionen. I. DSC-messungen zur quantitativen verfolgung der enthalpieänderungen von speicherstoffen für die hin- und rückreaktion. *Thermochim Acta* 1983;68:349–61. [http://dx.doi.org/10.1016/0040-6031\(83\)80237-8](http://dx.doi.org/10.1016/0040-6031(83)80237-8)
- [32] Fujioka K, Hatanaka K, Hirata Y. Composite reactants of calcium chloride combined with functional carbon materials for chemical heat pumps. *Appl Therm Eng* 2008;28:304–10. <http://dx.doi.org/10.1016/j.applthermaleng.2006.02.032>
- [33] Zhu D, Wu H, Wang S. Experimental study on composite silica gel supported CaCl<sub>2</sub> sorbent for low grade heat storage. *Int J Therm Sci* 2006;45:804–13. <http://dx.doi.org/10.1016/j.ijthermalsci.2005.10.009>
- [34] Okada K, Nakanome M, Kameshima Y, Isobe T, Nakajima A. Water vapor adsorption of CaCl<sub>2</sub>-impregnated activated carbon. *Mater Res Bull* 2010;45:1549–53. <http://dx.doi.org/10.1016/j.matresbull.2010.07.027>
- [35] Tokarev M, Gordelova I, Romannikov V, Glaznev I, Aristov Y. New composite sorbent CaCl<sub>2</sub> in mesopores for sorption cooling/heating. *Int J Therm Sci* 2002;41:470–4. [http://dx.doi.org/10.1016/S1290-0729\(02\)01339-X](http://dx.doi.org/10.1016/S1290-0729(02)01339-X)
- [36] Cortés FB, Chejne F, Carrasco-Marín F, Pérez-Cadenas AF, Moreno-Castilla C. Water sorption on silica- and zeolite-supported hygroscopic salts for cooling system applications. *Energy Convers Manage* 2012;53:219–23. <http://dx.doi.org/10.1016/j.enconman.2011.09.001>
- [37] Kuhmichel Abrasiv GmbH. Glass beads physical-chemical properties. *Glass Beads – GP 2014*. <<http://www.kuhmichel.com/116-1-Glass-Beads.html>>; [accessed 10.09.14].
- [38] Lide DR, Haynes WM “Mickey” (editors). *Thermal properties of Air* (Page 6–175). In: CRC handbook of chemistry and physics, internet version 2010. 90th Internet ed. Boca Raton, Florida, USA: CRC Press/Taylor and Francis; 2010.
- [39] Kristiansen J. The guide to expression of uncertainty in measurement approach for estimating uncertainty an appraisal. *Clin Chem* 2003;49:1822–9. <http://dx.doi.org/10.1373/clinchem.2003.021468>
- [40] Menard D, Py X, Mazet N. Activated carbon monolith of high thermal conductivity for adsorption processes improvement: Part B. Thermal regeneration. *Chem Eng Process: Process Intensif* 2007;46:565–72. <http://dx.doi.org/10.1016/j.cen.2006.07.013>
- [41] Tian B, Jin ZQ, Wang LW, Wang RZ. Permeability and thermal conductivity of compact chemical and physical adsorbents with expanded natural graphite as host matrix. *Int J Heat Mass Transfer* 2012;55:4453–9. <http://dx.doi.org/10.1016/j.ijheatmasstransfer.2012.04.016>
- [42] Smalc M, Skandakumaran P, Norley J. Thermal performance of natural graphite heat spreaders with embedded thermal vias. In: ASME proceeding InterPACK conference, vol. 1, San Francisco, California, USA; 2007. p. 607–17. doi: 10.1115/InterPACK2007-33215.
- [43] El-Dessouky H, Al-Juwayhel F. Effectiveness of a thermal energy storage system using phase-change materials. *Energy Convers Manage* 1997;38:601–17. [http://dx.doi.org/10.1016/S0196-8904\(96\)00072-6](http://dx.doi.org/10.1016/S0196-8904(96)00072-6)
- [44] Wang K, Wu JY, Wang RZ, Wang LW. Effective thermal conductivity of expanded graphite–CaCl<sub>2</sub> composite adsorbent for chemical adsorption chillers. *Energy Convers Manage* 2006;47:1902–12. <http://dx.doi.org/10.1016/j.enconman.2005.09.005>

Please cite this article in press as: Korhammer K et al. Sorption and thermal characterization of composite materials based on chlorides for thermal energy storage. *Appl Energy* (2015), <http://dx.doi.org/10.1016/j.apenergy.2015.08.037>

## **6. Paper IV**

Available online at [www.sciencedirect.com](http://www.sciencedirect.com)

ScienceDirect

Energy Procedia 91 (2016) 161 – 171

---



---

Energy  
**Procedia**


---



---

SHC 2015, International Conference on Solar Heating and Cooling for Buildings and Industry

## Reaction of calcium chloride and magnesium chloride and their mixed salts with ethanol for thermal energy storage

Kathrin Korhammer<sup>1\*</sup>, Christina Apel<sup>1</sup>, Thomas Osterland<sup>1</sup>, Wolfgang K. L. Ruck<sup>1</sup><sup>1</sup>Leuphana University Lüneburg, Scharnhorststraße 1, 21335 Lüneburg, Germany

---

### Abstract

The use of thermochemical energy storage systems increasingly gains interest in order to meet the energy targets of the European renewable energy directive. In this study the suitability of calcium chloride, magnesium chloride and mixed salt ethanolates as heat storage materials for practical implementation was determined by investigating specific thermodynamic properties and estimating the materials' lifetime at various operating conditions. It was proven that the reaction of the before mentioned metal salts with ethanol depends on the applied ethanol vapour pressure. The ethanol sorption increased in the following order:  $MgCl_2 < CaCl_2 < 2CaCl_2 * MgCl_2$ . The enthalpies followed the same sequence. Over-stoichiometric ethanol uptake, in particular for  $CaCl_2$  and  $2CaCl_2 * MgCl_2$  with increasing  $C_2H_5OH$  vapour pressure, was observed. However, the reaction systems  $CaCl_2 - C_2H_5OH$  and  $2CaCl_2 * MgCl_2 - C_2H_5OH$  showed the best sorption properties and cycle stability and thus have a great potential for low-grade thermal energy storage as well as cold storage due to their low reaction temperatures in comparison with salt-water-systems. In general, physically mixing of single salts from the same family with different chemical properties leads to superior thermal behaviour with higher heat storage capacities and material stabilities.

© 2016 The Authors. Published by Elsevier Ltd. This is an open access article under the CC BY-NC-ND license (<http://creativecommons.org/licenses/by-nc-nd/4.0/>).

Peer-review by the scientific conference committee of SHC 2015 under responsibility of PSE AG

**Keywords:** Thermal energy storage; TCM; calcium chloride; magnesium chloride; mixed salts, ethanol, TGA; sorption; cycle stability; reaction kinetics

---

### 1. Introduction

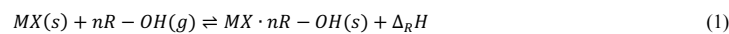
In the transformation process to a more environmentally friendly heat energy conservation and recovery the advancement of clean technologies can help meet the stricter government regulations on carbon dioxide emissions.

---

\* Corresponding author. Tel.: +49-4131-677-1768; fax: +49-4131-677-2822.  
 E-mail address: [kathrin.korhammer@leuphana.de](mailto:kathrin.korhammer@leuphana.de)

Low-grade heat storage systems using reversible chemical gas-solid reactions have the advantage of balancing weather-driven supply fluctuations and time-decoupled demand of heat, which is for instance produced as by-product during power generation from renewable energy sources. The operating temperature usually ranges from 30-150 °C. In the building sector the excess heat can be recovered and re-used for domestic space heating or hot water production. Compared to conventional technologies such as sensible and latent heat storage applications, thermochemical heat storage ensures loss-free, long-term, compact and cost-efficient storage of low-carbon heat.

In the last decades different binary reaction systems have been investigated by numerous scientists. In the low-temperature range inorganic metal salts and alcohols have been identified as potential working pairs. The underlying reaction scheme is given in equation (1):



During the exothermic discharging reaction the solid inorganic metal salt  $MX$  reacts with the gaseous alcohol  $R - OH$  forming the salt alcoholate  $MX \cdot nR - OH$ , where  $n$  is the stoichiometric number of alcohol molecules sorbed, and releasing the stored heat  $\Delta_R H$ . The reverse reaction (charging reaction) is endothermic. Heat energy must be supplied to surpass the activation energy. Fast reaction kinetics, precise temperature control and high reaction enthalpies make salt-alcohol-pairs an advantageous option. Moreover, in comparison to reaction systems with water as reaction partner they exhibit lower charging temperatures.

Up to now, the reaction of inorganic salts with alcohol for thermal energy applications has only drawn a few researchers' attention. Most research articles and publications report on the synthesis of salt alcoholates of different stoichiometric ratios and their characterisation via calorimetric and thermogravimetric analysis and X-ray diffraction. For instance, calcium chloride ( $CaCl_2$ ) and magnesium chloride ( $MgCl_2$ ) form various ethanulates with ethanol ( $C_2H_5OH$ ), in particular  $CaCl_2 \cdot 1C_2H_5OH$ ,  $CaCl_2 \cdot 2C_2H_5OH$ ,  $CaCl_2 \cdot 3C_2H_5OH$ ,  $CaCl_2 \cdot 4C_2H_5OH$  and  $MgCl_2 \cdot C_2H_5OH$  according to Iyimen-Schwarz and Lechner, Mar and Carling and Parker et al. [1,5,6]. The research group around Aristov at the Moscow State University has mainly carried out studies on the ethanol/methanol sorption and desorption behaviour of modified salt-porous-carrier-composites in gram-scale experiments [2,3]. Micro-scale thermogravimetric analysis has been conducted by Iyimen-Schwarz and Lechner, they have made pioneering scientific contributions to the usability of salt alcoholates based on  $CaCl_2$  and  $MgCl_2$  and ethanol for thermal energy storage. They have calculated the energy storage density from the forward and reverse reaction enthalpy determined in dynamic differential calorimetric measurements under vacuum with controlled temperature and alcohol vapour pressure. The total energy yield of the above mentioned reactions of  $CaCl_2$  with  $C_2H_5OH$  decreased to 65 % after 10 operation cycles, while for the  $MgCl_2$ - $C_2H_5OH$ -system the total energy yield remained constant at 99 % [1].

However, fundamental and systematic studies on the reaction of  $CaCl_2$  and  $MgCl_2$  and their mixed salts with  $C_2H_5OH$  are still lacking. By physically mixing two different salts of the same family, the overall performance can be improved compared to single untreated salts. Focus of this study is the characterisation of thermodynamic properties and reaction mechanisms as well as the successive cycling behaviour of above mentioned materials by thermal analysis.  $C_2H_5OH$  uptake and release and the associated reaction enthalpies have been calculated from single thermogravimetric analysis (TGA) measurements. The  $C_2H_5OH$  vapour pressure dependence of the sorption rate has been analysed by applying different flow rates during the sorption process. Preliminary results of desorption kinetics are presented. The model-free Kissinger method has been used to determine the activation energy and pre-exponential factor. A major requirement for use in heat storage systems is a good cycling performance under periodic operation. Thus, the stability of the materials has been examined in cycling tests.

#### Nomenclature

DSC	differential scanning calorimetry
DTG	differential thermogravimetry
TGA	thermogravimetric analysis
TG/MS	thermogravimetric mass spectrometry



$k_{max}$	maximum sorption rate (mg/min)
$mass\%$	change in mass (%)
$t_{50}$	time required to reach a degree of conversion of 50 % (min)
$t_{90}$	time required to reach a degree of conversion of 90 % (min)
$T_{max}$	maximum temperature / peak temperature (K)
$T$	reaction temperature ( $^{\circ}\text{C}$ )
<b>Greek symbols</b>	
$\alpha(t)$	conversion (l)
$\beta$	heating rate (K/min)

## 2. Experimental section

### 2.1. Materials

Anhydrous  $\text{CaCl}_2$  (Ph Eur, Merck), water-free  $\text{MgCl}_2$  (>98.5 %, Roth) and  $\text{C}_2\text{H}_5\text{OH}$  (99.8 %, max. 0.01 %  $\text{H}_2\text{O}$ , Merck) stored over 4 Å binderless molecular sieves Köstrolith® 4ABFK (Chemiewerk Bad Köstritz) were used in this study.  $\text{CaCl}_2$  and  $\text{MgCl}_2$  have been chosen because of their environmental benignity, satisfactory  $\text{C}_2\text{H}_5\text{OH}$  sorption capacity, low production costs and good economic procurement.  $\text{C}_2\text{H}_5\text{OH}$  has been favoured due to its low boiling point, high vapour pressure compared to water and low toxicity. The mixed salt ( $2\text{CaCl}_2 \cdot \text{MgCl}_2$ ) was prepared by physically mixing  $\text{CaCl}_2$  and  $\text{MgCl}_2$  in the ratio of 2:1 in a glove-box in an inert He-atmosphere. The mixture was thoroughly homogenised using pestle and mortar to ensure a perfect blend, dried under vacuum and stored in sealed sample vials over 4 Å binderless molecular sieves. It is assumed that the mixed salt is a mixture and does not form any compounds during preparation.

### 2.2. Methods

The sorption and desorption properties, the reaction temperature range, the reaction enthalpies and the cycle stability were determined by using a simultaneous thermogravimetric and differential scanning calorimetric analysis device (TGA/DSC 1) from Mettler Toledo. Open alumina crucibles with a volume of 70  $\mu\text{l}$  were used. All experiments were performed with small milligram quantities (10-12 mg), which were evenly distributed with no packing at the bottom of the crucible. The experimental setup is illustrated in Fig. 1

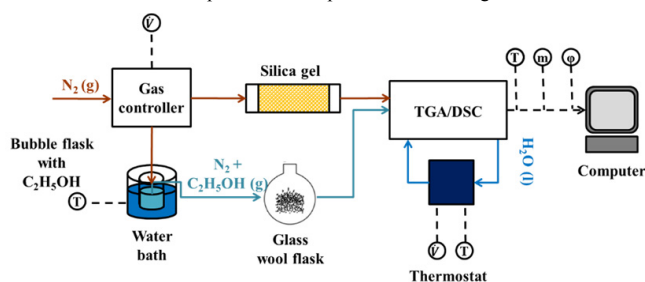


Fig. 1. Experimental setup.

The sorption process (discharging) was performed with an ethanol saturated carrier gas (nitrogen) under atmospheric pressure at 25  $^{\circ}\text{C}$ . The carrier gas was fed with  $\text{C}_2\text{H}_5\text{OH}$  by passing it through a bubble flask filled with

liquid  $C_2H_5OH$  (bubbler system). The water bath temperature of the bubbler system was set to 21 °C to produce ethanol vapour of an equilibrium pressure of 6.2 kPa. For the study on the dependence of the ethanol vapour on the sorption behaviour measurements with different carrier gas flow rates (50 ml/min, 75 ml/min and 100 ml/min) were carried out. During the measurement the reaction chamber was additionally purged with silica-gel dried nitrogen (50 ml/min) to remove released gaseous reaction products and to avoid any side reactions. The time-dependent  $C_2H_5OH$  uptake was studied by variation of the ethanolation time. For the kinetic studies and cycling tests the sample was exposed to a  $C_2H_5OH$ -saturated gas flux of 50 ml/min for 120 min, which is equivalent to an alcohol partial pressure of 3.1 kPa. Between the sorption and desorption phase the sample was stabilised for 60 min at 25 °C. In the desorption process the sample was heated to 180 °C with a heating rate of 3 K/min and stabilised at the final temperature for about 30 min while flushing it continuously with silica-gel dried nitrogen. In the last step the sample was cooled down to the initial temperature with a temperature ramp of -10 K/min. Kinetic data have been obtained under non-isothermal conditions using different heating rates (1 K/min, 3 K/min, 5 K/min and 10 K/min). Measurements with more than 20 cycles of operation were carried out for life cycle analysis. Prior to each measurement the specimen were thermally pre-treated to remove any residual moisture and impurities. The pre-treatment of the sample has a tremendous impact on its sorption behaviour towards the reactant, in particular in the first number of cycles.

Changes in mass and heat flux were recorded online as a function of time and temperature. The precision of the microbalance is given as  $\pm 1.0 \mu\text{g}$ . Temperature and heat flux referring to a reference material were simultaneously detected. The heat power can be determined to a precision of  $\pm 0.1 \text{ mW}$ . Experimental data were analysed by the Mettler Toledo STARE® software 11.00a. The reaction enthalpies were obtained by integrating the reaction peak area and were also referred to one mole of anhydrous sample. All measurement curves presented in this study were blank curve corrected in order to compensate buoyancy effects. The  $C_2H_5OH$  sorption in mole was calculated from the difference of the initial and final sample mass and was referred to one mole of anhydrous sample. The standard uncertainties of the calculated mass and enthalpy are 10-20 %. The change in mass  $mass\%$  was calculated as follows:

$$mass\% = \frac{m_t}{m_0} \times 100\% \quad (2)$$

where  $m_0$  is the initial sample mass and  $m_t$  the mass at the reaction time  $t$ . The total conversion  $\alpha(t)$  was calculated using the following equation:

$$\alpha(t) = \frac{m_0 - m_t}{m_0 - m_1} \quad (3)$$

where  $m_0$  is the initial sample mass,  $m_t$  the mass at the reaction time  $t$  and  $m_1$  the final sample mass.

### 3. Results

As the samples might undergo slight changes during storage and handling the pure salts as received and mixed salts were heated to 400 °C with a temperature ramp of 10 K/min to gain information on the actual water content and decomposition pattern. As assumed the water content measured was slightly higher than given by the supplier. Traces of coordinated water cannot properly be avoided in technical applications and thus were neglected for the evaluation of the materials sorption behaviour. The chemical formula of the received water-free  $CaCl_2$  and  $MgCl_2$  were calculated to be  $CaCl_2 \cdot 0.5H_2O$  and  $MgCl_2 \cdot 0.6H_2O$ , respectively. The mixed salt  $2CaCl_2 \cdot MgCl_2$ , prepared by physically mixing, contained 1.0 mole of  $H_2O$ .

#### 3.1. Influence of $C_2H_5OH$ vapour pressure on sorption properties

Both chemicals  $CaCl_2$  and  $MgCl_2$  and their mixed salts possess good sorption abilities towards  $C_2H_5OH$ . The sorption mechanism strongly depends on the  $C_2H_5OH$  vapour pressure. The given  $C_2H_5OH$  vapour pressures associated to the different flow rates are theoretical values and have been derived from the Antoine-equation. The

following results are summarised in Table 1. All values are average values of 5 runs. The results on the time-dependent  $C_2H_5OH$  sorption on  $CaCl_2$  and  $MgCl_2$  at a  $C_2H_5OH$  vapour pressure of 3.1 kPa showed that an ethanolisation time of 60 min is not sufficient to reach a sorption equilibrium state. With a total amount of  $C_2H_5OH$  sorbed per mole anhydrous  $CaCl_2$  or  $MgCl_2$  of 0.6 for  $CaCl_2$  ethanolates and 0.7 for  $MgCl_2$  ethanolates these values are considerably lower than obtained in stoichiometric gram-scale salt ethanolate synthesis or mentioned in the literature. The associated sorption enthalpy of  $CaCl_2$  ethanolates (-20 kJ/mol) is lower than the average desorption enthalpy (32 kJ/mol). The sorption enthalpy of  $MgCl_2$  ethanolates is -29 kJ/mol, more heat energy is required to induce the decomposition of  $MgCl_2$  ethanolates resulting in a higher desorption reaction enthalpy (45 kJ/mol).

Extension of the ethanolation segment resulted in higher ethanol/salt ratios and reactions enthalpies. An average sorption of 1.0 mole  $C_2H_5OH$  per mole anhydrous  $CaCl_2$  was reached. This value is lower than the theoretical stoichiometric value of 2 moles  $C_2H_5OH$  per mole  $CaCl_2$  due to the applied measuring method varying from the conditions given in the literature [1,4-5]. By doubling the ethanolation time double the sorption enthalpy (-44 kJ/mol) could be measured. An average desorption enthalpy of 57 kJ/mol was calculated. The energy yield was less than 61 %. Iyimen-Schwarz calculated an average energy yield of 65 % over 10 cycles [7]. Applying vacuum can potentially improve the sorption performance of this reaction system. Working at a higher  $C_2H_5OH$  vapour pressure of 3.7 kPa, which equals a flow rate of 75 ml/min, had a low impact on the total amount of  $C_2H_5OH$  sorbed by  $CaCl_2$ . The  $C_2H_5OH$  uptake was only 0.3 mole  $C_2H_5OH$  per mole  $CaCl_2$  higher than at 3.1 kPa. At 4.1 kPa a slight increase in the uptake to a value of 1.7 could be observed. Mar and Carling have suggested the possible existence of both  $CaCl_2 \cdot 1C_2H_5OH$  and  $CaCl_2 \cdot 2C_2H_5OH$ .

Table 1. Sorption characteristics of  $CaCl_2$  and  $MgCl_2$  and their mixed salt  $2CaCl_2 \cdot MgCl_2$  tested under different measurement conditions.  $C_2H_5OH$  sorption and reaction enthalpies are referred to one mole of  $C_2H_5OH$  for better comparison.

$C_2H_5OH$ vapour pressure (kPa)	$CaCl_2$				$MgCl_2$				$2CaCl_2 \cdot MgCl_2$		
	3.1	3.1	3.7	4.1	3.1	3.1	3.7	4.1	3.1	3.7	4.1
Sorption											
Sorption time (min)	60	120	120	120	60	120	120	120	120	120	120
$C_2H_5OH$ uptake (mol $C_2H_5OH$ /mol salt)	0.6	1.0	1.3	1.7	0.7	0.9	0.7	1.2	3.2	3.7	4.4
Enthalpy (kJ/mol salt)	-20	-44	-73	-79	-29	-59	-40	-65	-181	-201	-205
Enthalpy (kJ/mol $C_2H_5OH$ )	-33	-44	-56	-46	-41	-66	-57	-54	-57	-54	47
Desorption											
$C_2H_5OH$ release (mol $C_2H_5OH$ /mol salt)	-0.5	-0.8	-1.0	-1.2	-0.7	-0.8	-0.6	-1.1	-2.8	-3.0	-3.0
Enthalpy (kJ/mol salt)	32	57	63	59	45	36	32	48	149	145	159
Enthalpy (kJ/mol $C_2H_5OH$ )	64	72	63	49	64	45	53	44	53	48	53
Energy yield (%)	52	61	89	94	64	146	108	122	108	113	89

The normalised desorption reaction enthalpies are also listed in Table 1. They are partially higher than the sorption reaction enthalpies. At 3.1 kPa, the maximum amount of  $C_2H_5OH$  sorbed by anhydrous  $MgCl_2$  was only 0.9 in the extended sorption test. The prolonged exposure of  $MgCl_2$  to  $C_2H_5OH$  resulted in an increased sorption enthalpy of -59 kJ/mol. The calculated energy yield was with 145 % surprisingly high. Due to its chemical nature  $MgCl_2$  has a higher binding affinity towards  $C_2H_5OH$  than  $CaCl_2$  and thus stronger intermolecular interaction between these reactants are assumed. The data proposes that  $MgCl_2$  forms with  $C_2H_5OH$  only  $MgCl_2 \cdot 1C_2H_5OH$  compounds. A decline of the sorption capacity at 3.7 kPa compared to a lower  $C_2H_5OH$  vapour pressure of 3.1 kPa, and a jump at 4.1 kPa might be explained by an emerging drop in the sorption capacity and associated reaction enthalpy with increasing number of cycles at 3.1 kPa. The formation of gaseous side products is assumed. Iyimen-Schwarz has gained a sorption reaction enthalpy of -17 kJ/mol for both  $MgCl_2$  and  $CaCl_2$  mono-ethanolates in TGA

analysis experiments over 10 cycles [7]. The desorption enthalpies measured were with 19 kJ/mol and 26 kJ/mol much lower than reported in this study as the measurements were performed under vacuum at different conditions. Reactions are accelerated under vacuum and peak temperatures of desorption steps are shifted towards lower temperatures.

The sorption reaction enthalpy for  $\text{CaCl}_2 \cdot 2\text{C}_2\text{H}_5\text{OH}$  and the enthalpy of decomposition for  $\text{CaCl}_2 \cdot 1\text{C}_2\text{H}_5\text{OH}$  calculated by Carling et al. (-44 kJ/mol) and Mar and Carling (51 kJ/mol) are in closer agreement with the values of this work, which are ranging between -44 and -79 kJ/mol [4,5]. The latter enthalpy was derived from second-law analysis. The ethanolation and deethanolation enthalpies referred to one mole of  $\text{C}_2\text{H}_5\text{OH}$  for  $\text{MgCl}_2$  ethanolation measured by thermal analysis differ from enthalpies obtained from laboratory experiments, which were significantly lower. The mixed salt  $2\text{CaCl}_2 \cdot \text{MgCl}_2$  showed an excellent  $\text{C}_2\text{H}_5\text{OH}$  uptake. The  $\text{C}_2\text{H}_5\text{OH}$  capacity exceeded a value of 3.0 mole  $\text{C}_2\text{H}_5\text{OH}$  per mole anhydrous  $2\text{CaCl}_2 \cdot \text{MgCl}_2$ . The sorption enthalpy was remarkable. It is 6-9 times higher than the sorption enthalpy of pure  $\text{CaCl}_2$  and  $\text{MgCl}_2$ . The overall energy yield of 108 % is satisfying. The variation in the sorption and desorption enthalpy for  $\text{MgCl}_2$  and  $2\text{CaCl}_2 \cdot \text{MgCl}_2$  and given efficiencies over 100 % might be due to deviations in the enthalpy integration. The  $\text{C}_2\text{H}_5\text{OH}$  sorption increased at higher  $\text{C}_2\text{H}_5\text{OH}$  vapour pressure. During stabilisation at 25 °C between 0.4-1.4 mole  $\text{C}_2\text{H}_5\text{OH}$  were lost, which was probably non-coordinated  $\text{C}_2\text{H}_5\text{OH}$ . The higher the  $\text{C}_2\text{H}_5\text{OH}$  vapour pressure the more  $\text{C}_2\text{H}_5\text{OH}$  was released. Therefore, the total amount of coordinated, chemically sorbed  $\text{C}_2\text{H}_5\text{OH}$  was about 3.0 and seemed pressure independent.

Mass loss observed during the subsequent stabilisation phase regarding  $\text{CaCl}_2$  ethanolation indicates that an ethanolation time of 60 min might be too short for the  $\text{C}_2\text{H}_5\text{OH}$  to be incorporated into the crystal lattice and to be strongly bonded to the  $\text{CaCl}_2$ . Extended ethanolation at higher  $\text{C}_2\text{H}_5\text{OH}$  vapour pressure led to an even higher  $\text{C}_2\text{H}_5\text{OH}$  desorption during stabilisation. A steric hindrance is considered to occur between the  $\text{C}_2\text{H}_5\text{OH}$  and the calcium ion due to its higher cation size compared with the magnesium ion and thus a slower solvation process is assumed. However, the release of small amounts of  $\text{C}_2\text{H}_5\text{OH}$  from  $\text{MgCl}_2$  ethanolation at 25 °C is negligible. At lower temperatures mainly non-coordinated physically sorbed  $\text{C}_2\text{H}_5\text{OH}$  is given off. For proper validation of the reproducibility of above mentioned results repeated measurements have to be carried out.

### 3.2. Kinetic analysis of sorption process

The effect of the  $\text{C}_2\text{H}_5\text{OH}$  vapour pressure on the sorption behaviour of the pure and mixed salts was studied by applying different  $\text{C}_2\text{H}_5\text{OH}$  flow rates (Table 2). In order to compare the reaction kinetics of these substances the time required to achieve a conversion of 50 % ( $t_{50}$ ) and 90 % ( $t_{90}$ ) was calculated.

Table 2. Dependence of the sorption kinetics of the tested salts on the  $\text{C}_2\text{H}_5\text{OH}$  vapour pressure.

	3.1 kPa			3.7 kPa			4.1 kPa		
	$t_{50}$ (min)	$t_{90}$ (min)	$k_{max}$ (mg/min)	$t_{50}$ (min)	$t_{90}$ (min)	$k_{max}$ (mg/min)	$t_{50}$ (min)	$t_{90}$ (min)	$k_{max}$ (mg/min)
$\text{CaCl}_2$	35	77	0.14	27	61	0.16	25	62	0.26
$\text{MgCl}_2$	38	100	0.07	33	92	0.12	52	106	0.11
$2\text{CaCl}_2 \cdot \text{MgCl}_2$	27	72	0.12	25	68	0.14	28	83	0.16

In the thermograms of the tested materials are shown in Fig. 2 to Fig. 4. The sorption behaviour of the pure salts  $\text{CaCl}_2$  and  $\text{MgCl}_2$  and the mixed salt  $2\text{CaCl}_2 \cdot \text{MgCl}_2$  were varying in terms of the applied  $\text{C}_2\text{H}_5\text{OH}$  vapour pressure. Despite a higher  $\text{C}_2\text{H}_5\text{OH}$  uptake at higher  $\text{C}_2\text{H}_5\text{OH}$  vapour pressure (see Table 1), the sorption of  $\text{C}_2\text{H}_5\text{OH}$  on  $\text{CaCl}_2$  could be speed up as the  $\text{C}_2\text{H}_5\text{OH}$  vapour pressure increased resulting in a higher maximum sorption rate  $k_{max}$ . The sorption rate is defined as the amount of  $\text{C}_2\text{H}_5\text{OH}$  (mg) sorbed in one unit of time (min).

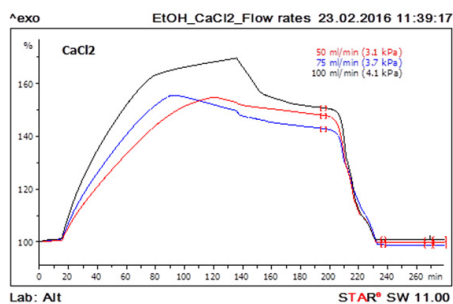


Fig. 2. Dependence of  $C_2H_5OH$  vapour pressure on  $C_2H_5OH$  sorption on  $CaCl_2$ . The sorption referred to the mass of the anhydrous salt (%) is plotted versus the reaction time (min).

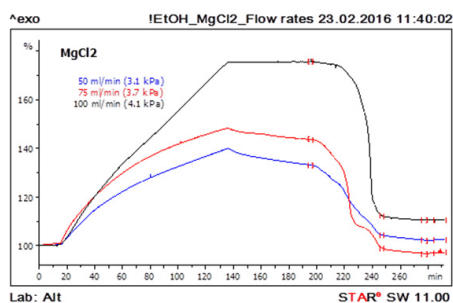


Fig. 3. Dependence of  $C_2H_5OH$  vapour pressure on  $C_2H_5OH$  sorption on  $MgCl_2$ . The sorption referred to the mass of the anhydrous salt (%) is plotted versus the reaction time (min).

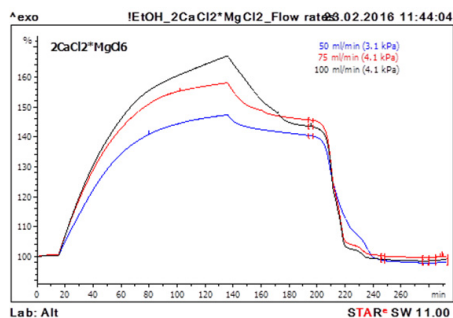


Fig. 4. Dependence of  $C_2H_5OH$  vapour pressure on  $C_2H_5OH$  sorption on  $2CaCl_2 \cdot MgCl_2$ . The sorption referred to the mass of the anhydrous salt (%) is plotted versus the reaction time (min).

Maximum sorption capacity was reached in less than 100 min in experiments at 3.1 kPa and 3.7 kPa. An over-stoichiometric uptake of  $C_2H_5OH$  was observed. This physically sorbed  $C_2H_5OH$  was immediately released.  $CaCl_2$

showed the fastest reaction with the highest sorption rate compared to  $MgCl_2$  and  $2CaCl_2 \cdot MgCl_2$ . For  $MgCl_2$  the fastest reaction occurred at 3.7 kPa as less  $C_2H_5OH$  was sorbed (0.7 mole  $C_2H_5OH$  per mole  $MgCl_2$ ) in comparison to the  $C_2H_5OH$  uptake at 3.1 kPa (0.9 mole  $C_2H_5OH$  per mole  $MgCl_2$ ) and 4.1 kPa (1.2 mole  $C_2H_5OH$  per mole  $MgCl_2$ ). The mixed salt possesses properties which are between the properties of its individual elements. The sorption rate was increasing with increasing pressure. However, at a pressure of 4.1 kPa the reaction proceeded the slowest.

### 3.3. Desorption behavior and kinetics

A literature study revealed that information about the thermal desorption behaviour and kinetics of  $CaCl_2$  and  $MgCl_2$  ethanولات is scarce. The release of  $C_2H_5OH$  from  $CaCl_2$  and  $MgCl_2$  ethanولات proceeded in three overlapping stages, which cannot be separated. The deethanolation process was completed below 150 °C. The deethanolation of  $2CaCl_2 \cdot MgCl_2$  followed a complex mechanism.  $C_2H_5OH$  is lost in up to 4 stages which are not clearly separable. In the first few cycles the stepwise desorption temperatures were varying over a small temperature interval, while with increasing cycle number  $C_2H_5OH$  was desorbed at similar peak temperatures. DTG plots were taken into account for the division of the stages. For  $2CaCl_2 \cdot MgCl_2$  ethanولات the desorption steps and hence desorption peaks varied in the first few cycles, but at higher cycle numbers the peaks and peak temperatures were congruent.

As demonstrated in Fig. 5 the heating rate affects the pattern of the reaction. The increase of the heating rate resulted in the shift of the desorption peaks towards higher temperatures (Fig. 5). Data on desorption reaction kinetics is of great importance for the determination of the material's thermal behaviour and the prediction of its stability in applications under periodic conditions. Results from non-isothermal differential thermal analysis measurements carried out at multiple heating rates  $\beta$  were used to calculate the activation energy  $E_A$  and the pre-exponential factor  $A$  by model-free Kissinger method as follows:

$$\ln \frac{\beta}{T_{max}^2} = \ln \frac{A \cdot R}{E_A} - \frac{E_A}{R \cdot T_{max}} \quad (4)$$

where  $T_{max}$  is the maximum or peak temperature corresponding to the maximum mass loss peak.  $R$  is the universal gas constant. The maximum or peak temperature was gained by integrating the first derivative of the mass curve. The Kissinger method is based on the assumption that the maximum temperature of the maximum mass loss rate is a function of the heating rate. By plotting  $\ln \frac{\beta}{T_{max}^2}$  against  $\frac{1}{T_{max}}$  and fitting a linear regression line to the data values (Fig. 6)  $E_A$  and  $A$  can be derived from the slope and intercept of equation (4).

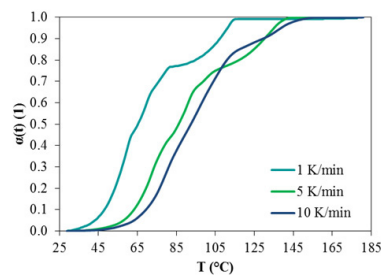


Fig. 5. Example of the degree of conversion over temperature at different heating rates for  $CaCl_2 \cdot 1.2C_2H_5OH$ .

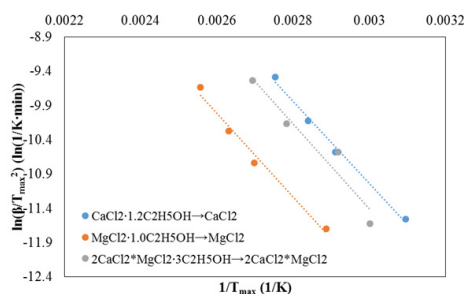


Fig. 6. Determination of desorption kinetic parameters by Kissinger analysis.

For desorption of 1.2 moles  $C_2H_5OH$  from 1 mole anhydrous  $CaCl_2$  an activation energy of 50 kJ/mol was needed. The corresponding pre-exponential factor was calculated to be  $6.48 \cdot 10^6$  1/min. Activation energies of 46 kJ/mol and 52 kJ/mol were obtained for  $MgCl_2 \cdot 1C_2H_5OH$  and  $2CaCl_2 \cdot MgCl_2 \cdot 3C_2H_5OH$ , respectively. The pre-exponential factors were  $3.13 \cdot 10^5$  1/min and  $7.52 \cdot 10^6$  1/min. The activation energies for desorbing  $C_2H_5OH$  are mostly congruent to the deethanolation enthalpies stated in 3.1. In general, the activation energy is equal to the minimum heat that can be stored or liberated. The activation energy obtained from the Kissinger equation is mainly valid for the rate-determining step. As the desorption of  $C_2H_5OH$  from salt ethanlates is a multi-step process as mentioned before, the activation energy changes in the course of the reaction with the degree of the conversion. A comparative study using different determination methods is currently ongoing.

#### 3.4. Cycle stability

One of the most important parameters for determining the suitability of thermochemical materials for heat storage applications is the material's lifespan. The runtime performance of a storage material can be predicted on micro-scale by long-term cycling tests. First stage cycling experiments have shown that the used substances possess stable ethanol uptakes over 5 sorption-desorption cycles. Thus, further experiments with extended cycles have been performed.

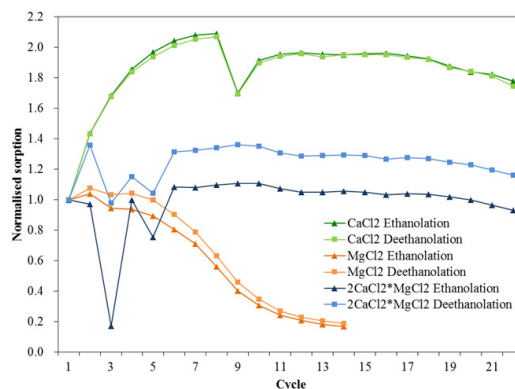


Fig. 7. Cycle stability of tested samples referred to the initial sample mass.

For a better comparison of the different salt-ethanol-systems the sorption and desorption have been normalised to the initial sorption value. In Fig. 7 the normalised sorption is plotted versus the number of operation cycles. The  $\text{CaCl}_2\text{-C}_2\text{H}_5\text{OH}$  -system had remarkable cycle stability over 36 successive cycles despite being tempered to 400 °C for pre-treatment prior to the measurement. Pre-treatment highly affects the reaction. It is assumed that baking-out might cause a change in the chemical structure and hence decrease the material's reactivity in the first cycles. The overall performance decreased only slightly by 15 % (referred to cycle number 8). Cycle stability can at least be guaranteed for a total amount of  $\text{C}_2\text{H}_5\text{OH}$  of 1.1-1.6 sorbed by one mole of  $\text{CaCl}_2$ . Stable  $\text{CaCl}_2$  ethanolates only exist up to  $\text{CaCl}_2 \cdot 1\text{C}_2\text{H}_5\text{OH}$ . However,  $\text{CaCl}_2$  was not fully ethanolated in order to prevent the material from forming crystalline ethanol solvates, which might cause a sharp performance decline.

Irreversible decomposition of  $\text{MgCl}_2$  with increasing cycle numbers probably strongly reduced the sample's sorption ability resulting in a poor reversibility. The performance starts already to drop in early stages and is continuously reduced so that the total degradation is about 85 % referred to the initial sorption. Thus, the cycling test was stopped after 15 cycles. Actually this is not the fully ethanolated state.  $\text{MgCl}_2$  can adsorb up to 4 moles of  $\text{C}_2\text{H}_5\text{OH}$  molecules. But with increasing number of molecules the result would probably be worse.

$2\text{CaCl}_2 \cdot \text{MgCl}_2$  exhibited only a marginal performance decline during cycling. The depicted amplitudes within the first 5 cycles are due to cooling problems of the system. Addition of 2  $\text{CaCl}_2$  to 1  $\text{MgCl}_2$  resulted in reversible and stable sorption-desorption cycles. From the 5<sup>th</sup> cycle onwards the performance declined only by 14 %.

During desorption gaseous degradation products such as ethylene chloride might be released regarding  $\text{MgCl}_2$  ethanolates and maybe also for  $2\text{CaCl}_2 \cdot \text{MgCl}_2$  ethanolates. In additional experiments, which are part of another study, the formation of ethylene chloride in high temperature regions could be confirmed by TG/MS and Raman. The degradation of  $\text{MgCl}_2$  ethanolates and production of ethylene chloride would explain the drastic decline in performance with increasing number of operation cycles. We assume that the alcohol forms complexes with the salts consisting of both build-in and free  $\text{C}_2\text{H}_5\text{OH}$  molecules as reported in other publications [4,7].

#### 4. Conclusions

The sorption behaviour of  $\text{CaCl}_2$ ,  $\text{MgCl}_2$  and their mixed salt  $2\text{CaCl}_2 \cdot \text{MgCl}_2$  strongly depends on the experimental conditions and can be controlled by variation of the  $\text{C}_2\text{H}_5\text{OH}$  vapour pressure, the discharging and charging temperature, the run time and temperature ramp of the desorption process. The experimental values on sorption and desorption ability and associated reaction enthalpies were coherent with literature and theoretical values. The molar  $\text{C}_2\text{H}_5\text{OH}$  /salt ratio referred to the anhydrous salt increased in the following order:  $\text{MgCl}_2 < \text{CaCl}_2 < 2\text{CaCl}_2 \cdot \text{MgCl}_2$ . The desorption enthalpies followed the same sequence. It could be proven that  $\text{C}_2\text{H}_5\text{OH}$  sorption is a function of the  $\text{C}_2\text{H}_5\text{OH}$  vapour pressure. Substances tend to over-stoichiometric ethanol uptake, in particular  $\text{CaCl}_2$  and  $2\text{CaCl}_2 \cdot \text{MgCl}_2$  with increasing  $\text{C}_2\text{H}_5\text{OH}$  vapour pressure. The reaction systems  $\text{CaCl}_2\text{-C}_2\text{H}_5\text{OH}$  and  $2\text{CaCl}_2 \cdot \text{MgCl}_2\text{-C}_2\text{H}_5\text{OH}$  showed the best sorption properties and long-term stability and thus have a great potential for low-grade thermal energy storage as well as cold storage due to their low reaction temperatures in comparison to salt-water-systems. Physically mixing of salts from the same family with different chemical properties leads to superior thermal behaviour with higher heat storage capacities compared with the single salts.

A comprehensive understanding of the thermal behaviour of salt ethanolates to be used in technical applications is required in order to forecast the material's stability. Reaction kinetic parameters of salt ethanolates are affected by various factors such as pre-treatment method, ethanolisation state and chemical composition. Future studies will focus on a detailed kinetic analysis using different mathematical models. A systematic study on the effect of the pre-treatment and history of the substance on the sorption ability is planned. During desorption irreversible decomposition of the materials might occur resulting in the production of chloride-based gaseous side products. Thus, the chemical composition of the gases given off will be analysed by combining thermogravimetric and mass spectrometer analysis. As salt ethanolates tend to solvation and agglomeration in bulk state during consecutive sorption-desorption cycles, optimization and modification methods will be addressed also.



### Acknowledgements

The study was part of a European cooperation-project with the Research Centre for Natural Sciences HAS Budapest and funded by the Federal Ministry of Education and Research.

### References

- [1] Iyimen-Schwarz Z, Lechner MD. Energiespeicherung durch chemische Reaktionen. I. DSC-Messungen zur quantitativen Verfolgung der Enthalpieänderungen von Speicherstoffen für die Hin- und Rückreaktion. *Thermochemica Acta* 1983;68:349-361.
- [2] Aristov YJ, Gordeeva LG. Sorption equilibrium of methanol on new composite sorbents "CaCl<sub>2</sub>/silica gel". *Adsorption* 2007; 13:121-127.
- [3] Gordeeva LG, Freni A, Restuccia J, Aristov YJ. Influence of Characteristics of Methanol Sorbents "Salts in Mesoporous Silica" on the Performance of Adsorptive Air Conditioning Cycle. *Ind. Eng. Chem. Res.* 2007;46:2747-2752.
- [4] Carling RW, Wondolowski AT, Macmillan DC. Enthalpy of formation of CaCl<sub>2</sub>·2CH<sub>3</sub>OH and CaCl<sub>2</sub>·2C<sub>2</sub>H<sub>5</sub>OH by solution calorimetry. *J. Chem. Thermodynamics* 1982;14:125-131.
- [5] Mar RW, Carling RW. The calcium chloride-ethanol system. *Thermochemica Acta* 1981;45:213-217.
- [6] Parker VB, Wagman DD, Evans WH. *Nat. Bur. Stand. Techn. Note* 1971:270-6.
- [7] Iyimen-Schwarz Z. Energiespeicherung durch chemische Reaktionen. Dissertation. Osnabrück: Osnabrück Universität; 1984.

## 7. Paper V



## Reversible formation of alcohol solvates and their potential use for heat storage

Kathrin Korhammer<sup>1</sup> · Judith Mihály<sup>2</sup> · Szabolcs Bálint<sup>2,3</sup> · László Trif<sup>2</sup> · Ádám Vass<sup>2</sup> · András Tompos<sup>2</sup> · Emília Tálás<sup>2</sup>

Received: 22 May 2018 / Accepted: 14 February 2019  
© The Author(s) 2019

### Abstract

In this study, CaCl<sub>2</sub>- and MgCl<sub>2</sub>-alcohol solvates of different stoichiometric quantities of ethyl alcohol (EtOH) and methyl alcohol (MeOH) were synthesized and characterized via coupled thermogravimetric–differential scanning calorimetry, thermogravimetric–mass spectrometric evolved gas analysis (TG-MS), spectroscopic analysis (Raman) methods as well as by X-ray diffraction. Correlations between the obtained calorimetric, thermodynamic, kinetic, and crystallographic data were carried out. The CaCl<sub>2</sub>-alcohol systems seem suitable for heat storage based on the feasible recovery of the salt. However, Raman spectroscopic results revealed that the MgCl<sub>2</sub>-EtOH solvates were instable compounds. Irreversible transformation of MgCl<sub>2</sub>-alcohol solvates related to the formation of alkyl chloride appeared upon heating, as proven by TG-MS and Raman spectroscopic measurements. Pure salt-alcohol solvates could not be prepared under technically applicable conditions. The samples contained at least traces of water. Appearance of side reactions resulting in magnesium oxychlorides, oxyhydroxides, and possible release of HCl with cycling may contribute to corrosion of reactor components. Based on these considerations, MgCl<sub>2</sub>-alcohol solvate systems are not recommended for heat storage.

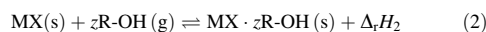
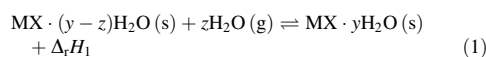
**Keywords** Heat storage · CaCl<sub>2</sub> · MgCl<sub>2</sub> · Alcohol solvates · Alkyl chloride formation

### Introduction

Storage and utilization of thermal energy are of utmost importance for a sustainable energy future. There are three main approaches in this field, e.g., sensible heat storage in water [1, 2], utilization of latent heat by phase change materials (PCM) [3–15], and conversion to chemical energy by different thermochemical reactions [16–22]. Heat storage via reversible thermochemical reactions has several benefits, such as high energy density per volume

material and low long-term losses. Space can be a limiting factor for many practical applications. Most mobile applications, for instance, demand high energy densities in small volumes.

To date, the reaction of inorganic salts with water to form salt hydrates under heat release (1) has mainly been studied and optimized [23–26]. Alcohols are known to undergo similar reactions with salts (2). These reactions have only been studied in a casual manner in terms of their application in thermal energy storage [27, 28], although the high vapor pressure and low freezing point of EtOH and MeOH facilitate low-temperature applications unlike the aqueous adducts.



During the exothermic association reaction (discharging mode), the solid inorganic salt MX reacts with the gaseous alcohol R-OH forming the salt-alcohol solvate (alcoholate) MX·zR-OH, where z is the stoichiometric coefficient. The

✉ Emília Tálás  
talas.emilia@tk.mta.hu

<sup>1</sup> Leuphana University of Lüneburg, Universitätsallee, 1, 21335 Lüneburg, Germany

<sup>2</sup> Institute of Materials and Environmental Chemistry, Research Centre for Natural Sciences, Hungarian Academy of Sciences, Magyar tudósok körútja 2, 1117 Budapest, Hungary

<sup>3</sup> Semilab Semiconductor Physics Laboratory, Prielle Kornélia utca 2, 1117 Budapest, Hungary

chemical energy stored in the reaction is released as heat of reaction  $\Delta_r H_2$ . The reverse reaction (charging mode) is endothermic. Heat energy must be supplied to initiate the dissociation of the  $MX \cdot zR-OH$  adduct. The gaseous product  $R-OH$  can be collected and condensed. Therefore, the storage volume can be reduced and the reaction products can be stored separately. As a result, a long-term storage without sensible heat losses is technically feasible. A schematic diagram of the operating principle of a closed thermochemical heat storage system is shown in Fig. 1.

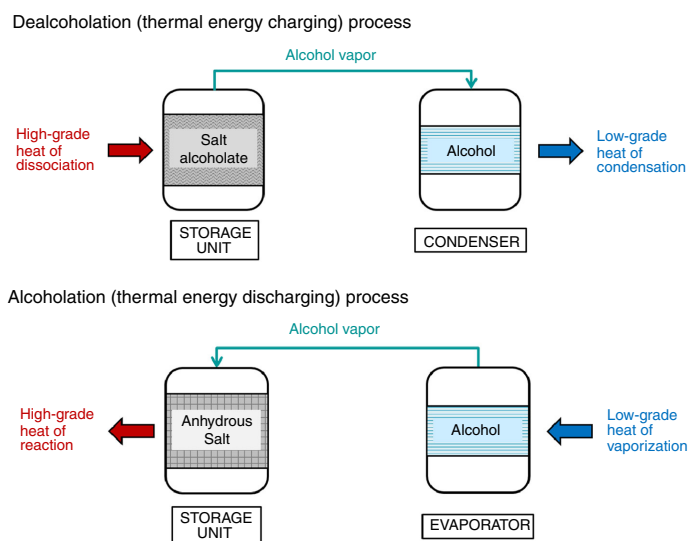
Fast reaction kinetics, precise thermodynamic control, and low regeneration temperatures make salt–alcohol pairs an advantageous option. Recently, the suitability of EtOH solvates of  $CaCl_2$ ,  $MgCl_2$ , and their mixtures as heat storage materials for practical implementations has been studied [29]. The EtOH sorption ability of  $CaCl_2$  was better than that of  $MgCl_2$ . At high EtOH vapor pressures, over-stoichiometric EtOH uptake occurred. The  $CaCl_2$ –EtOH reaction system exhibited convenient sorption properties coupled with good multi-cyclic stability. Consequently, it has a great potential for low-grade thermal energy storage. However, poor reversibility appeared in case of the  $MgCl_2$ –EtOH system with increasing number of cycles, probably caused by irreversible decomposition that strongly reduced the material's sorption performance [29].

Due to the variety of synthesis procedures and conditions, an apparent discrepancy of the stoichiometry of salt alcoholates is found in the published literature. Moreover, present work on the energy storage density is limited. The

aim of this work was to prepare and characterize salt–alcohol solvates of different stoichiometry based on anhydrous  $CaCl_2$  and  $MgCl_2$  by use of commercially available, specially non-purified chemicals with methods that can be relatively easily transposed into practice. The salt–alcohol solvates were prepared by direct synthesis from  $CaCl_2/MgCl_2$  and EtOH/MeOH. This preparation method is based on the operating principle of a thermochemical heat store and can easily be adapted to practice. The focus was laid not only on the detailed comparative study of the calorimetric behavior, but also on the mapping of the heat-induced changes in these solvates. Besides coupled thermogravimetric–mass spectrometric (TG-MS) [30, 31], thermogravimetric analysis/differential scanning calorimetric (TGA/DSC) [32] techniques are generally applied in heat storage studies. We believed that Raman spectroscopy [33, 34] and X-ray powder diffraction (XRD) [35] methods are informative in sample characterization. Use of above techniques on structural changes in salt alcoholates is quite unique. We tried to find relationships between structural changes in the salt–alcohol solvates and the cyclic stability during repeated alcoholation/dealcoholation reactions observed earlier [29].

In solid state, the solvent molecules could be in a well-localized form and in solution they could be located in the first, second, and so on solvation shell. The interaction energies between the solvent molecules and solvated ions can vary over a broad range. Conducting single-crystal diffraction experiments for each composition was not

**Fig. 1** Schematic diagram of the operating principle of a closed thermochemical heat storage system



possible and may be the subject of another work. Throughout this article, the term built-in form refers to the solvent molecules coordinated to the salt ions and also to the molecules loosely bound to the complexes studied, which dissociate upon crystallization or slightly elevating the temperature.

## Experimental

### Synthesis of salt–alcohol solvates

Anhydrous  $\text{CaCl}_2$  powder (Merck, Ph Eur), anhydrous  $\text{MgCl}_2$  powder (Roth,  $\geq 98.5\%$ ), absolute MeOH (max. 0.003%  $\text{H}_2\text{O}$ , Merck), and absolute EtOH (max. 0.01%  $\text{H}_2\text{O}$ , Merck) were used as starting materials. The  $\text{H}_2\text{O}$  content of pure  $\text{CaCl}_2$  and  $\text{MgCl}_2$  samples as received was determined by TGA. The powdered salts contained only traces of  $\text{H}_2\text{O}$ .

Alcohol–salt pairs in four combinations, i.e., MeOH/ $\text{CaCl}_2$ , EtOH/ $\text{CaCl}_2$ , MeOH/ $\text{MgCl}_2$ , EtOH/ $\text{MgCl}_2$ , were prepared setting different alcohol/salt molar ratios (Table 1). The alcohol/salt stoichiometric ratios varied between 2 and 8 mol of EtOH or MeOH per mole anhydrous  $\text{CaCl}_2$  or  $\text{MgCl}_2$ . Samples of 10 g of the respective salt were placed into a round bottom flask that was purged with dry nitrogen ( $\text{N}_2$ ) prior to each alcoholate synthesis

reaction. The flask was equipped with a magnetic stirrer and two thermometers. A stoichiometric amount of liquid alcohol was dropped onto the vigorously agitated salt under dry  $\text{N}_2$  atmosphere, while both the temperature of the sample and the vapor phase were measured. Changes in textural and optical properties of the alcoholated salts were recorded. Preparation and denomination of the samples obtained are summarized in Table 1. The prepared samples were stored in closed glass vessels in a vacuum desiccator over  $\text{P}_2\text{O}_5$ .

### Characterization methods

#### Simultaneous thermogravimetric analysis and differential scanning calorimetry

Experimental alcohol/salt ratios of the salt–alcohol solvates prepared at different theoretical stoichiometric molar ratios, according to Table 1, and associated heat absorptions were identified by simultaneous TGA/DSC. The horizontal furnace TGA/DSC 1 from Mettler Toledo was used. Specimens of 10–15 mg were uniformly placed into alumina crucibles of 70  $\mu\text{L}$  volume and kept isothermally at 30  $^\circ\text{C}$  for 15 min to stabilize the sample. Dynamic runs were carried out by scanning the specimen from 30 to 180  $^\circ\text{C}$  with a temperature ramp of 3  $^\circ\text{C min}^{-1}$  at atmospheric pressure. During subsequent isothermal

**Table 1** Preparation of salt–alcohol solvates by direct synthesis from liquid phase alcohols under neat conditions

Sample no.	Alcohol	Salt	Theoretical molar ratio/alcohol/salt	$n_{\text{alcohol}}/\text{mol}$	$n_{\text{salt}}/\text{mol}$	$V_{\text{alcohol}}/\text{mL}$	$m_{\text{salt}}/\text{g}$
1	MeOH	$\text{CaCl}_2$	2:1	0.180	0.090	7.29	10
2	MeOH	$\text{CaCl}_2$	3:1	0.270	0.090	10.94	10
3	MeOH	$\text{CaCl}_2$	4:1	0.360	0.090	14.58	10
4	MeOH	$\text{CaCl}_2$	6:1	0.541	0.090	21.87	10
5	MeOH	$\text{CaCl}_2$	8:1	0.721	0.090	29.16	10
6	EtOH	$\text{CaCl}_2$	2:1	0.180	0.090	10.51	10
7	EtOH	$\text{CaCl}_2$	3:1	0.270	0.090	15.76	10
8	EtOH	$\text{CaCl}_2$	4:1	0.360	0.090	21.02	10
9	EtOH	$\text{CaCl}_2$	6:1	0.541	0.090	31.53	10
10	MeOH	$\text{MgCl}_2$	2:1	0.210	0.105	8.50	10
11	MeOH	$\text{MgCl}_2$	3:1	0.315	0.105	12.75	10
12	MeOH	$\text{MgCl}_2$	4:1	0.420	0.105	16.99	10
13	MeOH	$\text{MgCl}_2$	6:1	0.630	0.105	25.49	10
14	MeOH	$\text{MgCl}_2$	8:1	0.840	0.105	33.99	10
15	EtOH	$\text{MgCl}_2$	2:1	0.210	0.105	12.25	10
16	EtOH	$\text{MgCl}_2$	3:1	0.315	0.105	18.37	10
17	EtOH	$\text{MgCl}_2$	4:1	0.420	0.105	24.50	10
18	EtOH	$\text{MgCl}_2$	6:1	0.630	0.105	36.75	10

MeOH methanol, EtOH ethanol. Calculation of theoretical stoichiometric molar ratios at standard conditions (20  $^\circ\text{C}$ , 1 atm) using the respective molar masses and densities of the different substances

stabilization at the final temperature, the mass was recorded until the reaction went to completion. The TGA/DSC instrument was purged with  $N_2$  at a flow rate of  $50 \text{ mL min}^{-1}$  during the entire measurement. Effects of buoyancy forces and temperature changes on the TGA and DSC signal were eliminated by automatic blank curve correction. For subtraction of the blank curve from the measurement curve, a blank curve was recorded under the same temperature conditions as the measurement curve, but using empty reference and sample crucibles. All measurements were performed under well-controlled laboratory conditions. The TGA/DSC device was calibrated with high purity metal standards (gallium, indium, lead, aluminum, and gold) over the temperature range of interest. For temperature and enthalpy calibration, the calibration substances were subjected to the same temperature and heating conditions as the samples analyzed. The measured onset temperature, which is assigned the start of the melting process, was compared with the reference melting point of the respective standard. The determined enthalpy of fusion was also validated by comparison with the reference value. The blank curve reproducibility was better than  $\pm 10 \mu\text{g}$  over the whole temperature range. The standard deviation of the enthalpy reproducibility was given as  $< 5\%$ . Mass changes and heat powers were determined with a precision of  $\pm 0.1 \mu\text{g}$  and  $\pm 1 \text{ mW}$ . The Mettler Toledo STARe software 11.00a was used for data processing.

Selected samples of the series of salt–alcohol solvates were characterized complimentary by Raman spectroscopy, TG-MS, and XRD. In case of the first two methods,  $N_2$  atmosphere was used for sample handling.

#### Raman spectroscopy

Raman spectra of samples in closed glass ampoules held at room temperature were recorded with a dynamically aligned Bio-Rad (Digilab) dedicated FT-Raman spectrometer equipped with a Spectra Physics Nd–YAG laser (1064 nm) and high sensitivity liquid- $N_2$ -cooled Ge detector. The excitation laser power used was about 250 mW at the samples. Increase in laser power up to 500 mW does not result in a significant change of the spectra that indicates the stability of the samples during the measurement. The resolution of the Raman instrument was ca.  $4 \text{ cm}^{-1}$ , and a backscattered geometry was used. For each spectrum, 256 individual spectra were averaged.

#### Thermogravimetric–mass spectrometric evolved gas analysis

The simultaneous thermogravimetric and mass spectrometric evolved gas analyses (TG-MS) were recorded on a Setaram LabsysEvo thermal analyzer, in high purity (99.9999%) helium atmosphere, with a flow rate of  $80 \text{ mL min}^{-1}$ . The measurements were done with a heating rate of  $20 \text{ }^\circ\text{C min}^{-1}$ ; the samples were weighed into  $100 \mu\text{L}$  aluminum crucibles in inert (dry  $N_2$ ) atmosphere. Exposure to moisture during sample transfer was prevented, and MS recording of evolved volatiles was enabled by closing the crucibles with aluminum lids pierced with a 700 micron hole by crimping. The measurements were performed in the  $25\text{--}500 \text{ }^\circ\text{C}$  temperature range. The obtained results were baseline corrected and then evaluated with the thermal analyzer's processing software (AKTS Calisto Processing, ver. 1.41). Parallel with the thermogravimetric measurements, the analysis of the evolved gases/volatiles was carried out on a Pfeiffer Vacuum OmniStar<sup>TM</sup> gas analysis system coupled to the above-described TGA. The gas splitter and transfer line to the mass spectrometer were preheated to  $250 \text{ }^\circ\text{C}$ . The scanned  $m/z$  interval was  $5\text{--}79 \text{ amu}$ , with a scan speed of  $20 \text{ ms amu}^{-1}$ . The mass spectrometer was operated in electron impact mode. During a measurement, the total ion current (TIC), the discrete ion current of all scanned masses (75 masses) and the analog spectra on each scan cycle (1 scan cycle was  $1.5 \text{ s}$  long) were obtained in parallel.

#### X-ray powder diffraction

XRD patterns were obtained in a Philips model PW 3710 based PW 1050 Bragg–Brentano parafocusing goniometer using  $\text{CuK}_\alpha$  radiation ( $\lambda = 0.15418 \text{ nm}$ ), graphite monochromator and proportional counter. Samples were placed in an Anton-Paar HTK2000 high-temperature oven chamber. Prior to measurements, the chamber was flushed with high purity  $N_2$  (99.9999%) and during XRD measurements a continuous slow  $N_2$  flow was ensured. The temperature steps chosen for the “temperature programmed” XRD were based on the results of the TG-MS measurement of the appropriate sample. First, XRD patterns were recorded at room temperature, which was followed by stepwise in situ heating. The heating rate was  $5 \text{ }^\circ\text{C min}^{-1}$ . XRD patterns were recorded at every temperature step. Finally, the samples were allowed to cool down ( $20 \text{ }^\circ\text{C min}^{-1}$ ) and the room temperature XRD pattern was again measured. For the phase analysis, reference cards from the ICDD PDF-4 (2010) database were used.

## Results and discussion

### Preliminary results of the direct synthesis of salt–alcohol solvate

During the formation of the different salt alcoholate solvates, heat was evolved and resulted in a change in the temperature. The temperature change in the sample and the surrounding vapor phase was calculated from the difference between the respective initial and final temperatures. The initial sample temperatures ranged from 24 to 27 °C. The increase in temperature in both the sample and vapor chamber laid in the interval of 15–25 °C for almost all salt–alcohol pairs (Fig. 2). Rather fast reactions occurred and maximum temperatures of 40–56 °C were reached within a time of less than 3 min. In general, the temperature rise was higher in the solid phase than in the vapor phase, except for some outliers. For CaCl<sub>2</sub>–alcohol solvates, higher temperature differences were measured when compared with that for MgCl<sub>2</sub>–alcohol solvates. Since the temperature difference of both CaCl<sub>2</sub>–MeOH and CaCl<sub>2</sub>–EtOH solvates varied between 20 °C and 25 °C, irrespective of the alcohol/salt molar ratio, similar stoichiometric compositions of the different salt–alcohol solvates were considered. It is assumed that some heat dissipated into the ambient.

Lower temperature differences compared with that of CaCl<sub>2</sub> hydrates [36, 37] indicate lower heat outputs and

corresponding enthalpies of reaction. Heterogeneous compounds were observed particularly for samples of higher stoichiometry. Some compositions consisted of two phases: a solid salt alcoholate phase and an excess liquid alcohol phase containing dissolved salt particles. Thus, further analysis was carried out using the solid salt–alcohol solvates only.

### Results of TGA/DSC measurements of all samples

The composition of the different salt–alcohol solvates synthesized according to Table 1 was analyzed by TGA/DSC technique. The respective alcohol/salt molar ratios were derived from the change in sample mass recorded as a function of both time and temperature.

### Thermal analysis of the CaCl<sub>2</sub>–MeOH system

The total amount of MeOH uptake of CaCl<sub>2</sub> was calculated to be 4 (Table 2). Samples decomposed in 2–3 overlapping stages over a temperature domain of 33–145 °C (Fig. 3). The majority of MeOH was given off below 100 °C. Peak temperatures of 57–94 °C, 80–114 °C, and 95–118 °C were measured (Table 2). As depicted in Fig. 3, the mass loss rate of the first decomposition step, also referred to as rate of dealcoholation, increased with increasing stoichiometric ratio despite similar sample masses. At theoretical alcohol/salt ratios of 2 and 3, a compound doubly

**Fig. 2** Temperature increase during the synthesis of salt–alcohol solvates, according to Table 1. *MeOH* methanol; *EtOH* ethanol; diamond—sample, square—vapor chamber

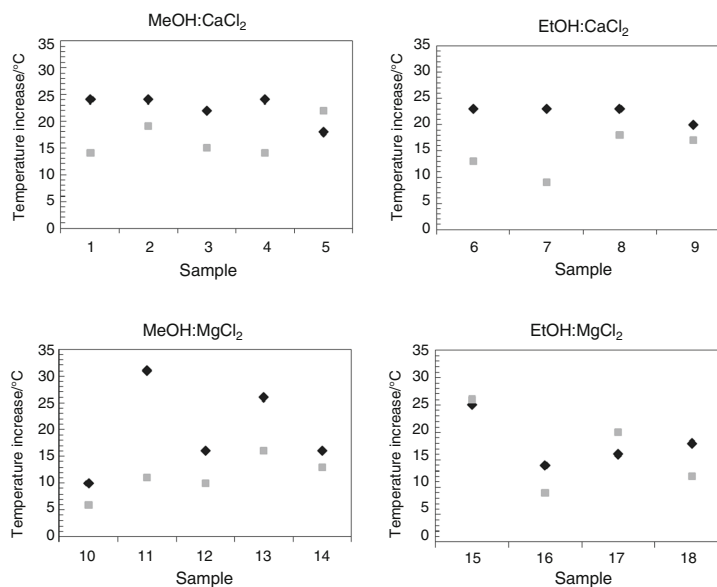


Table 2 Data obtained from TGA/DSC measurements

Sample no.	Salt	Alcohol	z	X/ %	Step 1		Step 2		Step 3		Step 4		$\Delta H^{\circ}/z$ kJ mol <sup>-1</sup>	$\Delta H^{\circ}/z$ kJ mol <sup>-1</sup>	$E_{in}/z$ kJ kg <sup>-1</sup>			
					$T_{initial}/^{\circ}\text{C}$	$T_{peak}/^{\circ}\text{C}$	$T_{initial}/^{\circ}\text{C}$	$T_{peak}/^{\circ}\text{C}$	$T_{initial}/^{\circ}\text{C}$	$T_{peak}/^{\circ}\text{C}$	$T_{initial}/^{\circ}\text{C}$	$T_{peak}/^{\circ}\text{C}$						
1	CaCl <sub>2</sub>	MeOH	2.1	38	54	100	92	100	113	110	113	127	118	101	49	1314	569	
2	CaCl <sub>2</sub>	MeOH	2.1	38	33	102	94	102	128	114				116	55	1337	649	
3	CaCl <sub>2</sub>	MeOH	3.1	47	34	100	93	100	117	108				108	35	1520	518	
4	CaCl <sub>2</sub>	MeOH	4.2	55	33	87	84	87	107	98	107	127	112	129	31	1771	525	
5	CaCl <sub>2</sub>	MeOH	4.0	54	33	63	57	63	85	80	85	145	95	151	38	1754	631	
6	CaCl <sub>2</sub>	EtOH	1.8	42	33	75	71	75	99	88	99	127	108	92	52	1303	475	
7	CaCl <sub>2</sub>	EtOH	1.9	44	35	78	71	78	101	92	101	127	118	127	178	168	1365	614
8	CaCl <sub>2</sub>	EtOH	2.0	45	34	78	72	78	97	89	97	126	116	130	65	1394	642	
9	CaCl <sub>2</sub>	EtOH	1.8	42	34	72	68	72	100	87	100	132	121	99	55	1326	507	
10	MgCl <sub>2</sub>	MeOH	0.9	22	33	103	94	103	132	132	132	177	136	69	77	890	555	
11	MgCl <sub>2</sub>	MeOH	1.9	39	33	74	74	74	102	76	102	177	120	93	49	1115	594	
12	MgCl <sub>2</sub>	MeOH	2.1	42	33	71	65	71	105	78	105	177	122	105	50	1167	643	
13	MgCl <sub>2</sub>	MeOH	3.1	52	33	70	66	70	97	76	97	177	124	183	59	1447	943	
14	MgCl <sub>2</sub>	MeOH	4.1	58	33	76	67	76	108	102	108	136	122	175	43	1639	770	
15	MgCl <sub>2</sub>	EtOH	1.9	48	33	81	65	81	176	140				65	34	1153	354	
16	MgCl <sub>2</sub>	EtOH	2.3	53	33	74	62	74	143	130	143	177	153	90	39	1272	449	
17	MgCl <sub>2</sub>	EtOH	4.6	69	33	68	61	68	126	102	126	145	136	145	177	149	1860	448
18	MgCl <sub>2</sub>	EtOH	3.5	63	33	76	67	76	142	101	142	177	149	158	45	1622	616	

z, stoichiometric coefficient (ethanolation/methanolation level); X, mass loss;  $T_{initial}$ , initial temperature;  $T_{final}$ , final temperature;  $T_{peak}$ , peak temperature;  $\Delta H^{\circ}$ , reaction enthalpy;  $\Delta H^{\circ}/z$ , reaction enthalpy per mole EtOH/MeOH;  $\Delta H^{\circ}$ , enthalpy of formation;  $E_{in}$ , gravimetric energy storage density; Step 1, step 2, step 3 and step 4 refer to the respective EtOH/MeOH release steps of the multi-stage dissociation reactions



Reversible formation of alcohol solvates and their potential use for heat storage

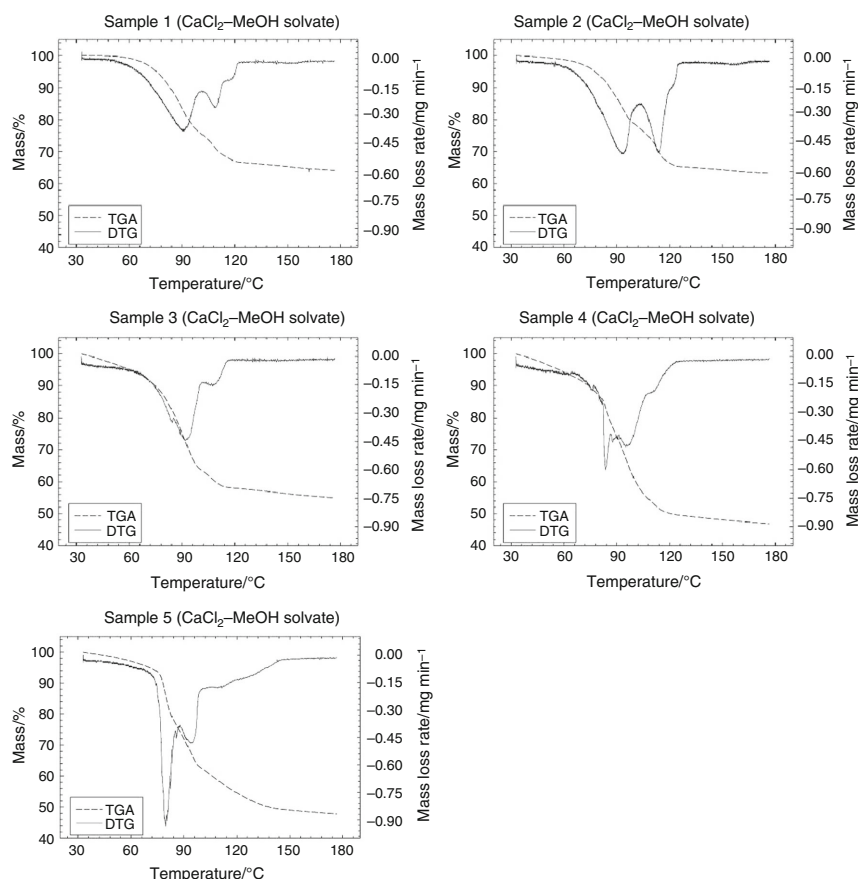


**Fig. 3** Mass (TGA) and mass loss rate (DTG) curves of the dealcoholation of  $\text{CaCl}_2$ -MeOH solvates prepared in neat at different MeOH/ $\text{CaCl}_2$  molar ratios (see Table 1), (measurement temperature interval: 30–180 °C; heating rate of 3 °C  $\text{min}^{-1}$ ; 20 min isotherm at 180 °C)

coordinated with MeOH was the only  $\text{CaCl}_2$ -MeOH solvate found. This result is consistent with the findings of other authors [27, 38–42]. With excess of absolute MeOH, even a  $\text{CaCl}_2$  trimethanolate and  $\text{CaCl}_2$  tetramethanolate could be synthesized (Table 2). Note that samples prepared at higher theoretical alcohol/salt ratios were a heterogeneous mixture of two phases: a solid phase and a liquid phase. The latter was discarded from analysis. The formation of  $\text{CaCl}_2$ -MeOH complexes of different stoichiometry has been claimed by other researchers. Gmelin [43] has reported the existence of  $\text{CaCl}_2$  monomethanolates and  $\text{CaCl}_2$  trimethanolates that have been identified in a study conducted by Gerhold and Kahovec. Bonnell [44] and Menschutkin [45] have obtained  $\text{CaCl}_2$

trimethanolates, too. MeOH solvates of  $\text{CaCl}_2$  with a molar ratio of 4 [43–48] and 6 [49] have been characterized by different analysis methods. The standard reaction enthalpies were deduced from the DSC curve by peak integration and varied between 101 and 151  $\text{kJ mol}^{-1}$  (Table 2).

#### Thermal analysis of the $\text{CaCl}_2$ -EtOH system

In  $\text{CaCl}_2$ -EtOH solvate complexes (Fig. 4), the EtOH was evolved in up to four inseparable steps with peak temperature around 68–72 °C, 87–92 °C, 108–121 °C, and 150–177 °C, respectively (Table 2). The decomposition started roughly at 33 °C and was completed at around 178 °C. The major amount of EtOH was desorbed below

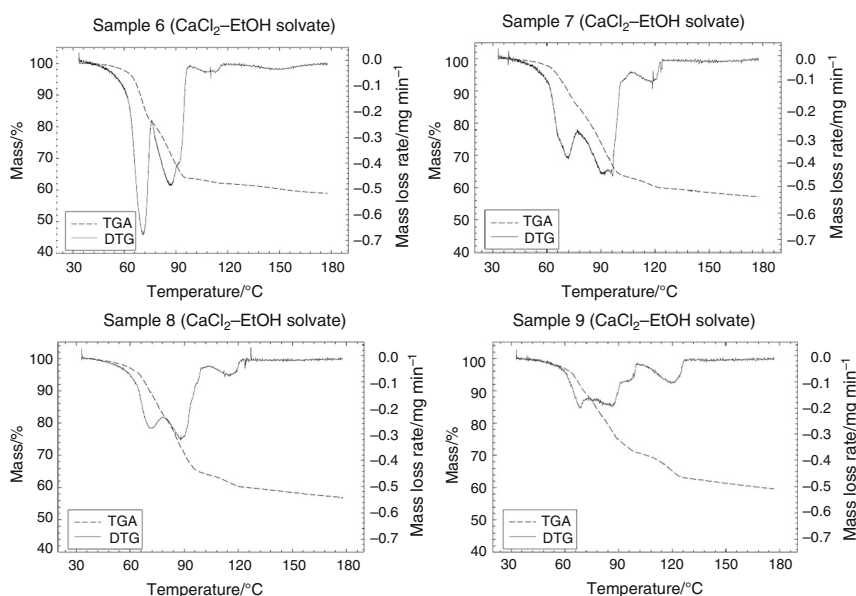


**Fig. 4** Mass (TGA) and mass loss rate (DTG) curves of the dealcoholation of  $\text{CaCl}_2$ -EtOH solvates prepared in neat at different EtOH/ $\text{CaCl}_2$  molar ratios (see Table 1), (measurement temperature interval: 30–180 °C; heating rate of 3 °C  $\text{min}^{-1}$ ; 20 min isotherm at 180 °C)

100 °C. The rate of deethanolation varied over a broad range and was not reproducible, as shown in Fig. 4. The calculated percentage of mass loss (Table 2) clearly showed that in each sample only 2 mol of EtOH was adsorbed per mole of anhydrous  $\text{CaCl}_2$ . However, a variation in the standard enthalpy of reaction with values between 92 and 130  $\text{kJ mol}^{-1}$  was observed. We suppose that  $\text{CaCl}_2$  could only hold up to two molecules of EtOH under the experimental conditions studied, irrespective of the initial stoichiometric ratio we used during sample preparation. These data are consistent with the findings described in the literature [27, 50]. According to published literature data, EtOH forms also a number of other  $\text{CaCl}_2$  ethanulates. Monoethanulates [43, 50, 51], triethanulates [43–45, 52, 53], and tetraethanulates [53–55] of  $\text{CaCl}_2$  have been reported previously. Their existence was not proven in this study.

#### Thermal analysis of the $\text{MgCl}_2$ -MeOH system

The experimental alcohol/salt ratios of the  $\text{MgCl}_2$  methanulates prepared, as listed in Table 1, varied significantly from the theoretical ones. Methanulates of lower methanolation states were formed when the absolute MeOH was added in excess under the conditions studied.

According to the obtained experimental data, about 1, 2, 3, and 4 MeOH molecules were sorbed by one molecule of  $\text{MgCl}_2$  (Table 2). Samples 13 and 14 were deliquescent and therefore we presume that both physically and chemically attached MeOH was present. Depending on the amount of MeOH, the dissociation reaction proceeded in 3–4 incomplete steps (Fig. 5) over the temperature region of 33–177 °C with peak temperatures of 65–94 °C, 76–103 °C, 120–136 °C, and 158 °C, respectively (Table 2). Trace amounts of MeOH continued to evolve during isothermal stabilization at 180 °C until the demethanolation went to completion. As plotted in Fig. 5, the mass loss rates are in general lower compared with that of the  $\text{CaCl}_2$ -MeOH and  $\text{CaCl}_2$ -EtOH solvates. The DSC peak integration yielded standard reaction enthalpy values of 69–183  $\text{kJ mol}^{-1}$  (Table 2). The obtained values were raised by increasing the alcohol/salt molar ratio. Recently,  $\text{MgCl}_2$  monomethanulates have only been reported by Iyimen-Schwarz [51]. Furthermore,  $\text{MgCl}_2$ -MeOH species with stoichiometric numbers of coordinated MeOH molecules of 2 [42, 51, 56], 3 [51, 57], 4 [28, 42, 56, 58, 59], and 6 [47, 49, 56, 57, 60–66] have been identified in the literature.

Reversible formation of alcohol solvates and their potential use for heat storage

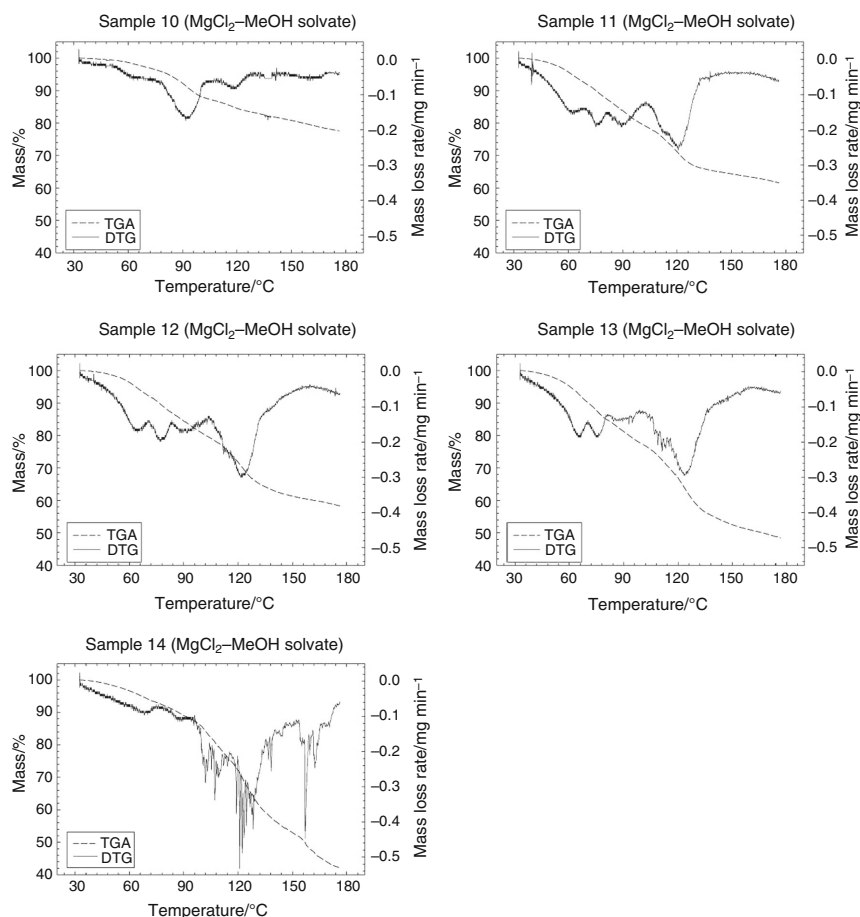


**Fig. 5** Mass (TGA) and mass loss rate (DTG) curves of the dealcoholation of  $\text{MgCl}_2$ -MeOH solvates prepared in neat at different MeOH/ $\text{MgCl}_2$  molar ratios (Table 1), (measurement temperature interval: 30–180 °C; heating rate of 3 °C  $\text{min}^{-1}$ ; 20 min isotherm at 180 °C)

#### Thermal analysis of the $\text{MgCl}_2$ -EtOH system

$\text{MgCl}_2$  formed ethanulates of different stoichiometry: stoichiometric ratios of 1.9, 2.3, 3.5, and 4.6 were identified under the experimental conditions studied (Table 2). The latter  $\text{MgCl}_2$ -4.6EtOH is doubtful as the maximum quantity of absolute EtOH added to anhydrous  $\text{MgCl}_2$  was 4. The dissociation reaction occurred in 2–4 steps (Fig. 6) between 33 and 177 °C with peak temperatures at 61–67 °C, 101–140 °C, and 136–153 °C (Table 2). Trace amounts of EtOH were desorbed during the subsequent isothermal stabilization segment until the reaction went to completion, as observed for  $\text{MgCl}_2$  methanulates (Fig. 5).

The EtOH released in a stepwise manner was probably uncoordinated and coordinated EtOH. The samples 17 and 18 consisted of a two phase mixtures: liquid and solid phase. The latter was used for characterization studies. Mass loss rates between 0.2 and 0.4  $\text{mg min}^{-1}$  were measured (Fig. 6). The calculated standard reaction enthalpies amounted to 65–158  $\text{kJ mol}^{-1}$  (Table 2); the standard reaction enthalpies per mole EtOH were surprisingly low (30–45  $\text{kJ mol}^{-1}$ ), partly lower than the standard enthalpy of vaporization of EtOH (41.680  $\text{kJ mol}^{-1}$ ) [67].  $\text{MgCl}_2$ -EtOH solvates have gained considerable interest among researchers for the synthesis of  $\text{MgCl}_2$ -supported Ziegler-Natta catalysts and subsequently a plethora of the

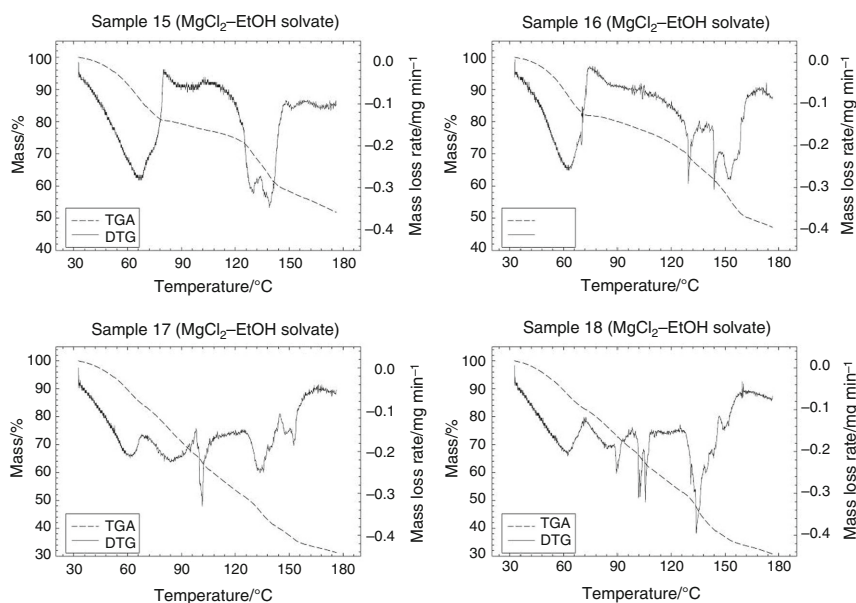


**Fig. 6** Mass (TGA) and mass loss rate (DTG) curves of the dealcoholation of  $\text{MgCl}_2$ -EtOH solvates prepared in neat at different EtOH/ $\text{MgCl}_2$  molar ratios (Table 1), (measurement temperature interval: 30–180 °C; heating rate of 3 °C  $\text{min}^{-1}$ ; 20 min isotherm at 180 °C)

literature exists. Besides well-defined compounds, addition compounds of non-integer stoichiometry have also been identified in several studies. Iyimen-Schwarz [51], Tewell et al. [68], Chadwick and Severn [69], and Bart and Roovers [70] have prepared  $\text{MgCl}_2$  ethanlates with a molar ratio of 0.47, 1, 1.1, and 1.25. The existence of  $\text{MgCl}_2$  diethanlates has been proven by Multani [56] and Di Noto et al. [71]. Furthermore, EtOH solvates of  $\text{MgCl}_2$  with molar ratios of 1.5 [72], 1.67 [68, 70], 2.05 and 2.1 [68, 69], 2.5 [70, 73], 2.8 [69, 72], and 3.33 [28, 70, 72] have been synthesized and investigated in detail. Complex compounds with higher stoichiometry of 4, 4.5, and 5 have been obtained by Bart and Roovers [70], Multani [56], and Tewell et al. [68]. The maximum coordination number observed in  $\text{MgCl}_2$ -EtOH complexes has been 6 according to various authors [56, 57, 63, 65–67, 70–72, 74, 75].

Comparing the decompositions temperatures of  $\text{CaCl}_2$  alcohol solvates indicates that obviously MeOH was stronger associated with the metal chloride than EtOH. For instance, the EtOH evolution from  $\text{CaCl}_2$ -EtOH solvates started at lower temperatures than the desorption of MeOH from  $\text{CaCl}_2$ -MeOH solvates; the last MeOH molecule was liberated at higher temperatures than the last EtOH molecule. This means that during thermal cycling, EtOH can be liberated with lower energy than MeOH. Analogous

reaction behavior was observed for  $\text{MgCl}_2$  alcohol solvates. Moreover,  $\text{MgCl}_2$ -alcohol solvates showed lower dealcoholation rates and thus slower alcoholation/dealcoholation reactions are assumed in comparison with  $\text{CaCl}_2$  alcohol solvates.

#### Energy analysis

Variation in the coordination numbers of the salt-alcohol solvates cited in the references and this study could be the result of the diversity in the synthesis procedures and conditions. According to Bart and Roovers [70], the synthesis method plays a crucial role with regard to the nature of the reactants. Salt-alcohol solvates can be prepared by direct synthesis, solution crystallization and elimination of excess solvent, or recrystallization, for example. The alcohol coordinates to the alkaline earth metal cations to form complexes with variable stoichiometry and structural properties that exist either in the solid state or in solution.

Note that the calculated enthalpies of reaction and dissociation (Table 2) tend to be inaccurate as no quantitative differentiation between alcohol molecules and possible  $\text{H}_2\text{O}$  molecules coordinated to one molecule of salt could be made at this stage. Samples contained probably trace amounts of  $\text{H}_2\text{O}$  that were neglected, since the freshly

prepared samples were immediately characterized via TGA/DSC.

A linear regression analysis of the experimentally obtained standard enthalpies of dissociation as a function of the number of alcohol molecules revealed that the applied model fitted well the data (Fig. 7). The coefficient of determination was close to one for each reaction system. Evidently, the standard enthalpy of dissociation increased along the homologous series of the alcohols studied. EtOH solvates possessed higher enthalpies of formation compared to MeOH solvates. The  $\text{Ca}^{2+}$  ion is of higher charge than the  $\text{Mg}^{2+}$  ion and has a greater polarizing power. Therefore, the standard enthalpies of formation of  $\text{CaCl}_2$ -alcohol complexes are comparatively higher.

The best fit ( $R^2 = 0.9981$ ) was achieved with the  $\text{CaCl}_2$ -EtOH reaction system confirming its chemical stability. The calculated enthalpies of dissociation for all  $\text{CaCl}_2$ -2EtOH solvates analyzed were in the range of  $1303$ – $1394 \text{ kJ mol}^{-1}$  (Table 2) and coincided with formation enthalpy and dissociation enthalpy data given in the published literature [27, 50] (Table 3).  $\text{CaCl}_2$ -EtOH complexes of higher ethanolated states as reported by Parker et al. [53] and those of lower ethanolated states [50, 51] could not be synthesized under the experimental conditions applied.

The  $\text{CaCl}_2$ -MeOH system exhibited an acceptable fit with a coefficient of determination of  $R^2 = 0.9967$ . The enthalpies of dissociation of the  $\text{CaCl}_2$ -2MeOH solvates with values of  $1314 \text{ kJ mol}^{-1}$  and  $1337 \text{ kJ mol}^{-1}$ , respectively, (Table 2) were slightly higher than literature values [27, 38, 42, 51] (Table 3). Enthalpies of reaction and formation/dissociation for  $\text{CaCl}_2$ -3MeOH and  $\text{CaCl}_2$ -4MeOH have not been determined yet. The enthalpy of

dissociation of  $\text{CaCl}_2$ -3MeOH and of  $\text{CaCl}_2$ -4MeOH was estimated at  $1520 \text{ kJ mol}^{-1}$  and  $1771 \text{ kJ mol}^{-1}$ /  $1754 \text{ kJ mol}^{-1}$ , respectively. The enthalpy of dissociation of  $\text{CaCl}_2$ -MeOH complexes increased with the number of alcohol molecules indicating a linear relationship. However, a nonlinear relationship could be observed when the standard enthalpies of reaction per mole of alcohol  $\frac{\Delta_r H^\circ}{z}$  were compared (Table 2). At levels of methanolation higher than 2, the enthalpies of reaction per mole MeOH varied between  $31$  and  $38 \text{ kJ mol}^{-1}$  (Table 2), which are close to the standard enthalpy of vaporization of MeOH ( $37.965 \text{ kJ mol}^{-1}$ ) [67]. Apparently, up to 2 molecules could be chemically bound as a ligand. In MeOH solvates of  $\text{CaCl}_2$  with higher molar ratios, the inclusion of MeOH molecules or physical incorporation of molecules into the crystal lattice could have caused the decrease in the standard enthalpy of reaction per mole of MeOH.

A linear relation between the enthalpy of dissociation and the number of alcohol molecules was also found for  $\text{MgCl}_2$ -EtOH and  $\text{MgCl}_2$ -MeOH solvate complexes (Fig. 7). The R-squared values of the  $\text{MgCl}_2$ -EtOH and  $\text{MgCl}_2$ -MeOH systems were  $R^2 = 0.9979$  and  $R^2 = 0.9971$ , respectively. Reference data are rarely available. Iyimen-Schwarz [51] has collected the enthalpies of formation and dissociation of  $\text{MgCl}_2$ -1EtOH,  $\text{MgCl}_2$ -1MeOH, and  $\text{MgCl}_2$ -3MeOH solvates from thermal cycling tests by DSC technique (Table 4). When compared with values determined in this study, a significant deviation appeared. The values given by Iyimen-Schwarz [51] are mean values averaged over 13 cycles for  $\text{MgCl}_2$ -MeOH solvates and 10 cycles for  $\text{MgCl}_2$ -EtOH solvates. Maximum formation and dissociation enthalpy values of  $31 \text{ kJ mol}^{-1}$ – $34 \text{ kJ mol}^{-1}$  and  $111 \text{ kJ mol}^{-1}$ – $103 \text{ kJ mol}^{-1}$  were derived for  $\text{MgCl}_2$ -1MeOH and  $\text{MgCl}_2$ -3MeOH. In the present study, the enthalpies of dissociation of  $\text{MgCl}_2$ -1MeOH,  $\text{MgCl}_2$ -2MeOH,  $\text{MgCl}_2$ -3MeOH, and  $\text{MgCl}_2$ -4MeOH ranged from  $891$  to  $1639 \text{ kJ mol}^{-1}$  (Table 2). The calculated enthalpies of reaction per mole MeOH of  $43$ – $77 \text{ kJ mol}^{-1}$  (Table 2) were higher than the standard enthalpy of vaporization of MeOH. However, the enthalpies of reaction per mole EtOH with values of  $30$ – $45 \text{ kJ mol}^{-1}$  (Table 2) were lower in comparison with the enthalpy of vaporization of EtOH ( $42 \text{ kJ mol}^{-1}$ ) [67]. Iyimen-Schwarz [51] has obtained even lower enthalpies of formation and dissociation and, respectively, enthalpies of reaction per mole of EtOH for  $\text{MgCl}_2$ -EtOH solvates (Table 3). These inconsistent and unreliable experimental results are ascribed to inherent instability issues of the  $\text{MgCl}_2$ -alcohol solvates.

To assess the suitability of the various salt-alcohol solvate systems for low-temperature heat storage, the gravimetric energy density was calculated from the

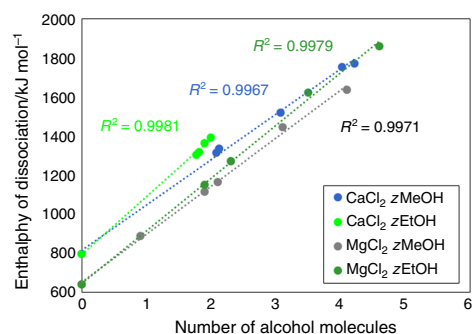


**Fig. 7** Experimentally obtained standard enthalpies of dissociation of various salt-alcohol solvates plotted against the number of alcohol molecules evolved during the dissociation reaction, *MeOH* methanol, *EtOH* ethanol. Linear regression analysis was applied to determine the coefficient of determination (R-squared)

**Table 3** Data available in the literature on experimental and theoretical standard enthalpies of reaction per mole salt alcoholate  $\Delta_r H^\circ$  and standard enthalpies of formation/dissociation  $\Delta_f H^\circ$  of  $\text{CaCl}_2$ -MeOH and  $\text{CaCl}_2$ -EtOH complexes of different stoichiometry  $z$ 

	$z = 1$		$z = 2$		$z = 3$		$z = 4$	
	$\Delta_r H^\circ /$ kJ mol <sup>-1</sup>	$\Delta_f H^\circ /$ kJ mol <sup>-1</sup>	$\Delta_r H^\circ /$ kJ mol <sup>-1</sup>	$\Delta_f H^\circ /$ kJ mol <sup>-1</sup>	$\Delta_r H^\circ /$ kJ mol <sup>-1</sup>	$\Delta_f H^\circ /$ kJ mol <sup>-1</sup>	$\Delta_r H^\circ /$ kJ mol <sup>-1</sup>	$\Delta_f H^\circ /$ kJ mol <sup>-1</sup>
<i>CaCl<sub>2</sub>-MeOH complexes</i>								
Aristov et al. [38]			- 120	- 1317				
Carling et al. [27]			- 113	- 1310				
Iyimen-Schwarz [51]			- 102	- 1299				
Iyimen-Schwarz [51]			103	1300				
Offenhartz et al. [42]			- 103	- 1300				
<i>CaCl<sub>2</sub>-EtOH complexes</i>								
Carling et al. [27]			- 127	- 1393				
Iyimen-Schwarz [51]	- 17	- 1048						
Iyimen-Schwarz [51]	26	1057						
Mar and Carling [50]	51		- 103	- 1369				
Mar and Carling [50]	- 51	- 1082	105	1371				
Parker et al. [53]					- 172	- 1673	- 219	- 1956

For the calculation of missing enthalpy data, a standard enthalpy of formation of  $- 796 \text{ kJ mol}^{-1}$  for solid  $\text{CaCl}_2$ , of  $- 201 \text{ kJ mol}^{-1}$  for gaseous MeOH and of  $- 235 \text{ kJ mol}^{-1}$  for gaseous EtOH was used, respectively [82]

**Table 4** Data available in the literature on experimental and theoretical standard enthalpies of reaction per mole salt alcoholate  $\Delta_r H^\circ$  and standard enthalpies of formation/dissociation  $\Delta_f H^\circ$  of  $\text{MgCl}_2$ -MeOH and  $\text{MgCl}_2$ -EtOH complexes of different stoichiometry  $z$ 

	$z = 1$		$z = 2$		$z = 3$		$z = 4$	
	$\Delta_r H^\circ /$ kJ mol <sup>-1</sup>	$\Delta_f H^\circ /$ kJ mol <sup>-1</sup>	$\Delta_r H^\circ /$ kJ mol <sup>-1</sup>	$\Delta_f H^\circ /$ kJ mol <sup>-1</sup>	$\Delta_r H^\circ /$ kJ mol <sup>-1</sup>	$\Delta_f H^\circ /$ kJ mol <sup>-1</sup>	$\Delta_r H^\circ /$ kJ mol <sup>-1</sup>	$\Delta_f H^\circ /$ kJ mol <sup>-1</sup>
<i>MgCl<sub>2</sub>-MeOH complexes</i>								
Iyimen-Schwarz [51]	- 19	- 861			- 52	- 1295		
Iyimen-Schwarz [51]	21	863			67	1310		
<i>MgCl<sub>2</sub>-EtOH complexes</i>								
Iyimen-Schwarz [51]	- 17	- 893						
Iyimen-Schwarz [51]	19	895						

For the calculation of missing enthalpy data, a standard enthalpy of formation of  $- 641 \text{ kJ mol}^{-1}$  for solid  $\text{MgCl}_2$ , of  $- 201 \text{ kJ mol}^{-1}$  for gaseous MeOH and of  $- 235.1 \text{ kJ mol}^{-1}$  for gaseous EtOH was used, respectively [82]

experimentally measured standard enthalpies of reaction. The gravimetric energy density is a thermochemical material characteristic. As a key performance metric, it is used to evaluate and compare the energy storage performance of thermal energy storage systems. The gravimetric energy density of the investigated salt-alcohol systems was similar, irrespective of the reaction pair combination and ranged from  $354$  to  $943 \text{ kJ kg}^{-1}$ , respectively. From the energetic point of view, salt-alcohol solvate systems for heat storage are not as good as salt-water solvate systems, as the measured standard enthalpies of reaction and

associated gravimetric energy densities are roughly half the respective values of the latter ones [76].

#### Raman spectroscopic characterization of selected samples

In a starting series of experiments, we increased the laser energy systematically from  $200 \text{ mW}$  to  $500 \text{ mW}$  and we found that spectra of sample 6 were not influenced by the change of the excitation energy. This observation let us to conclude that the alcohol solvate sample was stable enough

to be characterized by Raman spectroscopy. Raman spectra of several  $\text{CaCl}_2$ -alcohol solvates recorded at room temperature can be seen in Fig. 8. Comparing the spectrum of pure  $\text{CaCl}_2$ , (line d in Fig. 8a) to those of the different alcohol solvates (lines a, b, e, f in Fig. 8), it could be suggested that the very low wavenumber region was characteristic for  $\text{CaCl}_2$  and bands from  $\sim 450$  to  $\sim 3100 \text{ cm}^{-1}$  belonged to the alcohols. Although Raman spectroscopy is not actually sensitive to  $\text{H}_2\text{O}$ , a very weak band at about  $3400 \text{ cm}^{-1}$  indicated that  $\text{CaCl}_2$  contained a certain amount of coordinated  $\text{H}_2\text{O}$  (line e in Fig. 8b). As a comparison, the Raman spectrum of moisture exposed  $\text{CaCl}_2$  is also shown (line h in Fig. 8b).

The MeOH in sample 1 (line a in Fig. 8a) was mainly in built-in form as  $\nu_{\text{as}}$  of  $\text{CH}_3$  at  $2952 \text{ cm}^{-1}$  and  $\nu_{\text{s}}$  of  $\text{CH}_3$  at  $2844 \text{ cm}^{-1}$  and was shifted with  $\sim 10 \text{ cm}^{-1}$  comparing to those of the MeOH ( $2942 \text{ cm}^{-1}$  and  $2833 \text{ cm}^{-1}$ , line c in Fig. 8a). Bands at  $3013 \text{ cm}^{-1}$  and  $2982 \text{ cm}^{-1}$  in sample 1 indicated the presence of coordinated  $\text{OCH}_3$  (line a in Fig. 8a), while the band at  $\sim 3400 \text{ cm}^{-1}$  indicated the

presence of certain built-in  $\text{H}_2\text{O}$  (cf. line a and line d in Fig. 9a) that was somewhat more intensive than in the starting salt. As the Raman technique gives average information about the material, we could not decide, whether the sample consisted of the mixture of non-coordinated, OH-coordinated, and MeOH-coordinated units of the  $\text{CaCl}_2$  or units, which had MeOH and  $\text{H}_2\text{O}$  in the same coordination sphere.

Contrary to sample 1, sample 4 contained a large amount of free MeOH besides the coordinated MeOH witnessed by the doublet of  $\nu_{\text{s}}$   $\text{CH}_3$  band at  $2844 \text{ cm}^{-1}$  and  $2836 \text{ cm}^{-1}$ ; the latter belongs to non-coordinated MeOH. In addition, a double or triple band in the region  $\sim 3300 \text{ cm}^{-1}$  indicated that  $-\text{OH}$  and non-coordinated MeOH existed in this sample (cf. lines b and c in Fig. 8a). The appearance of a significant amount of non-coordinated MeOH in sample 4 (prepared at an alcohol/salt ratio of 6:1) confirmed that the maximum number of the coordinated MeOH could be 4, as it was already indicated previously (Sect. 3.1). It is worth noting that the Raman spectrum of sample 3 was very similar to that of sample 4,

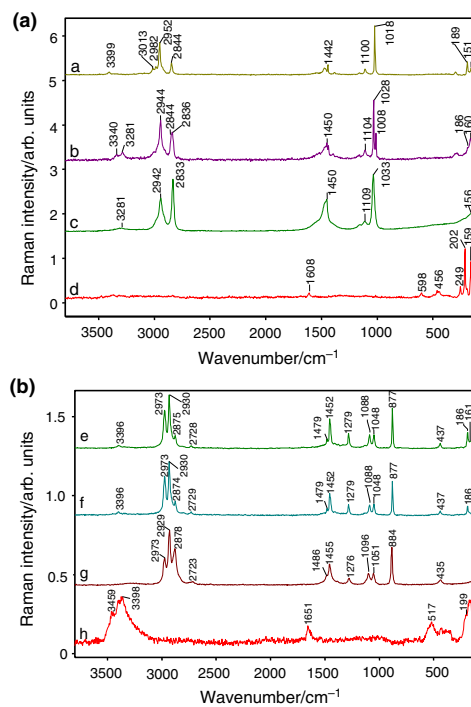


**Fig. 8** Raman spectra of alcohol solvates of  $\text{CaCl}_2$ . **a** MeOH solvates; **b** EtOH solvates; a: sample 1; b: sample 4; c: MeOH; d:  $\text{CaCl}_2$ ; e: sample 6; f: sample 9; g: EtOH; h: moisture exposed  $\text{CaCl}_2$

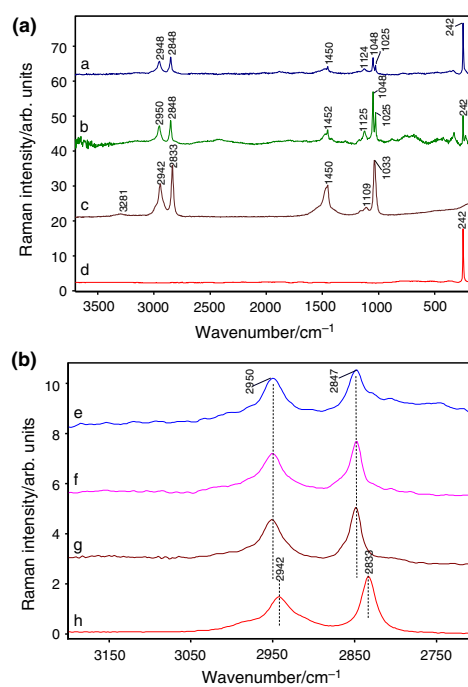


**Fig. 9** Raman spectra of MeOH solvates of  $\text{MgCl}_2$ . **a** overview spectra. **b** enlargement of  $\text{CH}_3$  region; a: sample 12; b: sample 13; c: MeOH; d:  $\text{MgCl}_2$ ; e: sample 10; f: sample 12; g: sample 13; h: MeOH

apart from the band of the non-coordinated MeOH, which was somewhat weaker in sample 3 than in sample 4.

Regarding the alcohol solvates obtained from  $\text{CaCl}_2$  and EtOH, no real difference between the Raman spectra of the samples prepared at different alcohol/salt ratios could be found (cf. line e and f in Fig. 8b) in accordance with the findings described in Sect. 3.1. Certain relative intensity changes in  $2973\text{ cm}^{-1}/\sim 2878\text{ cm}^{-1}$  of  $\nu_{\text{as}}\text{CH}_3/\nu_{\text{s}}\text{CH}_3$  in the region of EtOH (cf. lines e, f and g in Fig. 8b) indicated the presence of the EtOH incorporated into the crystal lattice. The shift of the  $\nu\text{C-O}$  bands at  $1096\text{ cm}^{-1}$  and  $1051\text{ cm}^{-1}$  to  $1088\text{ cm}^{-1}$  and  $1048\text{ cm}^{-1}$ , respectively, could support this idea. However, the appearance of a weak band at  $3396\text{ cm}^{-1}$  confirmed again the presence of coordinated  $\text{H}_2\text{O}$ .

Raman spectra of several  $\text{MgCl}_2$ -MeOH solvates are depicted in Fig. 9. Samples in these series were very similar to each other. The splitting of the  $\nu\text{C-O}$  band at  $1033\text{ cm}^{-1}$  indicated MeOH incorporation into the crystal structure. The intensity ratios of MeOH bands/Mg-Cl bands increased with the amount of introduced MeOH. The  $\nu_{\text{as}}$  of  $\text{CH}_3$  appeared at  $2950\text{ cm}^{-1}$  and  $\nu_{\text{s}}$  of  $\text{CH}_3$  appeared at  $2848\text{ cm}^{-1}$  in the  $\text{MgCl}_2$ -MeOH solvates. These values were shifted compared to that of free MeOH (cf. lines a, b, c and d in Fig. 9b), which indicated that MeOH definitely existed in built-in form in the samples 10, 12, and 13.

Regarding the  $\text{MgCl}_2$ -EtOH systems (Fig. 10), the spectra resembled the spectrum of EtOH showing only negligible band shifts; it was difficult to decide, whether the EtOH existed in a real built-in form or not (cf. line a and c in Fig. 10a). Surprisingly, a new C-H stretching band at high wavenumber appeared (better visualized for sample 18, and only as a shoulder for sample 15) that might be assigned to  $\nu\text{C-H}$  of halogen substituted methyl group. As a comparison, the library IR spectrum of ethyl chloride is also shown (Fig. 10b). It seems plausible that ethyl chloride was formed in  $\text{MgCl}_2$ -EtOH systems. Simultaneously, the  $\text{Ca-Cl}$  vibrational band at  $241\text{ cm}^{-1}$  almost completely disappeared (cf. line b in Fig. 10a).

As a conclusion,  $\text{MgCl}_2$ -EtOH solvates underwent certain decomposition resulting in ethyl chloride formation. Pure salt-alcohol solvates could not be obtained, because of the presence of a certain amount of salt hydrates.

#### TG-MS behavior of selected samples

As preliminary investigations, the starting materials, i.e., the  $\text{CaCl}_2$  and  $\text{MgCl}_2$ , were analyzed, and it was found that both of them contained roughly around 2%  $\text{H}_2\text{O}$  of crystallization (more precisely,  $\text{CaCl}_2$  contained 2.28%  $\text{H}_2\text{O}$ , while the  $\text{H}_2\text{O}$  content of  $\text{MgCl}_2$  was 2.36%).

Four samples were chosen for the TG-MS measurements, namely 3 (containing  $\text{CaCl}_2$  and MeOH), 7 (which

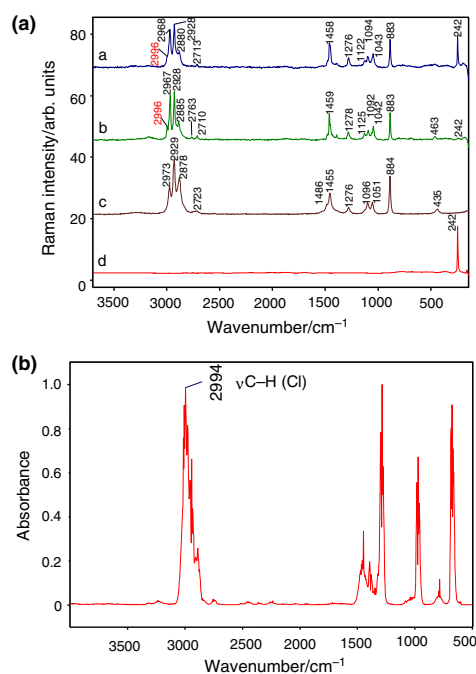


**Fig. 10** Raman spectra of  $\text{MgCl}_2$ -EtOH solvates. **a** EtOH solvates; **b** reference FT-IR spectrum of ethyl chloride from Aldrich Vapor FT-IR Spectral Library; **a**: sample 15; **b**: sample 18; **c**: EtOH; **d**:  $\text{MgCl}_2$

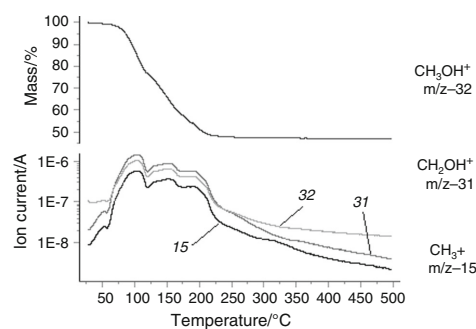


**Fig. 11** TG-MS trace of the sample 3 (mass loss on the upper part, while ion currents on the lower part of the graph), on the right side the formulae of the corresponding fragments/ions

contain  $\text{CaCl}_2$  and EtOH), 12 (containing  $\text{MgCl}_2$  and MeOH), and finally 18 (composed of  $\text{MgCl}_2$  and EtOH). In Fig. 11, the mass loss and some selected ion currents are plotted against the temperature obtained from sample 3,



while on the right side of the figure the chemical species corresponding to the chosen  $m/z$  values are also shown. On the TG curve, between 55 and 300.5 °C, three mass loss steps can be seen. The first mass loss step is between 55 and 123.5 °C, with a mass loss of 23.3%, the second step is between 123.5 and 178 °C, with 19.2% mass lost, and the last step between 178 and 300.5 °C resulting in 9.5% mass loss; the total mass loss during the measurement was 52.9%. Comparing the shape of the three ion currents, three overlapping peaks can be observed on each curve, which correspond to the appropriate mass loss step. The  $m/z$  32 is the molecular ion of MeOH, the  $m/z$  31 is the base peak of MeOH (and also a characteristic marker of aliphatic alcohols), while the  $m/z$  15 corresponds to the methyl ion ( $\text{CH}_3$ ). From the TG-MS measurement, it can be concluded that the evolution of MeOH starts at very low temperatures (around 30 °C). Some  $\text{H}_2\text{O}$  was also detected during the measurement (the ion current of  $\text{H}_2\text{O}$  is not shown), but its concentration variation was within one order of magnitude compared to the concentration variation of MeOH, which was 2 orders of magnitude ( $m/z$  31), thus confirming that the major volatile component formed during the measurement was MeOH. Moreover, no chlorinated compounds (e.g., methyl chloride) were detected. It can be seen that above 300 °C all three ion current curves are still decreasing, which implies that some MeOH is still lost, but this causes a very small mass loss, not detected by TG.

Considering the TG-MS trace of the sample 7 (Fig. 12), only two mass loss steps can be distinguished. The first mass loss step is between 55 and 95 °C, with a mass loss of 1.9%, while the second step is between 95 and 241 °C, with a mass loss of 48%; the total mass loss during the measurement was 50.3%. It can be seen that the formation of EtOH vapors ( $m/z$  46 is the molecular ion of EtOH,  $m/z$  45 is a deprotonated EtOH, while  $m/z$  31 is the base peak

of EtOH) begins at very low temperatures, as already observed in the case of sample 3.

A very small amount of  $\text{H}_2\text{O}$  can be detected between 152 and 235 °C, which means that the  $\text{H}_2\text{O}$  is much more strongly bound to the  $\text{CaCl}_2$  than the EtOH. No alkyl chloride was detected proving the thermal stability of the  $\text{CaCl}_2$ -alcohol solvate. Comparing the results of sample 3 and 7, it can be concluded that EtOH (sample 7) is lost in a narrower temperature range than MeOH (sample 3). Moreover, the temperature value, where the alcohol is practically lost decreases from 300.5 °C (sample 3) to 240 °C (sample 7). This means that during cyclic measurements, EtOH can be liberated with less energy than MeOH.

Replacing  $\text{CaCl}_2$  with  $\text{MgCl}_2$ , significant differences appear in the TG-MS trace of sample 12 and 18. On the mass loss curve of the sample 12 (Fig. 13), three mass loss steps can be identified. The first larger step is between 55 and 198 °C, with a mass loss of 40%, the second, smaller mass loss is between 198 and 306 °C (10% mass lost), and the last, very small step is from 306 °C up to the end of the measurement (up to 500 °C, 1.2% mass loss). Evaluating the ion current curves of four masses ( $m/z$  32 molecular ion of MeOH,  $m/z$  31 base peak of MeOH, while  $m/z$  52 is the molecular ion of methyl chloride, with the  $^{37}\text{Cl}$  isotope, and  $m/z$  50 is the molecular ion of methyl chloride, with the  $^{35}\text{Cl}$  isotope), it can be seen that MeOH is liberated below 180 °C. Above this temperature, besides MeOH, which is still the major component of the volatiles and some traces of  $\text{H}_2\text{O}$ , the formation of methyl chloride begins. This confirms that at higher temperatures,  $\text{MgCl}_2$  hydrolyzes and converts the MeOH into methyl chloride. Around the upper end of the temperature scale, a small amount of methyl chloride is still released between 410 and 490 °C (0.7% mass is lost).

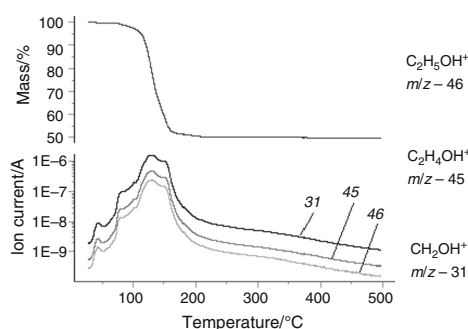


**Fig. 12** TG-MS trace of the sample 7, on the right side the formulae of the corresponding fragments/ions

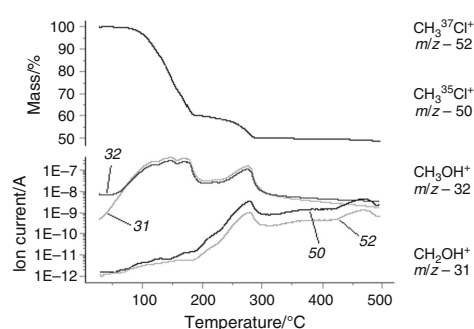


**Fig. 13** TG-MS trace of the sample 12, on the right side the formulae of the corresponding fragments/ions

Replacing the MeOH in the magnesium salt with EtOH (sample 18, Fig. 14), again a complicated, multi-step decomposition pattern is obtained. On the mass loss curve of sample 18, four decomposition steps can be identified (first step between 50 and 100 °C, mass loss 4.2%; second, larger step between 100 and 170 °C, mass loss 46.3%; third step between 170 and 212 °C, mass loss 13.3% and fourth step between 212 and 288 °C, mass loss 10.3%). It can be seen that below 140 °C, the mass loss is caused mainly by the evaporation of EtOH ( $m/z$  46 is the molecular ion of the EtOH,  $m/z$  45 is a deprotonated EtOH, while  $m/z$  31 is the base peak of EtOH) and some traces of H<sub>2</sub>O (ion curves not shown). Above 140 °C, the formation of ethyl chlorides ( $m/z$  66 is the molecular ion of ethyl chloride, with the <sup>37</sup>Cl isotope, while  $m/z$  64 is the molecular ion of ethyl chloride, with the <sup>35</sup>Cl isotope) can be detected. Ethyl chloride is formed over a broad temperature range (between 140 and 370 °C), additionally the concentration of ethanol decreases above 290 °C, while the ethyl chloride is still formed. The formation of ethyl chloride confirms the fact that MgCl<sub>2</sub> hydrolyzes and converts the EtOH into the corresponding alkyl chloride. Comparing the TG-MS results of sample 12 and 18, it can be seen that the alkyl chloride formation starts at lower temperatures in the case of sample 18 (140 °C). The end temperature value of the mass loss end is shifted toward lower temperatures (mass loss end temperature of sample 12 is 306 °C, while the corresponding value is 288 °C in the case of sample 18).

#### Temperature programmed XRD characterization of selected samples

Figure 15 shows the XRD patterns of four selected salt-alcohol solvate samples recorded by use of stepwise heating. The temperature steps were also chosen according to the TG curve obtained from the TG-MS measurement.

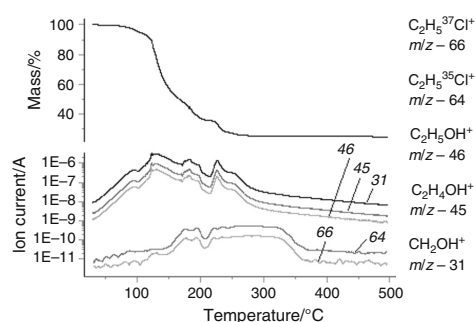


Fig. 14 TG-MS trace of the sample 18, on the right side the formulae of the corresponding fragments/ions

Sample 3 in its starting form (Fig. 15) consisted of MeOH-coordinated phases. The XRD diffraction pattern was somewhat more complicated at 55 °C than at 25 °C, which indicated the formation of a more complex system by the mild heating. These samples consisted of certain CaCl<sub>2</sub>xMeOH (H<sub>2</sub>O) phases. The most likely composition was the average CaCl<sub>2</sub>/MeOH/H<sub>2</sub>O = 1:1:3 ratio in the coordination sphere, which could be estimated from TG. Either a mixture of 1:4 and 1:2 coordinated samples of CaCl<sub>2</sub>-H<sub>2</sub>O and CaCl<sub>2</sub>-MeOH or samples with mixed coordination spheres could be imagined. At 120 °C, 177 °C, and 301 °C samples were CaCl<sub>2</sub>-like materials having amorphous part. At 500 °C, only the CaCl<sub>2</sub> phase existed. The sample after re-cooling was CaCl<sub>2</sub> with some Ca-hydroxide-carbonate. The XRD patterns at 120 °C, 177 °C, and 301 °C were very similar in spite of the large amount of MeOH that went away in the above temperature steps, which implies that a significant amount of MeOH was not really bound in the coordination sphere of the salt.

The diffraction pattern of sample 7 (Fig. 15b) did not change significantly during the heating up to 53 °C in accordance with the TG-MS results, which shows that no significant amount of EtOH or H<sub>2</sub>O was removed during the first some minutes. The starting solvate formed at 1:3 molar ratio could be imagined as a mixture of crystals with coordination sphere 1:2 and 1:4 or crystals with coordination sphere 1:2 and alcohol inclusions. The situation was complicated with the presence of H<sub>2</sub>O. Consequently, besides the pure CaCl<sub>2</sub>·zEtOH and pure CaCl<sub>2</sub>·zH<sub>2</sub>O crystals, CaCl<sub>2</sub>·(x-y)EtOH·yH<sub>2</sub>O structures could exist. Based on the XRD results it was impossible to give a more detailed description. Pure CaCl<sub>2</sub> phase could also be found in the region of 55–500 °C. Probably easily decomposable alcoholic, a relatively stable alcoholic and hydrous phases existed parallel in this sample. The final state was alcohol- and H<sub>2</sub>O-free CaCl<sub>2</sub>.

The composition of the initial sample 12 was rather complicated (Fig. 15c). A volatile part was removed at 56 °C that resulted in a slight change in the diffraction pattern. One might think that physisorbed solvent was removed during the heating from 25 up to 56 °C and the solid consisted of mainly several H<sub>2</sub>O-coordinated MgCl<sub>2</sub> and MeOH-coordinated MgCl<sub>2</sub> forms. Regarding the starting solvate, the TG-MS indicated parallel removing of MeOH and a significant amount of H<sub>2</sub>O. The TG-MS gave a MgCl<sub>2</sub>/MeOH ratio of 3.12 only instead of 4. Since the molar mass of H<sub>2</sub>O is smaller than that of MeOH, the difference might come from the presence of structures with coordination number 4, but both ligands were in the coordination sphere in different variation. Consequently, the starting solvate itself had to be a mixture. The slight changes in the XRD pattern of sample 12 at 56 °C compared to that at 25 °C resulted from the small variation of

Reversible formation of alcohol solvates and their potential use for heat storage

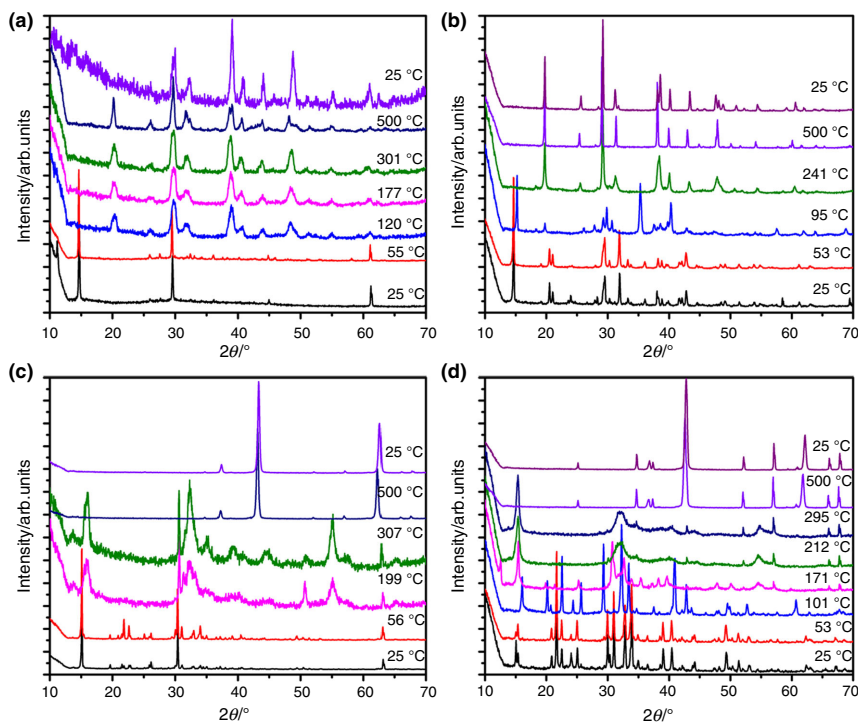


**Fig. 15** XRD patterns of selected alcohol solvates at different temperatures (temperature steps adjusted according to TG curve obtained from the TG-MS measurement; heating rate  $5\text{ }^{\circ}\text{C min}^{-1}$ ;

atmosphere: dry  $\text{N}_2$ ). **a** MeOH-CaCl<sub>2</sub> (sample 3); **b** EtOH-CaCl<sub>2</sub> (sample 7); **c** MeOH-MgCl<sub>2</sub> (sample 12); **d** EtOH/MgCl<sub>2</sub> (sample 18)

the individual components. At 200 °C, the broadenings in the XRD patterns indicated the formation of amorphous phases. A less crystalline form observed was supposed to be a mixture of MeOH- and H<sub>2</sub>O-coordinated materials. It is conceivable that MeOH and H<sub>2</sub>O bound to the salt more or less equally strongly. Some small peaks at about  $2\theta \sim 32^{\circ}$  and  $2\theta \sim 50^{\circ}$  decreased upon increasing the temperature, but we can only say that probably the decomposition of 1:2 complexes appeared. At 307 °C either H<sub>2</sub>O or MeOH could not be present according to TG-MS. The XRD pattern shows the presence of a certain amount of MgCl<sub>2</sub> and/or MgOCl besides amorphous phase(s). At 500 °C, the final material was more crystallized; the final state was MgO (with certain hydrate) and probable Mg-hydroxy-hydrate. The presence of certain MgOOH-HCl could be supposed, too. From these results, it is obvious that the MgCl<sub>2</sub> decomposed upon increasing the temperature from 307 to 500 °C. When the sample was

cooled to 25 °C, the XRD pattern (and of course the structure) formed at 500 °C was maintained.

The XRD patterns of sample 18 (Fig. 15d) at low temperatures (25 °C, 53 °C) were very similar to those of MgCl<sub>2</sub>·zH<sub>2</sub>O. However, TG-MS had shown the removal of mainly EtOH (fragments of EtOH). This observation excluded that the starting material was merely MgCl<sub>2</sub>·zH<sub>2</sub>O. We had to assume that MgCl<sub>2</sub>·zH<sub>2</sub>O is isostructural with MgCl<sub>2</sub>·zEtOH. Only a little shift of the peaks appeared in comparison with MgCl<sub>2</sub>·zH<sub>2</sub>O, which means that the point group was the same in both cases. Because the shift was small, the cell parameters were not altering significantly. This was very surprising considering the difference in the steric properties of H<sub>2</sub>O and EtOH. The very small change in the XRD pattern at 53 °C compared to the XRD pattern at 25 °C could be explained by the removal of a small amount of non-chemisorbed alcohol (physisorbed EtOH or inclusion of EtOH). In the

temperature region of 101–306 °C, the sample gradually lost the EtOH. According to TG-MS results, only EtOH was removed up to 171 °C; EtOH and a small amount of H<sub>2</sub>O went away between 171 and 306 °C. Nevertheless, ethyl chloride was also detected by TG-MS indicating a decomposition process. Increasing the temperature from 101 °C up to 212 °C resulted in a change in the XRD patterns with gradual formation of amorphous phases. MgOHCl, MgCl<sub>2</sub> (aq) probably existed at higher temperatures. The XRD pattern obtained at 500 °C indicated a cubic crystalline material. The pattern of MgO could be fitted well, but the coexistence of other cubic components could also be suggested. The “temperature programmed” XRD behavior of sample 18 was very similar to that of sample 12.

Results of XRD measurements led us to the following conclusions. Mixtures of different phases containing alcohol and H<sub>2</sub>O existed in all of our salt–alcohol solvate samples. CaCl<sub>2</sub> was retrievable from its alcohol solvate by bake out of the alcohol solvate, but irreversible processes appeared in case of MgCl<sub>2</sub>–alcohol solvates. Upon increasing the temperature up to 500 °C, MgO was obtained with elimination of hydrogen chloride similarly to the MgCl<sub>2</sub>·6H<sub>2</sub>O·1,4-C<sub>4</sub>H<sub>8</sub>O<sub>2</sub> [77] and MgCl<sub>2</sub>·6H<sub>2</sub>O system. Although the transformation of the MgCl<sub>2</sub> hydrates has long been known [78], clarifying of its mechanism is still in the focus of interest [79].

#### **Possible problems of the applications of salt–alcohol solvates in heat storage systems, based on the results of various techniques used**

Our results revealed that the MgCl<sub>2</sub>–EtOH solvates were instable compound; decomposition of these samples during storage, handling, and analysis was assumed. Raman spectroscopic measurements proved the appearance of ethyl chloride from MgCl<sub>2</sub>–EtOH without heating. Upon heating, both MeOH and EtOH solvates of MgCl<sub>2</sub> were involved in alkyl chloride release, as proven by TG-MS measurements. The alkyl chloride ion current increased slightly from the beginning of the heating and intensified above 140 °C. Although the heating rate can influence on the mechanism of the decomposition, TG-MS measurements by use of high heating rate indicated the formation of alkyl chloride as well as Raman spectroscopy without any heating. On the other hand, XRD measurements showed transformation of MgCl<sub>2</sub> in all MgCl<sub>2</sub>–alcohol solvate samples, which released alkyl chloride.

These observations were in accordance with the literature. Micro-calorimetric analysis has been conducted by

Iyimen-Schwarz [51], who has made pioneering scientific contributions to the usability of salt–alcohol solvates based on CaCl<sub>2</sub>/MgCl<sub>2</sub> and MeOH/EtOH for thermal energy storage. Iyimen-Schwarz [51] calculated the energy density from the forward and reverse reaction enthalpy determined in dynamic DSC measurements under vacuum at controlled temperatures and alcohol vapor pressures. Based on observations on both the shape of the MgCl<sub>2</sub>–MeOH solvate’s measurement curve and the change of the physical appearance, Iyimen-Schwarz suspected the decomposition of the MgCl<sub>2</sub>–MeOH solvate and the release of CH<sub>3</sub>Cl with successive cycling, analogous to the reaction of MgCl<sub>2</sub> with H<sub>2</sub>O, affecting the reproducibility of the measurements. According to his work, EtOH can be desorbed easily from the MgCl<sub>2</sub>–ethanol system. Iyimen-Schwarz further assumed that in this system the MgCl<sub>2</sub> is likely to decompose into C<sub>2</sub>H<sub>5</sub>Cl and HCl, due to unreproducible results of the measured dissociation enthalpy. Results of our TG-MS and Raman spectroscopic measurements fully support the conclusions of Iyimen-Schwarz and explain the poor cyclic stability of MgCl<sub>2</sub>–EtOH solvates [51].

For alkyl chloride formation in our system different pathways could be assumed. It has been reported that gas phase reaction of EtOH and HCl with formation of H<sub>2</sub>O over ZnCl<sub>2</sub>/Al<sub>2</sub>O<sub>3</sub> as a catalyst, is a suitable method for ethyl chloride preparation [80]. According to a possible explanation, the starting material (MgCl<sub>2</sub>) contains MgCl<sub>2</sub>·zH<sub>2</sub>O in the presence of traces of H<sub>2</sub>O. Heating the MgCl<sub>2</sub> hydrates results in MgOH<sub>x</sub>Cl<sub>x</sub> with probable formation of hydrochloric acid (HCl). At the same time, reaction of alcohols and HCl can lead to the formation of methyl chloride (CH<sub>3</sub>Cl), or ethyl chloride (C<sub>2</sub>H<sub>5</sub>Cl) via MgCl<sub>2</sub> acting as a catalyst. Deliberation of H<sub>2</sub>O carries on the decomposition of MgCl<sub>2</sub>. A direct interaction between the ligands (i.e., Cl<sup>−</sup> and alcohol) in the coordination sphere of the Mg<sup>2+</sup> can also be assumed. This idea does not need the H<sub>2</sub>O to assist in the alkyl chloride formation, but it can lead to the gradual hydrolysis of MgCl<sub>2</sub>. Although we do not have direct evidence for the first or second pathway, we believe that the direct way is more likely, since ethyl chloride formation appeared even at room temperature, while HCl release from MgCl<sub>2</sub>·2H<sub>2</sub>O was reported only at 167 °C [79]. It is worth to note that the final temperature in the cyclic stability test of MgCl<sub>2</sub>·zEtOH was 180 °C [29].

The results presented in Sect. 3.3–3.5 demonstrate that pure salt–alcohol solvates could not be prepared under technically applicable conditions; the samples contained at least traces of H<sub>2</sub>O. H<sub>2</sub>O could be introduced by both the preparation procedure and by the starting materials, despite the use of commercial absolutized solvents and N<sub>2</sub>

atmosphere for the preparation. The starting salts also contained 1–2% of H<sub>2</sub>O, which resulted in the presence of salt hydrates besides the mixture of salt–alcohol solvates. The possibility of the formation of salt hydrates implies the possibility of HCl formation during the thermal treatment above 167 °C [81]. In practical applications, an inert atmosphere cannot be maintained during the whole process, so that traces of H<sub>2</sub>O cannot be avoided. Additionally, the use of high purity grade H<sub>2</sub>O-free substances might be too expensive at technical scale. The appearance of side reactions and the release of HCl with cycling can contribute to corrosion of the reactor components. The decomposition of MgCl<sub>2</sub>–alcohol solvates results further in a degradation of the overall performance of the thermal energy storage system. In conclusion, the reaction system MgCl<sub>2</sub>–R–OH is not suitable for practical implementation, due to its instability and irreversibility. From the energetic point of view, this compound is also not favorable as the measured enthalpies of reaction and associated energy densities are lower than that of CaCl<sub>2</sub>–alcohol solvates and salt–H<sub>2</sub>O systems [76].

## Conclusions

Reversible chemical reactions are highly efficient in terms of storage volume, storage period, and sensible heat losses to the environment compared to other energy storage technologies. Different CaCl<sub>2</sub>- and MgCl<sub>2</sub>-alcohol solvates (EtOH, MeOH) were synthesized and their suitability for heat storage was examined by employing combined thermogravimetric analysis and differential scanning calorimetry (TGA/DSC), spectrometric and spectroscopic analysis (TG-MS, Raman) methods as well as by using X-ray diffraction (XRD). Due to their chemical nature, the CaCl<sub>2</sub>–EtOH systems exhibited lower energy densities than CaCl<sub>2</sub>–H<sub>2</sub>O systems. Decomposition of MgCl<sub>2</sub>–EtOH solvates accompanied by ethyl chloride formation started already during storage. Upon heating, both MeOH and EtOH solvates of MgCl<sub>2</sub> were affected by alkyl chloride release, as proven by TG-MS measurements. Our results fully support the assumptions of Iyimen-Schwarz [51] and explain the poor cycle stability of MgCl<sub>2</sub>–EtOH solvates reported previously. We also demonstrated that pure salt–alcohol solvates cannot be prepared under technically applicable conditions. Formation of salt hydrates implies the possibility of HCl formation during the thermal treatment. Appearance of side reactions and possible release of HCl with cycling may be conducive to corrosion. Conclusively, MgCl<sub>2</sub>–alcohol solvate systems are not recommended for heat storage, whereas CaCl<sub>2</sub>–alcohol systems are suitable demonstrating stable cycle performance. The information on the decomposition pattern and associated

changes in the structural integrity of the salt alcoholates obtained in this study are essential for selecting and designing efficient thermochemical energy stores. The fundamental data on the heat content of the parent salt provide the basis for the development of new two-component thermochemical materials with advanced properties.

**Acknowledgements** Open access funding provided by MTA Research Centre for Natural Sciences (MTA TTK). Project no. TÉT\_12\_DE-1-2013-0003 has been implemented with the support provided by the National Research, Development and Innovation Fund of Hungary, financed under the TÉT\_12\_DE funding scheme. This study received funding from the German Federal Ministry of Education and Research (BMBF) within the framework of a bilateral research collaborative project between the Leuphana University of Lüneburg and the Hungarian Academy of Sciences under grant agreement number 01DS14029. The authors thank Christina Apel for the preparation of salt–alcohol solvate samples.

**Open Access** This article is distributed under the terms of the Creative Commons Attribution 4.0 International License (<http://creativecommons.org/licenses/by/4.0/>), which permits unrestricted use, distribution, and reproduction in any medium, provided you give appropriate credit to the original author(s) and the source, provide a link to the Creative Commons license, and indicate if changes were made.

## Appendix 1: Calculations

The alcohol/salt molar ratios (levels of alcoholation) were derived from experimental data obtained by TGA. The percentage mass loss  $X$  is defined as the mass of alcohol  $m_{R-OH}$  desorbed per unit mass of salt alcoholate  $m_{MXzR-OH}$ :

$$X = \frac{m_{R-OH}}{m_{MXzR-OH}} 100\% \quad (3)$$

The level of alcoholation  $z$  is defined as the ratio of the number of alcohol molecules evolved during the endothermic dissociation reaction  $n_{R-OH}$  to the amount of anhydrous salt  $n_{MX}$  and was calculated from the following equation:

$$z = \frac{n_{R-OH}}{n_{MX}} = \frac{m_{R-OH}M_{MX}}{m_{MX}M_{R-OH}} \quad (4)$$

wherein  $m_{MX}$  and  $m_{R-OH}$  are the masses of the anhydrous salt and the alcohol desorbed, respectively.

The principle of thermochemical heat storage using reversible gas–solid reactions is based on the conversion of thermal energy into chemical energy required to break the chemical bonds of the reactants. At constant pressure, the amount of heat energy that must be supplied to induce the decomposition reaction equals the endothermic heat of reaction, also designated enthalpy of reaction. An infinitesimal change in the temperature results in a change

of the enthalpy by  $\Delta C_p dT$ . The enthalpy of reaction  $\Delta_r H$  under non-standard condition, in case of a reaction temperature  $T_1$  different from the standard state temperature  $T_0$  can be estimated from the standard reaction enthalpies and heat capacities of the reactants using Kirchhoff's law. The heat energy  $\Delta Q$  is then expressed by:

$$\Delta Q = \Delta_r H(T_1, p_0) = \Delta_r H^0(T_0, p_0) + \int_{T_0}^{T_1} \Delta C_p dT + \Delta_{Tr} H \quad (5)$$

where  $\Delta_r H^0(T_0)$  is the standard enthalpy of reaction at standard state conditions  $T_0 = 298.15$  K and  $p_0 = 1$  bar,  $C_p$  is the constant-pressure heat capacity and  $\Delta_{Tr} H$  is the enthalpy of transformation.

The enthalpy of reaction was obtained from DSC measurement by peak area integration. The energy that is liberated or absorbed as heat during a chemical reaction as a result of a temperature difference  $\Delta T$  can be quantitatively determined by heat flux DSC. This technique measures the thermally induced heat flux transferred between the sample and an inert reference that are connected by a low-resistance heat flow path. Thermocouples below the symmetrically positioned sample crucible and empty reference crucible detect and compare the temperature of the specimen to the temperature of the reference as a function of time under same conditions. The heat flux between sample and reference is proportional to the temperature difference:

$$\phi = E_{(T)} \text{DSC} = E_{(T)} \Delta T \quad (6)$$

wherein  $E_{(T)}$  and DSC are the calorimetric sensitivity and the measured DSC signal. Integration of the peak area under the baseline-subtracted DSC signal over time yields  $\Delta_r H^0$ :

$$\Delta_r H^0 = \int_{t_1}^{t_2} \text{DSC} dt = \int_{t_1}^{t_2} \frac{\phi}{E_{(T)}} dt \quad (7)$$

According to Hess Law, the value of the standard reaction enthalpy of the forward and reverse reaction must be equal and the same applies for the standard enthalpy of association and standard enthalpy of dissociation. The standard enthalpy of dissociation is the inverse of the standard enthalpy of formation. In general, the standard enthalpy of reaction is calculated from the difference of the

standard enthalpy of formation of the products and the standard enthalpy of formation of the reactants:

$$\Delta_r H^0 = \sum \Delta_f H^0_{\text{products}} - \sum \Delta_f H^0_{\text{reactants}} \quad (8)$$

Solving Eq. (8) for  $\Delta_r H^0_{\text{products}}$  gives the standard enthalpy of formation and hence the standard enthalpy of dissociation.

Different mathematical approaches are used to determine the specific energy storage density. Two types of energy densities are known: gravimetric and volumetric energy density. The gravimetric energy density  $E_m$  is defined as the capacity of heat energy stored at a defined temperature and pressure per unit mass of storage material and can be calculated from the ratio of the standard reaction enthalpy to the molar mass of the reactant  $M_{\text{MXzR-OH}}$ :

$$E_m = \frac{\Delta_r H^0}{M_{\text{MXzR-OH}}} \quad (9)$$

whereas the volumetric energy density  $E_v$  is related to the volume of storage material and is described as:

$$E_v = \frac{\Delta_r H^0}{M_{\text{MXzR-OH}}} \rho \quad (10)$$

The storage material volume is derived from the material's mass and bulk density  $\rho$ . The higher the level of alcoholation, the lower is the density. The volumetric energy density is an important key energy storage metric for designing and operating storage systems. It is also preferred for performance comparison studies. Space can be a limiting factor for many practical applications. There are no data available for the mass and bulk densities of the salt-alcohol systems studied and hence only the gravimetric energy density could be calculated.

## Appendix 2: Data processing—example of a TGA/DSC curve

Figure 16 displays the DSC measurement curve and corresponding TGA signal normalized to the sample mass for sample 6. To determine the heat content of the sample and the associated enthalpy of reaction, the area under the DSC peak was integrated. Similar curves were recorded for all other samples.

Reversible formation of alcohol solvates and their potential use for heat storage

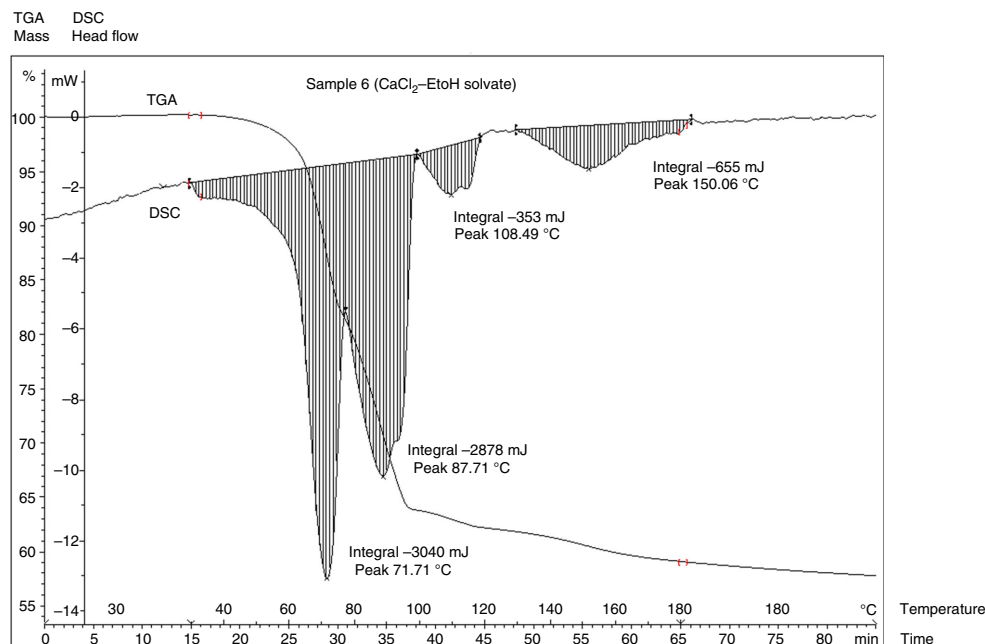


**Fig. 16** Example of a recorded TGA and DSC curve. The TGA curve or change in mass (%) and DSC curve or heat flow (mW) are given as a function of time (min) and temperature (°C). The sample was heated

from 30 to 180 °C at a heating rate of 3 K min<sup>-1</sup>. Since the signs of the thermal processes were inverted due to software issues, the signed number of the underlying endothermic reaction is negative

## References

- Dincer I, Rosen MA. Thermal energy storage systems and applications. Chichester: Wiley; 2002.
- Garg HP, Mullick SC, Bhargava AK. Solar thermal energy storage. Dordrecht: D. Reidel Publishing Company; 1985.
- Agyenim F, Hewitt N, Eames P, Smyth M. A review of materials, heat transfer and phase change problem formulation for latent heat thermal energy storage systems (LHTESS). *Renew Sustain Energy Rev.* 2010;14:615–28.
- Feczko T, Trif L, Horák D. Latent heat storage by silica-coated polymer beads containing organic phase change materials. *Sol Energy.* 2016;132:405–14.
- Kenfack F, Bauer M. Innovative phase change material (PCM) for heat storage for industrial applications. *Energy Proc.* 2014;46:310–6.
- Naumann R, Emons HH. Results of thermal analysis for investigation of salt hydrates as latent heat-storage materials. *J Therm Anal Calorim.* 1989;35:1009–31.
- Naumann R, Schatz O. Thermoanalytical investigation of some alkaline earth hydroxidehydrates on application as latent heat storage materials. *J Therm Anal Calorim.* 1992;38:665–71.
- Sharma A, Tyagi VV, Chen CR, Buddhi D. Review on thermal energy storage with phase change materials and applications. *Renew Sustain Energy Rev.* 2009;13:318–45.
- Zhang N, Yuan Y, Cao X, Du Y, Zhang Z, Gui Y. Latent heat thermal energy storage systems with solid–liquid phase change materials: a review. *Adv Eng Mater.* 2018;20:1700753. <https://doi.org/10.1002/adem.201700753>.
- Anghel EM, Georgiev A, Petrescu S, Popov R, Constantinescu M. Thermo-physical characterization of some paraffins used as phase change materials for thermal energy storage. *J Therm Anal Calorim.* 2014;117:557–66.
- Kong W, Lei Y, Jiang Y, Lei J. Preparation and thermal performance of polyurethane/PEG as novel form-stable phase change materials for thermal energy storage. *J Therm Anal Calorim.* 2017;130:1011–9.
- Guo L, Yu X, Gao D, Guo Y, Ma C, Deng T. Synthesis and thermal energy storage properties of a calcium-based room temperature phase change material for energy storage. *J Therm Anal Calorim.* 2018. <https://doi.org/10.1007/s10973-018-7610-3>.
- He Y, Zhang N, Yuan Y, Cao X, Sun L, Song Y. Improvement of supercooling and thermal conductivity of the sodium acetate trihydrate for thermal energy storage with  $\alpha$ -Fe<sub>2</sub>O<sub>3</sub> as additive. *J Therm Anal Calorim.* 2018;133:859–67.
- Cui W, Zhang H, Xia Y, Zou Y, Xiang C, Chu H, et al. Preparation and thermophysical properties of a novel form-stable CaCl<sub>2</sub>·6H<sub>2</sub>O/sepiolite composite phase change material for latent heat storage. *J Therm Anal Calorim.* 2018;131:57–63.
- Genc M, Karagoz Genc Z. Microencapsulated myristic acid–fly ash with TiO<sub>2</sub> shell as a novel phase change material for building application. *J Therm Anal Calorim.* 2018;131:2373–80.

16. Bevers ERT, Oonk HAJ, Haije WG, van Ekeren PJ. Investigation of thermodynamic properties of magnesium chloride amines by HPDSC and TG. *J Therm Anal Calorim.* 2007;90:923–9.
17. Jabbari-Hichri A, Bennici S, Aroux A. Water sorption heats on silica-alumina-based composites for interseasonal heat storage. *J Therm Anal Calorim.* 2014;118:1111–8.
18. Posern K, Osburg A. Determination of the heat storage performance of thermochemical heat storage materials based on SrCl<sub>2</sub> and MgSO<sub>4</sub>. *J Therm Anal Calorim.* 2018;131:2769–73.
19. Posern K, Kaps C. Humidity controlled calorimetric investigation of the hydration of MgSO<sub>4</sub> hydrates. *J Therm Anal Calorim.* 2008;92:905–9.
20. Lager D, Hohenauer W, Knoll C, Weinberger P, Werner A. Methodology to determine the apparent specific heat capacity of metal hydroxides for thermochemical energy storage. *J Therm Anal Calorim.* 2018;133:207–15. <https://doi.org/10.1007/s10973-017-6883-2>.
21. Bevers ERT, van Ekeren JP, Haije WG, Oonk HAJ. Thermodynamic properties of lithium chloride ammonia complexes for application in a high-lifftemperature chemical heat pump. *J Therm Anal Calorim.* 2006;86:825–32.
22. Ishitobi H, Uruma K, Takeuchi M, Ryu J, Kato Y. Dehydration and hydration behavior of metal-salt-modified materials for chemical heat pumps. *Appl Therm Eng.* 2013;50:1639–44.
23. Donkers PAJ, Pel L, Adan OCG. Experimental studies for the cyclability of salt hydrates for thermochemical heat storage. *J Energy Storage.* 2016;5:25–32.
24. Hamdan MA, Rossides SD, Haj Khalil R. Thermal energy storage using thermo-chemical heat pump. *Energy Convers Manag.* 2013;65:721–4.
25. Korhammer K, Druske MM, Fopah-Lele A, Rammelberg HU, Wegscheider N, Opel O, Osterland T, Ruck W. Sorption and thermal characterization of composite materials based on chlorides for thermal energy storage. *Appl Energy.* 2016;162:1462–72.
26. Posern K, Kaps Ch. Calorimetric studies of thermochemical heat storage materials based on mixtures of MgSO<sub>4</sub> and MgCl<sub>2</sub>. *Thermochim Acta.* 2010;502:73–6.
27. Carling RW, Wondolowski AT, Macmillan DC. Enthalpy of formation of CaCl<sub>2</sub>·2CH<sub>3</sub>OH and CaCl<sub>2</sub>·2C<sub>2</sub>H<sub>5</sub>OH by solution calorimetry. *J Chem Thermodyn.* 1982;14:125–31.
28. Cho HS, Lee WY. Synthesis of inorganic MgCl<sub>2</sub>-alcohol adduct via recrystallization method and its application in supported organometallic catalysts for the polymerization of ethylene with 1-hexene. *J Mol Catal A-Chem.* 2003;191:155–65.
29. Korhammer K, Apel C, Osterland T, Ruck WKL. Reaction of calcium chloride and magnesium chloride and their mixed salts with ethanol for thermal energy storage. *Energy Proc.* 2016;91:161–71.
30. Muroyama AP, Schrader AJ, Loutzenhiser PG. Solar electricity via an Air Brayton cycle with an integrated two-step thermochemical cycle for heat storage based on Co<sub>3</sub>O<sub>4</sub>/CoO redox reactions II: kinetic analyses. *Sol Energy.* 2015;122:409–18.
31. Olivares R, Edwards W. LiNO<sub>3</sub>-NaNO<sub>3</sub>-KNO<sub>3</sub> salt for thermal energy storage: thermal stability evaluation in different atmospheres. *Thermochim Acta.* 2013;560:34–42.
32. Kousksou T, Jamil CA, Gibout CS, Zeraoui YC. Thermal analysis of phase change emulsion. *J Therm Anal Calorim.* 2009;96:841–52.
33. Anghel EM, Georgiev A, Petrescu S, Popov R, Constantinescu M. Thermo-physical characterization of some paraffins used as phase change materials for thermal energy storage. *J Therm Anal Calorim.* 2014;117:557–66.
34. Wong B, Brown L, Buckingham R, Sweet W, Russ B, Gorenssek M. Sulfur dioxide disproportionation for sulfur based thermochemical energy storage. *Sol Energy.* 2015;118:134–44.
35. van Essen VM, Zondag HA, Gores JC, Bleijendaal LPJ, Bakker M, Schuitema R, van Helden WGJ, He Z, Rindt CCM. Characterization of MgSO<sub>4</sub> hydrate for thermochemical seasonal heat storage. *J Sol Energy Eng.* 2009;131:041014-1–7.
36. van Essen VM, Bleijendaal LPJ, Kikkert BWJ, Zondag HA, Bakker M, Bach PW. Development of a compact heat storage system based on salt hydrates. In: *Proceedings of the EUROSUN; 2010.*
37. Zondag H, van Essen M, Bleijendaal L, Cot J, Schuitema R, Planje W, Epema T, Oversloot H. Comparison of reactor concepts for thermochemical storage of solar heat. In: *Third International Renewable Energy Storage Conference, IRES; 2008:24–5.*
38. Aristov YI, Gordeeva LG, Pankratiev YD, Plyasova LM, Bikova IV, Freni A, Restuccia G. Sorption equilibrium of methanol on new composite sorbents “CaCl<sub>2</sub>/silica gel”. *Adsorption.* 2007;13:121–7.
39. Gillier-Pandraud H, Philoche-Levisalles M. Structure cristalline du composé CaCl<sub>2</sub>·CH<sub>3</sub>OH. *C R Acad Sci Ser C.* 1971;273:949–51.
40. Hirata Y, Fujioka K. Thermophysical properties and heat transfer characteristics of CaCl<sub>2</sub> heat pump reactor associated with structural change of reactive salts. In: *V Minsk international seminar “Heat pipes, heat pumps, refrigerators”; 2003.*
41. Lai H, Li C. Application of periodic reversal flow reactors to chemical heat pump systems based on solid/vapor non-catalytic reaction. *Chem Eng Sci.* 1996;51:2951–7.
42. Offenhartz PO'D, Brown FC, Mar RW, Carling RW. A heat pump and thermal storage system for solar heating and cooling based on the reaction of calcium chloride and methanol vapor. *J Sol Energy Eng.* 1980;102:59–65.
43. Gmelin L. *Handbuch der anorganischen chemie.* Weinheim: Verlag Chemie; 1966.
44. Bonnell DGR, Jones WJLH. The dissociation pressures of alcoholates. Part I. *J Chem Soc (Resumed).* 1926;129:321–8.
45. Menshutkin BN. Über einige Kristallalkoholate. *Zeitschrift für anorganische und allgemeine Chemie.* 1907;52:9–24.
46. Brusset H, Gillier-Pandraud H, Philoche-Levisalles M. Crystallographic data on compound CaCl<sub>2</sub>. *C R Acad Sci Ser C.* 1970;271:579.
47. Halut-Desportes S, Husson E. Spectres d'absorption infrarouge et calcul de champ de force de complexes de coordination: halogénures de magnésium et de calcium avec le méthanol ou l'éthanol. *Spectrochim Acta A Mol Spectr.* 1985;41:661–73.
48. Kane R. Beiträge zur Geschichte des Holzgeistes und seiner Verbindungen. *Eur J Org Chem.* 1836;19:164–83.
49. Halut-Desportes S, Philoche-Levisalles M. Structures comparées des solvates de formule MBr<sub>2</sub>·6CH<sub>3</sub>OH. *Acta Crystallogr B-Struct Crystallogr Cryst Chem.* 1978;34:432–5.
50. Mar RW, Carling RW. The calcium chloride-ethanol system. *Thermochim Acta.* 1981;45:213–7.
51. Iyimen-Schwarz, Z. *Energiespeicherung durch chemische Reaktionen.* Doctoral dissertation; 1984.
52. Heindl JB. Über krystallinische Verbindungen von Chlorcalcium mit Alkoholen. *Monatshefte für Chemie und verwandte Teile anderer Wissenschaften.* 1881;2:200–11.
53. Parker VB, Wagman DD, Evans WH. *NBS Technical Note 270-6. Selected values of thermodynamic properties.* Washington: US Government Printing Office; 1971.
54. von Chodnew A. Beiträge zur Kenntniss der Alkoholate und der salpetersauren Magnesia. *Eur J Org Chem.* 1849;71:241–65.
55. Graham T. XLVII. An account of the formation of alcohates, definite compounds of salts and alcohol analogous to the hydrates. *Philos Mag Ser.* 1828;2(4):265–72.
56. Multani RK. Action of magnesium chloride on alcohols. *Curr Sci.* 1964;33:430.



## Reversible formation of alcohol solvates and their potential use for heat storage

57. Olmer LJ, Quinet MLB. *Soc Chim Fr.* 1934;1:1579–81.
58. Choi JH, Chung JS, Shin HW, Song IK, Lee WY. The effect of alcohol treatment in the preparation of  $MgCl_2$  support by a recrystallization method on the catalytic activity and isotactic index for propylene polymerization. *Eur Polym J.* 1996;32:405–10.
59. Quinet MLB. *Soc Chim Fr.* 1936;3:1829.
60. Emons HH, Pollmer K. Studies on systems of salts and mixed solvents. XXXI. On the solubility and solvation behaviour of magnesium chloride in mixed aqueous organic solvents. *Zeitschrift für anorganische und allgemeine Chemie.* 1985;521:224–30.
61. Gnanakumar ES, Gowda RR, Kunjir S, Ajithkumar TG, Rajamohanan PR, Chakraborty D, Gopinath CS.  $MgCl_2 \cdot 6CH_3OH$ : a simple molecular adduct and its influence as a porous support for olefin polymerization. *ACS Catal.* 2013;3:303–11.
62. Kabisch G, Bader I, Emons HH, Pollmer K. A Raman spectroscopic investigation of the structure of magnesium salt solutions in methanol and methanol-water mixtures. *J Mol Liq.* 1983;26:139–57.
63. Lloyd E, Brown CB, Bonnell DGR, Jones WJ. XC.—Equilibrium between alcohols and salts. Part II. *J. Chem. Soc. (Resumed).* 1928;658–66. <https://doi.org/10.1039/JR9280000658>
64. Radnai T, Kalman E, Pollmer K. X-ray diffraction study of  $MgCl_2$  in methanol. *Z Naturforsch Pt A.* 1984;39:464–70.
65. Simon SE. Über die Verbindungen des Chlorlithiums und des Chlormagnesiums mit Alkoholen. *Adv Synth Catal.* 1879;20:371–7.
66. Turova NY, Turevskaya EP. Alkoxy-magnesium halides. *J Organomet Chem.* 1972;42:9–17.
67. Nasirzadeh K, Zimin D, Neueder R, Kunz W. Vapor-pressure measurements of liquid solutions at different temperatures: apparatus for use over an extended temperature range and some new data. *J Chem Eng Data.* 2004;49:607–12.
68. Tewell CR, Malizia F, Ager JW, Somorjai GA. An ultraviolet–Raman spectroscopic investigation of magnesium chloride–ethanol solids with a 0.47 to 6 molar ratio of  $C_2H_5OH$  to  $MgCl_2$ . *J Phys Chem B.* 2002;106:2946–9.
69. Chadwick JC, Severn JR. Single-site catalyst immobilization using magnesium chloride supports. *Kinet Catal.* 2006;47:186–91.
70. Bart JCJ, Roovers W. Magnesium chloride-ethanol adducts. *J Mater Sci.* 1995;30:2809–20.
71. Di Noto V, Zannetti R, Vivani M, Marega C, Marigo A, Bresadola S.  $MgCl_2$ -supported Ziegler–Natta catalysts: a structural investigation by X-ray diffraction and Fourier-transform IR spectroscopy on the chemical activation process through  $MgCl_2$ -ethanol adducts. *Macromol Chem Phys.* 1992;193:1653–63.
72. Malizia F, Fait A, Cruciani G. Crystal structures of Ziegler–Natta catalyst supports. *Chem Eur J.* 2011;17:13892–7.
73. Jiang X, Tian X, Fan Z. Crystal structure of ball-milled mixture of sodium chloride and magnesium chloride–ethanol adduct. *Mater Res Bull.* 2008;43:343–52.
74. Taveira Magalhaes DN, Do Coutto Filho O, Coutinho FMB. Ziegler–Natta catalyst for ethylene and propylene polymerization supported on adducts of magnesium chloride with methyl and ethyl alcohols. *Eur Polym J.* 1991;27:827–30.
75. Thushara KS, Gnanakumar ES, Mathew R, Ajithkumar TG, Rajamohanan PR, Bhaduri S, Gopinath CS.  $MgCl_2 \cdot 4((CH_3)_2CHCH_2OH)$ : a new molecular adduct for the preparation of  $TiCl_4/MgCl_2$  catalyst for olefin polymerization. *Dalton Trans.* 2012;41:11311–8.
76. N'Tsoukpoe KE, Schmidt T, Rammelberg HU, Watts BA, Ruck WK. A systematic multi-step screening of numerous salt hydrates for low temperature thermochemical energy storage. *Appl Energy.* 2014;124:1–16.
77. Jin M, Sun Y, Li P, Yu J, Ulrich J. The thermal decomposition study of  $MgCl_2 \cdot 6H_2O \cdot 1.4-C_4H_8O_2$ . *Chem Eng Res Des.* 2015;104:256–63.
78. Galwey AK, Laverty GM. The thermal decomposition of magnesium chloride dihydrate. *Thermochim Acta.* 1989;138:115–27.
79. Huang Q, Lu G, Wang J, Yu J. Mechanism and kinetics of thermal decomposition of  $MgCl_2 \cdot xH_2O$ . *Metall Mater Trans B.* 2010;41:1059–66.
80. Bukhanko N, Samikannu A, Larsson W, Shchukarev A, Leino AR, Kordás K, Warna J, Mikkola JP. Continuous gas-phase synthesis of ethyl chloride from ethyl alcohol and hydrochloric acid over  $Al_2O_3$  based catalysts: the “green” route. *ACS Sustain Chem Eng.* 2013;1:883–93.
81. Huang Q, Lu G, Wang J, Yu J. Thermal decomposition mechanisms of  $MgCl_2 \cdot 6H_2O$  and  $MgCl_2 \cdot H_2O$ . *J Anal Appl Pyrol.* 2011;91:159–64.
82. Wagman DD, Evans WH, Parker VB, Schumm RH, Halow I. The NBS tables of chemical thermodynamic properties. Selected values for inorganic and C1 and C2 organic substances in SI units. National Standard Reference Data System, 1982.

**Publisher's Note** Springer Nature remains neutral with regard to jurisdictional claims in published maps and institutional affiliations.

## 8. Paper VI

Available online at [www.sciencedirect.com](http://www.sciencedirect.com)

ScienceDirect

Energy Procedia 105 (2017) 4363 – 4369

Energy  
ProcediaThe 8<sup>th</sup> International Conference on Applied Energy – ICAE2016

## Micro-scale thermodynamic and kinetic analysis of a calcium chloride methanol system for process cooling

Kathrin Korhammer<sup>a\*</sup>, Karsten Neumann<sup>a</sup>, Oliver Opel<sup>a</sup>, Wolfgang K.L. Ruck<sup>a</sup><sup>a</sup>Leuphana University of Lüneburg, Scharnhorststraße 1, 21335 Lüneburg

### Abstract

Calcium chloride methanol addition compounds are promising sorbent candidates, which can not only be used for thermal energy storage but also for providing evaporative cooling in industrial applications using low-grade heat. The methanolate dissociation occurs within the working temperature range of low temperature cooling systems. Methanol has a low freezing point and high operating pressure and is less toxic and corrosive than ammonia as refrigerant. In solid-gas reactions the overall specific cooling capacity mainly depends on the sorption rate of the reaction. In general the reaction pattern follows a complex mechanism, in which the formation of intermediate phases and structural changes might occur. In this study a comprehensive micro-scale analysis on the effect of the methanol partial pressure, the thermal history of the calcium chloride, the dissociation temperature and subsequent sorption-desorption cycling on the sorption rate has been carried out. Results show that thermodynamic conditions as well as the thermal history and physicochemical properties of the material have a great influence on the sorption rate, whereas only a marginal dependence between the regeneration temperature and the sorption process was observed.

© 2017 The Authors. Published by Elsevier Ltd. This is an open access article under the CC BY-NC-ND license (<http://creativecommons.org/licenses/by-nc-nd/4.0/>).

Peer-review under responsibility of the scientific committee of the 8th International Conference on Applied Energy.

*Keywords:* Refrigeration, calcium chloride, methanol, TGA/DSC, kinetics, cycle stability

### 1. Introduction

Continuously increasing anthropogenic emissions contribute substantially to global warming. A major cause of rising global temperatures are CO<sub>2</sub> emissions emitted from industrial process refrigeration and air-conditioning. For process cooling conventional vapour compression refrigeration systems are most commonly being used, which are energy intensive and usually contain the environmentally critical and

\* Corresponding author. Tel.: +49-4131-677-1768; fax: +49-4131-677-2822.  
E-mail address: [kathrin.korhammer@leuphana.de](mailto:kathrin.korhammer@leuphana.de).

hazardous refrigerant hydrofluorocarbons (HFCs). In 2015, the European Union has adopted a new regulation on the restriction and limitation of the consumption of these fluorinated gases (F-gases) favouring the use of alternative, climate-friendly refrigerants [1]. The challenge of heat and fluorinated greenhouse gas reduction can be addressed by supplying cooling energy produced from waste heat-driven chemisorption systems. These systems, which are based on reversible chemical solid-gas reactions, demonstrate superior advantages compared with vapour compression, physisorption and absorption technologies [2,3]. The most widely and comprehensively studied alternative cooling systems have been adsorption refrigeration machines that use physisorption processes [2]. Physisorption or physical adsorption is generated by van der Waals forces. These are induced by dipole interactions between the molecules of the working fluid (adsorbate) and the surface of the polar substance (adsorbent). Physisorption results in weak, long-range attractive forces and low interaction energies and accordingly to low cooling capacities. Typical physisorption adsorbent materials are synthetic silica gels and zeolites. However, chemisorption is associated to strong chemical, short-range bonding resulting in the formation of stable adsorbate-adsorbent complexes. The observed enthalpies of formation and associated cooling capacities are comparatively high. The most common applied sorbents are metal halides such as calcium chloride. Chemisorption machines feature flexible operating conditions, low regeneration temperatures, non-delayed and time-decoupled supply of cooling [4]. Due to optional modular configuration and few moving parts these systems are easy-to-transport and highly attractive for both stationary and mobile applications. Additionally, the use of chemisorption systems can improve the energy efficiency by combining the production of heat and cold energy in integrated systems. At present no chemical-reaction-based refrigeration machine is commercially available [5]. Closed thermochemical sorption refrigeration machines basically consist of a sorption-desorption cycle. During the sorption phase, the refrigerant is chemically bound to the solid sorbent. This exothermic process is also referred to as discharging mode as the heat of reaction is released which causes a pressure drop within the system. As a result the fluid evaporates and absorbs surrounding heat below the ambient temperature producing a refrigerating effect. In the reverse process, which has an endothermic character, the sorption material can be regenerated by using low-level heat. Separation of the reaction products guarantees loss-free and infinite energy storage. Various reaction system types have been investigated in the last decades [3,6]. Data on the sorption-desorption characteristics of inorganic metal salt/ammonia systems are widely available at micro- and macro-scale, whereas the reaction of salts with alcohol has only been studied in casual manner. In cold energy storage the major system performance indicators for identifying and comparing different reaction system types at material level are the refrigerant uptake, the sorption rate, the energy storage capacity and the so-called specific cooling power (SCP). Systems using chemical reactions exhibit the highest cooling capacity among the various refrigeration systems as chemisorption involves higher energy compared to absorption and physisorption because of the associated formation of chemical bonds. Since chemical reactions generally follow a complex reaction mechanism proceeding via intermediate phases and are mainly affected by the reaction temperature, the partial pressure of the reactant and the alcoholate state, possible morphological and structural changes might occur during subsequent sorption-desorption cycling [7,8]. These changes might distinctively influence the kinetics and reversibility of the reaction. This paper will focus on a comprehensive micro-scale analysis of the dependency of the partial pressure, the dissociation temperature and the nature and thermal history of the reaction pair calcium chloride and methanol on the sorption kinetics under practical conditions. Cycle-dependent changes in the alcohol sorption and associated enthalpies of reaction were measured and compared. In a short-term cycling test the stability of the chosen reaction pair was evaluated.

## 2. Experimental section

### 2.1. Materials

The tested substances calcium chloride (Merck) and methanol (Merck) were waterfree and of high purity grade (Ph.Eur.). Methanol (CH<sub>3</sub>OH) was selected as refrigerant due to its high operating pressure, low regeneration temperature and low freezing point, which are necessary for cold storage applications. Moreover, CH<sub>3</sub>OH is a strong Lewis base with a high affinity to metal salts and less steric effects than other straight-chain primary alcohols such as ethanol or propanol. Calcium chloride (CaCl<sub>2</sub>) was selected as it is inexpensive, easily available and chemically stable. The methanolate dissociation occurs within the working temperature range of low temperature cooling systems. Calcium halides are soft Lewis acids and hence form with alcohol, analogous to salt hydrates, strong salt-alcohol complexes.

### 2.2. Characterisation

Thermal behaviour, sorption kinetics and cycle stability of CaCl<sub>2</sub>-CH<sub>3</sub>OH addition compounds were investigated using thermogravimetric analysis (TGA) and differential scanning calorimetry (DSC) techniques. A modified TGA/DSC 1 device from Mettler Toledo was used for all measurements. CH<sub>3</sub>OH sorption and desorption involve changes in sample weight and enthalpy over time that can simultaneously be detected and recorded with high precision. The TGA/DSC was connected to a bubbler system in order to measure dynamic methanol vapour sorption. A thermostat maintained the water bath of the bubbler system at a constant temperature of 21 °C. For sorption experiments dry nitrogen was used as carrier gas and purged through the bubbler system to produce a CH<sub>3</sub>OH-saturated nitrogen flux. The flow rates and hence the CH<sub>3</sub>OH partial pressures ( $p_{CH_3OH}$ ) were regulated by an external gas controller. During both sorption and desorption runs the whole apparatus was flushed with dry nitrogen. Specimen of 10 mg were evenly placed into a 70 µl alumina crucible and characterised with different temperature programmes. Sorption equilibrium tests were carried out at 25 °C at three different CH<sub>3</sub>OH partial pressures ( $p_{CH_3OH} = 6.8/8.2/9.1$  kPa) over 240 min. The dissociation pattern was studied by scanning the samples from 25 °C to 150 °C. In a quick multi-step screening the influence of the regeneration temperature on the CH<sub>3</sub>OH sorption characteristics and sorption kinetics was determined. The discharging-charging process consisted of the following segments: (1) discharging at 25 °C, (2) charging at 90 °C, (3) discharging at 25 °C, (4) charging at 100 °C, (5) discharging at 25 °C and (6) charging at 150 °C. The discharging time was set to 60 min and the  $p_{CH_3OH}$  was maintained at 6.8 kPa. The short-term cycling test was performed at the same sorption conditions as the multi-step screening. In the desorption behaviour study the temperature was elevated to 180 °C, which equals the maximum temperature available under field conditions. The same heating rates (3.0 K/min) were applied to each desorption measurement. The CH<sub>3</sub>OH uptake and the specific cooling power were calculated from the weight gain and weight gain rate (in the following also referred to as sorption rate). The cooling capacity was derived from the manual integration of the heat fluxes as a function of time using the Mettler Toledo STARe. Software 11.00a.

## 3. Results and discussion

In sorption equilibrium tests the maximum sorption of CaCl<sub>2</sub> towards CH<sub>3</sub>OH was determined. The total amount of sorbed CH<sub>3</sub>OH was calculated to be around 3 mol per mol anhydrous CaCl<sub>2</sub>, wherein only 2 mol of CH<sub>3</sub>OH are strongly coordinated to 1 mol of anhydrous CaCl<sub>2</sub>. About 1 mol is physically attached to the CaCl<sub>2</sub> surface. The experimental percentage weight losses are close to the theoretical values. The proposed chemical composition is therefore CaCl<sub>2</sub>·2CH<sub>3</sub>OH, which is in accordance with the literature [9,10]. CaCl<sub>2</sub> is a hygroscopic substance with a high deliquescence in an alcohol saturated atmosphere and therefore tends to an over-stoichiometric uptake of CH<sub>3</sub>OH. A thermodynamic control of the reaction is mandatory and can be achieved by choosing an appropriate pressure-temperature

relationship and reaction time. The methanolate decomposition ranges from 80-143 °C. Between 75-85 % of the total weight is lost below 118 °C with peak temperatures around 100 °C. Two overlapping decomposition stages are observed. Tailing indicates the removal of both non-coordinated and coordinated methanol below 80 °C. By applying lower heating rates or working under vacuum, the peaks temperature could be shifted towards lower regeneration temperatures. The specific cooling power is defined as the capacity of a system to produce a refrigerating effect in relation to the initial sorbent weight and was estimated from the maximum sorption rate. The maximum sorption rate was derived from the first derivative of the weight loss curve. In Fig. 1 the sorption rate was plotted against the extent of conversion. For a better comparison the conversion is related to a total sorption of 2 mol of CH<sub>3</sub>OH per mol CaCl<sub>2</sub> for each sample measured. It can be seen that the higher CH<sub>3</sub>OH partial pressure, the higher the sorption rate. The reaction can be accelerated so that the maximum chemical sorption is reached in a shorter time. In the initial phase the sorption rate rapidly increases over a narrow time frame and drops quickly. In the further course of the reaction the sorption rate increases only slightly and finally gradually decreases until the chemical reaction is completed. The sorption of CH<sub>3</sub>OH on CaCl<sub>2</sub> might follow a 2-step process as two sorption rate peaks can be observed. According to the experimental data a polynomial relation between the sorption rate and the CH<sub>3</sub>OH partial pressure is assumed. The decelerated course of the sorption towards the end of the reaction might indicate a temperature gradient and heat transfer limitation. The sorption rate also depends on various other variables such as the sample's initial weight, structure, particle size, thermal history and porosity that might have different effects. In a comparative study the influence of the pre-treatment method on the CH<sub>3</sub>OH uptake at 6.8 kPa was evaluated and is also shown in Fig. 1. Heating the sample slows down the sorption reaction resulting in a lower sorption rate and also a more stable final CaCl<sub>2</sub>-CH<sub>3</sub>OH-adduct as less physisorption is observed compared to the untreated starting material. For further investigations a CH<sub>3</sub>OH partial pressure of 6.8 kPa was chosen as the corresponding temperature is equal to the condenser temperature.

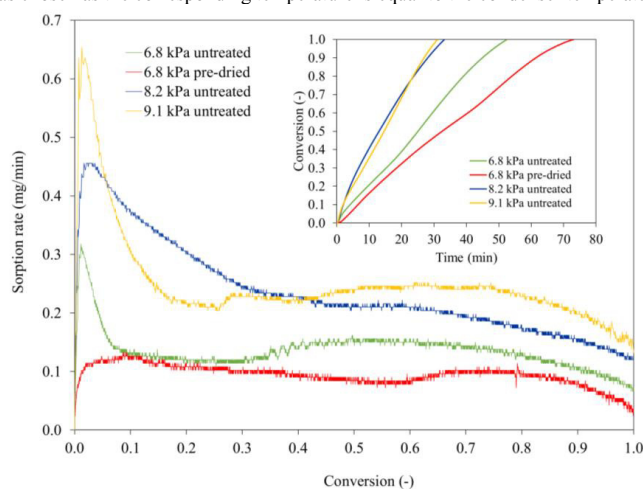


Fig. 1. The change in the sorption rate over the course of a reaction (extent of conversion) at different CH<sub>3</sub>OH partial pressures.

The effect of the desorption temperature, also referred to as regeneration temperature, was examined in a quick multi-step screening. The sample as received without any thermal pre-treatment was used. The CH<sub>3</sub>OH sorption is constant over the first two cycles. As part of the sorbed CH<sub>3</sub>OH is released during stabilisation at 25 °C physical sorption seems to appear. In the last cycle a slightly lower CH<sub>3</sub>OH uptake was measured. In total, sorption and desorption values are equal. Despite not being fully demethanolated the re-uptake of CH<sub>3</sub>OH is the same in each cycle which leads to the assumption that an equilibrium state has been reached under the applied measurement conditions. Below 90 °C and 100 °C the CaCl<sub>2</sub>·nCH<sub>3</sub>OH decomposes in one endothermic stage with a peak temperature at 83 °C and 99 °C, respectively, whereas above 100 °C two stages are present as aforementioned. The associated peak temperatures are 94 °C and 135 °C. The sorption rates (0.19/0.21/0.20 mg/min) are constant over three cycles, but appear to be slightly lower than the ones measured in the equilibrium test. Therefore the corresponding calculated cooling capacities were respectively lower. Other variables such as the initial sample mass and its porosity might also account for the lower value. The data reveals that the regeneration temperature affects the sorption rate only marginally. In order to validate this hypothesis a detailed characterization was carried out. The short-term performance of the CaCl<sub>2</sub>-CH<sub>3</sub>OH-adduct was tested in a cycle stability test consisting of 18 consecutive sorption-desorption cycles. Information on the cycling behaviour is of great importance as changes in the morphology and coordination structure of the methanolate and physical effects such as solvation and aggregation might occur that probably affect the sorption kinetics. The sample was dried at 105 °C prior to cycling. Due to the thermal pre-treatment the sample had to be activated resulting in an increase of the CH<sub>3</sub>OH-sorption over the first few cycles. As the amount of chemically and physically sorbed CH<sub>3</sub>OH varies greatly at the beginning, the formation of metastable phases is assumed. Non-coordinated CH<sub>3</sub>OH is evolved during stabilisation until a chemical equilibrium is reached and desorption begins. From the 10<sup>th</sup> cycle onwards sorption and desorption are constant and the amount of physically sorbed CH<sub>3</sub>OH is reduced. Even though the sorption reaction proceeds fast at the beginning of the methanolation phase indicated as a steep curve. The reaction decelerates with time and with higher extent of conversion. The high desorption temperature of 180 °C probably has only a marginal effect on the sorption characteristics and the sorption rate as seen in Fig. 2.

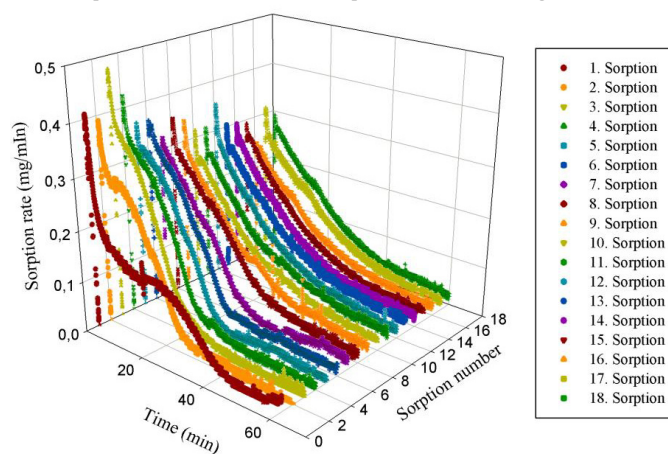


Fig. 2. Change of the sorption rate with subsequent short-term sorption-desorption cycling.

In the first and second sorption process the CH<sub>3</sub>OH uptake is lower compared with the third one, in which the highest sorption rate is attained. The subsequent maximum methanolation rates are ranging from 37-29 mg/min and show apparently a decreasing tendency with increasing number of cycles despite constant initial sample. The results indicate that cooling can be provided at a constant level at least during the initial discharging-charging cycles. The decomposition pattern, however, is inconsistent. The decomposition peaks vary within a narrow range from cycle to cycle and seem to be shifted with further cycling.

#### **4. Conclusion**

The usability of calcium chloride methanolates has been tested under different experimental conditions. Performance criteria such as methanol uptake, cooling capacity, sorption rate and sorption cooling power remarkably depend on the material's physical properties, nature and thermal history, surface phenomena and process conditions. In solid-gas reactions the sorption rate can be lifted by applying higher methanol partial pressures. It could be shown that the sorption rate of the initial sample is slow and increases with cycling until a constant value with little deviation is reached and proceeds with a decreasing tendency. The desorption temperature seems to have no significant influence on the sorption rate. Substitution of coordinated methanol molecules by water molecules in salt methanolates was considered to be neglected at micro-scale in this study. In laboratory scale investigation the test reactor system should be hermetically sealed.

#### **Acknowledgements**

This study was conducted within the framework of a ZIM project. The authors sincerely thank the German Federal Ministry of Economic Affairs and Energy for funding.



## References

- [1] [http://ec.europa.eu/clima/policies/f-gas/index\\_en.htm](http://ec.europa.eu/clima/policies/f-gas/index_en.htm), visited on 14/02/16.
- [2] Qun C, Gang T, Haijun C, Xinyue G, Huqing Y. Environmentally benign working pairs for adsorption refrigeration, *Energy*, Volume 30, Issues 2–4, February–March 2005, Pages 261–271, ISSN 0360-5442.
- [3] Gordeeva, Larisa G.; Freni, Angelo; Restuccia, Giovanni; Aristov, Yuri I. (2007): Influence of Characteristics of Methanol Sorbents “Salts in Mesoporous Silica” on the Performance of Adsorptive Air Conditioning Cycle. In: *Ind. Eng. Chem. Res* 46 (9), S. 2747–2752. DOI: 10.1021/ie060666n.
- [4] Wang LW, Bao HS, Wang RZ (2009): A comparison of the performances of adsorption and resorption refrigeration systems powered by the low grade heat. In: *Renewable Energy* 34 (11), S. 2373–2379. DOI: 10.1016/j.renene.2009.02.011.
- [5] Bundesministerium für Wirtschaft & Technologie BMWi (Hg.) (2014): Zahlen und Fakten. Energiedaten. Nationale und Internationale Entwicklung. Bundesministerium für Wirtschaft & Technologie BMWi. Online available on <http://www.bmwi.de/DE/Themen/Energie/energiedaten.html>.
- [6] Offenhartz PD, Brown FC, Mar RW, Carling RW. A Heat Pump and Thermal Storage System for Solar Heating and Cooling Based on the Reaction of Calcium Chloride and Methanol Vapor. *ASME. J. Sol. Energy Eng.* 1980;102(1):59-65. doi:10.1115/1.3266123.
- [7] Stanish, M. A. and Perlmutter, D. D. (1984), Rate processes in cycling a reversible gas-solid reaction. *AIChE J.*, 30: 56–62. doi:10.1002/aic.690300110.
- [8] Bart, J. C. J.; Roovers, W. (1995): Magnesium chloride - ethanol adducts. In: *Journal of Materials Science* 30 (11), S. 2809 – 2820. DOI: 10.1007/BF00349648.
- [9] Carling RW, Wondolowski AT, Macmillan DC. Enthalpy of formation of CaCl<sub>2</sub>·2CH<sub>3</sub>OH and CaCl<sub>2</sub>·2C<sub>2</sub>H<sub>5</sub>OH by solution calorimetry. *The Journal of Chemical Thermodynamics*, Volume 14, Issue 2, 1982, Pages 125–131, ISSN 0021-9614.
- [10] Iyimen-Schwarz, Z (1984): Energiespeicherung durch chemische Reaktionen. Dissertation. Osnabrück Universität, Osnabrück.



### Biography

Kathrin Korhammer is a PhD candidate at Leuphana University of Lüneburg. Her research focuses on the fundamentals of various salt-water and salt-alcohol systems as well as composite sorbents and binary mixtures for heating and cooling applications. She holds a degree in Chemical Engineering from KIT.

## **9. Paper VII**

Applied Energy 230 (2018) 1255–1278



Contents lists available at ScienceDirect

Applied Energy

journal homepage: [www.elsevier.com/locate/apenergy](http://www.elsevier.com/locate/apenergy)

## Thermodynamic and kinetic study of $\text{CaCl}_2\text{-CH}_3\text{OH}$ adducts for solid sorption refrigeration by TGA/DSC

Kathrin Korhammer<sup>a,\*</sup>, Karsten Neumann<sup>a</sup>, Oliver Opel<sup>a,b</sup>, Wolfgang K.L. Ruck<sup>a</sup>

<sup>a</sup> Leuphana University of Lüneburg, Scharnhorststraße 1, 21335 Lüneburg, Germany

<sup>b</sup> Westcoast University of Applied Sciences, Fritz-Thiedemann-Ring 20, 25746 Heide, Germany



### HIGHLIGHTS

- Thermal behavior and sorption characteristics of the  $\text{CaCl}_2\text{-CH}_3\text{OH}$  system are studied by TGA/DSC.
- SCPs and COPs are derived from thermogravimetric data.
- Cyclic reversibility is estimated in repeated methanolation/demethanolation cycles.
- Constant  $\text{CH}_3\text{OH}$  sorption and evolution of heat energy over cycling are observed.
- The working pair  $\text{CaCl}_2\text{-CH}_3\text{OH}$  possesses a good cyclability and reversible cooling output over 18 cycles.

### ARTICLE INFO

**Keywords:**  
Chemisorption refrigeration  
Calcium chloride  
Methanol  
TGA/DSC  
Kinetics  
Cycle stability

### ABSTRACT

Addition compounds of  $\text{CaCl}_2$  and  $\text{CH}_3\text{OH}$  are promising thermochemical materials for thermal energy storage and conversion. Achievable evaporation temperatures lie within the operating range of standard building and industrial refrigeration applications. In heterogeneous gas–solid reactions the cooling power of the respective reaction pair is mainly dependent on the uptake rate of the gaseous reactant. In this paper, a comprehensive study on the influence of various procedural parameters and thermal cycling on the cooling efficiency performance of  $\text{CaCl}_2$  methanolates was carried out at material scale to provide insights on application design principles. SCPs and cooling COPs were calculated from experimental data obtained by simultaneous TGA/DSC. SCPs, averaged over a methanolation time of 60 min, varied between 157 W/kg and 366 W/kg, whereas maximum SCPs reached values between 232 W/kg and 1029 W/kg depending on methanol partial pressure. The results indicate possible applications with evaporator temperatures around 10 °C, as for the cooling of buildings. COPs were within the range of 0.59 and 0.76. Results showed that thermodynamic conditions and thermo-physical properties of the material had a great impact on the methanolation/demethanolation reaction kinetics. Under periodic conditions a slight attenuation of the maximum cooling power was observed, whilst the more practically relevant average SCP was stable over a number of 18 cycles. With respect to application design, different regeneration (demethanolation) temperatures as well as the impact of the thermal history of the material were investigated. The reaction pair can also be used with regeneration temperatures of  $\leq 100$  °C.

### 1. Introduction

Continuously increasing anthropogenic greenhouse gases contribute substantially to global warming. A major cause of rising global temperatures are  $\text{CO}_2$  emissions [1], i.e. emitted from electricity-driven industrial process refrigeration and air conditioning. For process cooling, conventional vapor compression refrigeration systems are most frequently used, which are energy-intensive and usually contain environmentally critical and hazardous refrigerants. Stricter

environmental policies aim at phasing out ozone-depleting and high global-warming-potential (CFCs, HCFCs, HFCs) refrigerants. In 2015, the EU has adopted a new regulation on the restriction and limitation of the consumption of these fluorinated gases enforcing the use of climate-friendly, less or zero detrimental substitutes [2]. The challenge of well-conceived energy consumption and  $\text{CO}_2$  mitigation can be addressed by supplying cold energy produced from thermally-driven sorption systems. Sorption refrigeration technologies powered by low-grade temperature sources, encompassing i.e. biomass, waste heat or solar and

\* Corresponding author.

E-mail address: [korhammer@leuphana.de](mailto:korhammer@leuphana.de) (K. Korhammer).

<https://doi.org/10.1016/j.apenergy.2018.08.100>

Received 19 September 2017; Received in revised form 16 August 2018; Accepted 17 August 2018  
0306-2619/ © 2018 Elsevier Ltd. All rights reserved.

Nomenclature			
<b>Abbreviations</b>		$M_{\text{methanolate}}$	molar mass of the respective methanolate (g/mol)
DSC	differential scanning calorimetry	dm/dt	methanolation rate/demethanolation rate (mg/min)
G	gas phase	$m(t)$	sample mass at reaction time $t$ (mg)
Max	maximum	$N$	level of methanolation/methanolation state (1)
S	solid phase	$n_{\text{CaCl}_2}$	amount of calcium chloride anhydride (mol)
TCM	thermochemical material	$n_{\text{CH}_3\text{OH}}$	amount of methanol (mol)
TGA	thermogravimetric analysis	$p_{\text{reactive}}$	partial pressure of reactive gas (kPa)
<b>Latin symbols</b>		$p_{\text{MeOH}}$	partial vapor pressure of methanol (kPa)
COP	coefficient of performance (1)	$p_{\text{MeOH,S}}$	saturation vapor pressure of methanol (kPa)
$\Delta_r H$	molar enthalpy of reaction (kJ/mol)	$p_{\text{N}_2}$	partial pressure of nitrogen protective gas (kPa)
$\Delta_r H/N$	molar enthalpy of reaction per mole methanol (kJ/mol)	SCP	specific cooling power (W/kg)
$\Delta_r h$	specific enthalpy of reaction (J/g)	$t$	time (min)
$\Delta_r h_{\text{CH}_3\text{OH}}$	molar latent heat of vaporization of methanol (kJ/mol)	$T$	thermodynamic temperature (K)
$\Delta_r h_{\text{CH}_3\text{OH}}$	specific latent heat of vaporization of methanol (J/g)	$w_{\text{CH}_3\text{OH}}$	mass fraction of methanol (%)
$m$	sample mass (mg)	<b>Greek symbols</b>	
$m_0$	initial sample mass (mg)	$\alpha(t)$	extent of conversion (1)
$m_1$	final sample mass (mg)	d $\alpha$ /dt	reaction rate (1/s)
$m_{\text{CaCl}_2}$	mass of calcium chloride anhydride (mg)	$\phi$	heat flux (mW)
$M_{\text{CaCl}_2}$	molar mass of calcium chloride anhydride (g/mol)	$\vartheta$	celsius temperature (°C)
$m_{\text{CH}_3\text{OH}}$	mass of methanol (mg)	$\vartheta_{\text{evap}}$	evaporation temperature (°C)
$M_{\text{CH}_3\text{OH}}$	molar mass of methanol (g/mol)	$\vartheta_{\text{cond}}$	condensation temperature (°C)
		$\vartheta_{\text{reg}}$	regeneration temperature (°C)
		$\vartheta_{\text{peak}}$	peak temperature (°C)

geothermal energy, include a broad spectrum of technical applications such as dehumidification, air conditioning, food and medicine chilling and preservation, electronic appliance and data center cooling, etc. The type of application specifies the operating temperature range of the device and delimitates the choice of the respective refrigerant.  $\text{NH}_3$ ,  $\text{C}_2\text{H}_5\text{OH}$ ,  $\text{CH}_3\text{OH}$ , and  $\text{H}_2\text{O}$  are favored refrigerants [3]. Due to their high latent heat of vaporization, they are remarkably energy efficient.  $\text{NH}_3$ , for example, can provide average refrigerating temperatures between  $-20^\circ\text{C}$  and  $-10^\circ\text{C}$ .  $\text{H}_2\text{O}$  is preferably used for conventional cooling and air conditioning, because of its low vapor pressure.  $\text{C}_2\text{H}_5\text{OH}$  and  $\text{CH}_3\text{OH}$  are suitable for applications operating below the freezing point of  $\text{H}_2\text{O}$  and subatmospheric conditions; they are less toxic and corrosive than  $\text{NH}_3$  as refrigerant. Very low refrigeration temperatures can be produced by implementing advanced reactor concepts like cascading or multi-mode cycles.

Sorption systems are classified by their working principle into four categories: (i) liquid absorption, (ii) solid adsorption, (iii) thermochemical, and (iv) composite sorbent refrigeration [4,5]. Liquid absorption refrigeration is based on physical processes, wherein liquid adsorbents such as concentrated salt solutions are used instead of solid adsorbents [6]. According to standard classifications and terminologies established in this field of research, physisorption and chemisorption in

gas-solid reactions are termed thermochemical [7], even though physisorption processes involve no chemical bonding compared to chemisorption processes [8]. Since  $\text{H}_2\text{O}$  or  $\text{R-OH}$ , in case of crystalline salt hydrates or salt alcoholates, can be incorporated into the crystal lattice, chemisorption is occasionally denoted by the controversial term “solid absorption”. The prospective aqueous complexes usually have an odd number of ligands. In this paper, “chemisorption” and “thermochemical” are used interchangeably. A comparison of the features of different refrigeration principles is given in Table 1. Chemisorption systems based on reversible chemical gas-solid reactions have several remarkable advantages over conventional vapor compression, solid adsorption, and liquid absorption refrigeration technologies [9–13]. They feature flexible operating conditions, low regeneration temperatures, and non-delayed, time-decoupled supply of cooling. Due to optional modular configuration and few moving parts, these systems are easy-to-transport and highly attractive for both stationary and mobile applications.

### 1.1. Literature review

The utilization of solid sorption refrigeration systems dates back to the 19th century. A chemisorption system using the working pair  $\text{AgCl}$ -

**Table 1**  
Comparison of common refrigeration systems.

	Vapor compression refrigeration	Liquid absorption refrigeration	Solid adsorption refrigeration	Thermochemical refrigeration
Operating principle	Mechanical	Physisorption	Physisorption	Chemisorption
Temperature range	$\geq -60^\circ\text{C}$	$-25^\circ\text{C}$ to $15^\circ\text{C}$	$-10^\circ\text{C}$ to $15^\circ\text{C}$	$-20^\circ\text{C}$ to $15^\circ\text{C}$
Operating mode	Electrical energy	Low-/medium-grade heat	Low-/medium-grade heat	Low-/medium grade heat
Storage potential	No	Low	Medium	High
Mobile application	No	Low	Low	Yes
Size	Large	Large	Large	Compact
Moving parts	Many	Few	Few	Few
Modular construction	No	Critical	Yes	Yes
Investment costs	Low	High	High	Low
Operating costs	High	Low	Low	Low
Maintenance requirements	High	Low	Low	Low

NH<sub>3</sub> has already been introduced in 1848 by Faraday [14]. In the following decades, physisorption systems have attracted notable attention. Vital research has been carried out at renowned research institutes worldwide, including the Institute of Refrigeration and Cryogenics at the Shanghai Jiao Tong University, China, the Borekov Institute of Catalysis, Russia, and the School of Engineering at the University of Warwick, UK. A plethora of reviews on chemical heat pumps and solid adsorption refrigeration technologies exists. Wang and Oliveira [15] give an overview of various physisorption refrigeration systems at prototype level, including commercially manufactured adsorption chillers that have been developed in the last 50 years, and compare the efficiency performance of selected examples. Monocycle systems with H<sub>2</sub>O or CH<sub>3</sub>OH as refrigerant and activated carbon, zeolite, and silica gel as physical adsorbent achieved rather low SCPs (20 W/kg to 108 W/kg) and COPs (0.1–0.6). In a further review, Wang et al. [16] summarized work on physical adsorption systems addressing performance deterioration by improving system design and cycle mode. The implementation of dual-mode cycles with heat and/or mass recovery, cascading cycles, and advanced adsorption materials had a positive impact on the cooling effectiveness of the developed systems [17]. Wongsuwan et al. [10] presented a systematic review of the technology status, current application areas, and future trends of chemical heat pumps. Cot-Gores et al. [5] have also reviewed thermochemical cooling systems with focus on NH<sub>3</sub> and H<sub>2</sub>O as refrigerating fluid.

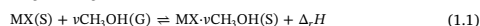
At present, solid adsorption refrigeration machines that use physisorption processes have been the most extensively investigated and implemented alternative refrigeration systems. Common physical adsorbents are activated carbons, activated carbon fibers, carbons, silica gels, molecular sieves, and metal organic frameworks. Among the diverse combinations of physical adsorbents and refrigerants, the adsorption working pairs silica gel/CH<sub>3</sub>OH [18], silica gel/H<sub>2</sub>O [19,20,21–29], activated carbon/NH<sub>3</sub> [30,31], activated carbon/C<sub>2</sub>H<sub>5</sub>OH [32–35], activated carbon/CH<sub>3</sub>OH [21,36–40], activated carbon fiber/NH<sub>3</sub> [41], carbon/ammonia [42–45], zeolite/CH<sub>3</sub>OH [39,46], zeolite/H<sub>2</sub>O [47–54], metal organic framework/C<sub>2</sub>H<sub>5</sub>OH [55], metal organic framework/CH<sub>3</sub>OH [56–58], and metal organic framework/H<sub>2</sub>O [57,59] have elicited great interest and been tested at material, laboratory, and pilot-plant scale. Among various inorganic salts, metal halides such as CaCl<sub>2</sub>, LiCl, LiBr, and SrBr<sub>2</sub> have been identified as promising TCMs for thermal energy storage. Research is still in its infancy, and only some prototypes have been developed so far. Inorganic salts that react with NH<sub>3</sub> have been thoroughly investigated for conventional adsorption cycle chemical heat pumps [60–67]. In chemical heat pumps based on the resorption thermochemical process a low temperature reactive salt bed (LTS) or a medium temperature reactive salt bed (MTS) and a high temperature reactive salt bed (HTS) are combined [68–71], instead of using a single bed reactor connected to an evaporator/condenser unit. This configuration minimizes safety risks, which might arise from the high pressure of the refrigerant. Attempts have been made to modify pure salts with the aim of tuning their thermophysical properties and enhancing the overall mass and heat transfer at different system levels. The usability of salts confined to porous supporting structures such as silica gel [72–76], MCM [77], zeolite [73,78–81], clay [82,83] as well as activated carbon [74,84–89], carbon fiber, carbon nanotube [60,90–93], expanded graphite [60,91,94–99], alumina [76,90], and metal organic framework [100] has been extensively studied by various researchers. Different approaches in composite preparation are prevalent among which the incipient wetness impregnation has been most frequently employed.

Chemical- and compound adsorbents paired with CH<sub>3</sub>OH for application in adsorption refrigeration systems have been scarcely investigated. In the 1980s, Offenhartz et al. [101] have carried out a fundamental study on the sorption equilibrium of CaCl<sub>2</sub> methanolate by thermogravimetric and XRD analysis and tested their feasibility for heating and cooling processes in a laboratory test rig. First subatmospheric thermal cycling experiments at material scale have been

performed by Iyimen-Schwarz [102] using DSC. Iyimen-Schwarz [102] has determined the thermal efficiency of the CaCl<sub>2</sub>-CH<sub>3</sub>OH system from the ratio of the formation enthalpy to the dissociation enthalpy. Lai and Li [103] have studied the system performance of a periodic flow reversal fixed-bed reactor utilizing CaCl<sub>2</sub> and CH<sub>3</sub>OH as working pair. Results of numerical simulations showed that significant improvement could be achieved with respect to existing traditional cycle operations of chemical heat pumps. Since heat transfer characteristics are also indispensable for designing prototype reactors, a thorough study on the changes in the thermophysical properties of the reaction pair CaCl<sub>2</sub>-CH<sub>3</sub>OH in a packed bed reactor has been conducted by Hirata and Fujioka [104]. The effective thermal conductivity of pure and reacted CaCl<sub>2</sub> is very low. For enhancing the thermal conductivity and thus intensifying the heat transfer, Fujioka et al. [91] have combined CaCl<sub>2</sub> with activated carbon and expanded graphite. Due to the heat promoting effect and porous structure of the matrices, the thermal conductivity could be improved and less volume expansion and contraction occurred. Gordeeva et al. [105] have synthesized various CH<sub>3</sub>OH sorbents “salts in mesoporous silica” for adsorption air conditioning, which showed higher sorption capacities than conventional physical CH<sub>3</sub>OH sorbents like activated carbon or zeolite. The best sorption efficiencies have been obtained with LiBr-based composites. Aristov et al. [106] have examined the CH<sub>3</sub>OH sorption of two types of mesoporous silica gel with different pore diameters (6 nm (S6) and 15 nm (S15)) that were impregnated with CaCl<sub>2</sub>. They have discovered profound differences in the CH<sub>3</sub>OH uptake depending on the pore diameter. The formation of solid crystalline CaCl<sub>2</sub> dimethanolate was observed in the S15 silica gel at low CH<sub>3</sub>OH vapor pressures, whereas the formation of a CaCl<sub>2</sub>-containing CH<sub>3</sub>OH solution occurred at higher CH<sub>3</sub>OH vapor pressures. The absence of a sorption plateau of the S6 silica gel hypothesis that a solid crystalline CaCl<sub>2</sub> methanolate phase coexisted with a CaCl<sub>2</sub>-CH<sub>3</sub>OH solution over the CH<sub>3</sub>OH vapor pressure range studied.

### 1.2. Thermochemical refrigeration

A closed thermochemical refrigeration system basically consists of a thermodynamic cycle. A detailed explanation of a basic thermodynamic cycle is given by Cot-Gores et al. [7] and Lai and Li [103]. The cycle can be described with the following generic equation for reversible heterogeneous gas-solid reactions:



wherein  $v$  is the stoichiometric coefficient. During the association reaction the gaseous reactant CH<sub>3</sub>OH is chemically bound to the solid reactant MX forming the solid product MX· $v$ CH<sub>3</sub>OH. This exothermic process is also referred to as discharging mode in which the stored heat of reaction  $\Delta H$  is released. The evolution of heat energy causes a pressure drop within the system and consequently the refrigerant evaporates and absorbs surrounding heat below the ambient temperature producing a refrigerating effect. In the thermally induced back reaction (charging mode), which has an endothermic character, the gaseous reactant CH<sub>3</sub>OH is evolved and the solid reactant MX is regenerated. Quick separation of the reaction products prevents synchronous reverse reactions and refrigerant reuptake, and guarantees loss-free and infinite thermal energy storage.

Chemical reactions generally follow complex reaction pathways and can proceed via intermediate steps. The formation and breaking of chemical coordination compounds is sometimes accompanied by structural reorganizations of the destabilized central atom [107]. Physical modifications and structural disintegration have been observed for several salt hydrates [108] and salt alcoholates [104]. These interventions may distinctively influence the kinetics and reversibility of multi-cyclic association/dissociation reactions. Fundamental data on thermodynamics and kinetics of salt ammoniates [62,109–111] or salt hydrates [112–114] are widely available, while the reaction of inorganic salts and alcohols [101,111,115–118] has only been studied in casual

manner. Information on the thermal behavior of single substances and limiting effects are of great practical importance for the development and assessment of the cooling performance of advanced materials, e.g. binary salt mixtures and salt composites that are tailored in terms of specific application requirements. A priori, three types of limiting effects may exist: binding kinetics of the gaseous molecules to the solid, mass transfer, and heat transfer [11]. The aim of the present paper is to comprehensively analyze the cooling efficiency, and reactivity characteristics of the reaction system  $\text{CaCl}_2\text{-CH}_3\text{OH}$  for use in an industrial adsorption cooling system. The paper presents results of a parametric study on the influence of (i) the  $\text{CH}_3\text{OH}$  partial pressure, (ii) the regeneration temperature, and (iii) the thermal history of pure bulk  $\text{CaCl}_2$  on the  $\text{CH}_3\text{OH}$  uptake kinetics under typical cooling application conditions. Thermal stability and cyclic changes in the  $\text{CH}_3\text{OH}$  uptake and associated heats of reaction are evaluated in a short-term cycling test. Energy storage densities, SCPs, and COPs are calculated from experimental data obtained with simultaneous thermogravimetric and micro-calorimetric analysis.

## 2. Materials and methods

### 2.1. Materials

From a preselected set of candidate materials, including metal halides, metal sulfates, and metal nitrates,  $\text{CaCl}_2$  was chosen owing to distinctive advantages compared with other salts. Despite its exceptional methanolation reaction kinetics,  $\text{LiCl}$  was discarded as a suitable material, because of its poor  $\text{CH}_3\text{OH}$  release below  $100^\circ\text{C}$  and overall low enthalpies of reaction.  $\text{CaCl}_2$  is an ubiquitous substance and has been the subject of several studies in the field of thermal energy storage as reviewed by N'Tsoukpoe et al. [119]. Theoretical calculations revealed that  $\text{CaCl}_2$  possesses a good sorption ability towards  $\text{CH}_3\text{OH}$ . According to thermodynamic equilibrium data (Fig. 2), the thermodynamic properties of the  $\text{CaCl}_2\text{-CH}_3\text{OH}$  system match well low-level temperature refrigeration applications. The  $\text{CaCl}_2$  methanolate dissociation occurs within the working temperature range of common low-grade heat sources.  $\text{CaCl}_2$  is an easily available, inexpensive, and chemically stable substance. As a soft Lewis acid it forms strong complexes with  $\text{CH}_3\text{OH}$ , analogous to salt hydrates. Anhydrous and high purity grade (Ph.Eur.)  $\text{CaCl}_2$  powder was purchased from Merck. The  $\text{CaCl}_2$  powder contained less than 5% of volatile components.

$\text{CH}_3\text{OH}$  was selected as refrigerant fluid, due to its high operating pressure and low freezing point, which are necessary for cold energy generation. The small size and the high polarity of the  $\text{CH}_3\text{OH}$  molecule appear to promise a reactivity similar to that of  $\text{H}_2\text{O}$  [101].  $\text{CH}_3\text{OH}$  has a lower latent heat of vaporization compared to  $\text{H}_2\text{O}$ , but can provide cold energy below zero degree centigrade [9]. Moreover,  $\text{CH}_3\text{OH}$  is a strong Lewis base [120] with high affinity to metal halides and has a lower steric hindrance than other straight-chain primary alcohols. The main drawbacks, flammability and toxicity, can be anticipated by an appropriate reactor design, i.e. operation in a hermetically closed system and adequate safety measures. Pure liquid  $\text{CH}_3\text{OH}$  (Merck) with a  $\text{H}_2\text{O}$  content of max. 0.003% was used. Selected thermodynamic and thermophysical properties of the materials used are listed in Table 2.

### 2.2. Experimental setup

Thermal behavior, reaction kinetics, and cycling performance of in-situ synthesized  $\text{CaCl}_2\text{-CH}_3\text{OH}$  addition compounds were experimentally studied by thermogravimetric analysis (TGA) and heat-flux differential scanning calorimetry (DSC). TGA/DSC is a standard technique in thermal analysis. It is an indispensable tool for composition identification of chemical compounds and examination of the heat transfer in chemical reactions.  $\text{CH}_3\text{OH}$  uptake (methanolation) and  $\text{CH}_3\text{OH}$  release (demethanolation) involve changes in the sample mass (TGA curve) and the enthalpy of reaction (DSC curve) that can easily be detected as a

function of time or temperature, whilst the sample is subjected to a predefined temperature program in a controlled atmosphere, and recorded with high precision.

All experiments were performed using a modified simultaneous TGA/DSC 1 device from Mettler Toledo. A schematic of the experimental setup is shown in Fig. 1. For in-situ synthesis of  $\text{CaCl}_2\text{-CH}_3\text{OH}$  compounds the TGA/DSC apparatus was connected to a  $\text{CH}_3\text{OH}$  vapor generation system. The evaporation system was equipped with a thermostated  $\text{H}_2\text{O}$  bath and a bubbler containing liquid  $\text{CH}_3\text{OH}$  for vapor dispersion. The  $\text{H}_2\text{O}$  bath was set at a constant temperature of  $21^\circ\text{C}$ . Dried high purity  $\text{N}_2$  was used as carrier gas and purged through the bubbler to evaporate the liquid  $\text{CH}_3\text{OH}$ , which had to be in vapor phase for the reaction. Before entering the TGA/DSC instrument, the  $\text{CH}_3\text{OH}$  droplets were homogenized by passing the  $\text{N}_2$  carrier gas saturated with  $\text{CH}_3\text{OH}$ , referred to as reactive gas, through glass wool. An external gas flow controller assured accurate gas flow rates. The reactive gas stream was mixed with the purge gas stream at the TGA/DSC inlet and passed over the specimen inside the TGA/DSC furnace. Different  $\text{CH}_3\text{OH}$  partial pressures were maintained by variation in the reactive gas flow rate. The relative  $\text{CH}_3\text{OH}$  vapor pressure at the TGA/DSC furnace inlet was derived from the ideal gas law [122]. Since experiments were carried out at high volumetric flow rates of the carrier and purge gas, the concentration and pressure of the  $\text{CH}_3\text{OH}$  vapor generated was low and the gas phase was considered to be ideal [123] with less than 1% error as has been determined via comparison with the van der Waals equation and experimentally confirmed by freezing out and determination of the methanol mass.  $\text{CH}_3\text{OH}$  is a highly volatile substance, due to its high vapor pressure at room temperature. To avoid any leakages, all tube connections were properly sealed. For purification of the exhaust gas stream the evolved  $\text{CH}_3\text{OH}$  vapor was captured and condensed in a cold trap connected to the TGA/DSC outlet (Fig. 1). The cold trap was chilled with a refrigeration circuit. To reach temperatures below  $0^\circ\text{C}$ , a  $\text{H}_2\text{O-HOCH}_2\text{CH}_2\text{OH}$  mixture with a ratio of 1:1 was used as refrigerant. During all methanolation/demethanolation cycles, the system was continuously purged with  $\text{N}_2$  gas (i) to protect the balance mechanism, (ii) to remove any residual moisture or impurities, and (iii) to prevent any reverse reactions by eliminating the reaction products from the reaction zone. The  $\text{N}_2$  protective gas was additionally passed over a silica gel desiccant with color indicator to visually indicate  $\text{H}_2\text{O}$  contamination in the purge gas line. All measurements were conducted at atmospheric pressure (1 atm).

Samples of small milligram quantities (10–12 mg) were used. The samples were distributed uniformly in an open  $70\ \mu\text{L}$   $\text{Al}_2\text{O}_3$  crucible (diameter: 6.0 mm, height: 4.5 mm). Small sample masses were chosen to avoid influences of  $\text{CH}_3\text{OH}$  vapor pressure gradients during methanolation and demethanolation runs. An automatic blank curve subtraction was performed to compensate the effect of buoyancy forces.  $\text{CH}_3\text{OH}$  uptake and  $\text{CH}_3\text{OH}$  release were calculated from the TGA curve. Methanolation/demethanolation rates and SCPs were derived from the

**Table 2**  
Thermodynamic and thermophysical properties of the anhydrous  $\text{CaCl}_2$  and the liquid  $\text{CH}_3\text{OH}$  used.

	$\text{CaCl}_2$	Reference	$\text{CH}_3\text{OH}$	Reference
Physical state	Solid		Liquid	
Molar mass	110.98 g/mol	Supplier	32.04 g/mol	Supplier
Melting point	$772^\circ\text{C}$	Supplier	$-98^\circ\text{C}$	Supplier
Boiling point			$64.5^\circ\text{C}$	Supplier
Water solubility	740 g/L ( $20^\circ\text{C}$ )	Supplier		
Density	2.15 g/cm <sup>3</sup> ( $20^\circ\text{C}$ )	Supplier	0.792 g/cm <sup>3</sup> ( $20^\circ\text{C}$ )	Supplier
Vapor pressure			12.8 kPa ( $20^\circ\text{C}$ )	Supplier
Molar specific heat capacity			81.6 (J/K mol) ( $25^\circ\text{C}$ )	[121]
Enthalpy of formation	795.8 (kJ/mol) ( $25^\circ\text{C}$ )	[121]	238.66 (kJ/mol) ( $25^\circ\text{C}$ )	[121]

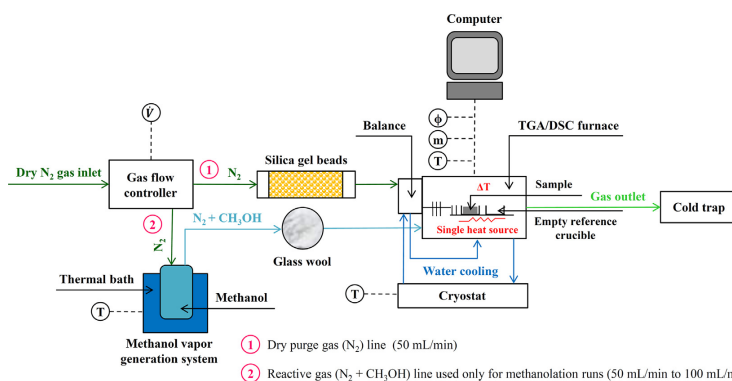


**Fig. 1.** Schematic flow diagram of the experimental setup for methanolation/demethanolation reaction cycles. The flow rate ( $\dot{V}$ ) of the refrigerant circuit containing H<sub>2</sub>O (indicated as blue solid line), the purge gas line (indicated as green solid line), and the reactive gas line (indicated as turquoise solid line), the temperature of the water bath, the furnace, the sample and the cryostat ( $T$ ) as well as the sample mass ( $m$ ), and the heat flux ( $\phi$ ) were recorded online. (For interpretation of the references to colour in this figure legend, the reader is referred to the web version of this article.)

first derivative of the TGA curve (DTG curve). For detecting changes in the heat flux and the corresponding onset and peak temperatures a reference crucible was used. The enthalpy of reaction was derived from manual integration of the heat flux as a function of time using the Mettler Toledo STARE Software 11.00a. The precision of the mass determination is given as  $\pm 1.0 \mu\text{g}$  (typical changes in mass were 2–10 mg). The heat power can be determined with a precision of  $\pm 0.1 \text{ mW}$  (typical heat powers were 2–10 mW). The measurement deviation of the experimental values ranged from 10% to 20%.

### 2.3. Experimental procedures

#### 2.3.1. Determination of the stoichiometric composition of $\text{CaCl}_2\text{-CH}_3\text{OH}$ compounds synthesized under different in-situ conditions

For the identification of the level of methanolation equilibrium tests were performed under isothermal (25 °C) and isobaric (1 atm) conditions at different CH<sub>3</sub>OH partial pressures over a methanolation time of 240 min followed by an isothermal stabilization segment in flowing dry N<sub>2</sub> atmosphere. The CH<sub>3</sub>OH partial pressure dependence of the methanolation rate was analyzed at three different CH<sub>3</sub>OH partial pressures (6.8 kPa, 8.2 kPa, and 9.1 kPa). The CH<sub>3</sub>OH vapor pressures applied correspond to evaporation temperatures of 8.5 °C, 11.7 °C, and 13.6 °C, respectively. Evaporation temperatures were calculated using the 2.5–5-form of the Wagner equation [124]. The dissociation reaction pattern was characterized by heating the samples from 25 °C to 150 °C with a temperature ramp of 3 K/min and stabilizing them at 150 °C for 30 min under dry N<sub>2</sub> with a flow rate of 50 mL/min.

#### 2.3.2. Determination of the influence of the CH<sub>3</sub>OH partial pressure on the methanolation and demethanolation reaction

The influence of the CH<sub>3</sub>OH partial pressure on the kinetics of the methanolation reaction and subsequent demethanolation reaction was studied under the same experimental conditions as described in Section 2.3.1.

#### 2.3.3. Determination of the influence of thermal pretreatment on the $\text{CaCl}_2$ methanolate formation

In a comparative study, the impact of thermal pretreatment on the CH<sub>3</sub>OH uptake of anhydrous CaCl<sub>2</sub> at a CH<sub>3</sub>OH partial pressure of 6.8 kPa and 9.1 kPa was investigated under the same isobaric and isothermal conditions as applied in the methanolation equilibrium test

described in Section 2.3.1. Samples were pre-dried by heating them with a ramp of 3 K/min from 25 °C to 105 °C in pure N<sub>2</sub> atmosphere. In a subsequent isothermal segment, the samples were stabilized at 105 °C until the mass remained constant and finally cooled down to 25 °C with a cooling rate of  $-10 \text{ K/min}$ . Thermal pretreatment is aimed to remove any residual adhering H<sub>2</sub>O and usually ranges from drying at temperatures slightly above the boiling point of H<sub>2</sub>O to drying at elevated temperatures.

#### 2.3.4. Determination of the influence of the regeneration temperature on the methanolation and demethanolation reaction

In a quick multi-step screening test the influence of the regeneration temperature on the CH<sub>3</sub>OH uptake characteristics and methanolation/demethanolation reaction kinetics was determined. The regeneration temperature was successively increased from 90 °C to 100 °C, and in the last demethanolation run up to 150 °C, while the methanolation conditions were unchanged. Three methanolation/demethanolation (discharging/charging) cycles were performed. These consisted of the following segments: (1) discharging at 25 °C, (2) charging at 90 °C, (3) discharging at 25 °C, (4) charging at 100 °C, (5) discharging at 25 °C, and (6) charging at 150 °C. The CH<sub>3</sub>OH uptake at a CH<sub>3</sub>OH partial pressure of 6.8 kPa and a temperature of 25 °C was measured over a methanolation period of 60 min. In a subsequent isothermal stabilization segment, the stability of the formed CaCl<sub>2</sub>-CH<sub>3</sub>OH complexes in pure N<sub>2</sub> was verified. The CaCl<sub>2</sub> methanolates were heated with a temperature ramp of 3 K/min from 25 °C to the final temperature of the corresponding segment under pure flowing N<sub>2</sub>. At the final temperature, the specimen were stabilized for several minutes, until the mass remained constant, and cooled down with a cooling rate of  $-10 \text{ K/min}$  to the initial temperature. The CaCl<sub>2</sub> sample as received without any thermal pretreatment was used.

In an additional systematic trial, the impact of the regeneration temperature on the cooling effect of the working pair CaCl<sub>2</sub>-CH<sub>3</sub>OH was investigated. For the target application, possible utilization of heat source temperatures below 100 °C (i.e. from combined heat-and-power units) would be favorable. Hence, desorption temperatures for demethanolation were varied over the interval 70 °C and 100 °C. The demethanolation was conducted at desorption temperatures of 70 °C, 80 °C, 90 °C, and 100 °C, respectively, in dry, flowing N<sub>2</sub>. Samples were heated from 25 °C to the final maximum temperature with a temperature ramp of 3 K/min. The methanolation was performed at a CH<sub>3</sub>OH

vapor pressure of 6.8 kPa at an evaporator temperature of 8.5 °C and a condenser temperature of 25 °C. A methanolation time of 60 min was set. In subsequent stabilization phases, the stability of the obtained  $\text{CaCl}_2\text{-CH}_3\text{OH}$  adducts at 25 °C and in dry  $\text{N}_2$  atmosphere was verified. Each measurement consisted of three consecutive methanolation/demethanolation cycles.

### 2.3.5. Determination of the cyclic stability of $\text{CaCl}_2$ methanolates

A short-term cycling test was conducted over 18 methanolation/demethanolation cycles. The virgin  $\text{CaCl}_2$  sample was predried at 105 °C prior to the first cycle to eliminate residual volatiles. The methanolation run was carried out at a  $\text{CH}_3\text{OH}$  partial pressure of 6.8 kPa and a temperature of 25 °C under atmospheric conditions. The methanolation time was 120 min. The methanolation run was followed by isothermal stabilization in dry  $\text{N}_2$  atmosphere. In the demethanolation run, the specimen was scanned from 25 °C to 180 °C at a constant heating rate of 3 K/min in pure flowing  $\text{N}_2$ . To ensure a complete demethanolation, the regeneration temperature was elevated to 180 °C. After stabilization at 180 °C for 30 min and cooling to 25 °C by a cooling rate of  $-10$  K/min, the remethanolation reaction was initiated.

## 3. Calculation

### 3.1. $\text{CH}_3\text{OH}$ sorption

The uptake and release of  $\text{CH}_3\text{OH}$  can be described by different key parameters. Since this study focuses on the methanolation process, exclusively methanolate formation related parameters are defined. The molar  $\text{CH}_3\text{OH}$  uptake ratio  $N$  is defined as the number of  $\text{CH}_3\text{OH}$  molecules  $n_{\text{CH}_3\text{OH}}$  associated with one mole of  $\text{CaCl}_2$  anhydride  $n_{\text{CaCl}_2}$  and is designated the level of methanolation or methanolation state:

$$N = \frac{n_{\text{CH}_3\text{OH}}}{n_{\text{CaCl}_2}} = \frac{m_{\text{CH}_3\text{OH}}}{m_{\text{CaCl}_2}} \times \frac{M_{\text{CaCl}_2}}{M_{\text{CH}_3\text{OH}}} \quad (3.1)$$

wherein  $m_{\text{CaCl}_2}$  is the initial dry mass of  $\text{CaCl}_2$  anhydride;  $M_{\text{CaCl}_2}$  is the molar mass of  $\text{CaCl}_2$  anhydride;  $m_{\text{CH}_3\text{OH}}$  is the mass of reacted  $\text{CH}_3\text{OH}$ , and  $M_{\text{CH}_3\text{OH}}$  is the molar mass of  $\text{CH}_3\text{OH}$ . The level of methanolation is given in mol  $\text{CH}_3\text{OH}$  per mol  $\text{CaCl}_2$ . The methanolation state is mainly dependent on several experimental variables such as  $\text{CH}_3\text{OH}$  partial pressure, reaction time, system pressure, and applied temperature. The reaction pathway also plays a crucial role.  $\text{CaCl}_2$  methanolates are addition compounds that can be synthesized by different methods resulting in a variation in the methanolation level, according to literature.

For a better comparison of the theoretical and experimental  $\text{CH}_3\text{OH}$  uptake the mass fraction of  $\text{CH}_3\text{OH}$  is introduced. The mass fraction of  $\text{CH}_3\text{OH}$   $w_{\text{CH}_3\text{OH}}$  (%) can be expressed as follows:

$$w_{\text{CH}_3\text{OH}} = \frac{m_{\text{CH}_3\text{OH}}}{m_{\text{CaCl}_2}} \times 100 \quad (3.2)$$

### 3.2. Chemical kinetics

Knowledge about the kinetic characteristics of the underlying gas-solid reaction is valuable for optimization of process conditions, numerical simulation, and reactor design purposes. In this study, both methanolation and demethanolation kinetics were evaluated. Methanolation and demethanolation rates were deduced from the first derivative of the TGA curve, which is called differential thermogravimetric (DTG) curve. The  $\text{CH}_3\text{OH}$  uptake rate, which is also denoted methanolation rate,  $\text{dm}/\text{dt}$  (mg/min) represents the change in sample mass that is linked to the amount of reacted methanol with time  $\Delta t$ :

$$\frac{\text{dm}}{\text{dt}} = \frac{m(t + \Delta t) - m(t)}{\Delta t} \quad (3.3)$$

For the kinetic analysis of the methanolation and demethanolation reactions, the extent of conversion  $\alpha(t)$  as a function of time was

determined from TGA measurements. The extent of conversion is defined as the current change in mass divided by the total change in mass that occurred throughout the reaction [125]:

$$\alpha(t) = \frac{m_0 - m(t)}{m_0 - m_1} \quad (3.4)$$

The term  $m_0$  is the initial sample mass;  $m(t)$  is the sample mass at the reaction time  $t$ , and  $m_1$  is the final sample mass. The extent of conversion can assume values between 0 and 1. An extent of conversion of 1, which is related to 100% completion, is assigned to a methanolation level of  $N = 2.0$ . For a better comparison of the results, the extent of conversion was related to a total uptake of two molecules of  $\text{CH}_3\text{OH}$  to one molecule of anhydrous  $\text{CaCl}_2$  for each sample tested. Therefore, values higher than 1 are ascribed to physisorption processes.

The determination of the extent of conversion is the basis for the calculation of the reaction rate  $d\alpha/\text{dt}$ . The reaction rate is the first derivative of the extent of conversion with respect to time and has the unit symbol 1/s.

### 3.3. Thermal analysis

The molar enthalpy of reaction was obtained from DSC measurements by peak area integration. The energy that is liberated or absorbed as heat during a chemical reaction as a result of a temperature difference  $\Delta T$  can be quantitatively determined by heat flux DSC. Heat flux DSC measures the difference in temperature of the specimen and an inert reference as a function of time under same conditions. Sample and reference crucible are symmetrically positioned on a horizontal sample holder below which six thermocouples are directly located. The heat flux  $\phi$  between sample and reference is proportional to the temperature difference, according with the following equation:

$$\phi = E_{(T)} \times \text{DSC} \quad (3.5)$$

where  $E_{(T)}$  and DSC are the calorimetric sensitivity and the measured DSC signal. Integration of the peak area under the DSC signal and above the baseline over time yields  $\Delta_r H$ :

$$\Delta_r H = \int_{t_1}^{t_2} \text{DSC} dt = \int_{t_1}^{t_2} \frac{\phi}{E_{(T)}} dt \quad (3.6)$$

The specific enthalpy of reaction  $\Delta_r h$  is defined as the capacity of heat energy stored per mass of TCM, which is equivalent to the molar reaction enthalpy divided by the molar mass of the respective methanolate  $M_{\text{methanolate}}$ :

$$\Delta_r h = \frac{\Delta_r H}{M_{\text{methanolate}}} \quad (3.7)$$

According to Hess Law, the value of the reaction enthalpy of the forward and reverse reaction are supposed to be equal. The heat absorbed or liberated by the sample as sensible heat is very low when compared with the heat of reaction. Therefore, sensible heat effects are negligible [126].

### 3.4. Refrigeration performance

In refrigeration applications, the major performance indicators for assessing and comparing different adsorption materials are the specific cooling power (SCP) and the coefficient of performance (COP). The SCP (W/kg) indicates the efficiency of a system to produce a refrigerating effect in relation to the initial adsorbent mass. It is defined as the fraction of the molar latent heat of vaporization of  $\text{CH}_3\text{OH}$   $\Delta_r H_{\text{CH}_3\text{OH}}$  and the molar mass of  $\text{CH}_3\text{OH}$   $M_{\text{CH}_3\text{OH}}$  and the initial mass of anhydrous  $\text{CaCl}_2$   $m_0$  multiplied by the methanolation rate  $\text{dm}/\text{dt}$ :

$$\text{SCP} = \frac{\text{dm}}{\text{dt}} \times \frac{\Delta_r H_{\text{CH}_3\text{OH}}}{m_0 \times M_{\text{CH}_3\text{OH}}} \quad (3.8)$$

The SCP is a function of heat and mass transfer. The heat capacity,



the thermal conductivity, and the methanolation reaction dynamics of the TCM are directly linked. Heat and mass transfer limitations can affect the reaction kinetics and result in a drop of the SCP. With increasing methanolation rate, the SCP is lifted. During the course of the methanolation reaction, the methanolation rate and accordingly the SCP changes with the degree of conversion. The maximum SCP was attained at the maximum methanolation rate. In addition to the maximum SCP, the average SCP was calculated. The average SCP is referred to either a methanolation time of 60 min and 120 min or a methanolation level of  $N = 2.0$ .

The efficiency in transforming heat provided from low-grade heat sources into useful cooling power, according to the First Law of thermodynamics, is characterized by the dimensionless cooling COP [127]. The COP for cooling is defined as the ratio of the cooling power output  $\Delta Q_{out}$  to the heat power input  $\Delta Q_{in}$ . According to Cacciola and Giordano [128], the efficiency of a cooling system using gas-solid reactions is the fraction of the vaporization enthalpy of the gaseous adsorbate  $\Delta_v H$  and the desorption enthalpy of the solid adsorbent  $\Delta_s H$ :

$$COP = \frac{\Delta Q_{out}}{\Delta Q_{in}} = \frac{|\Delta_v H|}{|\Delta_s H|} \quad (3.9)$$

The latent heat of vaporization of  $CH_3OH$  is a state function and dependent on the temperature. The specific vaporization enthalpy of  $CH_3OH$  at the respective evaporation temperatures was estimated with the PPDs equation [124],

$$\Delta_v h = RT_c \left[ A \times \left(1 - \frac{T}{T_c}\right)^{1/3} + B \times \left(1 - \frac{T}{T_c}\right)^{2/3} + C \times \left(1 - \frac{T}{T_c}\right) + D \times \left(1 - \frac{T}{T_c}\right)^2 + E \times \left(1 - \frac{T}{T_c}\right)^6 \right] \quad (3.10)$$

which is a useful correlation tool. The parameters are:  $A = 5.87513$ ,  $B = 13.91543$ ,  $C = -5.817880$ ,  $D = -5.692542$ ,  $E = 6.867206$ .  $T_c$  is the critical temperature of  $CH_3OH$  and is listed in Table 2. The molar vaporization enthalpy of  $CH_3OH$  was calculated by multiplying the specific vaporization enthalpy by the molar mass of  $CH_3OH$ .

## 4. Results and discussion

### 4.1. Stoichiometric composition of $CaCl_2$ - $CH_3OH$ compounds synthesized by in-situ TGA/DSC

Under the applied experimental conditions the maximum  $CH_3OH$  uptake was independent from the applied  $CH_3OH$  vapor pressure (Table 5). The methanolation level was calculated to be around three moles of  $CH_3OH$  per mole anhydrous  $CaCl_2$ , wherein only two moles of  $CH_3OH$  are strongly coordinated to one mole of anhydrous  $CaCl_2$ . About one mole is physically attached to the  $CaCl_2$  surface as structural  $CH_3OH$ . The experimental mass fractions of  $CH_3OH$  were close to theoretical values. The proposed chemical composition is  $CaCl_2 \cdot 2CH_3OH$ , which coincides with literature data (Table 3). The evolution of heat, which is ascribed to the DSC signal, affirms this assumption (Fig. 3b). The molar and specific reaction enthalpies were deduced from DSC peak integration. The calculated enthalpies of reaction per mole reacted  $CH_3OH$  for methanolation ranged from  $-51$  kJ/mol to  $-56$  kJ/mol (Table 5). The normalized demethanolation reaction enthalpies were comparatively high with values between 60 kJ/mol and 65 kJ/mol. Similar values have been published in the literature for methanolation and demethanolation reactions [101,102,106,116]. Offenhardt et al. [101] perceived a deviation from the theoretical level of methanolation depending on the geometry of the sample. Small pellets and powders exhibited a methanolation state of  $N = 1.9/2.0$ , whereas larger pellets were limited to  $N = 1.75$ .

In respect of the diversity in synthesis procedures, a variation in the stoichiometry has been reported. Five  $CaCl_2$  methanolate species with stoichiometric numbers of coordinated  $CH_3OH$  molecules of 1, 2, 3, 4 and 6 have been identified. In  $CaCl_2$  solutions with excess solvate the existence of a hexamethanolate solvate can be presumed.  $CaCl_2$  has an orthorhombic, distorted rutile-type structure and an octahedral geometry. The coordination number is six and hence up to six  $CH_3OH$  molecules can be theoretically coordinated to one  $Ca^{2+}$  ion. Solvates prepared from solution crystallization and drying yield lower  $CaCl_2$  methanolates. Inclusion of  $CH_3OH$  molecules inside the crystal during

**Table 3**  
Summary of published literature on the methanolation state of  $CaCl_2$ - $CH_3OH$  solvates.

Reference	Year	$N$	$w_{CH_3OH}$ (%)	$\Delta_v H$ (kJ/mol)	$\Delta_s H/N$ (kJ/mol)	Crystal structure	Method	Type of study
[130]	1966	1.0	29			Slabs	Raman analysis by Gerhold and Kahovec (1948)	Fundamental
[131]	1971	2.0	58			Polymeric polynuclear structure	$CaCl_2$ methanolate prepared by efflorescence from higher solvates	Fundamental
[101]	1980	2.0	58	-103.4	-51.7		Various	Applied
[116]	1982	2.0	58	-113	-56		Solution calorimetry (addition of stoichiometric quantity of liquid $CH_3OH$ to anhydrous $CaCl_2$ powder)	Fundamental
[102]	1984	2.0	58	-102	-51		In-situ methanolation reaction under vacuum by DSC	Fundamental
[102]	1984	2.0	58	103	51.5		Demethanolation reaction under vacuum by DSC	Applied
[103]	1996	2.0	58				Numerical simulation of a the system performance of a periodic flow reversal fixed-bed reactor	Fundamental
[104]	2003	2.0	58				Stoichiometric addition of $CH_3OH$ to anhydrous $CaCl_2$ in a glass vessel	Fundamental
[105]	2007	2.0	58				$CH_3OH$ uptake of a $CaCl_2$ -mesoporous silica gel composite	Fundamental
[106]	2007	2.0	58				$CH_3OH$ sorption on a $CaCl_2$ -mesoporous silica gel composite	Numerical
[132]	1907	3.0	87			Needles	Reaction of water-free $CaCl_2$ and absolute $CH_3OH$ above 55 °C, melting point at 177 °C to 178 °C	Applied
[115]	1926	3.0	87				Determination of the equilibrium dissociation pressure between trimethanolate/tetramethalae by dynamic method	Fundamental
[130]	1966	3.0	87			Slabs	Raman analysis by Gerhold and Kahovec (1948)	Fundamental
[133]	1836	4.0	115			Slabs	Methanolate crystallization from $CaCl_2$ saturated $CH_3OH$ solution upon cooling	Fundamental
[132]	1907	4.0	115			Plates	Reaction of water-free $CaCl_2$ and absolute $CH_3OH$ below 55 °C, decomposition to trimethanolate at 55 °C	Fundamental
[115]	1926	4.0	115				Determination of the equilibrium dissociation pressure between trimethanolate/tetramethalae by dynamic method	Fundamental
[130]	1966	4.0	115			Slabs	Raman analysis by Gerhold and Kahovec (1948)	Fundamental
[134]	1970	4.0	115			Discrete octahedral groups	Prepared by efflorescence from higher $CaCl_2$ - $CH_3OH$ solvates	Fundamental
[135]	1978	6.0	173					Fundamental

the growth period facilitates the presence of both coordinated and non-coordinated  $\text{CH}_3\text{OH}$  species. Crystalline  $\text{CaCl}_2\text{-CH}_3\text{OH}$  complexes with a defined structure were synthesized by adding a stoichiometric amount of  $\text{CH}_3\text{OH}$  to anhydrous  $\text{CaCl}_2$ . It can be concluded that experimental conditions have a notable impact on the methanolate formation.  $\text{CaCl}_2$  methanulates other than that identified in the present study may exist at pressures and temperatures outside the pressure-temperature range studied.

Thermodynamic equilibrium data on  $\text{CaCl}_2$  methanulates have been collected by few scientists so far (Fig. 2). To measure the decomposition pressure as a function of temperature, Offenhardt et al. [101] prepared  $\text{CaCl}_2$  methanulates with a stoichiometry of  $N = 0.5$  and  $N = 1.5$ . The results of the chemical equilibrium analysis indicated no significant difference. In an additional study, the authors synthesized samples with a composition of  $N = 1.0$  and  $N = 2.0$  by in-situ XRD technique and only found the existence of  $\text{CaCl}_2\cdot 2\text{CH}_3\text{OH}$ . Aristov et al. [106] have analyzed the sorption equilibrium of  $\text{CH}_3\text{OH}$  on a new composite sorbent prepared with KSK silica with a pore diameter of 15 nm as host matrix. They pointed out that  $\text{CaCl}_2$  dispersed in the pores exhibited a behavior similar to that of pure bulk  $\text{CaCl}_2$ .  $\text{CaCl}_2$  is a hygroscopic substance with a high deliquescence in  $\text{CH}_3\text{OH}$  saturated atmosphere and tends to an overstoichiometric uptake of  $\text{CH}_3\text{OH}$ . A continuous sorption until liquidation and formation of a  $\text{CaCl}_2\text{-CH}_3\text{OH}$  solution inside a mesoporous silica gel has been observed by Aristov et al. [106].

#### 4.2. Influence of the $\text{CH}_3\text{OH}$ partial pressure on the methanolation and demethanolation reaction

##### 4.2.1. Methanolation reaction

When  $\text{CaCl}_2$  was exposed to  $\text{CH}_3\text{OH}$  vapor, a rapid uptake was initiated (Fig. 3a). While the reaction temperature is below the equilibrium temperature, the methanolation will continue until a state of equilibrium is achieved. All methanolation reactions showed two waves of acceleration. Nucleation may contribute to an increase of the active reaction interface between reacted and unreacted phases and cause a second acceleration period. The  $\text{CH}_3\text{OH}$  uptake by  $\text{CaCl}_2$  powder is a solid-state process that can be phenomenologically explained as follows: After approaching the  $\text{CaCl}_2$  surface, the gaseous  $\text{CH}_3\text{OH}$  molecules diffuse through the porous crystal structure to which they are attracted by van der Waals forces, followed by surface adsorption. Strong interactions between the  $\text{CaCl}_2$  and  $\text{CH}_3\text{OH}$  molecules finally result in the formation of chemical bonds. These processes contribute to different extents to the reaction progress. Hirata and Fujioka [104] have comprehensively investigated the change of various thermophysical properties and heat transfer characteristics of porous  $\text{CaCl}_2$  formed and decomposed over a series of successive methanolation/demethanolation cycles. They calculated the volume occupied by one mole of gaseous  $\text{CH}_3\text{OH}$  chemisorbed in one mole of solid  $\text{CaCl}_2$ . The calculated value was close to the liquid molar volume for  $\text{CH}_3\text{OH}$ . Consequently, they presumed that  $\text{CH}_3\text{OH}$  is less influenced by surrounding atoms constituting the salt sphere than  $\text{H}_2\text{O}$  is.

A high  $\text{CH}_3\text{OH}$  partial pressure favored the methanolation reaction, according to Le Chatelier's principle. The pressure difference between the pressure inside and across the sample is the driving force for the  $\text{CH}_3\text{OH}$  vapor diffusion. By applying higher  $\text{CH}_3\text{OH}$  partial pressures, the reaction was accelerated so that the maximum chemical  $\text{CH}_3\text{OH}$  uptake was reached faster (Fig. 3a). Vice versa, when low  $\text{CH}_3\text{OH}$  partial pressures were applied, longer methanolation times were required for the reaction to yield 100% completion. For  $\text{CH}_3\text{OH}$  partial pressures of 9.1 kPa and 8.2 kPa similar reaction times for the formation of  $\text{CaCl}_2\cdot 2\text{CH}_3\text{OH}$  were measured. The initial sample masses were within the same range.

Methanolation rates and reaction rates were sensitive to the  $\text{CH}_3\text{OH}$  partial pressure and increased with increasing  $\text{CH}_3\text{OH}$  partial pressure. In all measurements, the  $\text{CH}_3\text{OH}$  uptake increased instantaneously over a narrow time frame in the initial phase and diminished quickly after

reaching a maximum. The calculated maximum methanolation rates varied between 0.13 mg/min and 0.65 mg/min (Table 5). In untreated samples, local minima were observed at extents of conversion of 0.1–0.3, which are assigned to methanolation levels of  $N = 0.2$ –0.6. In the further course of the reactions, the reaction rates rose only slightly, indicated by a second fairly small peak, and finally gradually decreased until the chemical reaction was completed (Fig. 3c). Maximum reaction rates attained at low extents of conversion and decelerating courses are attributed to an advancing  $\text{CH}_3\text{OH}$ /methanolate interface with nucleation and growth phenomenon. SCPs exhibited a similar trend (Fig. 3d).

When the  $\text{CH}_3\text{OH}$  partial pressure was decreased below the equilibrium pressure in a subsequent isothermal stabilization segment, the direction of the reactions slowly shifted to the reactants and the formed  $\text{CaCl}_2\text{-CH}_3\text{OH}$  compounds started to dissociate evolving physisorbed and chemisorbed  $\text{CH}_3\text{OH}$ . The calculated differences in the composition after the methanolation runs and before the demethanolation runs amounted to 0–15%.

##### 4.2.2. Influence of thermal pretreatment on the $\text{CaCl}_2$ methanolate formation

Predrying at 105 °C prior to the first methanolation/demethanolation cycle had an inhibitory effect on the kinetics of the methanolation reactions studied at a  $\text{CH}_3\text{OH}$  partial pressure of 6.8 kPa and 9.1 kPa. Considerable differences in the  $\text{CH}_3\text{OH}$  uptake arose. The methanolation reactions were slowed down upon heating and therefore longer reaction times were needed to reach an extent of conversion of 50% (Fig. 3a). As illustrated in Fig. 3c and d, maximum methanolation rates and accordingly maximum SCPs were drastically reduced, irrespective of the  $\text{CH}_3\text{OH}$  partial pressure applied. Changes in the crystal integrity of the  $\text{CaCl}_2$  samples may be the major reason for lower methanolation rates and rather constant  $\text{CH}_3\text{OH}$  uptakes. Due to the removal of traces of volatile constituents (i.e.  $\text{H}_2\text{O}$ ), the structures of the  $\text{CaCl}_2$  samples were presumably destabilized, collapsed, and consequently the bulk densities of the samples increased. Reduced porosities and fewer accessible active reaction sites lead to diffusion barriers inside the samples. Yet, a positive influence on the formation of the final  $\text{CaCl}_2$  methanulates was revealed in terms of physical stability. Thermal pretreatment gave stable addition compounds, as no change in mass and hence no continuous physisorption were detected. The

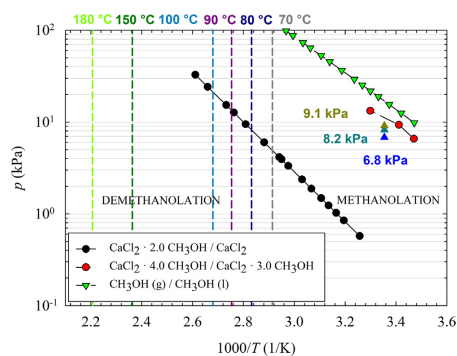
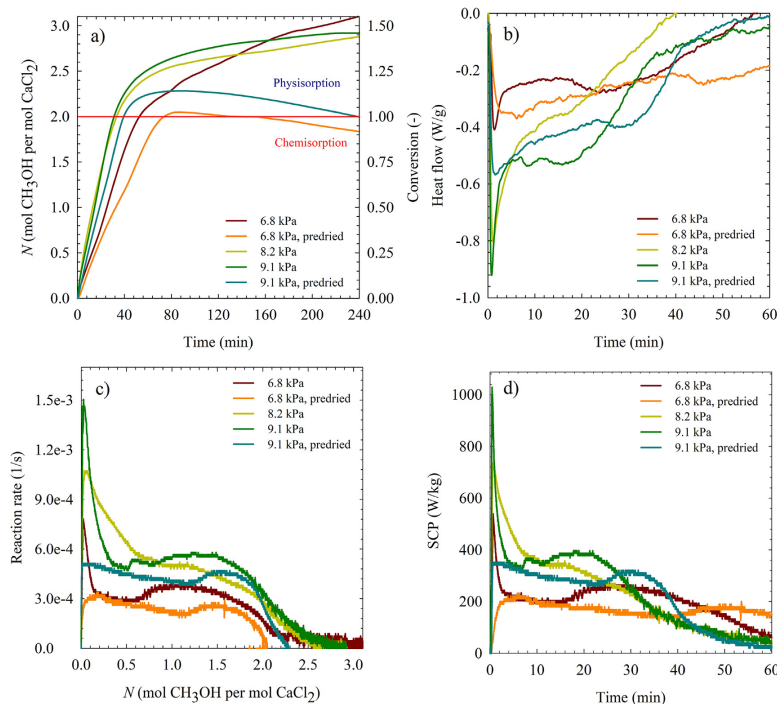


Fig. 2. Experimentally derived dissociation pressures of various  $\text{CaCl}_2\text{-CH}_3\text{OH}$  systems. All data were extracted from published literature [101,115,129]. In this study, isothermal methanolation experiments were carried out at  $\text{CH}_3\text{OH}$  partial vapor pressures of 6.8 kPa, 8.2 kPa, and 9.1 kPa and a temperature of 25 °C, as indicated in the diagram. To study the cooling efficiency under application-oriented conditions, the methanolated  $\text{CaCl}_2$  was regenerated over a charging temperature domain from 70 °C to 180 °C.



**Fig. 3.** Influence of  $p_{\text{CH}_3\text{OH}}$  variation and predrying on the methanolation reaction dynamics and cooling performance of  $\text{CaCl}_2$  methanolate species: (a)  $\text{CH}_3\text{OH}$  uptake, (b) heat flow normalized to the initial sample mass, (c) reaction rate, and (d) cooling power. Methanolation levels higher than  $N = 2.0$  indicate the presence of  $\text{CaCl}_2$  methanulates of non-coordinated form. Methanolation reactions were performed at  $p_{\text{CH}_3\text{OH}} = 6.8 \text{ kPa}$  ( $\vartheta_{\text{vap}} = 8.5^\circ\text{C}$ ),  $p_{\text{CH}_3\text{OH}} = 8.2 \text{ kPa}$  ( $\vartheta_{\text{vap}} = 11.7^\circ\text{C}$ ), and  $p_{\text{CH}_3\text{OH}} = 9.1 \text{ kPa}$  ( $\vartheta_{\text{vap}} = 13.6^\circ\text{C}$ ) under isothermal conditions ( $\vartheta_{\text{cond}} = 25^\circ\text{C}$ ). In dynamic demethanolation runs, the specimen was scanned from  $25^\circ\text{C}$  to  $150^\circ\text{C}$  with  $3 \text{ K/min}$  in dry  $\text{N}_2$ .

methanolation levels were roughly  $N = 2.0$ . Chemical equilibrium conditions were attained inside the samples, while exposed to  $\text{CH}_3\text{OH}$  saturated  $\text{N}_2$  atmosphere. A stepwise  $\text{CH}_3\text{OH}$  uptake was also observed for predried samples (Fig. 3c). In comparison to the untreated samples, the reaction rate values of the first and second step were of the same magnitude. However, the second step started at higher conversions, precisely at conversions of  $0.5$ – $0.6$ , which are equal to methanolation levels of  $N = 1.1$ – $1.2$ . Iyimen-Schwarz [102] also reported the uptake of  $\text{CH}_3\text{OH}$  in two clearly visible, though indistinct stages.

#### 4.2.3. Demethanolation reaction

Since information on the thermal decomposition kinetics of salt alcoholates is not available in the literature, the dissociation behavior was studied in detail. The demethanolation reactions followed a different pattern compared to the methanolation reactions. The rather sigmoidal curves with induction periods are presented in Fig. 4a. Methanolation levels higher than one result from overstoichiometric methanolation. Thermal hysteresis appears when the rate of the forward and the rate of the reverse reaction are not equal. Because of overstoichiometric  $\text{CH}_3\text{OH}$  uptakes during the methanolation reactions, the methanolation levels at the beginning of the demethanolation segments were different for the samples analyzed. The predried samples lost roughly about  $N = 0.3$  during the subsequent isothermal stabilization,

possibly due to equilibrium disturbances. The high vapor pressure of  $\text{CaCl}_2$  methanulates at room temperature stimulates the dissociation reaction. However, at the start of the demethanolation reaction the samples showed a stable behavior with no change in mass. Release of the remaining adsorbed  $\text{CH}_3\text{OH}$  proceeded in several clearly separable stages compared to the indistinct stages of the methanolation reactions. The untreated  $\text{CaCl}_2$  methanulates dissociated between  $84^\circ\text{C}$  and  $143^\circ\text{C}$  (Fig. 4a). Below  $80^\circ\text{C}$  mainly physisorbed  $\text{CH}_3\text{OH}$  was given off. Between  $75\%$  and  $85\%$  of the total mass was lost in the first step below  $120^\circ\text{C}$  with peak temperatures around  $101^\circ\text{C}$  to  $106^\circ\text{C}$ . The inflection point of the TGA curve is correspondent with the maximum peak temperature of the DSC curve. In Fig. 4d, the evolution of non-coordinated  $\text{CH}_3\text{OH}$  in samples with  $N > 2.0$  is well depicted. Tailing of the DSC curve in the low temperature region means that the prevailing  $\text{CH}_3\text{OH}$  removed was physisorbed  $\text{CH}_3\text{OH}$ . The liberation of weakly attached methanol is associated with low heat flows (Fig. 4b). The peak temperatures of the second peaks ranged from  $135^\circ\text{C}$  to  $136^\circ\text{C}$ .

Thermal pretreatment affected the dissociation reaction (Fig. 4a). The predried  $\text{CaCl}_2$  methanulates decomposed in three overlapping endothermic steps of different shapes with peak temperatures at  $92^\circ\text{C}$ . The decomposition of the under stoichiometric methanulates started at temperatures close to the boiling point of  $\text{CH}_3\text{OH}$  ( $64.5^\circ\text{C}$ , 1 atm) [124] and was completed at lower final temperatures compared to the

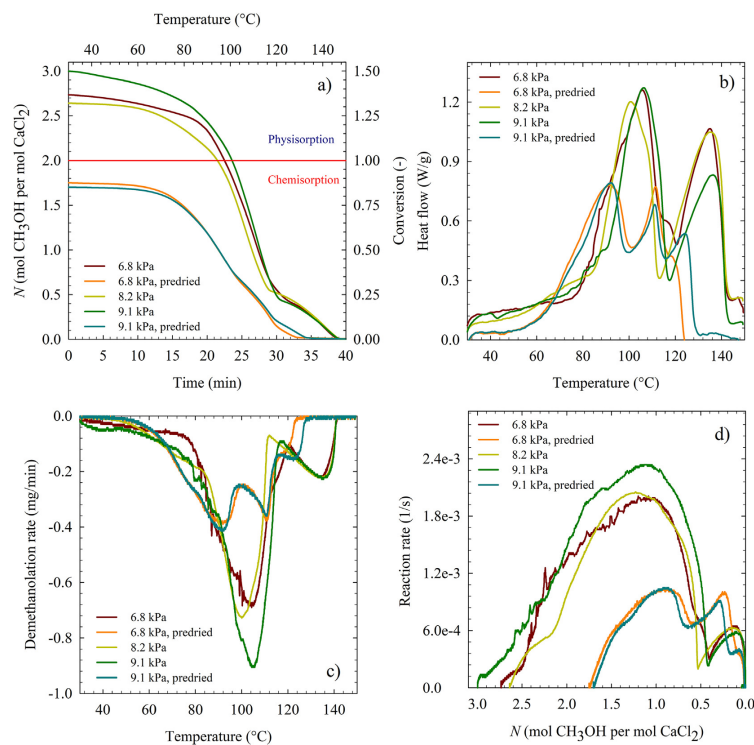


**Fig. 4.** Influence of  $p_{\text{CH}_3\text{OH}}$  variation and predrying on the demethanolation reaction dynamics of  $\text{CaCl}_2$  methanolate species: (a)  $\text{CH}_3\text{OH}$  release, (b) heat flow normalized to the initial sample mass, (c) demethanolation rate, and (d) reaction kinetics. Methanolation levels higher than  $N = 2.0$  indicate the presence of methanolates of non-coordinated form. Methanolation reactions were performed at  $p_{\text{CH}_3\text{OH}} = 6.8 \text{ kPa}$  ( $\vartheta_{\text{vap}} = 8.5^\circ\text{C}$ ),  $p_{\text{CH}_3\text{OH}} = 8.2 \text{ kPa}$  ( $\vartheta_{\text{vap}} = 11.7^\circ\text{C}$ ), and  $p_{\text{CH}_3\text{OH}} = 9.1 \text{ kPa}$  ( $\vartheta_{\text{vap}} = 13.6^\circ\text{C}$ ) under isothermal conditions ( $\vartheta_{\text{cond}} = 25^\circ\text{C}$ ). In dynamic demethanolation runs, the specimen was scanned from  $25^\circ\text{C}$  to  $150^\circ\text{C}$  with a constant temperature ramp of  $3 \text{ K/min}$  in dry  $\text{N}_2$ .

decomposition of the untreated methanolates (Fig. 4b). Since in samples with higher methanolation levels the  $\text{CH}_3\text{OH}$  pressure increases and more gaseous  $\text{CH}_3\text{OH}$  must be transported through the pores to the surface of the sample, a slower diffusion and a shift of the equilibrium position to higher temperatures is presumed. In Fig. 4c and d, demethanolation and reaction rates are plotted against the methanolation level. Higher levels of methanolation yielded higher demethanolation and reaction rates in the first dissociation step, respectively. This correlation can be explained by gas transfer and surface properties. Peak heat flows were considerably lower, as a result of the lower methanolation levels, when compared with the untreated samples (Fig. 4b).

Up to two moles of  $\text{CH}_3\text{OH}$  of a total uptake of three moles of  $\text{CH}_3\text{OH}$  per mole anhydrous  $\text{CaCl}_2$ , including physisorbed and chemisorbed species, were desorbed in one single step (Fig. 4d). In the second and third step, which appeared in the  $100^\circ\text{C}$  to  $143^\circ\text{C}$  temperature range, up to  $N = 0.6$  were removed. A very distinct second step was observed at regeneration temperatures above  $100^\circ\text{C}$  in the demethanolation reaction of the multi-step screening. A similar pattern occurred in the methanolation/demethanolation cycling experiments.  $\text{CaCl}_2$  methanolates appear to decompose in more than two steps, in particular at methanolation levels much higher than  $N = 2.0$  as well as at

higher methanolation rates under the experimental conditions studied. Measurements at lower heating rates may probably give a better description of the thermal effects, as the observed steps can be better distinguished.

Offenhardt et al. [101] have rapidly screened numerous salts including anhydrous  $\text{CaCl}_2$  that reacted with  $\text{CH}_3\text{OH}$  vapor equilibrated with liquid at  $15^\circ\text{C}$  by thermogravimetric analysis. They encountered that  $\text{CaCl}_2 \cdot 1.96\text{CH}_3\text{OH}$ , which was formed between  $65^\circ\text{C}$  and  $47^\circ\text{C}$ , decomposed between  $109^\circ\text{C}$  and  $132^\circ\text{C}$ . Since this finding is coherent with results obtained in this paper, the application of similar experimental conditions is assumed. Iyimen-Schwarz [102] has characterized the thermal behavior of the  $\text{CaCl}_2 \cdot 2\text{CH}_3\text{OH}$  compound in 10 consecutive methanolation/demethanolation reaction cycles with a heating rate of  $5 \text{ K/min}$  and a cooling rate of  $-3 \text{ K/min}$  by DSC. The methanolation and demethanolation reactions have been carried out at low pressures of  $1.0 \text{ kPa}$ . In that study, a single decomposition stage between  $70^\circ\text{C}$  and  $80^\circ\text{C}$ , and  $150^\circ\text{C}$  and  $180^\circ\text{C}$  has been detected. It is assumed that differences in the decomposition patterns resulted (i) from resistances to mass and heat transfers inside the sample, (ii) from different starting materials and (iii) from different experimental conditions. By applying lower heating rates or working under vacuum peak temperatures can be

shifted to lower temperatures, which favors the use of low-grade industrial waste heat or solar thermal energy for adsorption cooling.

The presence of intermediate phases can be explained by several hypotheses. The reaction between  $\text{CaCl}_2$  and  $\text{CH}_3\text{OH}$  is a heterogeneous reaction that involves three phases: (i) solid  $\text{CaCl}_2$ ,  $\text{CH}_3\text{OH}$  vapor and solid  $\text{CaCl}_2$  methanolate. Chemical reactions usually occur at the interfaces between these participating phases and are preceded by changes in the crystal structure [136]. A structural reorganization from the polynuclear structure of  $\text{CaCl}_2 \cdot 2\text{CH}_3\text{OH}$ , which has been identified by Gillier-Pandraud and Philoche-Levisalles [137], to the orthorhombic structure of  $\text{CaCl}_2$  anhydride may produce intermediate methanolates. If no equilibrium condition is maintained throughout the dissociation reaction, anhydrous  $\text{CaCl}_2$  and  $\text{CaCl}_2 \cdot 2\text{CH}_3\text{OH}$  could be present at the same time. During the demethanolation reaction, heat penetrates into the sample and initiates the gradual decomposition of the  $\text{CaCl}_2$  methanolate. Because heat is transferred by thermal conductance in solid compounds, the thermal conductivity of the solid has a great influence. Variances in the thermal conductivities of the participating phases may limit the heat transfer. The result is an unsteady distribution of heat inside the sample.  $\text{CaCl}_2$  methanolates possess higher heat capacities and thermal conductivities than anhydrous  $\text{CaCl}_2$  as determined by Hirata and Fujoka [104] and Offenhardt et al. [101]. Due to thermal resistances, small quantities of  $\text{CH}_3\text{OH}$ , chemically bound or evaporated, may remain inside the sample and hence non-integer decomposition steps appear. To remove the trapped  $\text{CH}_3\text{OH}$ , a sufficient amount of heat is necessary. The low thermal conductivity of anhydrous

$\text{CaCl}_2$  [138] is a major constraint that restricts its use in large-scale applications. A systematic complimentary research is mandatory to verify these hypotheses. Thermogravimetric analysis is limited to the determination of the quantitative composition of compounds. Conformational transformations cannot be substantiated and thus different solid-state forms, in this case single  $\text{CaCl}_2$  methanolates and admixtures of  $\text{CaCl}_2$  anhydride and  $\text{CaCl}_2$  methanolates, cannot be differentiated.

#### 4.3. Influence of the regeneration temperature on the methanolation and demethanolation reaction

Results obtained from the multi-step screening test are summarized in Figs. 5 and 6. In the first two cycles, the  $\text{CH}_3\text{OH}$  uptake was similar with  $\Delta moles = 2.1$  and  $\Delta moles = 1.9$  (Table 4). Since a small part of the  $\text{CH}_3\text{OH}$  was already released after the first methanolation reaction, during the stabilization segment at 25 °C, a true state of equilibrium was apparently not achieved and few  $\text{CH}_3\text{OH}$  was loosely bound to the  $\text{CaCl}_2$  surface. Despite being partially demethanolated at temperatures below 100 °C, the reuptake of  $\text{CH}_3\text{OH}$  was not remarkably affected in the second methanolation reaction (Fig. 5a). In the methanolation reaction of the third cycle a slightly lower  $\text{CH}_3\text{OH}$  uptake with  $\Delta moles = 1.4$  was measured compared to the first and second one. No significant loss occurred during the subsequent isothermal stabilization segments of the second and third methanolation reaction. This leads to the assumption that chemical equilibrium was attained in both reactions.

Due to the evolution of a significant amount of  $\text{CH}_3\text{OH}$  during the

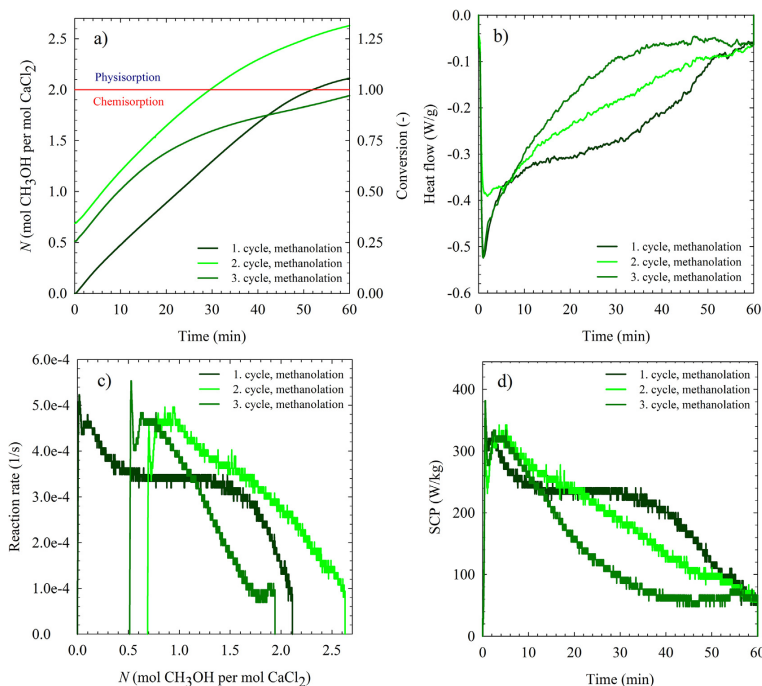


Fig. 5. Influence of the regeneration temperature on (a) the  $\text{CH}_3\text{OH}$  sorption pattern of  $\text{CaCl}_2$  methanolates, (b) the associated heat flow, (c) the chemical kinetics, and (d) the cooling power. Methanolation runs were performed at  $p_{\text{CH}_3\text{OH}} = 6.8$  kPa and  $\vartheta_{\text{vap}} = 8.5$  °C under isothermal conditions at 1 atm. The regeneration temperature was 90 °C in the 1st, 100 °C in the 2nd and 150 °C in the 3rd cycle.

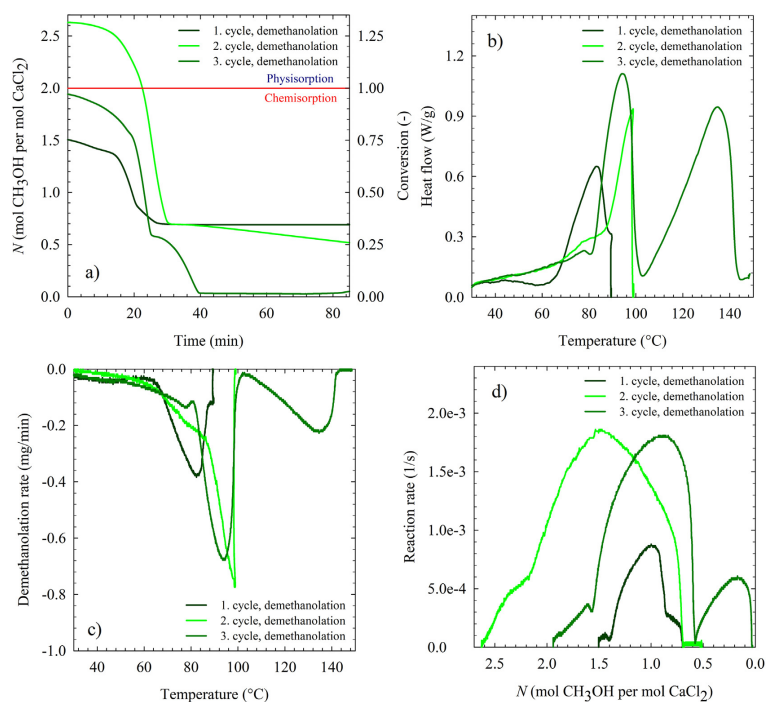


Fig. 6. Influence of the regeneration temperature on (a) the CH<sub>3</sub>OH desorption pattern of CaCl<sub>2</sub> methanolates, (b) the associated heat flow, (c) the demethanolation rate, and (d) the chemical kinetics. Methanolation runs were performed at  $p_{\text{CH}_3\text{OH}} = 6.8 \text{ kPa}$  and  $\varphi_{\text{vap}} = 8.5^\circ\text{C}$  under isothermal conditions at 1 atm. The regeneration temperature was 90 °C in the 1st, 100 °C in the 2nd and 150 °C in the 3rd cycle.

first stabilization segment, the lowest CH<sub>3</sub>OH desorption was ascribed to the first demethanolation (Fig. 6a). At the start of the second methanolation reaction the methanolation level amounted to  $N = 0.7$  (Table 4). In the second demethanolation reaction, the CH<sub>3</sub>OH release was slightly higher compared to the previous CH<sub>3</sub>OH reuptake. CH<sub>3</sub>OH taken up during the second remethanolation reaction was probably physically built into the crystal lattice, the total level of methanolation exceeded  $N = 2.0$ . An overstoichiometric CaCl<sub>2</sub> methanolate of  $N = 2.6$  existed. Upon heating to 100 °C about 2.1 mol of CH<sub>3</sub>OH of non-coordinated and coordinated form were liberated. A small amount of CH<sub>3</sub>OH of about  $N = 0.5$  remained inside the sample, which was finally liberated during the last demethanolation reaction in conjunction with the CH<sub>3</sub>OH taken up during the third methanolation reaction.

Since overstoichiometric methanolation took place, the degree of conversion exceeds the value of 1, which is assigned to an uptake of two moles of CH<sub>3</sub>OH per mole CaCl<sub>2</sub>. The associated heat flow development is depicted in Fig. 5b. In the first and second methanolation reaction with conversions less than 30%, a pointed heat flow peak was detected. Below regeneration temperatures of 90 °C and 100 °C, the CaCl<sub>2</sub>-CH<sub>3</sub>OH compounds decomposed in one endothermic step with peak temperatures at 83 °C and 99 °C, respectively (Table 4). In the third demethanolation phase with a regeneration temperature above 100 °C, two stages were detected, as aforementioned. The associated peak temperatures were 94 °C and 135 °C, respectively.

In the multi-step thermal cycling, the influence of the regeneration temperature on the methanolation and reaction rate of the

remethanolation reactions was marginal (Fig. 5c). The maximum methanolation rates with 0.22 mg/min, 0.22 mg/min, and 0.24 mg/min were constant over the methanolation/demethanolation reaction cycles tested, but slightly lower compared with those measured in the equilibrium test. Lower sample porosity may account for lower maximum methanolation rate values. Increase in the regeneration temperature resulted in changes in the demethanolation reaction kinetics (Fig. 6c). The lowest maximum demethanolation rate was observed after the first methanolation reaction, whereas the highest maximum demethanolation rate was measured in the second methanolation/demethanolation cycle for a regeneration temperature of 100 °C. In the third demethanolation run, in which the sample was heated to 150 °C, the demethanolation rate slightly decreased. This is attributed to a variation in the CH<sub>3</sub>OH uptake and initial and final level of methanolation per cycle.

The maximum reaction rate values for methanolation are within the same range (Fig. 5c). The highest maximum reaction rate was achieved in the third methanolation reaction, which is in accordance with the maximum methanolation rate. The CaCl<sub>2</sub> methanolate at the start of the second methanolation reaction possessed a higher thermal conductivity and a higher void fraction than pure CaCl<sub>2</sub> anhydride. This, however, didn't induce an accelerating effect on the reaction rate. Fig. 5d indicates that the reaction rate of the methanolation reaction is dependent on the initial level of methanolation. The maximum reaction rates for demethanolation in the second and third demethanolation reaction were twice as high as the one in the first demethanolation reaction (Fig. 6d). The reaction rate was apparently doubled, when the amount

**Table 4**  
Influence of the regeneration temperature  $\vartheta_{reg}$  on the  $\text{CH}_3\text{OH}$  sorption, the reaction kinetics, the energy storage density, and cooling performance of the methanolation/demethanolation reaction of  $\text{CaCl}_2$  and its methanolates. Average methanolation rates and average SCPs are referred to a methanolation time of 60 min. The given  $P_{\text{CH}_3\text{OH}}$  and corresponding  $\vartheta_{\text{cond}}$  are based on theoretical calculations.

Reaction	$N_0$	$N_1$	$\Delta n_{\text{Meth}}$	$w_{\text{CH}_3\text{OH}}$ (%)	Peak heat flow (W/g)	Max dm/dt (mg/min)	Average dm/dt (mg/min)	Max dz/dt (1/s)	$\vartheta_{\text{max}}$ (°C)	$\Delta H$ (kJ/mol)	$\Delta H/N$ (kJ/mol)	$\Delta H$ (J/g)	$\Delta H$ (J/g)	$P_{\text{CH}_3\text{OH}}$ (kPa)	$\vartheta_{\text{evap}}$ (°C)	$\vartheta_{\text{cond}}$ (°C)	$\vartheta_{\text{reg}}$ (°C)	Max SCP (W/kg)	Average SCP (W/kg)	COP
1. methanolation	0.0	2.1	2.1	61	-0.52	0.22	0.12	5.23E-04	83	-123	-58	-686	6.8	8.5	25	202	0.68			
1. demethanolation	1.5	0.7	-0.8	19	0.65	-0.38	-0.09	8.82E-04	66	46	57	290	90	8.5	25	186	0.75			
2. methanolation	0.7	2.6	1.9	56	-0.39	0.22	0.12	4.96E-04	99	-91	-47	-527	6.8	8.5	25	342	0.59			
2. demethanolation	2.6	0.5	-2.1	38	0.94	-0.77	-0.09	1.86E-03	74	107	51	541	100	8.5	25	382	0.59			
3. methanolation	0.5	1.9	1.4	41	-0.52	0.24	0.09	5.53E-04	94/135	-75	-53	-480	6.8	8.5	25	137	0.59			
3. demethanolation	1.9	0.0	-1.9	36	1.11	-0.68	-0.15	1.81E-03	80/109	125	65	724	150	8.5	25	382	0.59			

of  $\text{CH}_3\text{OH}$  released was doubled.

The methanolation reaction enthalpies varied over a broad range ( $-75$  kJ/mol to  $-123$  kJ/mol). The normalized reaction enthalpies ranged from  $-47$  kJ/mol to  $-58$  kJ/mol. The reaction enthalpies for demethanolation were with values of 46 kJ/mol to 125 kJ/mol similar to the methanolation reaction enthalpies. In the first demethanolation reaction, only a small amount of  $\text{CH}_3\text{OH}$  was released, as indicated by the low reaction enthalpy of 46 kJ/mol. However, the reaction enthalpy per mole  $\text{CH}_3\text{OH}$  was 57 kJ/mol and within the same range as the other normalized demethanolation enthalpies (51 kJ/mol to 65 kJ/mol) (Table 4).

Changes in geometry and structure of the samples were not investigated. To optically examine thermally induced physical transitions of  $\text{CaCl}_2$  methanolates upon methanolation and demethanolation, DSC combined with hot stage microscopy could be employed.

The impact of the desorption temperature on the overall cooling efficiency was analyzed over three methanolation/demethanolation cycles. Figs. 7 and 8 depict the results obtained for the third methanolation/demethanolation cycle. The first methanolation/demethanolation cycle significantly differed from the following ones, as observed in the cycle stability experiment described in Section 2.3.5. Methanolation runs were carried out under the following boundary conditions:  $P_{\text{CH}_3\text{OH}} = 6.8$  kPa,  $\vartheta_{\text{evap}} = 8.5$  °C, and  $\vartheta_{\text{cond}} = 25$  °C. Experimental results demonstrate that the desorption temperature notably affects the reaction dynamics of the consecutive remethanolation reaction. The methanol uptake (Fig. 7a) was similar in every methanolation step and amounted to  $N = 2.3 \pm 0.1$ . The sample regenerated at a temperature of 80 °C showed an overall slow reuptake of  $\text{CH}_3\text{OH}$ , when compared with the remethanolation processes of the samples demethanolated at 70 °C, 90 °C, and 100 °C. The slow reactivity and low total thermal power per total material mass (Fig. 7b) cannot be systematically explained and obviously results from variations in the initial sample mass, permeability and/or contact with the heat source in this single measurement. In case of the other samples, a continuous evolution of heat with decreasing trend over the first 20–30 min was measured. As the reaction progressed, the thermal power declined. The enthalpies of reaction per mole  $\text{CH}_3\text{OH}$  were within the range of  $-46$  kJ/mol to  $-52$  kJ/mol.

Scrutinizing the reaction dynamics reveals that high rates of reaction were reached at low degrees of conversion within seconds indicating a fast initial reactivity (Fig. 7c). The pointed peak was followed by a flat region with the progress of the methanolation reaction. The subsequent methanolation region is controlled by diffusion of  $\text{CH}_3\text{OH}$  vapor through the reacted part resulting in a stable cooling output. The desorption temperature influences the microstructure of the sample. An enlargement of the pore network and surface area, ascribed to the expansion of reacted particles, leads to a fast initial reaction. The rapid remethanolation process is primary attributable to a change in the topology, specifically the overall void fraction of the reactive bed. At the anhydrous state, the void fraction of the sample exposed to a methanolation/demethanolation cycle is higher than that of the unreacted  $\text{CaCl}_2$  [104]. The void fraction decreases with the evolution of the reaction and with increasing  $\text{CH}_3\text{OH}$  adsorption. At the desorption temperatures investigated, traces of methanolated  $\text{CaCl}_2$  present at the beginning of the methanolation phase are likely to serve as nuclei. The fast adsorption of  $\text{CH}_3\text{OH}$  molecules accompanied by a local temperature lift, which leads to the development of a temperature gradient, suggests condensation of the  $\text{CH}_3\text{OH}$  in gaseous state on the salt surface and liquid film formation, which promotes an accelerated remethanolation. The  $\text{CaCl}_2$  methanolate content of the sample increased with decreasing desorption temperature. Below desorption temperatures of 100 °C, the release of  $\text{CH}_3\text{OH}$  adsorbed to the  $\text{CaCl}_2$  was not complete, which means that very small quantities of  $\text{CH}_3\text{OH}$  remained inside the sample. Samples examined at desorption temperatures of 70 °C and 80 °C stuck to the crucible bottom after thermal cycling indicating the formation of a salt solution and agglomeration of adjacent

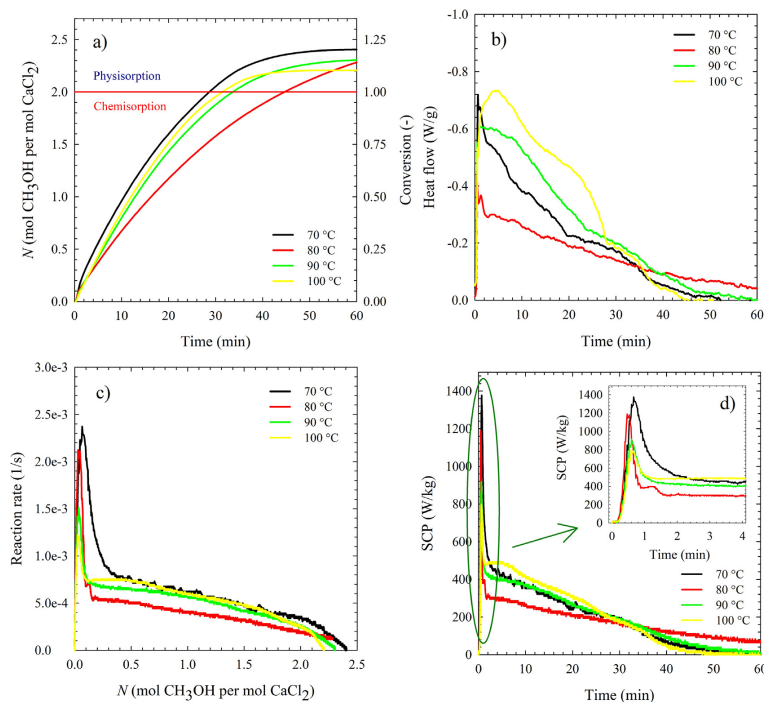


**Fig. 7.** Influence of the desorption temperature on the methanolation process (a), the thermal power normalized to the initial sample mass (b), the conversion rate (c), and the specific cooling power (d) of  $\text{CaCl}_2$  methanolates regenerated at different maximum demethanolation temperatures. Results from the 3rd methanolation run are depicted. Demethanolation reactions were conducted at temperatures of 70 °C, 80 °C, 90 °C, and 100 °C. Samples were heated from 25 °C to the final maximum temperature with 3 K/min in dry  $\text{N}_2$  atmosphere. In total, three consecutive methanolation/demethanolation cycles were performed.

particles during the methanolation/demethanolation reaction phase. The reaction rate and simultaneously the SCP decreased with increasing maximum desorption temperature and cycle time, as shown in Fig. 7d. From an energetic viewpoint, short cycle times for methanolation are preferable.

The demethanolation reactions proceeded similar up to a degree of conversion of 0.1, as shown in Fig. 8c, regardless of the desorption temperature applied. As the reaction progressed, the reaction rates described different patterns, which is ascribed to the different starting compounds. The sample regenerated at 80 °C shows reduced reactivity (Fig. 8a). During stabilization in  $\text{CH}_3\text{OH}$ -free, flowing  $\text{N}_2$ , some non-coordinated  $\text{CH}_3\text{OH}$  was evolved and hence the methanolation level at the start of the demethanolation step differed from the methanolation level reached at the end of the methanolation step indicating the presence of metastable phases. The initial methanolation state was between  $N = 1.1$  and  $N = 1.7$ . The thermal power per gram dry adsorbent material increased, when the regeneration temperature was increased, due to larger heat input (Fig. 8b). Heat transfer limitations prevented a continuous heat flow inside samples regenerated at temperatures of 70 °C and 100 °C. The onset temperature ranged from 62 °C to 80 °C in all demethanolation reactions. Peak temperatures were shifted to higher values by applying higher regeneration temperatures (Fig. 8b). The demethanolation reaction enthalpies normalized to one mole of reacted  $\text{CH}_3\text{OH}$  varied from 43 kJ/mol to 63 kJ/mol. The value

of 43 kJ/mol measured for a desorption temperature of 80 °C is slightly underestimated. A raise in the desorption temperature resulted in an increased demethanolation reaction enthalpy along with an increased heat capacity of the methanolated  $\text{CaCl}_2$ .

At milligram scale, the demethanolation at low fractional conversions facilitates structural deformations and positively influences the remethanolation, whereas cooling is rather supplied non-uniformly, as indicated by a steep peak maximum. The formation of a solution was identified as a drawback. The subsequent demethanolation reactions are likely to contribute to a lesser extent to the adsorbent expansion, since lower reaction rates were measured (Fig. 8c). The demethanolation process proceeded at slow rates in indistinct stages and was proven to be a major constraint for potential use in large-scales. The results imply that in scaled-up reactors, in which uniform TCM distribution is difficult to realize, the increased height and density of the adsorbent reactive bed, a fortiori, will reduce the overall speed of the methanolation and demethanolation reaction and result in the formation of a local reaction front, particularly when low regeneration temperatures are applied.



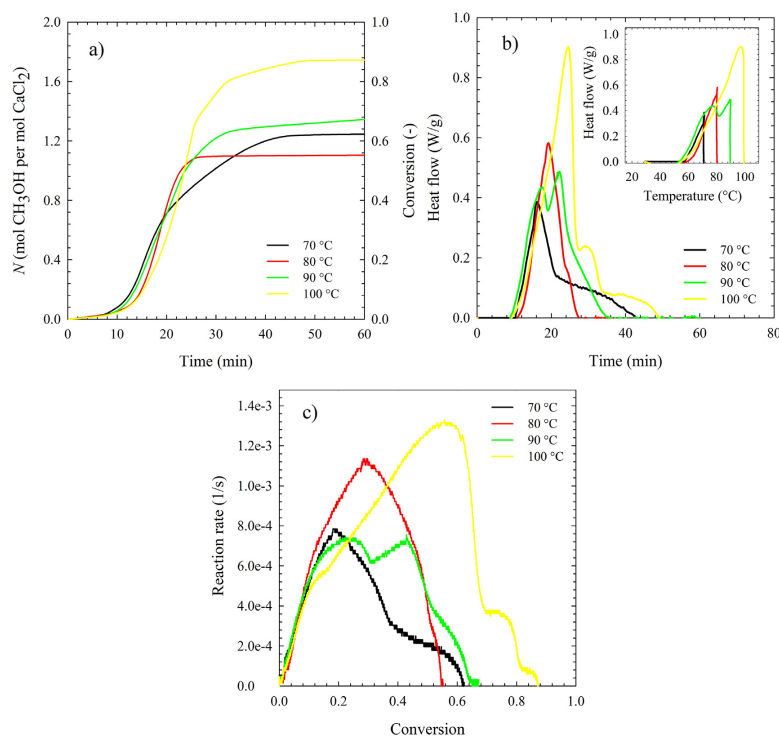


**Fig. 8.** Influence of the desorption temperature on the demethanolation reaction pattern (a), the thermal power normalized to the initial sample mass (b), the reaction kinetics behavior (c) of  $\text{CaCl}_2$  methanolates regenerated at different maximum demethanolation temperatures. Results from the 3rd demethanolation run are shown. Demethanolation reactions were conducted at temperatures of 70 °C, 80 °C, 90 °C, and 100 °C. Samples were heated from 25 °C to the final maximum temperature with 3 K/min in dry, flowing  $\text{N}_2$  atmosphere. In total, three consecutive methanolation/demethanolation cycles were performed.

#### 4.4. Influence of thermal cycling on the stability and reversible capacity of $\text{CaCl}_2$ methanolates

##### 4.4.1. Cycle stability of the methanolation reaction

The thermal cyclability of the  $\text{CaCl}_2\text{-CH}_3\text{OH}$  adduct was investigated in a cycling test with 18 methanolation/demethanolation cycles. Knowledge about the cyclic behavior of pure  $\text{CaCl}_2$  is of great practical importance. In this study, the virgin  $\text{CaCl}_2$  anhydride was dried at 105 °C prior to cycling.

Due to the thermal pretreatment, an unstable  $\text{CH}_3\text{OH}$  uptake occurred in the first few cycles (Fig. 9a and c). As the amount of reacted  $\text{CH}_3\text{OH}$  varied greatly at the beginning, owing to an overstoichiometric reaction, the formation of metastable phases is assumed. From the 10th cycle onwards the uptake and release of  $\text{CH}_3\text{OH}$  were constant and the amount of physisorbed  $\text{CH}_3\text{OH}$  was similar in each cycle (Fig. 9b and d). Over a methanolation time of 60 min about  $N = 2.1 \pm 0.1$  were adsorbed. At the end of the methanolation run with a duration of 120 min, the average methanolation level reached a value of  $N = 2.3 \pm 0.2$ . No significant change in the enthalpy of reaction, both methanolation and demethanolation, was measured (Fig. 13b). Considering the stable  $\text{CH}_3\text{OH}$  uptake and constant associated reaction enthalpies, the  $\text{CaCl}_2\text{-CH}_3\text{OH}$  system possesses a good reversible performance.

A detailed assessment of the methanolation reaction kinetics revealed that the time to reach an extent of conversion of 50% was extended with cycling, despite a rather stable  $\text{CH}_3\text{OH}$  uptake (Fig. 10e and f). This implies that the methanolation reaction slowed down with cycling. Even though the reaction proceeded fast at the beginning of the methanolation phase, indicated by a steep curve, the reaction decelerated with time and with higher extent of conversion. The highest maximum methanolation rate was measured in the third cycle (Fig. 10a). The subsequent maximum methanolation rates ranged from 0.25 mg/min to 0.42 mg/min and showed a decreasing tendency with increasing cycle number, while the sample masses stayed rather constant (Fig. 10b). Methanolation rates averaged over a time period of 60 min and 120 min were considerably lower with 0.09 mg/min to 0.11 mg/min and 0.05 mg/min to 0.06 mg/min, respectively. With increasing methanolation rate, the SCP was also lifted, due to direct proportionality (Fig. 10c and d).

##### 4.4.2. Cycle stability of the demethanolation reaction

Since the remethanolation rate is a function of the demethanolation conditions, the demethanolation reaction kinetics were also assessed. Non-coordinated  $\text{CH}_3\text{OH}$  was evolved during stabilization until chemical equilibrium was attained and the demethanolation run started (Fig. 11a and b). The dissociation reaction pattern was inconsistent

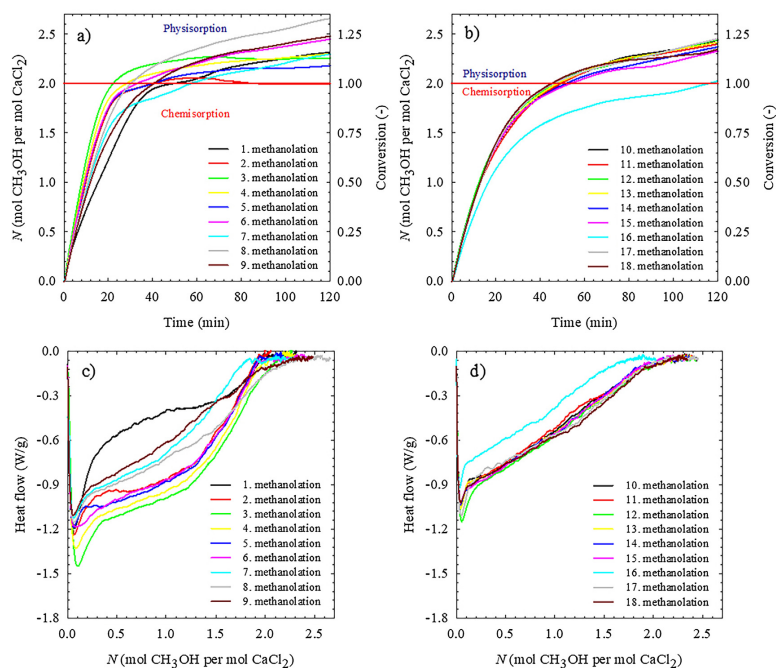


**Fig. 9.** Cycle performance test of the CaCl<sub>2</sub>-CH<sub>3</sub>OH system: change in the CH<sub>3</sub>OH uptake over the first 9 methanolation/demethanolation cycles (a) and over the last 9 methanolation/demethanolation cycles (b). DSC curves with change in the heat flow normalized to the initial sample mass of the 1st–9th methanolation reaction (c) and of the 10th–18th methanolation reaction (d). Methanolation runs were carried out at  $p_{\text{CH}_3\text{OH}} = 6.8 \text{ kPa}$  and  $\vartheta_{\text{trap}} = 8.5^\circ\text{C}$  under isothermal conditions ( $\vartheta_{\text{cond}} = 25^\circ\text{C}$ ). Dynamic demethanolation measurements were performed from  $25^\circ\text{C}$  to  $180^\circ\text{C}$  with a temperature ramp of  $3 \text{ K/min}$  in dry N<sub>2</sub>.

with variation in the number of decomposition stages and peak temperatures (Fig. 11c and d). The first methanolation/demethanolation reaction cycle significantly differed from the subsequent ones. The CaCl<sub>2</sub> methanolates decomposed in 2–3 stages within a narrow temperature domain with onset temperatures between  $75^\circ\text{C}$  and  $88^\circ\text{C}$ . Physisorbed CH<sub>3</sub>OH was completely removed below  $100^\circ\text{C}$ . From the 2nd cycle onwards, the peak temperatures were gradually shifted towards slightly higher temperatures ( $100^\circ\text{C}$  to  $104^\circ\text{C}$ ) with cycling. Higher initial methanolation levels resulted in higher maximum peak temperatures. The lowest maximum peak temperatures with values of  $94/95^\circ\text{C}$  were measured in the 4th, 5th, and 6th demethanolation runs in which the initial methanolation levels were around  $N = 1.7$ .

An increase in the maximum demethanolation rate with increasing number of cycles was observed (Fig. 12a and b). Reaction rates followed the same trend (Fig. 12c and d). As seen in Fig. 13a, the reaction rates of the demethanolation reaction were much higher compared to the reaction rates of the methanolation rates. Demethanolation reactions were performed under dynamic conditions by heating the specimen with a defined temperature ramp. The temperature gradient in the CaCl<sub>2</sub> methanolate is the thermodynamic driving force for the demethanolation reaction. In the first cycles the reaction, rate of the demethanolation reaction varies significantly, but from the 11th cycle onwards, it approaches a stable value. Three domains are observed, as displayed in Fig. 12d. The first domain ranges approximately between  $N = 2.4$ – $1.6$ , the second between  $N = 1.7$ – $0.1$ , and the third one between  $N = 0.2$ – $0.0$ .

The nature of the compound altered with successive cycling. During the methanolation reaction, the sample undergoes a volume expansion, due to phase change. After cycling, the sample had a porous framework and the sample size increased. High CH<sub>3</sub>OH vapor pressures necessitate high volumetric changes. The formed CaCl<sub>2</sub> methanolate has a higher volume and occupies more space than anhydrous CaCl<sub>2</sub>. A reduced total void fraction results in a better internal thermal contact and higher thermal conductivity of the CaCl<sub>2</sub> methanolate. In the subsequent demethanolation reaction, CH<sub>3</sub>OH is successively evolved. N<sub>2</sub> flows over the sample from one side only, which means that CH<sub>3</sub>OH removal is predominated by one-dimensional transport. Fast release of CH<sub>3</sub>OH located in the outer layers of the sample occurred. Residual CH<sub>3</sub>OH is retained inside the sample, which in turn displaces the chemical equilibrium. The dissociation of lower methanolates is shifted towards higher temperatures. When the sample is cooled down, the bulk density of the sample may slightly increase again, because of volume contraction. Less accessible diffusion pathways are responsible for decelerated remethanolation and reaction rates. In the repeated thermally induced demethanolation reactions, the liberation of CH<sub>3</sub>OH proceeds at faster rates, due to formation of cracks and tunnels inside the sample and reduced bulk density. Heat transfer limitations resulting from slow heat distribution and partial self-cooling may additionally negatively influence the methanolation/demethanolation reaction scheme.

For a comprehensive validation of the obtained data, complementary experimental approaches should be used. However, the determination of textural modifications and phase transitions, e.g. via SEM and

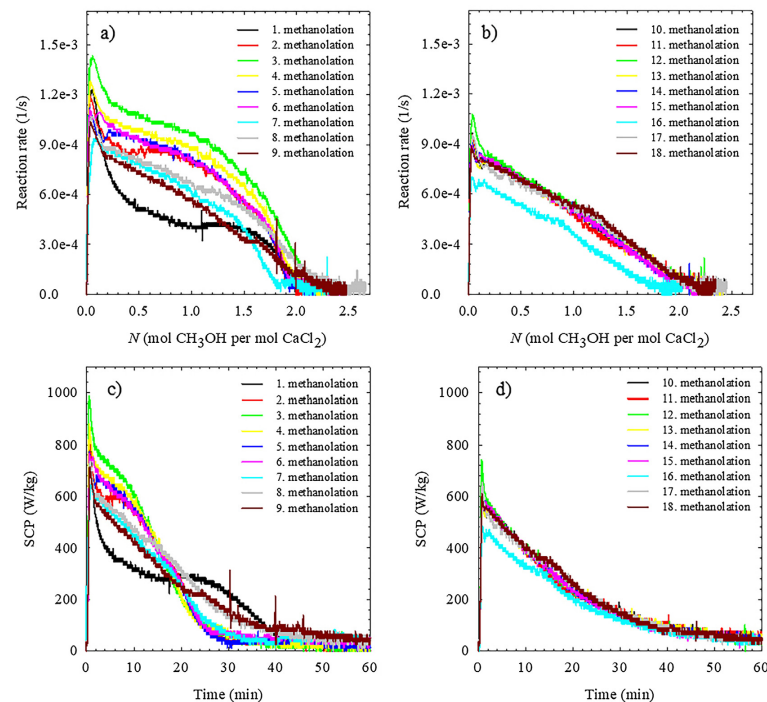


Fig. 10. Results on the methanolation reaction kinetics of  $\text{CaCl}_2$  methanolates cycled over 18 dynamic methanolation/demethanolation cycles: (a) reaction rate of the 1st–9th methanolation, (b) reaction rate of the 10th–18th methanolation, (c) SCP as a function of the cycle time for the 1st–9th methanolation, and (d) SCP as a function of the cycle time for the 10th–18th methanolation. Methanolation runs were performed at  $p_{\text{CH}_3\text{OH}} = 6.8 \text{ kPa}$  and  $\theta_{\text{evap}} = 8.5^\circ\text{C}$  under isothermal conditions ( $\theta_{\text{cond}} = 25^\circ\text{C}$ ). In dynamic demethanolation runs, the specimen was scanned from  $25^\circ\text{C}$  to  $180^\circ\text{C}$  with a constant heating rate of  $3 \text{ K/min}$  in dry  $\text{N}_2$  atmosphere.

XRD, were not within the scope of this study.

#### 4.5. Determination of the SCP and COP

Predrying led to a smoother progress of the methanolation reaction. The shapes of the curves depicted in Fig. 3d reflect that cold energy can be constantly provided over the time period investigated. In real applications sharp and narrow cooling peaks are not ideal, as a rather uniform cooling output is desirable. Results from the equilibrium and multi-step test are summarized in Tables 4 and 5. Since higher  $\text{CH}_3\text{OH}$  partial vapor pressures resulted in higher methanolation rates, the maximum SCPs increased as well, while the enthalpy of vaporization of  $\text{CH}_3\text{OH}$  slightly decreased. The maximum SCPs were in the range of  $232 \text{ W/kg}$  to  $1029 \text{ W/kg}$ . At a  $\text{CH}_3\text{OH}$  partial vapor pressure of  $9.1 \text{ kPa}$  corresponding to an evaporator temperature of  $13.6^\circ\text{C}$ , the SCP even reached a value of  $1029 \text{ W/kg}$ . Due to textural modifications and mass transfer limitations in predried samples, reduced maximum SCPs of  $232 \text{ W/kg}$  ( $6.8 \text{ kPa}$ ,  $8.5^\circ\text{C}$ ) and  $351 \text{ W/kg}$  ( $9.1 \text{ kPa}$ ,  $13.6^\circ\text{C}$ ) were achieved. The more practice-oriented average SCPs were also calculated and compared (Table 5). Higher  $\text{CH}_3\text{OH}$  partial pressures induced higher SCP maxima, but SCPs averaged over a methanolation level of  $N = 2.0$  varied only over a comparably narrow range ( $157\text{--}366 \text{ W/kg}$ ), however there is a significant increase between  $6.8 \text{ kPa}$  ( $8.5^\circ\text{C}$ ) and  $8.2 \text{ kPa}$  ( $11.7^\circ\text{C}$ ) indicating possible applications with evaporator

temperatures around or above  $10^\circ\text{C}$  as for the cooling of buildings, for example. The condensation temperature was  $25^\circ\text{C}$  in each measurement. The experimental COPs were very close to theoretical COP values with  $0.62\text{--}0.63$ . Samples predried at  $105^\circ\text{C}$  and methanolated at a  $\text{CH}_3\text{OH}$  vapor pressure of  $6.8 \text{ kPa}$  and  $9.1 \text{ kPa}$  exhibited similar COPs of  $0.59$  and  $0.59$ , respectively (Table 5).

In the multi-step screening test, the calculated maximum SCPs were lower with values of  $361 \text{ W/kg}$ ,  $342 \text{ W/kg}$ , and  $382 \text{ W/kg}$ , respectively, compared to the maximum SCP ( $539 \text{ W/kg}$ ) obtained in the equilibrium test under equivalent methanolation conditions (Table 4). The methanolation was performed at a  $\text{CH}_3\text{OH}$  partial vapor pressure of  $6.8 \text{ kPa}$ , which corresponds to an evaporation temperature of  $8.5^\circ\text{C}$ . With average SCPs between  $137 \text{ W/kg}$  and  $202 \text{ W/kg}$ , a considerable impact of multi-step cycling with higher initial methanolate levels at low regeneration temperatures on the reaction kinetics is assumed. The average SCP decreased with cycling, although the maximum methanolation rates were similar (Fig. 5d). However, the average methanolation rate of the third methanolation reaction was about 25% lower than that of the first and second one. The methanolation rates of the latter were similar. Same tendency was observed for the COP, which fluctuated between  $0.68$ ,  $0.75$ , and  $0.59$ , respectively, resulting in performance attenuation. Sample geometry and particle size affected by thermal and mechanical pretreatment contributed to a deteriorated performance. On the basis of the obtained experimental data, a non-

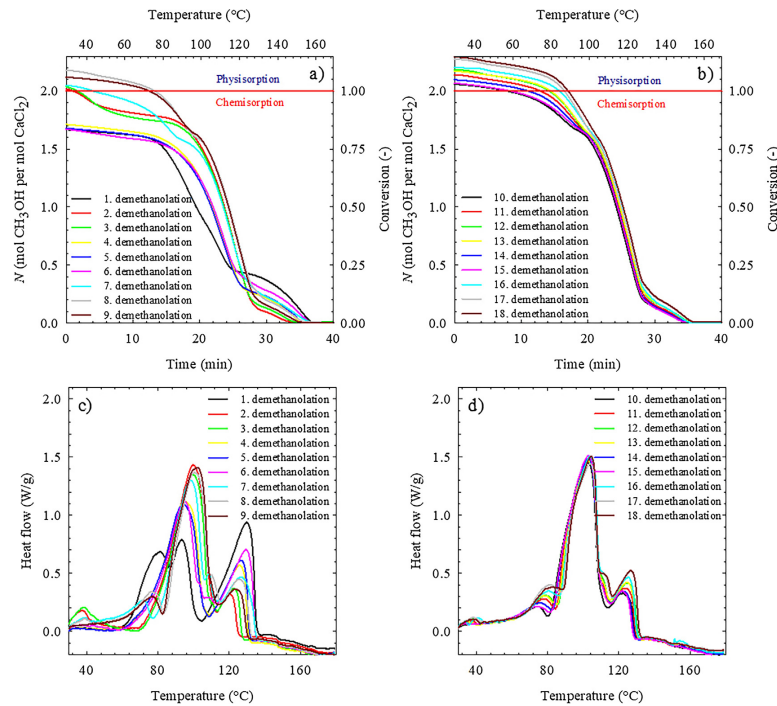


Fig. 11. Short-term thermal cycling test of the CaCl<sub>2</sub>-CH<sub>3</sub>OH system: (a) CH<sub>3</sub>OH release in the 1st–9th cycle, (b) CH<sub>3</sub>OH release in the 10th–18th cycle, and associated heat flow for the 1st–9th cycle (c), and the 10th–18th cycle (d). Methanolation runs were carried out at  $p_{\text{CH}_3\text{OH}} = 6.8 \text{ kPa}$  and  $\vartheta_{\text{evap}} = 8.5^\circ\text{C}$  under isothermal conditions ( $\vartheta_{\text{cond}} = 25^\circ\text{C}$ ). Dynamic demethanolation measurements were performed in the temperature range of 25–180 °C with a ramp of 3 K/min in dry N<sub>2</sub>.

linear relationship between the SCP and the CH<sub>3</sub>OH partial vapor pressure is considered. A high efficacy is subjected to a sufficient CH<sub>3</sub>OH vapor pressure. Precise prediction of the SCP by TGA/DSC is subjected to uncertainties, because of variables such as the initial mass, crystal structure, particle size distribution, and total surface area of the specimen that may also affect the cooling power output besides the parameters evaluated. Additionally, the sample preparation method, e.g. distribution of the specimen in the crucible and compaction pressure, contributes to certain discrepancies.

Fig. 14a shows the variation of the cooling COP and SCP as a function of the regeneration temperature. Evidently, the regeneration temperature has a significant impact on the cooling effect of repeated methanolation/demethanolation reaction cycles. Changes in the maximum SCPs over cycling occurred, regardless of the desorption temperature (Fig. 14b), as determined in the cycle stability test. The maximum SCP increased with thermal cycling and decreased with increasing desorption temperature. At desorption temperatures below 90 °C, maximum SCPs even reached values higher than 1000 W/kg producing a remarkable instant cooling effect. SCPs averaged over a reaction time of 60 min attained values around 200 W/kg, irrespective of the desorption temperature applied (Fig. 14a). The initial sample masses ranged from 11.26 mg to 13.04 mg. The smaller sample mass at the beginning of the (re-) methanolation reaction of the sample regenerated at a temperature of 70 °C (11.26–11.61 mg) probably contributed to a specific extent to higher SCP, when compared with the

fairly heavier samples.

Since the cooling efficiency of the material decreases, when the thermal energy input is increased, the thermodynamic cooling COP was slightly reduced with the rise in the desorption temperature. The maximum cooling COP was measured for a regeneration temperature of 80 °C, as depicted in Fig. 14a. The experimentally obtained demethanolation reaction enthalpy was slightly underestimated and consequently the calculated cooling COP was systematically overestimated.

In the cycle stability test, which was carried out at  $\vartheta_{\text{evap}} = 8.5^\circ\text{C}$ ,  $\vartheta_{\text{cond}} = 25^\circ\text{C}$ , and  $\vartheta_{\text{reg}} = 180^\circ\text{C}$ , the SCP of the first methanolation reaction of the predried sample was significantly higher than the SCP measured in the equilibrium test, which is attributed to the smaller sample mass ( $\Delta m = 15\%$ ). Smaller sample quantities or lower sample thicknesses promote better methanolation, as resistance to the methanol transport is reduced. Stanish and Perlmutter [108] have examined the suitability of the K<sub>2</sub>CO<sub>3</sub>-H<sub>2</sub>O system for low-temperature heat pumps. They reported that the hydration increased, when the pore diameter of salt particles was decreased, due to improved heat transfer. As seen in Fig. 15, the maximum SCP displayed a decreasing tendency. An elongation of the reaction time that produces the highest cold output was noticed over cycling. Both maximum methanolation rate and maximum SCP declined gradually up to 30% after 18 cycles compared to the value of the first methanolation process. The maximum SCP averaged over 18 cycles was  $(715 \pm 118) \text{ W/kg}$ . The maximum methanolation rate averaged  $(0.34 \pm 0.06) \text{ mg/min}$  over 18 cycles.

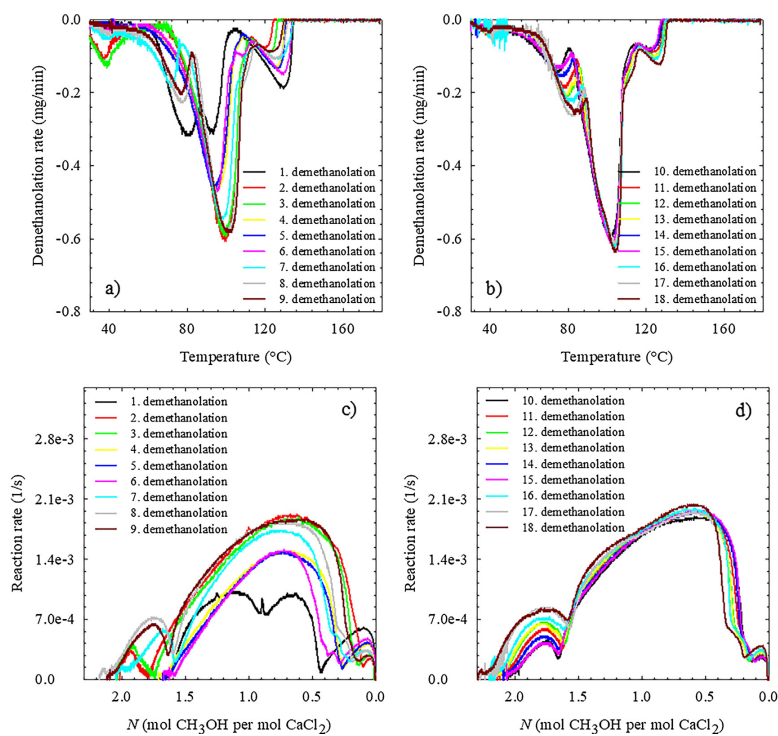


Fig. 12. Results on the demethanolation reaction kinetics of CaCl<sub>2</sub> methanolates cycled over 18 dynamic methanolation/demethanolation cycles: (a) demethanolation rate of the 1–9th demethanolation reaction, (b) demethanolation rate of the 10th–18th demethanolation reaction, (c) reaction rate of the 1st–9th demethanolation reaction, and (d) reaction rate of the 10th–18th demethanolation reaction. Methanolation runs were performed at  $p_{\text{CH}_3\text{OH}} = 6.8$  kPa and  $\dot{q}_{\text{vap}} = 8.5$  °C under isothermal conditions ( $\dot{q}_{\text{cond}} = 25$  °C). In dynamic demethanolation runs, the specimen was scanned from 25 °C to 180 °C with 3 K/min in flowing dry N<sub>2</sub>.

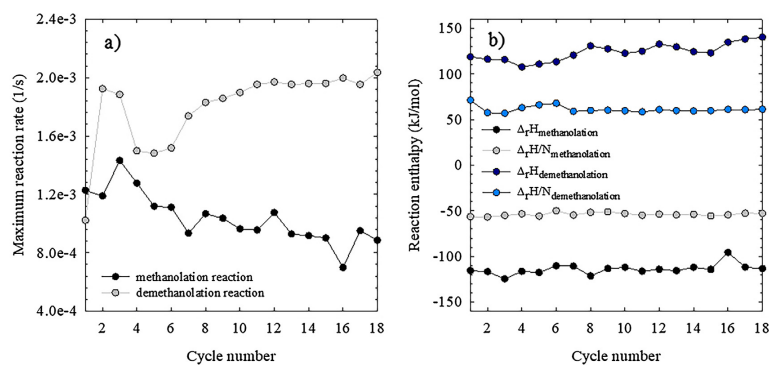


Fig. 13. Effect of thermal cycling of the reaction pair CaCl<sub>2</sub>-CH<sub>3</sub>OH on the maximum reaction rates (a), on the reaction enthalpies (b), and on the reaction enthalpies normalized to one mole of CH<sub>3</sub>OH (b) of the methanolation and demethanolation reactions. Methanolation runs were performed at  $p_{\text{CH}_3\text{OH}} = 6.8$  kPa and  $\dot{q}_{\text{vap}} = 8.5$  °C under isothermal conditions ( $\dot{q}_{\text{cond}} = 25$  °C). In dynamic demethanolation runs, the specimen was scanned from 25 °C to 180 °C with 3 K/min in flowing dry N<sub>2</sub>.

**Table 5**  
Influence of  $P_{\text{CH}_3\text{OH}}$  on the  $\text{CH}_3\text{OH}$  sorption, the thermal behavior, the reaction kinetics, the energy storage density, and the cooling performance of the methanolation/demethanolation reaction of  $\text{CaCl}_2$  and its methanolates. Average methanolation rates and average SCPs are referred to  $\text{CH}_3\text{OH}$  uptakes of 2 mol of  $\text{CH}_3\text{OH}$  per mole  $\text{CaCl}_2$  anhydride. The given  $P_{\text{CH}_3\text{OH}}$  and corresponding  $\delta_{\text{max}}$  are based on theoretical calculations.

$P_{\text{CH}_3\text{OH}}$ (kPa)	Sample history	$m_0$ (mg)	$N$	$w_{\text{CH}_3\text{OH}}$ (%)	Peak heat flow (W/g)	Max dm/dt (mg/min)	Average dm/dt (mg/min)	Max dm/dt (mg/min)	$\delta_{\text{max}}$ (°C)	$\delta_{\text{min}}$ (°C)	$\delta_{\text{peak}}$ (°C)	$\Delta H$ (kJ/mol)	$\Delta H/N$ (kJ/mol)	$\Delta h$ (J/g)	$\delta_{\text{des}}$ (°C)	$\delta_{\text{max}}$ (°C)	Max SCP (W/kg)	Average SCP (W/kg)	COP
6.8	Untreated	11.74	2.0	58	-0.41	0.32	0.13	7.83E-04	8.5	25	106/135	-105	-52	-498	8.5	25	539	218	0.63
	Predicted	11.32	2.0	58	-0.37	0.13	0.09	3.37E-03	8.5	25	92/112	-112	-56	-637	8.5	25	232	157	0.59
	Untreated	12.31	2.0	58	-0.80	0.46	0.21	1.07E-03	11.7	25	101/135	-106	-53	-521	11.7	25	735	344	0.62
	Predicted	12.58	2.0	58	-0.92	0.65	0.23	1.50E-03	13.6	25	106/136	-105	-53	-514	13.6	25	1029	366	0.62
9.1	Untreated	11.83	2.0	58	-0.57	0.21	0.17	5.14E-04	13.6	25	92/111/124	-116	-51	-629	13.6	25	351	290	0.59
	Predicted	16.96	-1.7	33	0.79	-0.41	-0.14	1.05E-03	69/98/105	84/117	106/135	165	60	831	150	150	150	150	150
6.8	Untreated	16.30	-2.7	44	1.26	-0.69	-0.20	2.01E-03	84/117	106/135	165	60	831	150	150	150	150	150	150
	Predicted	18.04	-1.8	34	0.78	-0.39	-0.13	1.04E-03	65/97	92/112	114	65	680	150	150	150	150	150	150
	Untreated	20.86	-2.6	43	1.20	-0.73	-0.19	2.05E-03	88/112	101/135	161	61	824	150	150	150	150	150	150
	Predicted	16.96	-1.7	33	0.79	-0.41	-0.14	1.05E-03	69/98/105	84/117	106/135	165	60	831	150	150	150	150	150

However, the average SCPs were unchanged. The arithmetic average of the SCPs averaged over a methanolation time of 60 min amounted to  $(203 \pm 12)$  W/kg. Since the total  $\text{CH}_3\text{OH}$  uptake remained constant, the lower maximum SCP resulted in a more stable cooling process and capacity over time. Thermal cycling of  $\text{CaCl}_2$  methanolates under constant methanolation/demethanolation reaction conditions had only a slight influence on the cooling COP. The COP ranged from 0.67 to 0.75 and its arithmetic average was  $0.63 \pm 0.03$ . SCP and cooling COP values obtained by TGA/DSC are comparable with literature values [101,139].

Main results on the cooling performance of the reaction pair  $\text{CaCl}_2$  and  $\text{CH}_3\text{OH}$  over the desorption temperature domain of 70–180 °C are summarized in Table 6. The overall COP stabilizes at temperatures above 100 °C, which signifies that desorption temperatures higher than 100 °C do not noticeably improve the material performance. The findings indicate that desorption temperatures below 90 °C result in good COPs and average SCPs. Since high maximum SCPs were measured for desorption temperatures of 70 °C, 80 °C, and 90 °C, which correspond to high peak loads of cold exposure, the application of desorption temperatures higher than 90 °C will give more static cold supply, and hence they are favored under the boundary conditions studied. Moreover, the amount of methanolated  $\text{CaCl}_2$  remaining in the system is limited and agglomeration phenomena can be reduced. In the present study, the cooling COPs are referred to the cooling performance at material scale. Specifications and operating parameters of an adsorption cooling system, including the influence of the heat exchanger, the reactor material, the share of the sensible heat, thermal losses, etc., were not taken into account. In the real application, the achievable cooling COPs are presumably lower than the ones presented in this study, as disclosed by Bao et al. [71], who observed a reduction of the maximum possible COP of 29–32%.

## 5. Conclusions

At material scale, TGA/DSC analysis is an indispensable tool for estimation of the energy storage and cooling efficiency of TCMs. In this paper, the potential of  $\text{CaCl}_2$  and its methanolates for solid adsorption refrigeration has been studied. Experimental data on thermodynamic and kinetic characteristics of the methanolation/demethanolation reaction have been obtained from simultaneous TGA/DSC measurements. In general, methanolation and demethanolation are multi-causal processes and are implicitly influenced by multiple parameters. In refrigeration applications, the most important key performance indicators are the SCP and the cooling COP. Variation of the operating conditions remarkably affected the cooling power and cooling performance. Influence of the physical properties and the thermal history of the material tested, the partial pressure of the reactant, the regeneration temperature, and repeated thermal cycling was investigated. The methanolation rate of the heterogeneous gas-solid reaction was lifted by applying higher  $\text{CH}_3\text{OH}$  partial vapor pressures, which resulted in a higher maximum cold output at higher evaporation temperatures. Thermal predrying at 105 °C gave stable addition compounds, irrespective of the  $\text{CH}_3\text{OH}$  vapor pressure. However, maximum and average SCPs and COPs were significantly reduced. In a dynamic cyclic reversibility test, it was shown that the reaction rate for demethanolation of the virgin sample was slow, but increased with increasing number of cycles until a rather stable value with little deviation was reached. In contrast, the maximum reaction rate of the methanolation reaction decreased by 28% compared to the initial value. Consequently, the maximum SCP showed a decreasing trend, whereas the more practically relevant average SCP remained constant. Application-wise, desorption temperatures are a critical aspect of system design.  $\text{CaCl}_2$  methanolates show good reaction kinetics if regenerated at  $\leq 100$  °C. However in practice, demethanolation kinetics are limiting efficiency. With lower regeneration temperatures longer demethanolation cycles are needed, since peak desorption temperatures ( $> 90$  °C) may not be reached.

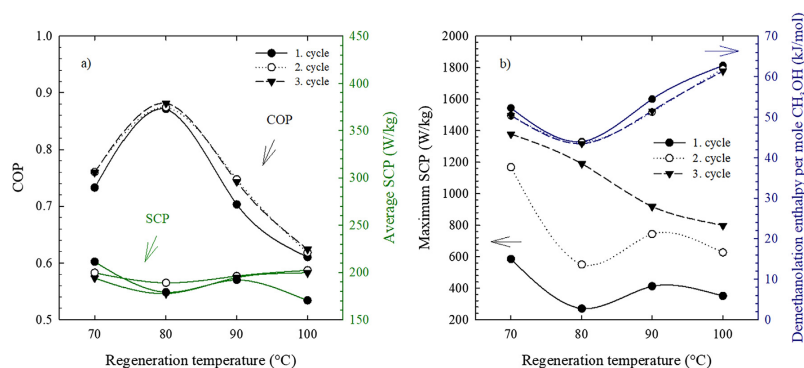


Fig. 14. Dependence of the COP and SCP on the regeneration temperature. In total, three consecutive methanolation/demethanolation cycles were performed, denoted by 1. cycle, 2. cycle, and 3. cycle. Demethanolation processes were carried out at temperatures of 70 °C, 80 °C, 90 °C, and 100 °C. Methanolation reactions were run at at  $P_{\text{CH}_3\text{OH}} = 6.8 \text{ kPa}$  and  $\delta_{\text{evap}} = 8.5^\circ\text{C}$  under isothermal conditions ( $\delta_{\text{cond}} = 25^\circ\text{C}$ ).

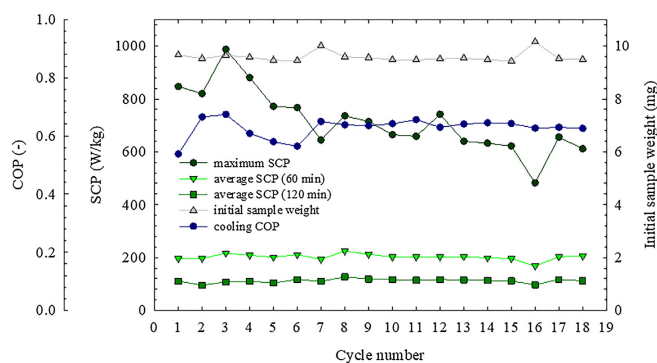


Fig. 15. Change in the maximum and average SCP and cooling COP with repeated thermal cycling of  $\text{CaCl}_2$  methanolates. Methanolation reactions were carried out at  $P_{\text{CH}_3\text{OH}} = 6.8 \text{ kPa}$  and  $\delta_{\text{evap}} = 8.5^\circ\text{C}$  under isothermal conditions ( $\delta_{\text{cond}} = 25^\circ\text{C}$ ). In dynamic demethanolation runs, the specimen was scanned from 25 °C to 180 °C ( $\delta_{\text{reg}} = 180^\circ\text{C}$ ) with a temperature ramp of 3 K/min in dry  $\text{N}_2$  atmosphere.

Table 6

Overview of the thermodynamic cooling efficiency of the working pair  $\text{CaCl}_2$  and  $\text{CH}_3\text{OH}$  under different operating conditions. The values were averaged over 18 cycles or are referred to one single cycle. For desorption temperatures of 70 °C, 80 °C, 90 °C, and 100 °C results from the 3rd demethanolation/methanolation reaction cycle are presented. The reaction time of 60 min is referred to a conversion of 100% indicating the uptake of 2.0 to 2.4 mol of  $\text{CH}_3\text{OH}$  per mole  $\text{CaCl}_2$ .

$\delta_{\text{evap}}$ (°C)	$\delta_{\text{cond}}$ (°C)	$\delta_{\text{reg}}$ (°C)	Sorption quantity (g/g)	$\Delta_r H/v$ (kJ/mol)	Max SCP (W/kg)	Average SCP (W/kg)	COP	Time (min)	Number of cycles
8.5	25	70	0.66	50	1378	194	0.76	60	3
8.5	25	80	0.69	43	1190	178	0.88	60	3
8.5	25	90	0.67	52	918	195	0.74	60	3
8.5	25	100	0.64	61	798	200	0.62	60	3
8.5	25	180	$0.61 \pm 0.04$	$61 \pm 4$	$715 \pm 118$	$203 \pm 12$	$0.63 \pm 0.03$	60	18

Furthermore, at lower temperatures, chemically bound  $\text{CH}_3\text{OH}$  is not fully desorbed, limiting the sorption capacity of the adsorbent. At 70–80 °C, samples showed liquefaction. To overcome constraints on the thermodynamic and kinetic behavior, material modification methods are verified. Methanolation/demethanolation cycling experiments of composite adsorbents, i.e.  $\text{CaCl}_2$  incorporated into expanded vermiculite and biochar, are being currently carried out.

#### Acknowledgements

The authors gratefully acknowledge the financial support from the Federal Ministry for Economic Affairs and Energy. This study was conducted within the framework of a ZIM cooperation project under grant number KF2098305ZG4. The authors would like to thank Holger Urs Rammelberg, Christina Apel, and Armand Fopah-Lele for assistance

in the modification of the experimental setup and scientific discussions.

## References

- [1] International Energy Agency. Climate change 2016 < <http://www.iaea.org/topics/climatechange/> > [accessed February 16, 2016].
- [2] European Commission. Fluorinated greenhouse gases | Climate Action 2016. < [https://ec.europa.eu/clima/policies/f-gas\\_en](https://ec.europa.eu/clima/policies/f-gas_en) > [accessed February 15, 2016].
- [3] Critoph RE. Performance limitations of adsorption cycles for solar cooling. *Sol Energy* 1988;41:21–31. [https://doi.org/10.1016/0038-092X\(88\)90111-9](https://doi.org/10.1016/0038-092X(88)90111-9).
- [4] Yu N, Wang RZ, Wang LW. Sorption thermal storage for solar energy. *Prog Energy Combust Sci* 2013;39:489–514. <https://doi.org/10.1016/j.pecs.2013.05.004>.
- [5] Meunier F. Sorption solar cooling. *Renew Energy* 1994;5:422–9. [https://doi.org/10.1016/0960-1481\(94\)90409-X](https://doi.org/10.1016/0960-1481(94)90409-X).
- [6] N'Tsoukpoe KE, Le Pierrès N, Luo L. Experimentation of a LiBr–H<sub>2</sub>O absorption process for long-term solar thermal storage: prototype design and first results. *Energy* 2013;53:179–98. <https://doi.org/10.1016/j.energy.2013.02.023>.
- [7] Cui-Gores J, Castell A, Cabeza LF. Thermochemical energy storage and conversion: A state-of-the-art review of the experimental research under practical conditions. *Renew Sustain Energy Rev* 2012;16:5207–24. <https://doi.org/10.1016/j.rser.2012.04.007>.
- [8] McQuarrie DA, Simon JD. Physical chemistry: A molecular approach. Sausalito, CA: University Science Books; 1997.
- [9] Cui Q, Tao G, Chen H, Guo X, Yao H. Environmentally benign working pairs for adsorption refrigeration. *Energy* 2005;30:261–71. <https://doi.org/10.1016/j.energy.2004.05.005>.
- [10] Wongsuwan W, Kumar S, Neveu P, Meunier F. A review of chemical heat pump technology and applications. *Appl Therm Eng* 2001;21:1489–519. [https://doi.org/10.1016/S1359-4311\(01\)00022-9](https://doi.org/10.1016/S1359-4311(01)00022-9).
- [11] Meunier F. Solid sorption: an alternative to CFCs. *Heat Recover Syst CHP* 1993;13:289–95. [https://doi.org/10.1016/0890-4332\(93\)90051-V](https://doi.org/10.1016/0890-4332(93)90051-V).
- [12] Meunier F. Solid sorption heat powered cycles for cooling and heat pumping applications. *Appl Therm Eng* 1998;18:715–29. [https://doi.org/10.1016/S1359-4311\(97\)00122-1](https://doi.org/10.1016/S1359-4311(97)00122-1).
- [13] Pons M, Meunier F, Cacciola G, Critoph RE, Groll M, Puigjaner L, et al. Thermodynamic based comparison of sorption systems for cooling and heat pumping: comparison des performances thermodynamiques des systèmes de pompes à chaleur à sorption dans des applications de refroidissement et de chauffage. *Int J Refrig* 1999;22:5–17. [https://doi.org/10.1016/S0140-7007\(98\)00048-6](https://doi.org/10.1016/S0140-7007(98)00048-6).
- [14] Critoph RE, Zhong Y. Review of trends in solid sorption refrigeration and heat pumping technology. *Proc Inst Mech Eng Part E J Process Mech Eng* 2005;219:285–300. <https://doi.org/10.1243/095440805X6982>.
- [15] Wang RZ, Oliveira RG. Adsorption refrigeration – an efficient way to make good use of waste heat and solar energy. *Prog Energy Combust Sci* 2006;32:424–58. <https://doi.org/10.1016/j.pecs.2006.01.002>.
- [16] Wang DC, Li YH, Li D, Xia YZ, Zhang JP. A review on adsorption refrigeration technology and adsorption deterioration in physical adsorption systems. *Renew Sustain Energy Rev* 2010;14:344–53. <https://doi.org/10.1016/j.rser.2009.08.001>.
- [17] Wang RZ, Xia ZZ, Wang LW, Lu ZS, Li SL, Li TX, et al. Heat transfer design in adsorption refrigeration systems for efficient use of low-grade thermal energy. *Energy* 2011;36:5425–39. <https://doi.org/10.1016/j.energy.2011.07.008>.
- [18] Oertel K, Fischer M. Adsorption cooling system for cold storage using methanol/silicagel. *Appl Therm Eng* 1998;18:773–86. [https://doi.org/10.1016/S1359-4311\(97\)00107-5](https://doi.org/10.1016/S1359-4311(97)00107-5).
- [19] Núñez T, Mittelbach W, Henning HM. Development of an adsorption chiller and heat pump for domestic heating and air-conditioning applications. *Appl Therm Eng* 2007;27:2205–12. <https://doi.org/10.1016/j.applthermaleng.2005.07.024>.
- [20] Akahira A, Alam KCA, Hamamoto Y, Akisawa A, Kashiwagi T. Mass recovery four-bed adsorption refrigeration cycle with energy cascading. *Appl Therm Eng* 2005;25:1764–78. <https://doi.org/10.1016/j.applthermaleng.2004.10.006>.
- [21] El-Sharkawy II, Hassan M, Saha BB, Koyama S, Nasr MM. Study on adsorption of methanol on carbon based adsorbents. *Int J Refrig* 2009;32:1579–86. <https://doi.org/10.1016/j.ijrefrig.2009.06.011>.
- [22] Saha BB, Koyama S, Kashiwagi T, Akisawa A, Ng KC, Chua HT. Waste heat driven dual-mode, multi-stage, multi-bed regenerative adsorption system. *Int J Refrig* 2003;26:749–57. [https://doi.org/10.1016/S0140-7007\(03\)00074-4](https://doi.org/10.1016/S0140-7007(03)00074-4).
- [23] Saha BB, Akisawa A, Kashiwagi T. Silica gel water advanced adsorption refrigeration cycle. *Energy* 1997;22:437–47. [https://doi.org/10.1016/S0360-5442\(96\)00102-8](https://doi.org/10.1016/S0360-5442(96)00102-8).
- [24] Wang DC, Wu JY, Xia ZZ, Zhai H, Wang RZ, Dou WD. Study of a novel silica gel-water adsorption chiller. Part II Experimental study. *Int J Refrig* 2005;28:1084–91. <https://doi.org/10.1016/j.ijrefrig.2005.03.002>.
- [25] Yang GZ, Xia ZZ, Wang RZ, Keletigui D, Wang DC, Dong ZH, et al. Research on a compact adsorption room air conditioner. *Energy Convers Manage* 2006;47:2167–77. <https://doi.org/10.1016/j.enconman.2005.12.005>.
- [26] Grisel RJH, Smeding SF, de Boer R. Waste heat driven silica gel/water adsorption cooling in trigeneration. *Appl Therm Eng* 2010;30:1039–46. <https://doi.org/10.1016/j.applthermaleng.2010.01.020>.
- [27] Chang WS, Wang CC, Shieh CC. Design and performance of a solar-powered heating and cooling system using silica gel/water adsorption chiller. *Appl Therm Eng* 2009;29:2100–5. <https://doi.org/10.1016/j.applthermaleng.2008.10.021>.
- [28] Lu Z, Wang R, Xia Z. Experimental analysis of an adsorption air conditioning with micro-porous silica gel-water. *Appl Therm Eng* 2013;50:1015–20. <https://doi.org/10.1016/j.applthermaleng.2012.07.041>.
- [29] Hildbrand C, Dind P, Pons M, Buchter F. A new solar powered adsorption refrigerator with high performance. *Sol Energy* 2004;77:311–8. <https://doi.org/10.1016/j.solener.2004.05.007>.
- [30] Passos E, Meunier F, Gianola JC. Thermodynamic performance improvement of an intermittent solar-powered refrigeration cycle using adsorption of methanol on activated carbon. *J Heat Recover Syst* 1986;6:259–64. [https://doi.org/10.1016/0198-7593\(86\)90010-X](https://doi.org/10.1016/0198-7593(86)90010-X).
- [31] Al Mers A, Azzabakh A, Mimet A, El Kalkha H. Optimal design study of cylindrical finned reactor for solar adsorption cooling machine working with activated carbon-ammonia pair. *Appl Therm Eng* 2006;26:1866–75. <https://doi.org/10.1016/j.applthermaleng.2006.01.021>.
- [32] El-Sharkawy II, Kuwahara K, Saha BB, Koyama S, Ng KC. Experimental investigation of activated carbon fibers/ethanol pairs for adsorption cooling system application. *Appl Therm Eng* 2006;26:859–65. <https://doi.org/10.1016/j.applthermaleng.2005.10.010>.
- [33] Kil HS, Kim T, Hata K, Ideta K, Ohba T, Kanoh H, et al. Influence of surface functionalities on ethanol adsorption characteristics in activated carbons for adsorption heat pumps. *Appl Therm Eng* 2014;72:160–5. <https://doi.org/10.1016/j.applthermaleng.2014.06.018>.
- [34] Brancato V, Gordeeva LG, Sapienza A, Freni A, Frazzica A. Dynamics study of ethanol adsorption on microporous activated carbon for adsorptive cooling applications. *Appl Therm Eng* 2016;105:28–38. <https://doi.org/10.1016/j.applthermaleng.2016.05.148>.
- [35] Uddin K, El-Sharkawy II, Miyazaki T, Saha BB, Koyama S. Thermodynamic analysis of adsorption refrigeration cycles using parent and surface treated Maxsorb III/ethanol pairs. *Int. Refrig. Air Cond. Conf.*, 2014, p. Paper 1493.
- [36] Wang LW, Wu JY, Wang RZ, Xu YX, Wang SG. Experimental study of a solidified activated carbon-methanol adsorption ice maker. *Appl Therm Eng* 2003;23:1453–62. [https://doi.org/10.1016/S1359-4311\(03\)00103-0](https://doi.org/10.1016/S1359-4311(03)00103-0).
- [37] Gordeeva LG, Aristov YI. Dynamic study of methanol adsorption on activated carbon ACM-35.4 for enhancing the specific cooling power of adsorptive chillers. *Appl Therm Eng* 2014;117:127–33. <https://doi.org/10.1016/j.apenergy.2013.11.073>.
- [38] Henninger SK, Schickanz M, H?genell PPC, Sievers H, Henning HM. Evaluation of methanol adsorption on activated carbons for thermally driven chillers part I: Thermophysical characterisation. *Int J Refrig* 2012;35:543–53. doi: 10.1016/j.ij-refrig.2011.10.004.
- [39] Pons M, Guilleminot JJ. Design of an experimental solar-powered, solid-adsorption ice maker. *J Sol Energy Eng* 1986;108:332–7.
- [40] Boubakri A, Arsalane M, Yous B, Ali-Moussa L, Pons M, Meunier F, et al. Experimental study of adsorptive solar-powered ice makers in Agadir (Morocco)—I. Performance in actual site. *Renew Energy* 1992;2:7–13. [https://doi.org/10.1016/0960-1481\(92\)90054-7](https://doi.org/10.1016/0960-1481(92)90054-7).
- [41] Vasiliev LL, Mishkinis DA, Antukh AA, Vasiliev LL. Solar-gas solid sorption heat pump. *Appl Therm Eng* 2001;21:573–83. [https://doi.org/10.1016/S1359-4311\(00\)00069-7](https://doi.org/10.1016/S1359-4311(00)00069-7).
- [42] Critoph RE. Towards a one tonne per day solar ice maker. *Renew Energy* 1996;9:626–31. [https://doi.org/10.1016/0960-1481\(96\)88366-2](https://doi.org/10.1016/0960-1481(96)88366-2).
- [43] Critoph RE. Multiple bed regenerative adsorption cycle using the monolithic carbon-ammonia pair. *Appl Therm Eng* 2002;22:667–77.
- [44] Tamainot-Telto Z, Critoph RE. Monolithic carbon for sorption refrigeration and heat pump applications. *Appl Therm Eng* 2001;21:37–52. [https://doi.org/10.1016/S1359-4311\(00\)00030-2](https://doi.org/10.1016/S1359-4311(00)00030-2).
- [45] Critoph RE. Evaluation of alternative refrigerant-adsorbent pairs for refrigeration cycles. *Appl Therm Eng* 1996;16:891–900. [https://doi.org/10.1016/1359-4311\(96\)00008-7](https://doi.org/10.1016/1359-4311(96)00008-7).
- [46] Restuccia G, Freni A, Russo F, Vasta S. Experimental investigation of a solid adsorption chiller based on a heat exchanger coated with hydrophobic zeolite. *Appl Therm Eng* 2005;25:1419–28. <https://doi.org/10.1016/j.applthermaleng.2004.09.012>.
- [47] Hauer A. Adsorption systems for TES—Design and demonstration projects. In: Paksoy HÖ, editor. *Therm. energy storage Sustain. energy Consum.* 234th ed., Dordrecht: Springer Netherlands; 2007, p. 409–27. doi: 10.1007/978-1-4020-5290-3\_25.
- [48] Lang R, Roth M, Stricker M, Westerfeld T. Development of a modular zeolite-water heat pump. *Heat Mass Transf* 1999;35:229–34. <https://doi.org/10.1007/s002310050318>.
- [49] Poyelle F, Guilleminot J-J, Meunier F. Experimental tests and predictive model of an adsorptive air conditioning unit. *Ind Eng Chem Res* 1999;38:298–309. <https://doi.org/10.1021/ie9802008>.
- [50] Solmuş I, Yamali C, Kafanoglu B, Baker D, Çağlar A. Adsorption properties of a natural zeolite-water pair for use in adsorption cooling cycles. *Appl Energy* 2010;87:2062–7. <https://doi.org/10.1016/j.apenergy.2009.11.027>.
- [51] Zhang LZ. Design and testing of an automobile waste heat adsorption cooling system. *Appl Therm Eng* 2000;20:103–14. [https://doi.org/10.1016/S1359-4311\(99\)00009-5](https://doi.org/10.1016/S1359-4311(99)00009-5).
- [52] Jiangzhou S, Wang RZ, Lu YZ, Xu YX, Wu JY. Experimental investigations on adsorption air-conditioner used in internal-combustion locomotive driver-cabin. *Appl Therm Eng* 2002;22:1153–62. [https://doi.org/10.1016/S1359-4311\(02\)00036-4](https://doi.org/10.1016/S1359-4311(02)00036-4).
- [53] Lai HM. Enhanced adsorption cycle operated by periodic reversal forced convection. *Appl Therm Eng* 2000;20:595–617. [https://doi.org/10.1016/S1359-4311\(99\)00036-8](https://doi.org/10.1016/S1359-4311(99)00036-8).
- [54] Douss N, Meunier FE, Sun LM. Predictive model and experimental results for a two-adsorbent solid adsorption heat pump. *Ind Eng Chem Res* 1988;27:310–6. <https://doi.org/10.1021/ie00074a017>.
- [55] Rezk A, Al-Dadah R, Mahmoud S, Elsayed A. Investigation of ethanol/metal



- organic frameworks for low temperature adsorption cooling applications. *Appl Energy* 2013;112:1025–31. <https://doi.org/10.1016/j.apenergy.2013.06.041>.
- [56] Saha BB, El-Sharkawy II, Miyazaki T, Koyama S, Henninger SK, Herbst A, et al. Ethanol adsorption onto metal organic framework: theory and experiments. *Energy* 2015;79:363–70. <https://doi.org/10.1016/j.energy.2014.11.022>.
- [57] Jeremias F, Fröhlich D, Janiak C, Henninger SK. Water and methanol adsorption on MOFs for cycling heat transformation processes. *New J Chem* 2014;38:1846–52. <https://doi.org/10.1039/C3NJ01556D>.
- [58] Nguyen BT, Nguyen HL, Nguyen TC, Cordova KE, Furukawa H. High methanol uptake capacity in two new series of metal-organic frameworks: promising materials for adsorption-driven heat pump applications. *Chem Mater* 2016;28:6243–9. <https://doi.org/10.1021/acs.chemmater.6b02431>.
- [59] Janiak C, Henninger SK. Porous coordination polymers as novel sorption materials for heat transformation processes. *Chimia (Aarau)* 2013;67:419–24. <https://doi.org/10.2533/chemia.2013.419>.
- [60] Spinner B. Ammonia-based thermochemical transformers. *Heat Recover Syst CHP* 1993;13:301–7. [https://doi.org/10.1016/0890-4332\(93\)90053-X](https://doi.org/10.1016/0890-4332(93)90053-X).
- [61] Goetz V, Marty A. A model for reversible solid-gas reactions submitted to temperature and pressure constraints: simulation of the rate of reaction in solid-gas reactor used as chemical heat pump. *Chem Eng Sci* 1992;47:4445–54. [https://doi.org/10.1016/0009-2509\(92\)85122-R](https://doi.org/10.1016/0009-2509(92)85122-R).
- [62] Neveu P, Castaing J. Solid-gas chemical heat pumps: Field of application and performance of the internal heat of reaction recovery process. *Heat Recover Syst CHP* 1993;13:233–51. [https://doi.org/10.1016/0890-4332\(93\)90014-M](https://doi.org/10.1016/0890-4332(93)90014-M).
- [63] Lebrun M, Neveu P. Conception, simulation, dimensioning and testing of an experimental chemical heat pump. *ASHRAE Trans* 1992;98:3483–95.
- [64] Lepinasse E, Goetz V, Crosat G. Modelling and experimental investigation of a new type of thermochemical transformer based on the coupling of two solid-gas reactions. *Chem Eng Process Process Intensif* 1994;33:125–34. [https://doi.org/10.1016/0255-2701\(94\)90002-7](https://doi.org/10.1016/0255-2701(94)90002-7).
- [65] Lebrun M, Spinner B. Models of heat and mass transfers in solid–gas reactors used as chemical heat pumps. *Chem Eng Sci* 1990;45:1743–53. [https://doi.org/10.1016/0009-2509\(90\)87052-T](https://doi.org/10.1016/0009-2509(90)87052-T).
- [66] Neveu P, Castaing-Lasvignottes J. Development of a numerical sizing tool for a solid-gas thermochemical transformer—I. Impact of the microscopic process on the dynamic behaviour of a solid-gas reactor. *Appl Therm Eng* 1997;17:501–18. [https://doi.org/10.1016/S1359-4311\(96\)00065-8](https://doi.org/10.1016/S1359-4311(96)00065-8).
- [67] Mbaye M, Aidoun Z, Valkov V, Legault A. Analysis of chemical heat pumps (CHPs): basic concepts and numerical model description. *Appl Therm Eng* 1998;18:131–46. [https://doi.org/10.1016/S1359-4311\(97\)00027-6](https://doi.org/10.1016/S1359-4311(97)00027-6).
- [68] Li TX, Wang RZ, Wang LW. High-efficient thermochemical sorption refrigeration driven by low-grade thermal energy. *Chinese Sci Bull* 2009;54:885–905. <https://doi.org/10.1007/s11434-009-0117-3>.
- [69] Goetz V, Spinner B, Lepinasse E. A solid-gas thermochemical cooling system using BaCl<sub>2</sub> and NiCl<sub>2</sub>. *Energy* 1997;22:49–58. [https://doi.org/10.1016/S0360-5442\(96\)00081-3](https://doi.org/10.1016/S0360-5442(96)00081-3).
- [70] Gao P, Wang LW, Wang RZ, Zhang XF, Li DP, Liang ZW, et al. Experimental investigation of a MnCl<sub>2</sub>/CaCl<sub>2</sub>-NH<sub>3</sub> two-stage solid sorption freezing system for a refrigerated truck. *Energy* 2016;103:16–26. <https://doi.org/10.1016/j.energy.2016.02.145>.
- [71] Bao HS, Wang RZ, Oliveira RG, Li TX. Resorption system for cold storage and long-distance refrigeration. *Appl Energy* 2012;93:479–87. <https://doi.org/10.1016/j.apenergy.2011.12.022>.
- [72] Aristov YI, Restuccia G, Cacciola G, Parmon VN. A family of new working materials for solid sorption air conditioning systems. *Appl Therm Eng* 2002;22:191–204. [https://doi.org/10.1016/S1359-4311\(01\)00072-2](https://doi.org/10.1016/S1359-4311(01)00072-2).
- [73] Cortés FB, Chejne F, Carrasco-Marín F, Pérez-Cadenas AF, Moreno-Castilla C. Water sorption on silica- and zeolite-supported hygroscopic salts for cooling system applications. *Energy Convers Manage* 2012;53:219–23. <https://doi.org/10.1016/j.enconman.2011.09.001>.
- [74] Tso CY, Chao CYH. Activated carbon, silica-gel and calcium chloride composite adsorbents for energy efficient solar adsorption cooling and dehumidification systems. *Int J Refrig* 2012;35:1626–38. <https://doi.org/10.1016/j.jrefrig.2012.05.007>.
- [75] Restuccia G, Freni A, Vasta S, Aristov YI. Selective water sorbent for solid sorption chiller: experimental results and modelling. *Int J Refrig* 2004;27:284–93. <https://doi.org/10.1016/j.jrefrig.2003.09.003>.
- [76] Dawoud B, Aristov YI. Experimental study on the kinetics of water vapor sorption on selective water sorbents, silica gel and alumina under typical operating conditions of sorption heat pumps. *Int J Heat Mass Transf* 2003;46:273–81. [https://doi.org/10.1016/S0017-9310\(02\)00288-0](https://doi.org/10.1016/S0017-9310(02)00288-0).
- [77] Tokarev MM, Gordeeva LG, Romannikov V, Glaznev IS, Aristov YI. New composite sorbent CaCl<sub>2</sub> in mesopores for sorption cooling/heating. *Int J Therm Sci* 2002;41:470–4. [https://doi.org/10.1016/S1290-0729\(02\)01339-X](https://doi.org/10.1016/S1290-0729(02)01339-X).
- [78] Sadeghlu A, Yari M, Mahmoudi SMS, Dizaji HB. Performance evaluation of zeolite 13X/CaCl<sub>2</sub> two-bed adsorption refrigeration system. *Int J Therm Sci* 2014;80:76–82. <https://doi.org/10.1016/j.ijthermalsci.2014.02.001>.
- [79] Chan KC, Chao CYH, Sze-To GN, Hui KS. Performance predictions for a new zeolite 13X/CaCl<sub>2</sub> composite adsorbent for adsorption cooling systems. *Int J Heat Mass Transf* 2012;55:3214–24. <https://doi.org/10.1016/j.ijheatmasstransfer.2012.02.054>.
- [80] Nonnen T, Beckert S, Gleichmann K, Brandt A, Unger B, Kerskes H, et al. A Thermochemical long-term heat storage system based on a salt/zeolite composite. *Chem Eng Technol* 2016;39:2427–34. <https://doi.org/10.1002/ceat.201600301>.
- [81] Whiting GT, Grondin D, Stosic D, Bennici S, Auroux A. Zeolite-MgCl<sub>2</sub> composites as potential long-term heat storage materials: Influence of zeolite properties on heats of water sorption. *Sol Energy Mater Sol Cells* 2014;128:289–95. <https://doi.org/10.1016/j.solmat.2014.05.016>.
- [82] Tretiak CS, Abdallah NB. Sorption and desorption characteristics of a packed bed of clay-CaCl<sub>2</sub> desiccant particles. *Sol Energy* 2009;83:1861–70. <https://doi.org/10.1016/j.solener.2009.06.017>.
- [83] Veselovskaya JV, Tokarev MM. Novel ammonia sorbents "porous matrix modified by active salt" for adsorptive heat transformation: 4. Dynamics of quasi-isobaric ammonia sorption and desorption on BaCl<sub>2</sub>/vermiculite. *Appl Therm Eng* 2011;31:566–72. <https://doi.org/10.1016/j.applthermaleng.2010.10.018>.
- [84] Li TX, Wang RZ, Wang LW, Lu ZS. Experimental investigation of an innovative dual-mode chemisorption refrigeration system based on multifunction heat pipes. *Int J Refrig* 2008;31:1104–12. <https://doi.org/10.1016/j.jrefrig.2007.11.018>.
- [85] Lu ZS, Wang RZ, Wang LW, Chen CJ. Performance analysis of an adsorption refrigerator using activated carbon in a compound adsorbent. *Carbon N Y* 2006;44:747–52. <https://doi.org/10.1016/j.carbon.2005.09.016>.
- [86] Tokarev MM, Veselovskaya JV, Yanagi H, Aristov YI. Novel ammonia sorbents "porous matrix modified by active salt" for adsorptive heat transformation: 2. Calcium chloride in ACF felt. *Appl Therm Eng* 2010;30:845–9. <https://doi.org/10.1016/j.applthermaleng.2009.12.016>.
- [87] Wang LW, Wang RZ, Xia ZZ, Wu JY. Studies on heat pipe type adsorption ice maker for fishing boats. *Int J Refrig* 2008;31:989–97. <https://doi.org/10.1016/j.jrefrig.2008.01.002>.
- [88] Okada K, Nakanome M, Kameshima Y, Isobe T, Nakajima A. Water vapor adsorption of CaCl<sub>2</sub>-impregnated activated carbon. *Mater Res Bull* 2010;45:1549–53. <https://doi.org/10.1016/j.matresbull.2010.07.027>.
- [89] Bandosz TJ, Petit C. On the reactive adsorption of ammonia on activated carbons modified by impregnation with inorganic compounds. *J Colloid Interface Sci* 2009;338:329–45. <https://doi.org/10.1016/j.jcis.2009.06.039>.
- [90] Grekova AD, Girmik IS, Nikulin VV, Tokarev MM, Gordeeva LG, Aristov YI. New composite sorbents of water and methanol "salt in anodic alumina": evaluation for adsorption heat transformation. *Energy* 2016;106:231–9. <https://doi.org/10.1016/j.energy.2016.03.050>.
- [91] Fujioaka K, Hatanaka K, Hirata Y. Composite reactants of calcium chloride combined with functional carbon materials for chemical heat pumps. *Appl Therm Eng* 2008;28:304–10. <https://doi.org/10.1016/j.applthermaleng.2006.02.032>.
- [92] Dellerio T, Sarneo D, Touzain P. A chemical heat pump using carbon fibers as additive. Part I: enhancement of thermal conduction. *Appl Therm Eng* 1999;19:991–1000. [https://doi.org/10.1016/S1359-4311\(98\)00104-5](https://doi.org/10.1016/S1359-4311(98)00104-5).
- [93] Zajackowski B, Króllicki Z, Jezowski A. New type of sorption composite for chemical heat pump and refrigeration systems. *Appl Therm Eng* 2010;30:1455–60. <https://doi.org/10.1016/j.applthermaleng.2010.03.005>.
- [94] Oliveira RG, Wang RZ. A consolidated calcium chloride-expanded graphite compound for use in sorption refrigeration systems. *Carbon N Y* 2007;45:390–6. <https://doi.org/10.1016/j.carbon.2006.09.007>.
- [95] Oliveira RG, Wang RZ, Wang C. Evaluation of the cooling performance of a consolidated expanded graphite-calcium chloride reactive bed for chemisorption icemaker. *Int J Refrig* 2007;30:103–12. <https://doi.org/10.1016/j.jrefrig.2006.08.003>.
- [96] Wang K, Wu JY, Wang RZ, Wang LW. Effective thermal conductivity of expanded graphite-CaCl<sub>2</sub> composite adsorbent for chemical adsorption chillers. *Energy Convers Manage* 2006;47:1902–12. <https://doi.org/10.1016/j.enconman.2005.09.005>.
- [97] Wu S, Li TX, Yan T, Wang RZ. Experimental study on a solar-powered thermochemical sorption refrigeration system using strontium chloride/EG-ammonia working pair. *Proc 16th Int Refrig Air Cond Conf, Purdue* 2016.
- [98] Maurán S, Prades P, L'Haridon F. Heat and mass transfer in consolidated reacting beds for thermochemical systems. *Heat Recover Syst CHP* 1993;13:315–9. [https://doi.org/10.1016/0890-4332\(93\)90055-Z](https://doi.org/10.1016/0890-4332(93)90055-Z).
- [99] Fujioaka K, Suzuki H. Thermophysical properties and reaction rate of composite reactant of calcium chloride and expanded graphite. *Appl Therm Eng* 2013;50:1627–32. <https://doi.org/10.1016/j.applthermaleng.2011.08.024>.
- [100] Permyakova A, Wang S, Courbon E, Nouar F, Heymans N, D'Ans P, et al. Design of salt-metal organic framework composites for seasonal heat storage applications. *J Mater Chem A* 2017;5:12889–98. <https://doi.org/10.1039/C7TA9J1>.
- [101] Offenhardt PO, Brown FC, Mar RW, Carling RW. A heat pump and thermal storage system for solar heating and cooling based on the reaction of calcium chloride and methanol vapor. *J Sol Energy Eng* 1980;102:59–65.
- [102] Iyimen-Schwarz Z. Energiespeicherung durch chemische Reaktionen. Universität Osnabrück 1984.
- [103] Lai H, Li C. Application of periodic reversal flow reactors to chemical heat pump systems based on solid/vapor non-catalytic reaction. *Chem Eng Sci* 1996;51:2951–7. [https://doi.org/10.1016/0009-2509\(96\)00180-7](https://doi.org/10.1016/0009-2509(96)00180-7).
- [104] Hirata Y, Fujioaka K. Thermophysical properties and heat transfer characteristics of CaCl<sub>2</sub> heat pump reactor associated with structural change of reactive salts. *V Minsk Int Semin Heat Pipes, Heat Pumps, Refrig* 2003;2:287–98.
- [105] Gordeeva LG, Freni A, Restuccia G, Aristov YI. Influence of characteristics of methanol sorbents "salts in mesoporous silica" on the performance of adsorptive air conditioning cycle. *Ind Eng Chem Res* 46 2007 2747 52 doi: 10.1021/ie060666n.
- [106] Aristov YI, Gordeeva LG, Pankratiev YD, Plyasova LM, Bikova IV, Freni A, et al. Sorption equilibrium of methanol on new composite sorbents "CaCl<sub>2</sub>/silica gel". *Adsorption* 2007;13:121–7. <https://doi.org/10.1007/s10450-007-9012-x>.
- [107] Galwey AK. Structure and order in thermal dehydrations of crystalline solids. *Thermochim Acta* 2000;355:181–238. [https://doi.org/10.1016/S0040-6031\(00\)00448-2](https://doi.org/10.1016/S0040-6031(00)00448-2).
- [108] Stanish MA, Perlmutter DD. Rate processes in cycling a reversible gas-solid reaction. *AIChE J* 1984;30:56–62. <https://doi.org/10.1002/aic.690300110>.

- [109] Carling RW. Dissociation pressures and enthalpies of reaction in  $\text{MgCl}_2 \cdot n\text{H}_2\text{O}$  and  $\text{CaCl}_2 \cdot n\text{H}_2\text{O}$ . *J Chem Thermodyn* 1981;13:503–12. [https://doi.org/10.1016/0021-9614\(81\)90105-1](https://doi.org/10.1016/0021-9614(81)90105-1).
- [110] Hart AB, Partington JR. 36. Dissociation pressures of compounds of ammonia and trideterammonia with some metallic salts. *J Chem Soc* 1943;104–18. <https://doi.org/10.1039/JR9430000104>.
- [111] Fujioka K, Kato S-I, Fujiki S, Hirata Y. Variations of molar volume and heat capacity of reactive solids of  $\text{CaCl}_2$  used for chemical heat pumps. *J Chem Eng Jpn* 1996;29:858–64. <https://doi.org/10.1252/jcej.29.858>.
- [112] Eckhardt RC, Fichte PM, Flanagan TB. Kinetics of rehydration of crystalline anhydrides. Manganous formate. *Trans Faraday Soc* 1971;67:1143–54. <https://doi.org/10.1039/TF9716701143>.
- [113] Koga N, Tanaka H. A physico-geometric approach to the kinetics of solid-state reactions as exemplified by the thermal dehydration and decomposition of inorganic solids. *Thermochim Acta* 2002;388:41–61. [https://doi.org/10.1016/S0040-6031\(02\)00051-5](https://doi.org/10.1016/S0040-6031(02)00051-5).
- [114] Lyakhov NZ, Boldyrev VV. Kinetics and mechanism of the dehydration of crystal hydrates. *Russ Chem Rev* 1972;41:919.
- [115] Bonnell DGR, Jones WJ. XLII.—The dissociation pressures of alcoholates. Part I. *J Chem Soc* 1926;129:321–8. <https://doi.org/10.1039/JR9262900321>.
- [116] Carling RW, Wondolowski AT, Macmillan DC. Enthalpy of formation of  $\text{CaCl}_2 \cdot 2\text{C}_2\text{H}_5\text{OH}$  and  $\text{CaCl}_2 \cdot 2\text{C}_2\text{H}_5\text{OH}$  by solution calorimetry. *J Chem Thermodyn* 1982;14:125–31. [https://doi.org/10.1016/0021-9614\(82\)90024-6](https://doi.org/10.1016/0021-9614(82)90024-6).
- [117] Lloyd E, Brown CB, Bonnell DGR, Jones WJ. XC.—Equilibrium between alcohols and salts. Part II. *J Chem Soc* 1928;658–66. <https://doi.org/10.1039/JR9280000658>.
- [118] Graham TX. An account of the formation of alcohates, definite compounds of salts and alcohol analogous to the hydrates. *Trans R Soc Edinburgh* 1828;11:175–93. <https://doi.org/10.1017/S0008945680002189X>.
- [119] N'Tsoukpoe KE, Rammelberg HU, Lele AF, Korhammer K, Watts BA, Schmidt T, et al. A review on the use of calcium chloride in applied thermal engineering. *Appl Therm Eng* 2015;75:513–31. <https://doi.org/10.1016/j.applthermaleng.2014.09.047>.
- [120] Pearson RG. Hard and soft acids and bases, HSAB, part II: Underlying theories. *J Chem Educ* 1968;45:643. <https://doi.org/10.1021/ed045p643>.
- [121] Atkins PW, de Paula J, Bär M, Schleitzer A, Heinisch C. *Physikalische Chemie*. Wiley; 2006.
- [122] Dortmund Data Bank. Vapor pressure calculation by Antoine equation 2015 < <http://databases.dbst.com/AntoineCalculation/AntoineCalculationCGI.exe> > [accessed September 1, 2015].
- [123] Fopah Lele A, Kuznik F, Rammelberg HU, Schmidt T, Ruck WKL. Thermal decomposition kinetic of salt hydrates for heat storage systems. *Appl Energy* 2015;154:447–58. <https://doi.org/10.1016/j.apenergy.2015.02.011>.
- [124] Kleiber M, Joh R, Span R. VDI heat atlas. In: VDI-Gesellschaft Verfahrenstechnik und Chemieingenieurwesen, editor. VDI heat atlas. 2nd ed. Berlin, Heidelberg: Springer; 2010. p. 301–418.
- [125] Vyazovkin S, Chrissafis K, Di Lorenzo M, Koga N, Pijolat M, Roduit B, et al. ICTAC Kinetics Committee recommendations for collecting experimental thermal analysis data for kinetic computations. *Thermochim Acta* 2014;590:1–23. <https://doi.org/10.1016/j.tca.2014.05.036>.
- [126] Michel B, Mazet N, Neveu P. Experimental investigation of an open thermochemical process operating with a hydrate salt for thermal storage of solar energy: Local reactive bed evolution. *Appl Energy* 2016;180:234–44. <https://doi.org/10.1016/j.apenergy.2016.07.108>.
- [127] Kiplagat JK, Wang RZ, Li TX, Oliveira RG. Enhancement of heat and mass transfer in solid gas sorption systems. *Int J Air-Conditioning Refrig* 2012;20. <https://doi.org/10.1142/S2010132511300011>.
- [128] Cacciola G, Giordano N. Chemical processes for energy storage and transmission. *Appl Energy* 1986;25:315–37. [https://doi.org/10.1016/0306-2619\(86\)90032-2](https://doi.org/10.1016/0306-2619(86)90032-2).
- [129] Ambrose D, Sprake CHS. Thermodynamic properties of organic oxygen compounds XXV. Vapour pressures and normal boiling temperatures of aliphatic alcohols. *J Chem Thermodyn* 1970;2:631–45. [https://doi.org/10.1016/0021-9614\(70\)90038-8](https://doi.org/10.1016/0021-9614(70)90038-8).
- [130] Becker R, Hartwig H, Köppe H, Vanecek H, Velić P, Warncke R, et al. *Gmelin Handbuch der Anorganischen Chemie*. Berlin, Heidelberg: Springer; 1978. 10.1007/978-3-662-06224-1.
- [131] Bois C, Philoche-Levisalles M, L'Haridon P. Structures cristallines des composés  $\text{CaBr}_2 \cdot 4\text{CH}_3\text{OH}$  et  $\text{CaBr}_2 \cdot 4\text{C}_2\text{H}_5\text{OH}$ . *Acta Crystallogr Sect B* 1978;34:1463–6. doi: 10.1107/S0567740878005919.
- [132] Menschutkin BN. Über einige Kristallalkoholate. *Zeitschrift Für Anorg Chemie* 1907;52:9–24. <https://doi.org/10.1002/zaac.19070520103>.
- [133] Kane R. Beiträge zur Geschichte des Holzgeistes und seiner Verbindungen. *Ann Der Pharm* 1836;19:164–83. <https://doi.org/10.1002/jlac.18360190205>.
- [134] Brusset H, Gillier-Pandraud H, Philoche-Levisalles M. Crystallographic data on compound  $\text{CaCl}_2$ . *Comptes Rendus l'Académie Des Sci* 1970;271:C579.
- [135] Halut-Desportes S, Philoche-Levisalles M. Structures compar(é)es des solvates de formule  $\text{MBr}_2 \cdot 6\text{CH}_3\text{OH}$ . *Acta Crystallogr Sect B* 1978;34:432–5. doi: 10.1107/S0567740878003295.
- [136] Galvey AK, Brown ME. *Thermal decomposition of ionic solids*. 1st ed. Elsevier Science; 1999.
- [137] Bart J CJ, Roovers W. Magnesium chloride – ethanol adducts. *J Mater Sci* 1995;30:2809–20. <https://doi.org/10.1007/BF00349648>.
- [138] Korhammer K, Druske M-M, Fopah-Lele A, Rammelberg HU, Wegscheider N, Opel O, et al. Sorption and thermal characterization of composite materials based on chlorides for thermal energy storage. *Appl Energy* 2016;162:1462–72. <https://doi.org/10.1016/j.apenergy.2015.08.037>.
- [139] Offenhardt PO, Rye TV, Malsberger RE, Schwartz D. Methanol-based heat pump for solar heating, cooling, and storage. Phase III. Final Report. United States; 1981. doi: 10.2172/5353616.



## **10. Paper VIII**

## Energy storage and adsorption cooling efficiency of novel composite adsorbents

Kathrin Korhammer<sup>a</sup>, Oliver Opel<sup>\*a,b</sup>, Wolfgang K.L. Ruck<sup>a</sup>

<sup>a</sup> Leuphana University of Lüneburg, Universitätsallee 1, 21335 Lüneburg, Germany

<sup>b</sup> FH Westküste University of Applied Sciences, Fritz-Thiedemann-Ring 20, 25746 Heide, Germany

\* Corresponding Author. Tel.: +49 (0) 481 8555-375; Email address: opel@fh-westkueste.de

### Abstract

Calcium chloride was combined with different types of host matrices varying in the shape and pore framework structure. Natural clinoptilolite, binderless zeolite 13X, biochar, expanded graphite, and vermiculite were considered as promising supports. Ethanol and methanol were chosen as adsorbates. The composite adsorbents were designed for utilization in a closed thermal energy storage system powered by low temperature heat. Thermal and kinetic behavior were investigated by simultaneous TGA/DSC. Different experimental procedures were applied for deethanolation/ethanolation and demethanolation/methanolation measurements. Material intrinsic energy storage density, specific cooling power, and cooling coefficient of performance were calculated from experimentally obtained data. Multiple repeated reaction cycles were carried out to examine the life-cycle performance of the chemical and composite adsorbents. Energy storage densities ranged from 177 kJ kg<sup>-1</sup> to 319 kJ kg<sup>-1</sup> for the working pair adsorbent-ethanol and from 455 kJ kg<sup>-1</sup> to 540 kJ kg<sup>-1</sup> for the working pair adsorbent-methanol. SCPs were averaged to 49 W kg<sup>-1</sup> to 162 W kg<sup>-1</sup> in respect of the working fluid ethanol. The corresponding COPs were in the range of 0.34 to 0.88. The working pair adsorbent-methanol yielded average SCPs of 153 W kg<sup>-1</sup> to 220 W kg<sup>-1</sup> and cooling COPs between 0.63 and 0.73 under the conditions studied.

### Nomenclature

#### Abbreviations

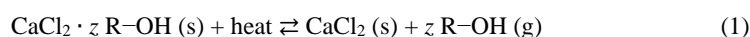
BC	Biochar
COP	Coefficient of performance
DSC	Differential scanning calorimetry
ENG	Expanded natural graphite
EV2	Expanded vermiculite
SCP	Specific cooling power
TCM	Thermochemical material
TGA	Thermogravimetric analysis
Z13X	Binderless zeolite 13X
ZNC	Zeolite natural clinoptilolite

**Symbols**

$N$	Adsorbate level	$\text{mol mol}^{-1}$
$\Delta_r H$	Molar reaction enthalpy	$\text{kJ mol}^{-1}$
$\Delta_r h$	Specific reaction enthalpy	$\text{kJ kg}^{-1}$
$T_{\text{Onset}}$	Onset temperature	$^{\circ}\text{C}$
$T_{\text{Peak}}$	Peak temperature	$^{\circ}\text{C}$

**1 Introduction**

Sustainable management and integration of thermal energy from renewables and heat recovery processes can be addressed through spatial and temporal decoupling using thermochemical energy storage systems. Heat energy can be harnessed to supply a broad range of energy demands, encompassing space and water heating, air conditioning, and refrigeration [1]. From an energy point of view, thermally intensive processes have been the largest consumer of energy in the last decades in Germany [2]. To date, the major share of thermal energy is generated from fossil fuels that are main sources of greenhouse gas emissions [3]. Low temperature thermochemical energy stores that use gas-solid reactions are appealing alternative technologies for heating and cooling purposes. They convert heat energy provided from renewable energy and waste heat sources into chemical energy and can effectively contribute to load balancing and carbon dioxide mitigation. In the low temperature regime, calcium chloride ( $\text{CaCl}_2$ ) can be employed as thermochemical material (TCM) in pair with aliphatic primary alcohols such as ethanol [4,5] or methanol [4–9] as adsorbate. During the thermal energy yielding (charging) mode, the inorganic salt  $\text{CaCl}_2$  is exposed to alcohol ( $\text{R-OH}$ ) in gas state and reacts exothermally to form salt alcoholates of different stoichiometry ( $z$ ) while releasing the energy stored. Evaporation of the alcohol in liquid state produces a cooling effect, which can be utilized for air conditioning or chilling. In the discharging mode, the endothermic decomposition reaction is initiated upon heating and  $\text{CaCl}_2$  anhydride is regenerated, as shown in the following generic equation:



The volatile product can be easily condensed. Separation of the working pairs and storage of the TCM at ambient temperature facilitates long-term heat storage with negligible sensible thermal losses [10]. For hybrid adsorption heating and cooling systems reasonable material intrinsic energy storage density and efficient cooling power are demanded. The performance is strongly dependent on the thermodynamics and kinetics of the reaction pair applied. Internal diffusion resistances relating to physical stability issues, sorption/desorption hysteresis, salt swelling, along with slow heat transfer, due to low thermal conductivities of  $\text{CaCl}_2$  and its complexes, impact the reversibility of the reaction system and therefore pose severe obstacles to the implementation in full-scale plants. To improve structural integrity and mass transfer, several researchers have confined  $\text{CaCl}_2$  and other alkali and alkaline earth metal salts into porous and high-surface matrices [11–26]. The working pair  $\text{CaCl}_2$  and silica gel has elicited much interest, because of its good methanol [14,25]

and ethanol [21] adsorption ability. Less attention has been paid to combine  $\text{CaCl}_2$  and carbonaceous [11] or aluminosilicate supports. In the present paper, various composite adsorbents were prepared and their suitability for thermal energy storage was verified by thermal analysis.  $\text{CaCl}_2$  was incorporated into natural clinoptilolite, binderless zeolite 13X, biochar, expanded graphite, and expanded natural vermiculite. Multi-cyclic measurements were conducted via TGA/DSC to study thermal and kinetic properties of the composite adsorbents and single  $\text{CaCl}_2$ .

## 2 Materials and methods

### 2.1 Materials

Calcium chloride anhydride of high purity (p.A.) from Merck was used as reference reagent and as impregnating agent for the preparation of the composite materials studied in this paper. The content of volatiles was less than 5%.  $\text{CaCl}_2$  is an abundant, environmental benign, non-toxic, and economically viable reagent that is predominantly obtained as by-product in the production of soda ash by Solvay process [27].

Five distinct natural and synthetic porous materials were chosen as host matrices for the composite adsorbents: (i) expanded natural graphite, (ii) binder-free zeolite 13X, (iii) natural clinoptilolite, (iv) biochar, and (v) natural expanded vermiculite. The host matrices belong to different classes and are distinguished by their internal pore width. The IUPAC originally defined three different classes [28]. Micropore materials have pores of internal width less than 2 nm, mesopore materials possess pores of internal width between 2 nm and 50 nm, and macropore materials exhibit pores of internal width greater than 50 nm. Mesoporous expanded natural graphite (ENG) pellets with an area density of  $750 \text{ g m}^{-2}$  were supplied by the SGL Carbon Group. Synthetic binder-free zeolite 13X (Z13X) spheres with particle sizes of 2.5  $\mu\text{m}$  to 3.5  $\mu\text{m}$  and bulk densities of  $620 \text{ g dm}^{-3}$  to  $700 \text{ g dm}^{-3}$  were provided by the Chemiewerk Bad Köstritz. Expanded graphite has an anisotropic structure and features a superb thermal conductivity. The zeolite 13X, which belongs to the zeolite type NaX, is highly hydrophilic and possesses good hygrothermal stability under cyclic conditions. Clinoptilolite zeolite (ZNC) powder from Zeolith Umwelttechnik with particle sizes between 0.0  $\mu\text{m}$  and 0.5  $\mu\text{m}$  was used as a low-cost alternative for synthetic zeolites. Clinoptilolite is a naturally occurring aluminosilicate with good water sorption ability. Biochar (BC) with high carbon content and medium particle size (0.0  $\mu\text{m}$  to 2.0  $\mu\text{m}$ ) was received from Bioenergy Concept. Biochar is a final product of organic waste incineration and displays an appealing sustainable host matrix. Natural expanded vermiculite (EV2) with grain sizes of 2.0  $\mu\text{m}$  to 6.0  $\mu\text{m}$  was obtained from Deutsche Vermiculite. Vermiculite is a natural layer-type aluminosilicate clay mineral. Expanded vermiculite, which has a large macroporous volume, is produced by exfoliation during high temperature treatment.

The sorbates ethanol ( $\text{C}_2\text{H}_5\text{OH}$ ) and methanol ( $\text{CH}_3\text{OH}$ ) were purchased from Merck. The grade of purity was >99.9% and p.A., respectively. Ethanol contained  $\leq 0.01\%$  and methanol about 0.003% of water. Some physico-chemical and thermodynamic properties of the sorbates are summarized in Table 1.

Table 1. Physical and thermodynamic properties of the working fluids used. Data were either provided by the supplier or taken from literature [29].

	Methanol	Ethanol
Chemical formula	CH <sub>3</sub> OH	C <sub>2</sub> H <sub>5</sub> OH
Molecular weight (g mol <sup>-1</sup> )	32.04	46.07
State	Liquid	Liquid
pH		7.0 (20 °C, 10 g L <sup>-1</sup> , 1013 hPa)
Density (g cm <sup>-3</sup> )	0.792 (20 °C)	0.790-0.793 (20 °C)
Pressure (hPa)	128 (20 °C)	59 (20 °C)
Melting point (°C)	-98.0	-114.5
Boiling point (°C)	64.5 (1013 hPa)	78.3 (1013 hPa)
Vaporization enthalpy (kJ mol <sup>-1</sup> )	35 (64.5 °C)	39 (78.3 °C)
	38 (8.5 °C)	43 (9.5 °C)
Molar vaporization enthalpy (kJ kg <sup>-1</sup> )	1102 (64.5 °C)	850 (78.3 °C)
	1195 (8.5 °C)	935 (9.5 °C)

## 2.2 Preparation of the composite adsorbents

The two-component composite adsorbents were synthesized by using two different impregnation procedures, wet impregnation and wet impregnation under subatmospheric pressure, referred to as vacuum impregnation.

The composites CaCl<sub>2</sub>-ENG and CaCl<sub>2</sub>-EV2 were prepared by wet impregnation under vacuum. The host matrices, compacted ENG and granular EV2 that were initially dried at 200 °C, were impregnated with a saturated aqueous solution of CaCl<sub>2</sub> in a vacuum-tight reactor vessel at 10 mbar and at room temperature. Prior to the impregnation process, the vessel was degassed and evacuated with a membrane pump. After separation of the excess solution and the composite adsorbent, the composite adsorbents were flushed with dry nitrogen at room temperature and at atmospheric pressure to remove any moisture inside the pores as well as on the internal and external surfaces. The samples were finally dried to constant mass at 200 °C.

For the synthesis of the composite CaCl<sub>2</sub>-BC, the predried biochar was soaked in a saturated aqueous CaCl<sub>2</sub> solution at room temperature. The excess solvent was eliminated by successive evaporation below the boiling point of the CaCl<sub>2</sub> solution. To determine the evaporation temperature, the boiling point elevation of the salt solution was calculated using the Clausius-Clapeyron equation. The evaporation temperature was set to 100 °C based upon the calculation. In the final step, the composite material was calcinated at 200 °C.

Before impregnation, the synthetic zeolite 13X and natural zeolite clinoptilolite had to be modified by ion exchange. Zeolites possess high cation exchange capacities. In the zeolites used, sodium cations constitute the major exchangeable functional sites. Since the zeolites are more selective towards cations of higher valence and atomic weight as well as smaller radii, the alkali cations were exchanged by alkaline earth cations to prevent spontaneous replacement by the calcium cations of the impregnation solvent during impregnation. The affinity towards bivalent



cations increases in the order  $\text{Mg}^{2+} < \text{Ca}^{2+} < \text{Sr}^{2+} < \text{Ba}^{2+}$ . Based on this selectivity order, a saturated barium acetate solution was chosen for ion exchange. The ion exchange was performed in batch mode at room temperature while shaking for 20 h. After drying, a saturated  $\text{CaCl}_2$  aqueous solution, whose volume exceeded the pore volume of the support, was added to the zeolites. The impregnated zeolites were dried in two subsequent steps overnight. The final drying temperature was 200 °C.

The content of the  $\text{CaCl}_2$  confined to the composite adsorbents was determined by weighting the dry sample before and after impregnation. The  $\text{CaCl}_2$  content ranged from 16 wt% to 83 wt% depending on impregnation method, synthesis condition, and support material. Specifications of the synthesized composite adsorbents are listed in Table 2.

Since zeolites can catalyze the conversion of  $\text{CH}_3\text{OH}$  to water and dimethyl ether (DME) at the temperature of interest [30], the reaction systems  $\text{CaCl}_2\text{-ZNC-CH}_3\text{OH}$  and  $\text{CaCl}_2\text{-Z13X-CH}_3\text{OH}$  are considered ineligible for heat and cold storage. Therefore, these working pair combinations were not tested.

Table 2. Overview of composite adsorbents studied.

Sample ID	Host matrix	Salt	Method	Salt content wt%	Reaction partner
$\text{CaCl}_2\text{-ENG}$	ENG	$\text{CaCl}_2$	Vacuum impregnation	64	$\text{C}_2\text{H}_5\text{OH}$
$\text{CaCl}_2\text{-Z13X}$	Z13X	$\text{CaCl}_2$	Wet impregnation	16	$\text{C}_2\text{H}_5\text{OH}$
$\text{CaCl}_2\text{-ZNC}$	ZNC	$\text{CaCl}_2$	Wet impregnation	30	$\text{C}_2\text{H}_5\text{OH}$
$\text{CaCl}_2\text{-BC}$	BC	$\text{CaCl}_2$	Wet impregnation	83	$\text{CH}_3\text{OH}$
$\text{CaCl}_2\text{-EV2}$	EV2	$\text{CaCl}_2$	Vacuum impregnation	69	$\text{CH}_3\text{OH}$

### 2.3 Thermal and kinetic analysis by simultaneous TGA/DSC

Simultaneous thermogravimetric analysis (TGA) and differential scanning calorimetry (DSC) coupled with an alcohol vapor generation system was employed to characterize thermochemical and kinetic properties of the pure  $\text{CaCl}_2$  and the designed composite materials under cyclic conditions (Figure 1). TGA measured the change in mass of the specimen during programmed temperature heating in a controlled  $\text{N}_2$  atmosphere as a function of time or temperature. Sorption ability of the samples, stoichiometry, and desorption temperature range of the respective reactions were determined from the overall mass loss/gain. Influences of the supporting structures on the degree of conversion over time and rate of reaction were also studied by TGA. Heat-flux DSC was applied to measure the amount of heat absorbed or liberated during reaction. In heat-flux DSC, the DSC signal equals the thermal energy transferred to or from the specimen relative to a reference material. Enthalpies of reaction were obtained from manual integration of the peak area under the baseline-subtracted DSC signal over time.

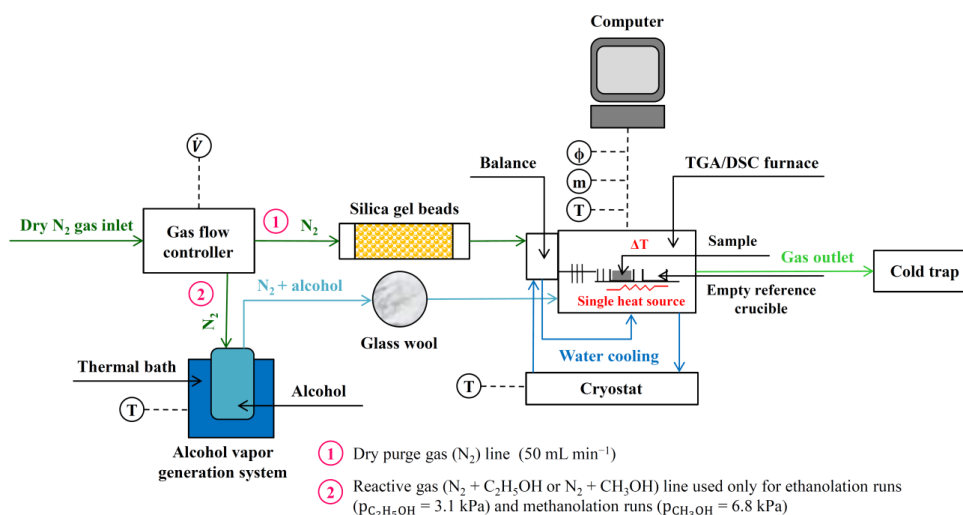


Figure 1. Schematic of the experimental setup. The water bath temperature  $T$ , the cryostat  $T$ , the furnace temperature  $T$ , the sample mass  $m$ , and the heat flux  $\phi$  were recorded online.

In this study, all measurements were carried out using the TGA/DSC 1 from Mettler Toledo. Measurement curves were blank curve corrected to eliminate effects of buoyancy forces. The Mettler Toledo STARe<sup>®</sup> software 11.00a was used for data processing. The precision of the mass and heat power determination are given as  $\pm 1.0 \mu\text{g}$  and  $\pm 0.1 \text{ mW}$ , respectively. The standard uncertainties of the calculated mass and enthalpy are 10% to 20%. Thermal analysis was performed under varying operating conditions depending on the sorbate applied. Sample masses amounted to  $(11 \pm 1) \text{ mg}$  and were spread evenly into open alumina crucibles with a volume of  $70 \mu\text{L}$ .

To simulate the heat storage (charging) and heat release (discharging) mode of the working pairs  $\text{CaCl}_2\text{-C}_2\text{H}_5\text{OH}$ ,  $\text{CaCl}_2\text{-ZnCl}_2\text{-C}_2\text{H}_5\text{OH}$ ,  $\text{CaCl}_2\text{-ZnCl}_2\text{-C}_2\text{H}_5\text{OH}$ , and  $\text{CaCl}_2\text{-ENG-C}_2\text{H}_5\text{OH}$  in a closed thermochemical energy store, ethanolation/demethanolation reaction cycles comprising isothermal ethanolation and dynamic demethanolation measurements were conducted via TGA/DSC. Prior to the ethanolation reaction, the sample was stabilized at  $25 \text{ }^\circ\text{C}$  for 15 min. In the subsequent ethanolation process, a  $\text{C}_2\text{H}_5\text{OH}$  saturated  $\text{N}_2$  carrier gas flow with a  $\text{C}_2\text{H}_5\text{OH}$  partial vapor pressure of 3.1 kPa, which is equal to an evaporator temperature of  $9.5 \text{ }^\circ\text{C}$ , was passed over the sample for 120 min at  $25 \text{ }^\circ\text{C}$ . After 60 min of stabilization in dry flowing  $\text{N}_2$  gas at  $25 \text{ }^\circ\text{C}$ , the sample was heated to  $180 \text{ }^\circ\text{C}$  with a constant heating rate of  $3 \text{ K min}^{-1}$ , followed by an isothermal step at  $180 \text{ }^\circ\text{C}$  for 30 min. In the last step, the sample was cooled down to the initial temperature at  $-10 \text{ K min}^{-1}$ .

The cycle stability of the reaction pairs  $\text{CaCl}_2\text{-CH}_3\text{OH}$ ,  $\text{CaCl}_2\text{-BC-CH}_3\text{OH}$ , and  $\text{CaCl}_2\text{-EV2-CH}_3\text{OH}$  was tested under dynamic methanolation and demethanolation conditions. In the first step, the sample was heated to  $150 \text{ }^\circ\text{C}$  and kept isothermally at this temperature for 5 min. In the second step the sample was cooled down to  $25 \text{ }^\circ\text{C}$  with a cooling rate of  $-1 \text{ K min}^{-1}$  while exposed to a

CH<sub>3</sub>OH vapor pressure of 6.8 kPa. This corresponds to an evaporation temperature of 8.5 °C. After isothermal stabilization at 25 °C for 15 min, the sample was demethanolated by scanning from 25 °C to the initial temperature of 150 °C at a linear ramp of 1 K min<sup>-1</sup> in flowing N<sub>2</sub> atmosphere. The first methanolation/demethanolation cycle differed from the subsequent ones and was excluded from analysis. Low heating rates were applied to minimize mass and heat transfer limitations. In real applications, heating rates between 0 K min<sup>-1</sup> and 3 K min<sup>-1</sup> can be expected.

## 2.4 Energy storage and cooling performance analysis

DSC is well suited for analyzing the energy storage and cooling performance of TCMs. The C<sub>2</sub>H<sub>5</sub>OH and CH<sub>3</sub>OH adsorption abilities were calculated from the mass gain during the ethanolation and methanolation phase and referred to the dry mass of the CaCl<sub>2</sub> and composite samples tested. The specific reaction enthalpies were determined by dividing the experimentally obtained molar reaction enthalpies by the molar mass of CaCl<sub>2</sub>. The gravimetric energy density is an important key performance indicator and quantifies the thermal energy storage efficiency of the TCM in relation to the respective ethanolated or methanolated CaCl<sub>2</sub>.

The specific cooling power (SCP) per dry mass of pure CaCl<sub>2</sub> and composite adsorbent during the cooling phase was derived from the adsorption rate and the enthalpy of vaporization of the respective refrigerant. The adsorption rates were obtained from the first derivative of the TGA curve. The SCP changes over the time and the course of the reaction. The peak SCP was attained at the greatest rate of mass change indicated by the inflection point of the DTG curve. The average SCP is referred to the time required for the reactions to reach 100% completion. The cooling efficiency of a thermochemical energy store operating with gas-solid reactions is the ratio of the useful cooling effect to the heat energy provided from a heat source [31] and is called the cooling coefficient of performance (COP). The COP at material scale was calculated from the enthalpy of vaporization of the particular sorbate and the measured reaction enthalpy of the desorption reaction. The enthalpies of vaporization at the specific evaporation temperatures were estimated with the PPDS equation [29]. Note that the SCPs and COPs presented in this study are ideal values. At system scale, practical values will be lower than the values identified by TGA/DSC.

## 3 Results and discussion

### 3.1 Thermal and kinetic analysis of different CaCl<sub>2</sub>-based adsorbents and C<sub>2</sub>H<sub>5</sub>OH as adsorbate

#### 3.1.1 The working pair CaCl<sub>2</sub>-C<sub>2</sub>H<sub>5</sub>OH

The reaction pair CaCl<sub>2</sub>-C<sub>2</sub>H<sub>5</sub>OH was cycled over three consecutive ethanolation/deethanolation runs. As seen in Figure 2, a maximum ethanolation level of 1.2 was reached during all ethanolation operations. Since some C<sub>2</sub>H<sub>5</sub>OH was given off during subsequent stabilization at 25 °C in flowing N<sub>2</sub> atmosphere, the ethanolation level dropped to 0.9 to 1.0 moles of C<sub>2</sub>H<sub>5</sub>OH per mole CaCl<sub>2</sub>. In published literature, the existence of CaCl<sub>2</sub> monoethanolate [32–

34] and dimethanolate [4,32] has been described. The dissociation proceeded in several indistinct stages and was completed at temperatures of 130 °C to 132 °C (Table 3). Findings are in accordance with previously reported results [35,36].

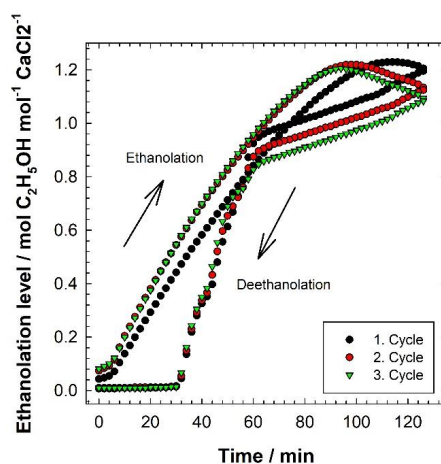


Figure 2. Change of the state of ethanolation of pure  $\text{CaCl}_2$  and its ethanolates over three consecutive ethanolation/deethanolation reaction cycles as a function of time. The ethanolation was carried out at a  $\text{C}_2\text{H}_5\text{OH}$  vapor pressure of 3.1 kPa and at a temperature of 25 °C under atmospheric conditions. The deethanolation was performed from 25 °C to 180 °C with a temperature ramp of 3  $\text{K min}^{-1}$  in a continuous dry  $\text{N}_2$  gas stream.

Besides valuable information on the thermal behavior of the reaction system, a solid understanding of the sorbate diffusion and kinetics is of high interest for the design of a high-efficient hybrid heating and cooling system. As seen in Figure 3, the speed of the ethanolation reaction increased over thermal cycling. The time to reach an extent of conversion of 50% reduced about 18% from 44 min to 36 min and the reaction was accelerated by 22-25%. The ethanolation reaction followed a sigmoidal curve with fast reaction at low conversions. With progress of the reaction, a continuous reaction rate with decreasing tendency was encountered (Figure 3). In the third ethanolation run, a pointed reaction rate peak ( $3.5 \times 10^{-4} \text{ s}^{-1}$ ) occurred. The evolution of non-coordinated  $\text{C}_2\text{H}_5\text{OH}$  in flowing  $\text{N}_2$  during the stabilization phase is indicated by very low deethanolation reaction rates (Figure 4). After approximating an ethanolation state of one mole  $\text{C}_2\text{H}_5\text{OH}$  per mole  $\text{CaCl}_2$ , the deethanolation reaction rate was elevated. The coordinated  $\text{C}_2\text{H}_5\text{OH}$  was lost in three non-integer steps with maximum reaction rates between  $2.8 \times 10^{-4} \text{ s}^{-1}$  and  $7.4 \times 10^{-4} \text{ s}^{-1}$  (Figure 4). The deethanolation reaction rates appeared to be higher than the ethanolation reaction rates as a result of the different experimental procedures. Deethanolation was carried out under dynamic heating. The temperature gradient inside the sample provides the thermodynamic driving force for the heat transfer. If the heating rate is too high, the temperature gradient raises and limitations in the heat transfer occur. The forced decomposition hindered the diffusion of  $\text{C}_2\text{H}_5\text{OH}$  and caused non-integer release of  $\text{C}_2\text{H}_5\text{OH}$ . Ethanolation and deethanolation are slow processes and hence low heating rates are favored.

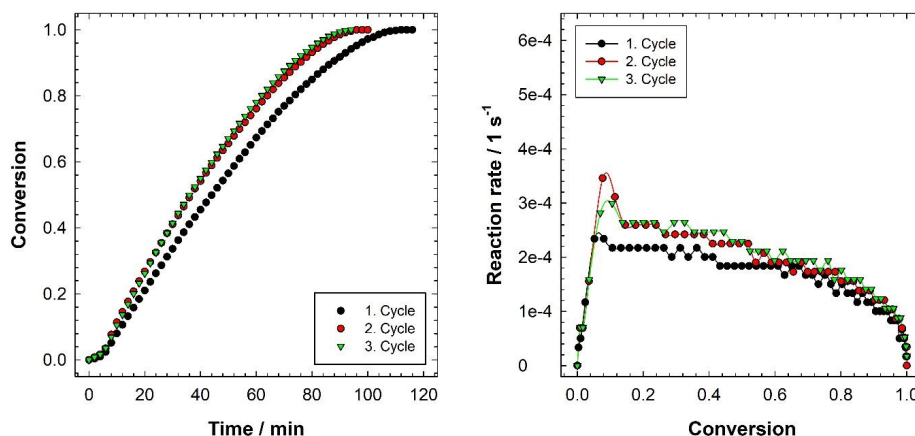


Figure 3. Reaction kinetics of the isothermal ethanolation of  $\text{CaCl}_2$ . Variation in the degree of conversion over time (left) and the reaction rate as a function of the degree of conversion (right) over three successive ethanolation/deethanolation reaction cycles.

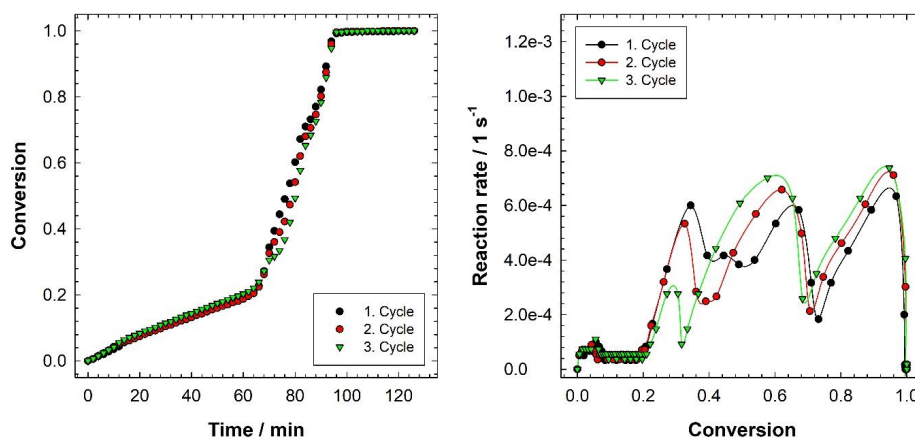


Figure 4. Reaction kinetics of the dynamic deethanolation of  $\text{CaCl}_2$ . Variation in the degree of conversion over time (left) and the reaction rate as a function of the degree of conversion (right) over three successive ethanolation/deethanolation reaction cycles.

The reaction enthalpies for ethanolation and deethanolation per mole  $\text{C}_2\text{H}_5\text{OH}$ , which were obtained from integration of the area under the exothermic and endothermic DSC peak and are listed in Table 3, were coincident with literature data [4,32,33,35,36]. The normalized ethanolation enthalpies ranged from  $-46 \text{ kJ mol}^{-1}$  to  $-56 \text{ kJ mol}^{-1}$ , whereas the normalized deethanolation

enthalpies reached values of  $59 \text{ kJ mol}^{-1}$  to  $60 \text{ kJ mol}^{-1}$ . The deethanolation reaction enthalpies are slightly higher, due to the higher heat capacity of the ethanolated  $\text{CaCl}_2$ .

Table 3. Characteristics of the ethanolation and deethanolation reaction of the reaction system  $\text{CaCl}_2\text{-C}_2\text{H}_5\text{OH}$ .

Cycle	Ethanolation		Deethanolation		
	$N$	$\Delta_r H$	$\Delta_r H$	Step 3 $T_{\text{Onset}}$	$T_{\text{Peak}}$
	( $\text{mol mol}^{-1}$ )	( $\text{kJ mol}^{-1}$ )	( $\text{kJ mol}^{-1}$ )	( $^{\circ}\text{C}$ )	( $^{\circ}\text{C}$ )
1	1.2	-56	59	102	130
2	1.2	-46	59	102	132
3	1.2	-48	60	101	132

### 3.1.2 The working pair $\text{CaCl}_2\text{-ZnO-C}_2\text{H}_5\text{OH}$

The confinement of  $\text{CaCl}_2$  to clinoptilolite resulted in overall higher ethanolation levels when compared to pure  $\text{CaCl}_2$ , as depicted in Figure 5. The maximum state of ethanolation was between 1.3 and 1.5 per cycle. Due to the overstoichiometric uptake of  $\text{C}_2\text{H}_5\text{OH}$ , a considerable amount of loosely bound  $\text{C}_2\text{H}_5\text{OH}$  was desorbed in dry  $\text{N}_2$  atmosphere so that the final ethanolation level ranged from 0.9 to 1.1.

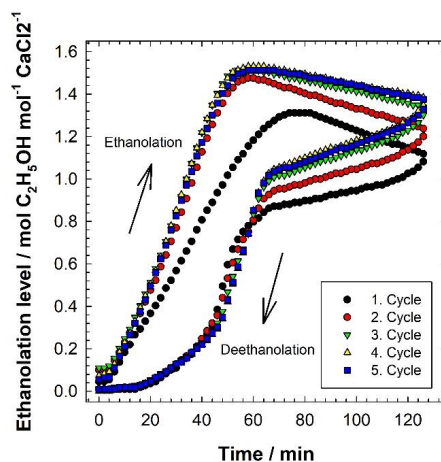


Figure 5. Five consecutive ethanolation/deethanolation reaction cycles of the composite adsorbent  $\text{CaCl}_2\text{-ZnO}$  as a function of time. The ethanolation was carried out at a  $\text{C}_2\text{H}_5\text{OH}$  vapor pressure of 3.1 kPa and at a temperature of  $25^{\circ}\text{C}$  under atmospheric conditions. The deethanolation was performed from  $25^{\circ}\text{C}$  to  $180^{\circ}\text{C}$  with a temperature ramp of  $3 \text{ K min}^{-1}$  in a continuous dry  $\text{N}_2$  gas stream.

The deethanolation reaction pattern changed over cycling. In the first demethanolation reaction, one distinct peak was measured, while in the subsequent reactions two main peaks were detected, which imply that the adsorbed  $\text{C}_2\text{H}_5\text{OH}$  was gradually removed in two overlapping steps (Figure 7). The peak temperatures values of the first and second stages ( $81^{\circ}\text{C}$  to  $92^{\circ}\text{C}$ ) may be

below 100 °C and thus lower than that of the last deethanolation stage of the deethanolation reaction of untreated CaCl<sub>2</sub>, but the desorption occurred over the whole temperature interval. Broad smeared out DSC peaks confirmed the slow desorption process, in particular at desorption temperatures higher than 100 °C and high extents of conversion.

Scrutinizing the kinetics of the ethanolation reaction reveals that the C<sub>2</sub>H<sub>5</sub>OH uptake was similar in the second to the fifth ethanolation/deethanolation cycle, as shown in Figure 6. A time of 28 min to 30 min was necessary to attain 50% completion. The shape of the ethanolation reaction rate curve remarkably differed from that observed for pure CaCl<sub>2</sub>. Maximum ethanolation reaction rates varied from  $3.6 \times 10^{-4} \text{ s}^{-1}$  and  $4.9 \times 10^{-4} \text{ s}^{-1}$  over five ethanolation/deethanolation runs. A small loss of C<sub>2</sub>H<sub>5</sub>OH was measured at 25 °C in dry N<sub>2</sub> gas flow (Figure 7). With increasing temperature, C<sub>2</sub>H<sub>5</sub>OH was continuously evolved reaching deethanolation reaction rates of  $5.9 \times 10^{-4} \text{ s}^{-1}$  to  $8.5 \times 10^{-4} \text{ s}^{-1}$ . The results highlight the distinct behavior of CaCl<sub>2</sub> incorporated into clinoptilolite. The hybrid material showed an adsorption behavior between pure CaCl<sub>2</sub> and natural clinoptilolite. The increase in the C<sub>2</sub>H<sub>5</sub>OH loading and speed of the ethanolation reaction over the first two ethanolation/deethanolation cycles suggests changes in the structural integrity of the composite adsorbent CaCl<sub>2</sub>-ZNC.

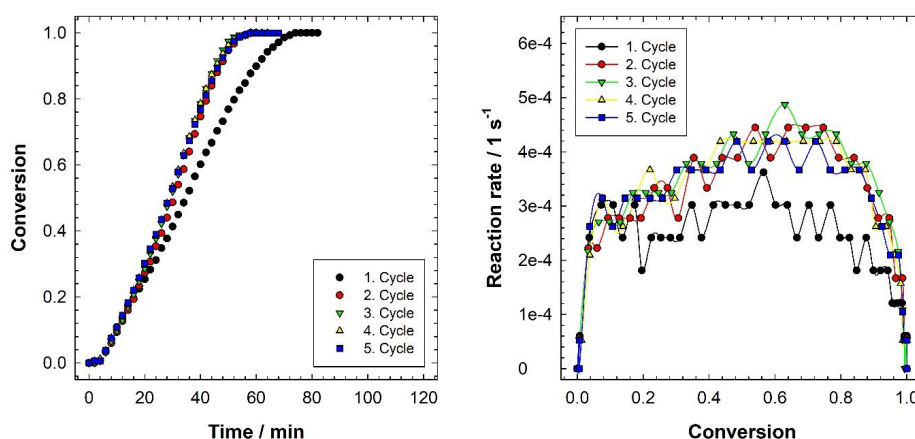


Figure 6. Reaction kinetics of the isothermal ethanolation of the composite CaCl<sub>2</sub>-ZNC. Variation in the degree of conversion over time (left) and the reaction rate as a function of the degree of conversion (right) over five successive ethanolation/deethanolation reaction cycles.

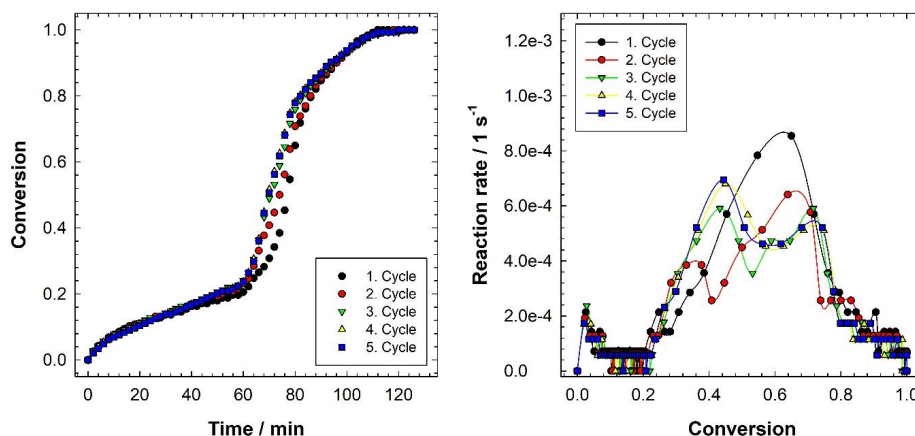


Figure 7. Reaction kinetics of the dynamic deethanolation of the composite  $\text{CaCl}_2\text{-ZNC}$ . Variation in the degree of conversion over time (left) and the reaction rate as a function of the degree of conversion (right) over five successive ethanolation/deethanolation reaction cycles.

For the adsorbent composite  $\text{CaCl}_2\text{-ZNC}$ , ethanolation and deethanolation reaction enthalpies referred to one mole of  $\text{C}_2\text{H}_5\text{OH}$  per mole  $\text{CaCl}_2$  were between  $-56 \text{ kJ mol}^{-1}$  and  $-62 \text{ kJ mol}^{-1}$ , and  $48 \text{ kJ mol}^{-1}$  and  $63 \text{ kJ mol}^{-1}$ , respectively (Table 4). The ethanolation reaction enthalpies were noticeably higher than that observed for pure  $\text{CaCl}_2$ . The zeolite clinoptilolite apparently contributed to the adsorption process. According to Knowlton et al. [37], natural clinoptilolite can incorporate three types of water, specifically external water, loosely bound water, and tightly bound water, which are differentiated by their dissociation temperatures and enthalpies. The results imply that the  $\text{C}_2\text{H}_5\text{OH}$  associated with the composite adsorbent  $\text{CaCl}_2\text{-ZNC}$  is also of different nature.

Table 4. Characteristics of the ethanolation and deethanolation reaction of the reaction system  $\text{CaCl}_2\text{-ZNC-C}_2\text{H}_5\text{OH}$ .

Cycle	Ethanolation		Deethanolation				
	$N$	$\Delta_r H$	$\Delta_r H$	Step 1		Step 2	
				$T_{\text{Onset}}$	$T_{\text{Peak}}$	$T_{\text{Onset}}$	$T_{\text{Peak}}$
( $\text{mol mol}^{-1}$ )	( $\text{kJ mol}^{-1}$ )	( $\text{kJ mol}^{-1}$ )	( $^{\circ}\text{C}$ )	( $^{\circ}\text{C}$ )	( $^{\circ}\text{C}$ )	( $^{\circ}\text{C}$ )	
1	1.3	-62	63	71	92		
2	1.5	-56	53	29	53	65	87
3	1.5	-59	51	54	55	68	85
4	1.5	-57	48	28	58	61	82
5	1.5	-60	52	28	55	61	81



### 3.1.3 The working pair CaCl<sub>2</sub>-Z13X

The dispersion of CaCl<sub>2</sub> inside the binderless 13X molecular sieve was observed to have a pronounced impact on the C<sub>2</sub>H<sub>5</sub>OH adsorption reaction profile. Figure 8 shows the ethanolation/deethanolation reaction over four repetitive measurements. The composite material exhibited good cyclic reproducibility. The ethanolation level did not exceed a value of 1.0. This phenomenon can be theoretically supported by the theory of pore closure. Literature surveys revealed that ion exchange in NaX-type zeolites closes the pore structure, while ion exchange in NaY-type zeolites is accompanied by pore opening [38]. When NaX-type zeolites are soaked in solutions of bivalent cations, two monovalent sodium ions will be displaced by one bivalent ion to ensure electroneutrality. The accumulation of CaCl<sub>2</sub> inside the narrow zeolite pore network during impregnation reduces the internal pore volume and makes it inaccessible to further C<sub>2</sub>H<sub>5</sub>OH molecules, as the ethanolation reaction progresses. However, the ethanolated CaCl<sub>2</sub>-Z13X exhibited a good stability upon exposure to pure flowing N<sub>2</sub>. By heating the ethanolated CaCl<sub>2</sub>-Z13X to 180 °C, the C<sub>2</sub>H<sub>5</sub>OH was expelled in a single step over a broad temperature range. The peak temperature of 175 °C was comparatively high (Table 5). The adsorption and desorption curves resembled the sorption profiles of pure zeolite 13X. This characteristic is attributed to the low salt content of the composite material containing 16% of CaCl<sub>2</sub>. The adsorption of C<sub>2</sub>H<sub>5</sub>OH on zeolite is described by a type I adsorption isotherm common for microporous zeolites [28].

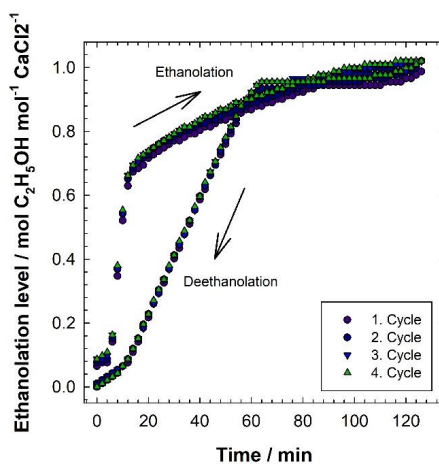


Figure 8. Four repetitive ethanolation/deethanolation reaction cycles of the composite adsorbent CaCl<sub>2</sub>-Z13X as a function of time. The ethanolation was carried out at a C<sub>2</sub>H<sub>5</sub>OH vapor pressure of 3.1 kPa at 25 °C under atmospheric conditions. The deethanolation was performed from 25 °C to 180 °C with a heating rate of 3 K min<sup>-1</sup> in a continuous flow of dry N<sub>2</sub> gas.

A rapid initial C<sub>2</sub>H<sub>5</sub>OH adsorption was experienced for the composite adsorbent CaCl<sub>2</sub>-Z13X (Figure 9). A conversion of 50% was achieved after a reaction time of around 10 min. The reaction rates constantly increased up to degrees of conversion of 0.3 to 0.4 and steadily declined afterwards.

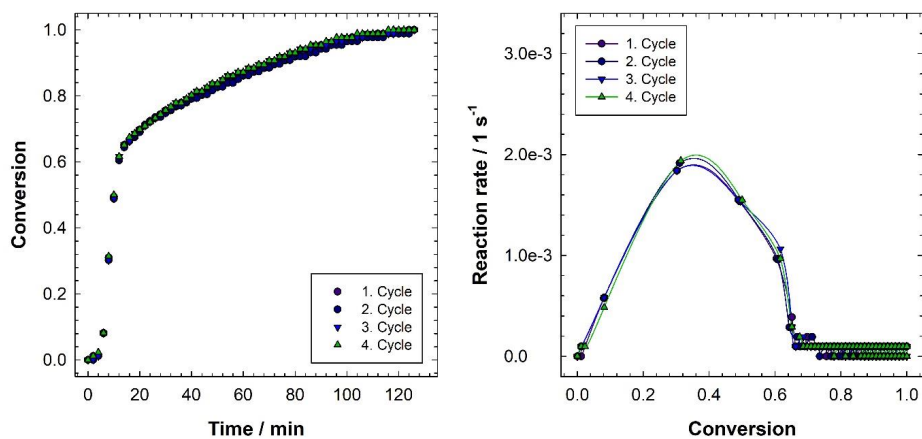


Figure 9. Reaction kinetics of the isothermal ethanolation of the composite  $\text{CaCl}_2\text{-Z13X}$ . Variation in the degree of conversion over time (left) and the reaction rate as a function of the degree of conversion (right) over four successive ethanolation/deethanolation reaction cycles.

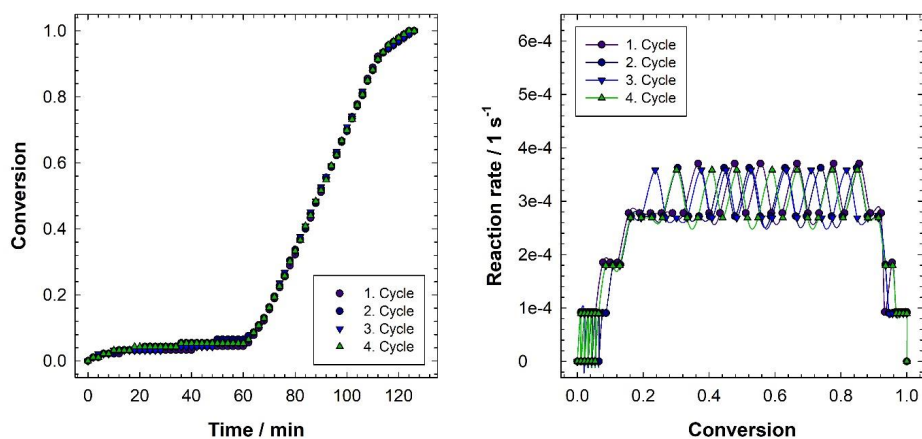


Figure 10. Reaction kinetics of the dynamic deethanolation of the composite  $\text{CaCl}_2\text{-Z13X}$ . Variation in the degree of conversion over time (left) and the reaction rate as a function of the degree of conversion (right) over four successive ethanolation/deethanolation reaction cycles.

Above a fractional conversion of 0.6, the reaction slowed down indicated by very low apparent rates of reaction. Ethanolation reaction rate maxima were between  $3.8 \times 10^{-3} \text{ s}^{-1}$  and  $3.9 \times 10^{-3} \text{ s}^{-1}$ . Jänchen et al. [39] have investigated the  $\text{H}_2\text{O}$  adsorption thermal storage and hydrothermal stability of binderless zeolite 13XBF and also found that the time to reach

equilibrium was significantly shorter when compared with binder-containing zeolites. The binderless zeolite contained mainly macro pores as secondary pore system and improved accessible surface area, which enhanced the kinetics. After stabilization at 25 °C for 60 min, the desorption process was initiated by applying heat. The C<sub>2</sub>H<sub>5</sub>OH was removed slowly in one broad step and as a result the reaction rate mainly fluctuated between  $2.7 \times 10^{-4} \text{ s}^{-1}$  and  $3.7 \times 10^{-4} \text{ s}^{-1}$ . Slow desorption kinetics and high desorption temperatures are due to strong interactions between the active sites in the zeolite and the adsorbate.

The ethanolation and deethanolation reaction enthalpies ranged from  $-129 \text{ kJ mol}^{-1}$  to  $-140 \text{ kJ mol}^{-1}$  and from  $120 \text{ kJ mol}^{-1}$  to  $129 \text{ kJ mol}^{-1}$ , respectively, as summarized in Table 5. The calculated values are approximately twice as high as the standard molar reaction enthalpies for the association and dissociation reaction of CaCl<sub>2</sub> ethanulates. Zeolites commonly display differential heats of H<sub>2</sub>O adsorption between  $-40 \text{ kJ mol}^{-1}$  and  $-100 \text{ kJ mol}^{-1}$  depending on the adsorbed amount of H<sub>2</sub>O [40–42]. According to literature, enthalpies of C<sub>2</sub>H<sub>5</sub>OH adsorption of the same magnitude ( $-60 \text{ kJ mol}^{-1}$  to  $-135 \text{ kJ mol}^{-1}$ ) were calculated for MFI-type zeolites [43,44]. Since comparative data is unavailable, overestimation errors could not be identified.

Table 5. Characteristics of the ethanolation and deethanolation reaction of the reaction system CaCl<sub>2</sub>-Z13X-C<sub>2</sub>H<sub>5</sub>OH.

Cycle	Ethanolation		Deethanolation		
	<i>N</i>	$\Delta_r H$	$\Delta_r H$	Step 1	
	(mol mol <sup>-1</sup> )	(kJ mol <sup>-1</sup> )	(kJ mol <sup>-1</sup> )	<i>T</i> <sub>Onset</sub> (°C)	<i>T</i> <sub>Peak</sub> (°C)
1	1.0	-140	126	28	175
2	1.0	-135	126	28	175
3	1.0	-129	120	28	175
4	1.0	-129	129	28	175

### 3.1.4 The working pair CaCl<sub>2</sub>-ENG-C<sub>2</sub>H<sub>5</sub>OH

The thermally conductive matrix expanded graphite is well known for its enhancement effect on the heat transfer in thermal energy storage materials [11,45]. Results on the adsorption and desorption behavior of the composite compound CaC<sub>2</sub>-ENG plotted in Figure 11 show that the incorporation of CaCl<sub>2</sub> into compacted ENG pellets facilitated the mass and thermal transport over thermal cycling. The maximum level of ethanolation varied from 1.2 in the first to 1.5 to 1.7 in the subsequent cycles.

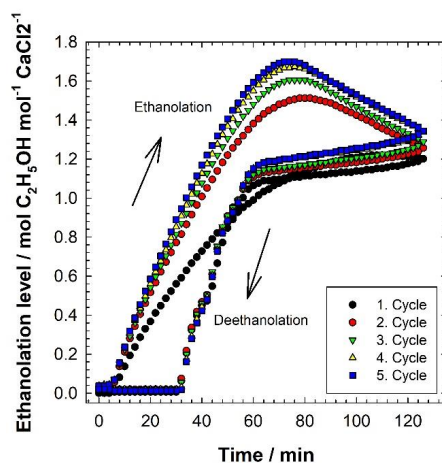


Figure 11. Five successive ethanolation/deethanolation reaction cycles of the composite adsorbent  $\text{CaCl}_2\text{-ENG}$  as a function of time. The ethanolation was carried out at a  $\text{C}_2\text{H}_5\text{OH}$  vapor pressure of 3.1 kPa at 25 °C under atmospheric conditions. The deethanolation was performed from 25 °C to 180 °C with a temperature ramp of 3 K  $\text{min}^{-1}$  in continuous dry  $\text{N}_2$  gas flow.

In the first cycle, the  $\text{C}_2\text{H}_5\text{OH}$  uptake proceeded slowly, whereas in the second to the fifth ethanolation measurement, a reaction time of 30 min to 34 min was needed to reach a conversion of 50% (Figure 12). In Figure 12, a conversion of 100% is assigned to an ethanolation level of 1.7 moles  $\text{C}_2\text{H}_5\text{OH}$  per mole  $\text{CaCl}_2$ . The reaction rate profile for the first ethanolation reaction differed from the following ones, as shown in Figure 12. A sharp peak appeared between an extent of conversion of 0% and 20% with maximum reaction rates from  $3.1 \times 10^{-4} \text{ s}^{-1}$  to  $4.4 \times 10^{-4} \text{ s}^{-1}$ . The reaction rates decreased with proceeding reaction. The overall curves were similar to that obtained for pure  $\text{CaCl}_2$ . Since  $\text{CaCl}_2$  is the key adsorbent, as confirmed by thermal analysis of the parent ENG, and the  $\text{CaCl}_2$  monoethanolate is the only thermodynamically stable coordination complex, ethanolates with an ethanolation level higher than one mole of  $\text{C}_2\text{H}_5\text{OH}$  per mole  $\text{CaCl}_2$  were unstable and dissociated in dry  $\text{N}_2$ . At the beginning of the deethanolation run, the ethanolation state levelled at 1.1 to 1.2. Concerning the release of  $\text{C}_2\text{H}_5\text{OH}$  upon heating, the composite  $\text{CaCl}_2\text{-ENG}$  showed a similar behavior as single  $\text{CaCl}_2$ , as seen in Figure 13. The sample decomposed in three overlapping steps with peak temperatures at 61 °C to 72 °C, 88 °C to 97 °C, and 124 °C to 125 °C. The corresponding onset and peak temperatures are listed in Table 6. The maximum deethanolation reaction rates were with values of  $4.4 \times 10^{-4} \text{ s}^{-1}$  to  $1.0 \times 10^{-3} \text{ s}^{-1}$  slightly higher than those for single  $\text{CaCl}_2$ . The higher reaction rates are primary ascribed to the higher initial amount of  $\text{C}_2\text{H}_5\text{OH}$  adsorbed inside the composite. Thermal and mechanical stresses altered the structure of the  $\text{CaCl}_2\text{-ENG}$  sample during the cycling test resulting in physical instability.

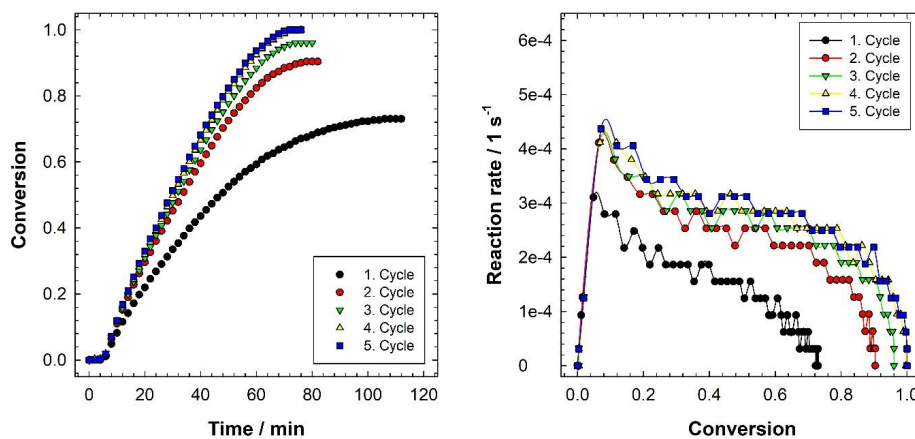


Figure 12. Reaction kinetics of the isothermal ethanolation of the composite CaCl<sub>2</sub>-ENG. Variation in the degree of conversion over time (left) and the reaction rate as a function of the degree of conversion (right) over four successive ethanolation/deethanolation reaction cycles. A conversion of 1 equals an ethanolation state of 1.7 moles of C<sub>2</sub>H<sub>5</sub>OH per mole CaCl<sub>2</sub>.

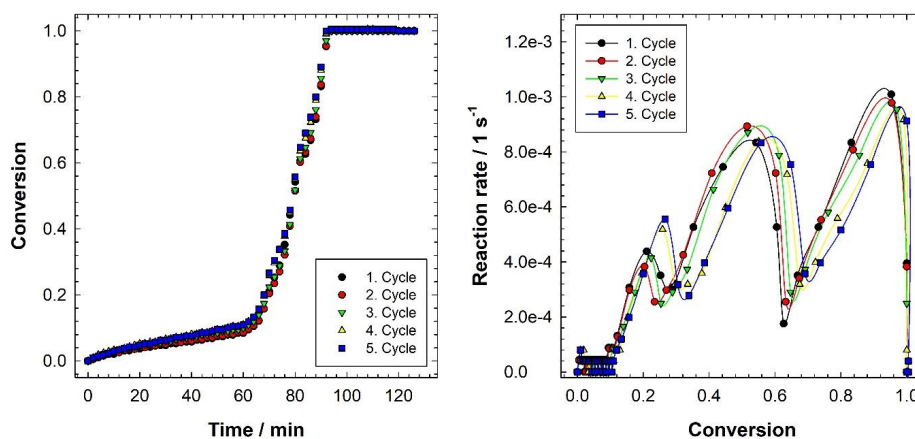


Figure 13. Reaction kinetics of the dynamic deethanolation of the composite CaCl<sub>2</sub>-ENG. Variation in the degree of conversion over time (left) and the reaction rate as a function of the degree of conversion (right) over four successive ethanolation/deethanolation reaction cycles. A conversion of 1 equals an ethanolation state of 1.7 moles of C<sub>2</sub>H<sub>5</sub>OH per mole CaCl<sub>2</sub>.

The composite material CaCl<sub>2</sub>-ENG yielded ethanolation reaction enthalpies of  $-42 \text{ kJ mol}^{-1}$  to  $-63 \text{ kJ mol}^{-1}$  and deethanolation reaction enthalpies between  $58 \text{ kJ mol}^{-1}$  and  $64 \text{ kJ mol}^{-1}$  (Table 6). The values were normalized to one mole of C<sub>2</sub>H<sub>5</sub>OH.

Table 6. Characteristics of the ethanolation and deethanolation reaction of the reaction system  $\text{CaCl}_2\text{-ENG-C}_2\text{H}_5\text{OH}$ .

Cycle	Ethanolation		Deethanolation						
	<i>N</i>	$\Delta_r H$	$\Delta_r H$	Step 1		Step 2		Step 3	
	(mol mol <sup>-1</sup> )	(kJ mol <sup>-1</sup> )	(kJ mol <sup>-1</sup> )	$T_{\text{Onset}}$ (°C)	$T_{\text{Peak}}$ (°C)	$T_{\text{Onset}}$ (°C)	$T_{\text{Peak}}$ (°C)	$T_{\text{Onset}}$ (°C)	$T_{\text{Peak}}$ (°C)
1	1.2	-42	63	54	63	71	88	102	124
2	1.5	-59	64	53	72	67	89	104	125
3	1.6	-63	63	50	61	72	96	103	125
4	1.7	-58	60	52	62	68	96	103	124
5	1.7	-58	58	54	62	72	97	101	124

### 3.2 Energy analysis of different $\text{CaCl}_2$ -based adsorbents and $\text{C}_2\text{H}_5\text{OH}$ as adsorbate

The composite materials studied were engineered for utilization in dual thermal energy storage systems operable by low potential heat sources. Besides appealing intrinsic energy storage performances, an efficient production of cold energy is demanded. Energy storage density, specific cooling power, and cooling coefficient of performance are highly determined by the operating conditions applied, in particular the adsorption and desorption temperature as well as the vapor pressure of the sorbate. The compound adsorbents yielded  $\text{C}_2\text{H}_5\text{OH}$  uptakes of 0.10 g g<sup>-1</sup> to 0.41 g g<sup>-1</sup> and specific reaction enthalpies between 195 kJ kg<sup>-1</sup> and 323 kJ kg<sup>-1</sup>. The specific reaction enthalpies were referred to the dry mass of the composite. Consequently, the corresponding energy storage densities, normalized to the ethanolated composite mass, only amounted to 177 kJ kg<sup>-1</sup> and 213 kJ kg<sup>-1</sup>, respectively. The energy density increased in the order of the  $\text{CaCl}_2$  content. Pure  $\text{CaCl}_2$  exhibited the best efficiency.

Table 7. Energy storage and cooling performance specifications of materials paired with  $\text{C}_2\text{H}_5\text{OH}$  as sorbate. Measurements were carried out at a  $\text{C}_2\text{H}_5\text{OH}$  vapor pressures of 3.1 kPa corresponding to an evaporator temperature of 9.5 °C and a condensation temperature of 25 °C. The materials were regenerated at a maximum desorption temperature of 180 °C. The SCP was averaged over the total  $\text{C}_2\text{H}_5\text{OH}$  adsorption.

Material	Ethanol uptake (g g <sup>-1</sup> )	$\Delta_r h$ (kJ kg <sup>-1</sup> )	E (kJ kg <sup>-1</sup> )	$\text{SCP}_{\text{max}}$ (W kg <sup>-1</sup> )	$\text{SCP}_{\text{average}}$ (W kg <sup>-1</sup> )	COP (-)	Number of cycles
$\text{CaCl}_2$	0.51 ± 0.00	451 ± 47	319 ± 25	253 ± 43	145 ± 8	0.88 ± 0.01	3
$\text{CaCl}_2\text{-ZNC}$	0.18 ± 0.01	234 ± 11	198 ± 8	137 ± 19	91 ± 13	0.81 ± 0.08	5
$\text{CaCl}_2\text{-Z13X}$	0.10 ± 0.00	195 ± 6	177 ± 6	210 ± 6	49 ± 6	0.34 ± 0.01	4
$\text{CaCl}_2\text{-ENG}$	0.41 ± 0.05	323 ± 43	213 ± 38	322 ± 37	162 ± 38	0.70 ± 0.03	5

Regarding the suitability of the materials for cooling applications, the composite adsorbent  $\text{CaCl}_2\text{-ENG}$  showed the highest average specific cooling power (Figure 14). The  $\text{CaCl}_2\text{-ENG}$  constantly provided cold energy over 70 min. Only with single  $\text{CaCl}_2$  satisfactory cooling over 80 min was produced. The  $\text{CaCl}_2\text{-Z13X}$  possessed excellent adsorption energetics and kinetics.

The fast reaction kinetics and limited adsorption capacity of the composite material resulted in high and short cooling output. Generally, the cooling power output is influenced by the speed of the reaction. At molecular level, some of the major factors controlling the reaction rate are chemical reactions occurring at the reactant/product interface, changes in the reaction interface geometry with proceeding reaction and diffusion of reagents to and from the reaction interface [46].

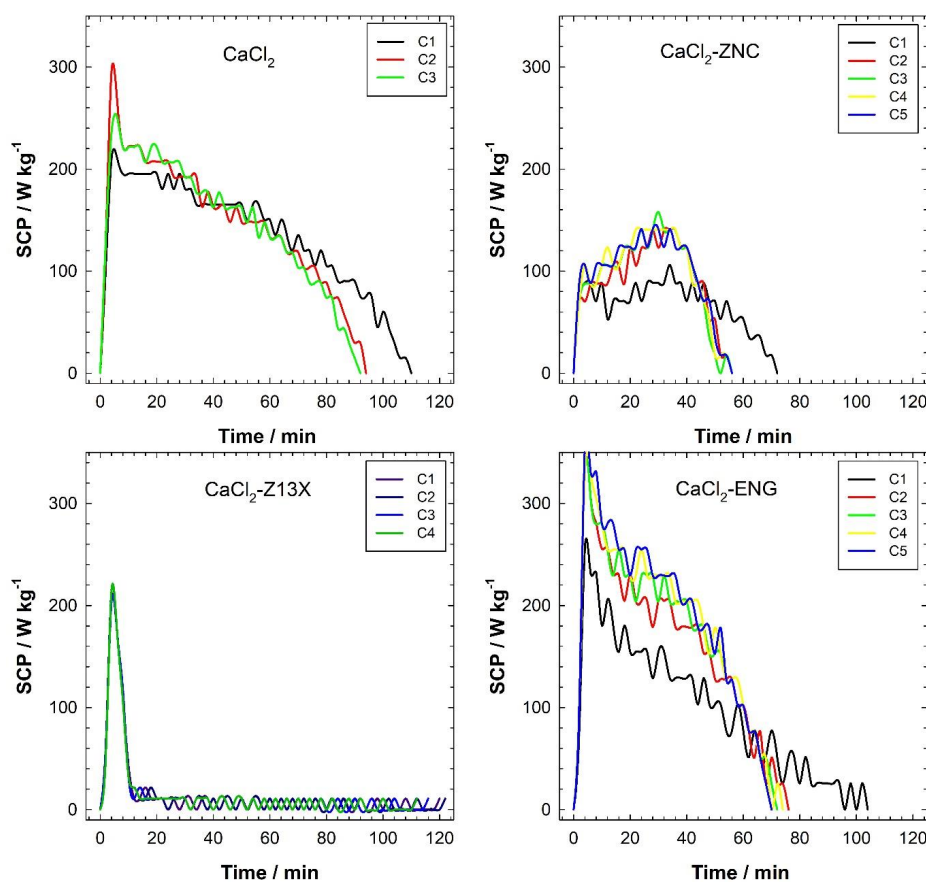


Figure 14. Specific cooling power as a function of time of the materials tested at an evaporator temperature of  $9.5\text{ }^{\circ}\text{C}$  and a condensation temperature of  $25\text{ }^{\circ}\text{C}$ . The materials were regenerated at a maximum desorption temperature of  $180\text{ }^{\circ}\text{C}$ .

A comparison of the results on the  $\text{C}_2\text{H}_5\text{OH}$  adsorption onto the composite  $\text{CaCl}_2\text{-Z13X}$  presented in this study with results obtained for binderless zeolite 13XBF, which was purchased from the same supplier, by Herzog and Jänchen [47], imply that ion exchange and deposition of  $\text{CaCl}_2$  inside the zeolite pores reduced the  $\text{C}_2\text{H}_5\text{OH}$  uptake. Herzog and Jänchen [47] reported a

$\text{C}_2\text{H}_5\text{OH}$  adsorption capacity of  $0.24 \text{ g g}^{-1}$  at  $25 \text{ }^\circ\text{C}$  under a relative pressure of 0.99. The instantaneous  $\text{C}_2\text{H}_5\text{OH}$  adsorption and accordingly high temperature lift over a narrow time frame of the composite based on zeolite 13X promises quick heat supply. However, the composite  $\text{CaCl}_2\text{-Z13X}$  is not easy to regenerate and requires high regeneration temperatures. Cui et al. [48], who studied the  $\text{C}_2\text{H}_5\text{OH}$  desorption behavior of zeolite 13X, draw similar conclusions. Main drawback of the molecular sieves used as supporting structures is the apparent high charging temperature and slow mass transport in the charging mode, which makes them unfavorable for low temperature applications. Deformations in the material structure were observed for the composite materials  $\text{CaCl}_2\text{-ZNC}$  and  $\text{CaCl}_2\text{-ENG}$  resulting in changes in the  $\text{C}_2\text{H}_5\text{OH}$  adsorption behavior over cycling. In terms of physical stability, these materials are not recommended at the current stage of development.

### 3.3 Thermal and kinetic analysis of different $\text{CaCl}_2$ -based adsorbents and $\text{CH}_3\text{OH}$ as adsorbate

#### 3.3.1 The working pair $\text{CaCl}_2\text{-CH}_3\text{OH}$

Since the use of  $\text{CH}_3\text{OH}$  can provide cooling at lower temperatures at higher vapor pressures, this refrigerant is advantageous over  $\text{C}_2\text{H}_5\text{OH}$ . Therefore, the reaction system  $\text{CaCl}_2\text{-CH}_3\text{OH}$  was examined in multi-cycle dynamic methanolation and demethanolation reactions. Results obtained by TGA show that the  $\text{CH}_3\text{OH}$  adsorption and desorption followed a sigmoidal reaction curve (Figure 15).

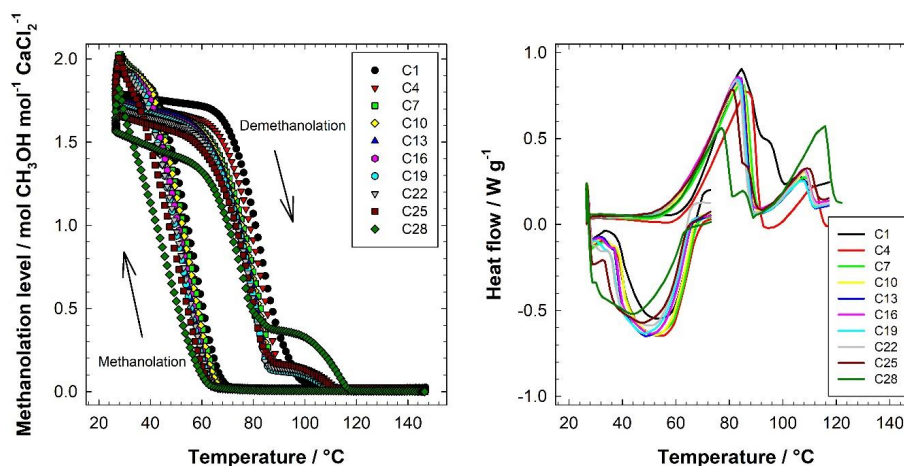


Figure 15. Methanolation/demethanolation cycles of single  $\text{CaCl}_2$  (left). Exothermic and endothermic heat evolution as a function of temperature over cycling (right). The methanolation was carried out at a  $\text{CH}_3\text{OH}$  vapor pressure of 6.8 kPa under dynamic conditions. The initial temperature was set at  $150 \text{ }^\circ\text{C}$ ; the cooling rate was  $-1 \text{ K min}^{-1}$ . The demethanolation was performed from  $25 \text{ }^\circ\text{C}$  to  $150 \text{ }^\circ\text{C}$  with a heating rate of  $1 \text{ K min}^{-1}$  in flowing dry  $\text{N}_2$  gas.



As seen in Figure 16, the  $\text{CH}_3\text{OH}$  uptake accelerated over the course of the reaction. The total amount of  $\text{CH}_3\text{OH}$  adsorbed in a single step during the methanolation phase was 2.0 and is in agreement with literature data [4,6,8,33].

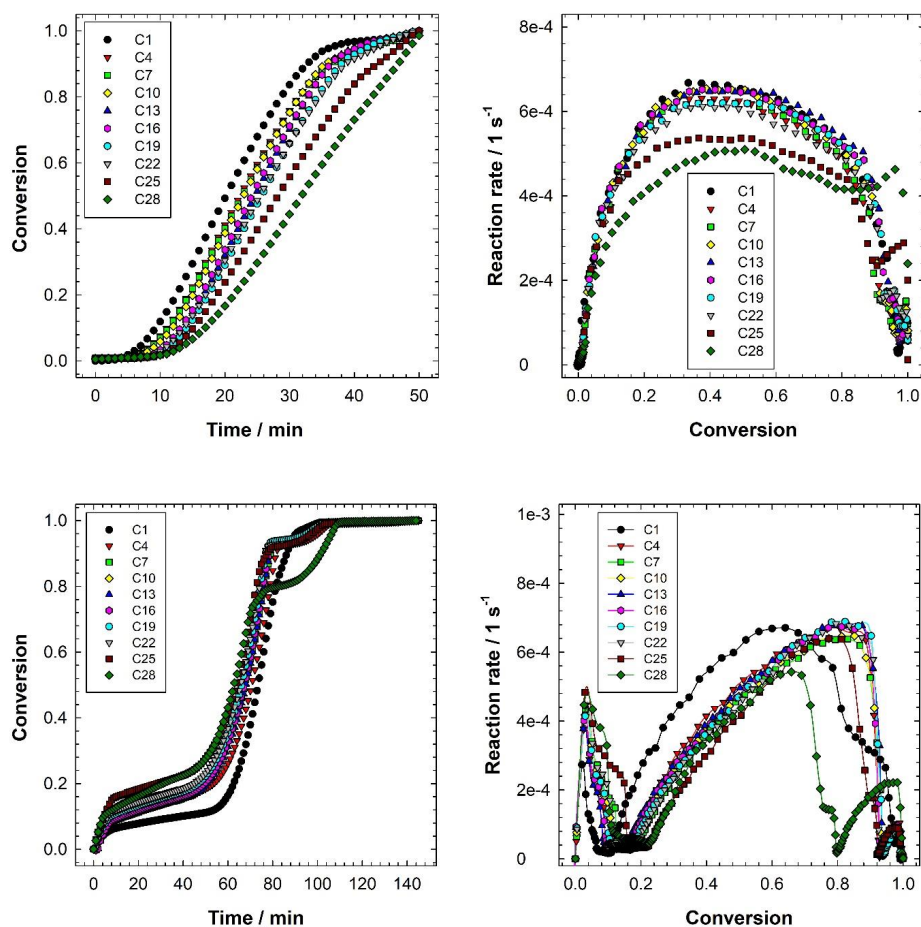


Figure 16. Methanolation (top) and demethanolation (bottom) reaction kinetics of the adsorbent  $\text{CaCl}_2$ . The methanolation was carried out at a  $\text{CH}_3\text{OH}$  vapor pressure of 6.8 kPa under dynamic conditions. The initial temperature was set at 150 °C; the cooling rate was  $-1 \text{ K min}^{-1}$ . The demethanolation was performed from 25 °C to 150 °C with a heating rate of  $1 \text{ K min}^{-1}$  in flowing dry  $\text{N}_2$  gas.

In the subsequent stabilization phase, the  $\text{CH}_3\text{OH}$  was partially desorbed at 25 °C in dry  $\text{N}_2$  atmosphere. Due to the fragile stability of the  $\text{CaCl}_2$  dimethanolate, the material requires precise control of the storage conditions. Decomposition indicates that true equilibrium was not reached under the experimental conditions applied. Some loosely bound  $\text{CH}_3\text{OH}$  was immediately released.

A stepwise dissociation was observed during the demethanolation phase (Figure 15). The major amount of  $\text{CH}_3\text{OH}$  was removed below  $100^\circ\text{C}$ . The second peak is attributed to limitations in the heat transfer. The onset temperatures of the main peaks were  $65^\circ\text{C}$  to  $71^\circ\text{C}$  for the methanolation reaction and  $60^\circ\text{C}$  to  $65^\circ\text{C}$  for the demethanolation reaction. The methanolation and demethanolation peak temperatures of the main peaks were determined at  $48^\circ\text{C}$  to  $57^\circ\text{C}$  and  $81^\circ\text{C}$  to  $86^\circ\text{C}$ , respectively. In the last cycles, the  $\text{CH}_3\text{OH}$  supply was interrupted and as a result onset and peak were shifted towards lower temperatures. The remethanolation process slowed down and a distinct demethanolation peak became clearly visible between conversions of 0.8 and 1.0. The peak was caused by mass transfer limitations inside the sample. From thermal and kinetic analysis it is apparent that the sample underwent structural changes with thermal cycling (Figure 15 and Figure 16). Microscopic analysis confirmed a volume expansion of the  $\text{CaCl}_2$  sample during the cycle test.

Figure 16 shows a continuous uptake of  $\text{CH}_3\text{OH}$  with increasing reaction rates between a conversion degree of 0% and 50%, which is equal to a methanolation level of one mole  $\text{CH}_3\text{OH}$  per mole  $\text{CaCl}_2$ . From a conversion of 50% to 100%, the reaction rates decreased again. Maximum methanolation reaction rates varied from  $4.6 \times 10^{-4} \text{ s}^{-1}$  to  $6.7 \times 10^{-4} \text{ s}^{-1}$ . The release of  $\text{CH}_3\text{OH}$  without heating is characterized by a narrow reaction rate peak (Figure 16). During demethanolation, maximum reaction rates ( $5.4 \times 10^{-4} \text{ s}^{-1}$  to  $6.9 \times 10^{-4} \text{ s}^{-1}$ ) are shifted to higher extents of conversion. The course of the demethanolation reaction rates confirm the non-integer decomposition of  $\text{CaCl}_2$  under the conditions tested.

Despite an overall heterogeneous methanolation and demethanolation pattern, the enthalpies of reaction were constant over twenty-five methanolation/demethanolation cycles, as demonstrated in Figure 17.

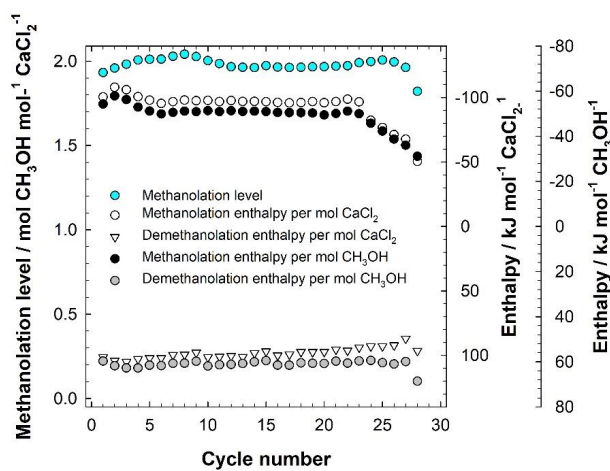


Figure 17. Molar enthalpy of methanolation and demethanolation for  $\text{CaCl}_2$  over thermal cycling in terms of the methanolation level.

Variation of both the reaction enthalpy per mole  $\text{CaCl}_2$  and per mole  $\text{CH}_3\text{OH}$  occurred over the first five cycles. The average methanolation and demethanolation enthalpy were calculated to  $(-93 \pm 12) \text{ kJ mol}^{-1}$  and  $(98 \pm 4) \text{ kJ mol}^{-1}$ , respectively. The corresponding normalized reaction enthalpies averaged to  $(-49 \pm 6) \text{ kJ mol}^{-1}$  and  $(61 \pm 2) \text{ kJ mol}^{-1}$ , respectively, and were close to values stated in literature [8]. During the last cycles, the interrupted  $\text{CH}_3\text{OH}$  supply decelerated not only the reaction, but also affected the processing of the methanolation reaction enthalpy data. The underestimation of the reaction enthalpy of methanolation, which gradually dropped to  $-31 \text{ kJ mol}^{-1}$ , arose from integration issues due to a displaced baseline and does not represent the real heat content of the material. In conclusion, single  $\text{CaCl}_2$  showed a good cycle stability regarding the thermal properties, but is susceptible to structural deterioration through hygrothermal cycling.

### 3.3.2 The working pair $\text{CaCl}_2\text{-BC-CH}_3\text{OH}$

To eliminate the intrinsic physical instability problem of  $\text{CaCl}_2$  and its methanolates, the salt was dispersed within a biochar matrix with open pore network. Results on the methanolation/demethanolation behavior are illustrated in Figure 18.

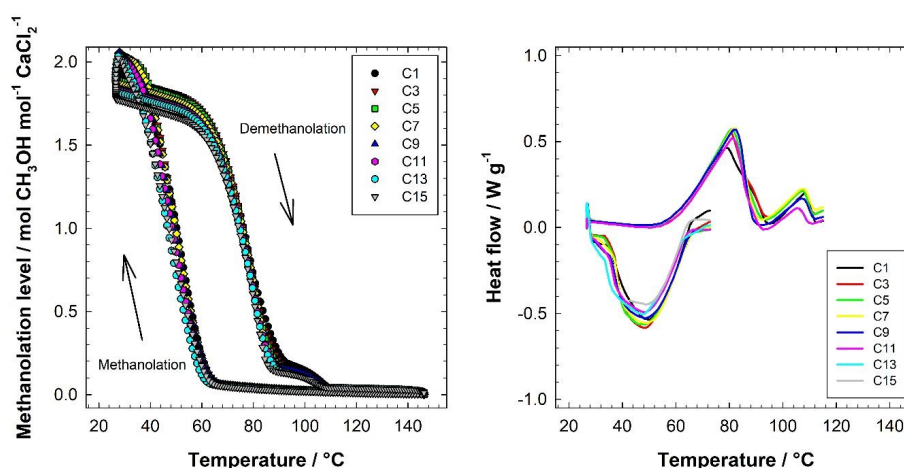


Figure 18. Methanolation/demethanolation cycles of the compound composite  $\text{CaCl}_2\text{-BC}$  (left). Exothermic and endothermic heat evolution as a function of temperature over cycling (right). The methanolation was carried out at a  $\text{CH}_3\text{OH}$  vapor pressure of 6.8 kPa under dynamic conditions. The initial temperature was set at 150  $^\circ\text{C}$ ; the cooling rate was  $-1 \text{ K min}^{-1}$ . The demethanolation was performed from 25  $^\circ\text{C}$  to 150  $^\circ\text{C}$  with a heating rate of  $1 \text{ K min}^{-1}$  in flowing dry  $\text{N}_2$  gas.

The composite displayed a cyclic stability over sixteen cycles. The overall thermal power remained unchanged. However, the exothermic heat flow peak decreased over cycling. As the material was stabilized between the methanolation and demethanolation phase at 25  $^\circ\text{C}$  in pure  $\text{N}_2$ , small amounts of  $\text{CH}_3\text{OH}$  were given off. Hysteresis occurred, which means a difference in the methanolation and demethanolation pattern. The hysteresis loops, which are peculiar to gas-solid

reactions, were smaller and smoother than that for  $\text{CaCl}_2$ . The methanolation level fluctuated around two moles of  $\text{CH}_3\text{OH}$  per mole  $\text{CaCl}_2$ . A high content of  $\text{CH}_3\text{OH}$  was successfully desorbed below  $100^\circ\text{C}$  indicating improved heat diffusion through the material (Figure 18). The methanolation and demethanolation onset temperatures of the main stages were within the range of  $64^\circ\text{C}$  to  $67^\circ\text{C}$  and  $59^\circ\text{C}$  to  $62^\circ\text{C}$ , respectively. The corresponding peak temperatures varied from  $46^\circ\text{C}$  to  $50^\circ\text{C}$  for the methanolation reaction and from  $79^\circ\text{C}$  to  $83^\circ\text{C}$  for the demethanolation reaction.

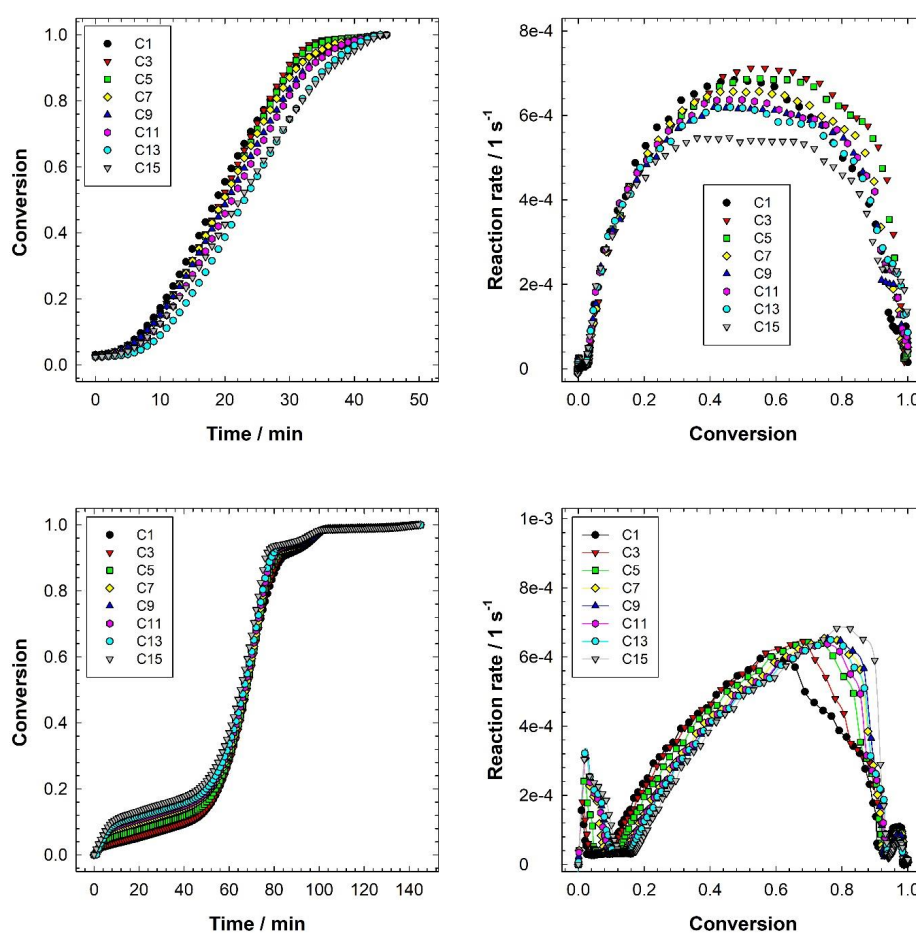


Figure 19. Methanolation (top) and demethanolation (bottom) reaction kinetics of the composite  $\text{CaCl}_2\text{-BC}$ . The methanolation was carried out at a  $\text{CH}_3\text{OH}$  vapor pressure of  $6.8\text{ kPa}$  under dynamic conditions. The initial temperature was set at  $150^\circ\text{C}$ ; the cooling rate was  $-1\text{ K min}^{-1}$ . The demethanolation was performed from  $25^\circ\text{C}$  to  $150^\circ\text{C}$  with a heating rate of  $1\text{ K min}^{-1}$  in flowing dry  $\text{N}_2$  gas.

As shown in Figure 19, no significant improvement of the reactivity was realized by using biochar. Over the first few cycles, the reaction rate marginally increased and reached maxima of  $6.8 \times 10^{-4} \text{ s}^{-1}$  to  $7.1 \times 10^{-4} \text{ s}^{-1}$ . The maximum demethanolation reaction rates ranged from  $6.0 \times 10^{-4} \text{ s}^{-1}$  to  $7.0 \times 10^{-4} \text{ s}^{-1}$ . In the seventh methanolation run, a reaction time of 20 min was necessary to reach 50% completion under dynamic methanolation conditions in comparison to the methanolation of pure  $\text{CaCl}_2$ . With pure  $\text{CaCl}_2$ , a degree of conversion of 50% was attained after 23 min. The conversion curves for methanolation and demethanolation of the composite adsorbent  $\text{CaCl}_2\text{-BC}$  and the single salt  $\text{CaCl}_2$  have similar shapes. That implies that  $\text{CaCl}_2$  is the major adsorbent. Due to reduced  $\text{CH}_3\text{OH}$  vapor pressure in the system during the last cycles, a decline in the methanolation reaction rate was experienced.

The insufficient supply of  $\text{CH}_3\text{OH}$  to the sample caused an underestimation of the methanolation reaction enthalpy. The reaction enthalpy for methanolation per mole  $\text{CH}_3\text{OH}$  diminished from  $-53 \text{ kJ mol}^{-1}$  to  $-37 \text{ kJ mol}^{-1}$  (Figure 20). The latter value is unrepresentative and resulted from problems with the integration of the DSC peak area because of a shift in the baseline. The associated methanolation enthalpies ranged from  $-102 \text{ kJ mol}^{-1}$  to  $-69 \text{ kJ mol}^{-1}$ . The demethanolation reaction enthalpies were not affected and thus varied only over a small interval. The calculated average was  $(49 \pm 2) \text{ kJ mol}^{-1}$  per mole  $\text{CH}_3\text{OH}$ . The composite  $\text{CaCl}_2\text{-BC}$  analyzed by TGA/DSC presented a subtly enhanced heat transfer and cyclic reversibility. No notable structural and textural changes in the sample geometry were optically detected after cycling. The addition of biochar can be beneficial to improve the thermal performance of  $\text{CaCl}_2$ . However, the composite is not recommended for practical application in its current form. Further material tuning is prerequisite to create a composite material with defined pore structure that is stable against mechanical and thermal shock on system scale.

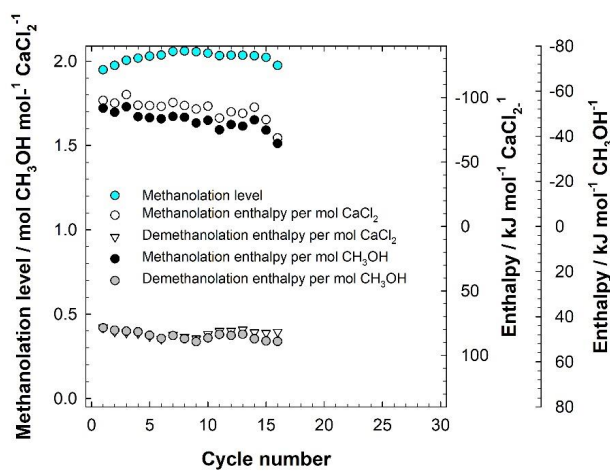


Figure 20. Molar enthalpy of methanolation and demethanolation for the composite material  $\text{CaCl}_2\text{-BC}$  over thermal cycling in terms of the methanolation level.

### 3.3.3 The working pair $\text{CaCl}_2\text{-EV2-CH}_3\text{OH}$

The confinement of  $\text{CaCl}_2$  to expanded natural vermiculite resulted in a narrower methanolation/demethanolation hysteresis compared with that of pure  $\text{CaCl}_2$  (Figure 21). The total  $\text{CH}_3\text{OH}$  loading numbered two moles of  $\text{CH}_3\text{OH}$  per mole  $\text{CaCl}_2$ . The first two demethanolation reactions exhibited a different reaction curve as the subsequent ones. The majority of  $\text{CH}_3\text{OH}$  was desorbed below  $90^\circ\text{C}$ . Traces of  $\text{CH}_3\text{OH}$  remained inside the sample indicated by a fairly small peak between a conversion of 0.9 and 1.0 (Figure 22). The methanolated  $\text{CaCl}_2\text{-EV2}$  showed a good stability during stabilization at  $25^\circ\text{C}$  in dry  $\text{N}_2$  gas as expressed by a small reaction rate peak between a conversion of 0% and 10%, except in the last methanolation/demethanolation run. The methanolation reaction happened in a single step. Local fluctuations in the temperature accounted for changes in the heat flow peak of the exothermic reaction over thermal cycling followed by subsequent stabilization, as seen in Figure 21. Methanolation onset and peak temperatures shifted from  $69^\circ\text{C}$  to  $63^\circ\text{C}$  and from  $52^\circ\text{C}$  to  $46^\circ\text{C}$ , respectively during the first thirteen cycles, as observed for pure  $\text{CaCl}_2$ . Onset and peak temperatures of  $66^\circ\text{C}$  to  $58^\circ\text{C}$  and  $83^\circ\text{C}$  to  $77^\circ\text{C}$  were measured for the demethanolation reaction. The thermal behavior of the composite  $\text{CaCl}_2\text{-EV2}$  signifies that the structure of the composite was disrupted by consecutive methanolation and demethanolation.

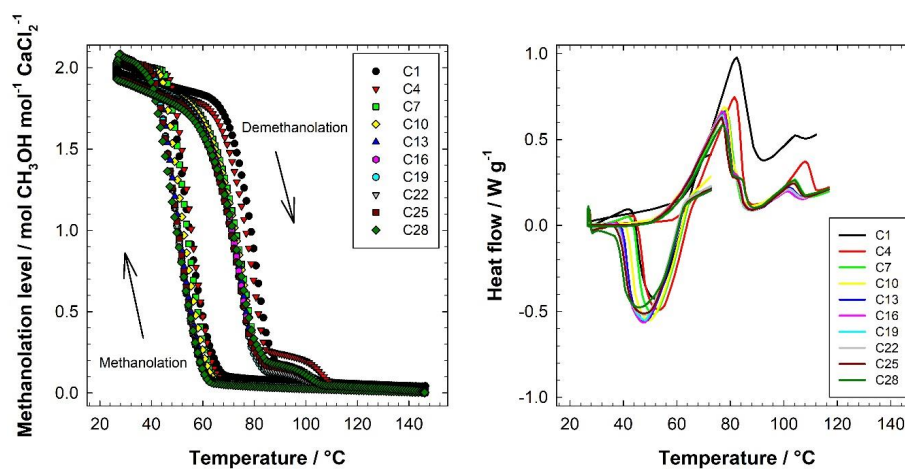


Figure 21. Methanolation/demethanolation cycles of the composite adsorbent  $\text{CaCl}_2\text{-EV2}$  (left). Exothermic and endothermic heat evolution as a function of temperature over cycling (right). The methanolation was carried out at a  $\text{CH}_3\text{OH}$  vapor pressure of 6.8 kPa under dynamic conditions. The initial temperature was set at  $150^\circ\text{C}$ ; the cooling rate was  $-1\text{ K min}^{-1}$ . The demethanolation was performed from  $25^\circ\text{C}$  to  $150^\circ\text{C}$  with a heating rate of  $1\text{ K min}^{-1}$  in flowing dry  $\text{N}_2$  gas.

For the composite material  $\text{CaCl}_2\text{-EV2}$ , the speed of the methanolation and demethanolation varied over thermal cycling, as displayed in Figure 22. To reach a conversion of 50%, a reaction time of 21 min was needed in the seventh methanolation reaction. The conversion rate profiles were similar to that obtained for pure  $\text{CaCl}_2$ .

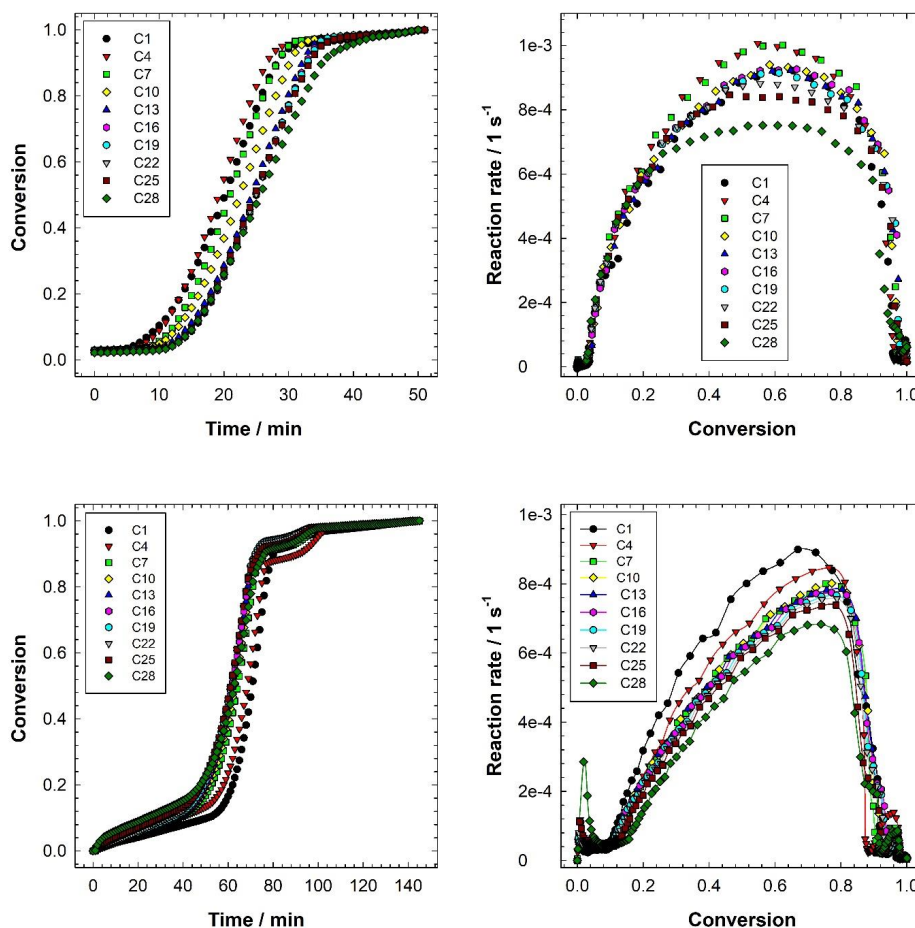


Figure 22. Methanolation (top) and demethanolation (bottom) reaction kinetics of the composite  $\text{CaCl}_2\text{-EV2}$ . The methanolation was carried out at a  $\text{CH}_3\text{OH}$  vapor pressure of 6.8 kPa under dynamic conditions. The initial temperature was set at 150 °C; the cooling rate was  $-1 \text{ K min}^{-1}$ . The demethanolation was performed from 25 °C to 150 °C with a heating rate of  $1 \text{ K min}^{-1}$  in flowing dry  $\text{N}_2$  gas.

Apparently, the methanolation and demethanolation reaction slowed down in the first ten cycles. Maximum methanolation reaction rates amounted to  $6.8 \times 10^{-4} \text{ s}^{-1}$  to  $1.0 \times 10^{-3} \text{ s}^{-1}$ , whereas slower maximum demethanolation reaction rates ( $6.5 \times 10^{-4} \text{ s}^{-1}$  to  $9.0 \times 10^{-4} \text{ s}^{-1}$ ) were measured. The overall high conversion rates are principally assignable to two factors. The sample mass was about 15% smaller when compared with the  $\text{CaCl}_2$  sample at the beginning of the methanolation reaction and thus a lower sample thickness facilitated the  $\text{CH}_3\text{OH}$  diffusion. The same applies to the demethanolation reaction in which the initial sample and consequently the amount of  $\text{CaCl}_2$  inside

the sample was 22% lower. According to the results, the reaction rate of the methanolation process was accelerated by 38% compared with single  $\text{CaCl}_2$ . Therefore, this vigorous enhancement is also ascribed to the formation of cracks and diffusion channels by thermal volume expansion and shrinkage during methanolation and demethanolation. Hence, the  $\text{CH}_3\text{OH}$  desorption from the reacted  $\text{CaCl}_2\text{-EV2}$  started at slightly lower temperatures. The moderate temperature shift of the methanolation reaction resulted from local variations in the  $\text{CH}_3\text{OH}$  partial pressure and thermodynamic equilibrium. From Figure 22, it is evident that the methanolation reaction rate declined gradually with increasing number of cycles, in particular in the last cycles.

Thermal analysis results disclosed that heat absorption and release remained constant over cyclic methanolation/demethanolation under dynamic conditions. The material intrinsic enthalpies of reaction per mole  $\text{CH}_3\text{OH}$  averaged to  $(-52 \pm 2) \text{ kJ mol}^{-1}$  for methanolation and  $(-53 \pm 1) \text{ kJ mol}^{-1}$  for demethanolation. Over the first eleven cycles fluctuations in the reaction enthalpy occurred. The molar enthalpies of methanolation and demethanolation were calculated to  $(-102 \pm 4) \text{ kJ mol}^{-1}$  and  $(-93 \pm 3) \text{ kJ mol}^{-1}$ , respectively. The material was examined with a microscopic camera after cycling. The images showed a highly porous calcareous sample indicating that the  $\text{CaCl}_2\text{-EV2}$  lost its structural integrity. Note that vermiculite tends to swelling under specific boundary conditions depending on the chemical composition [49].

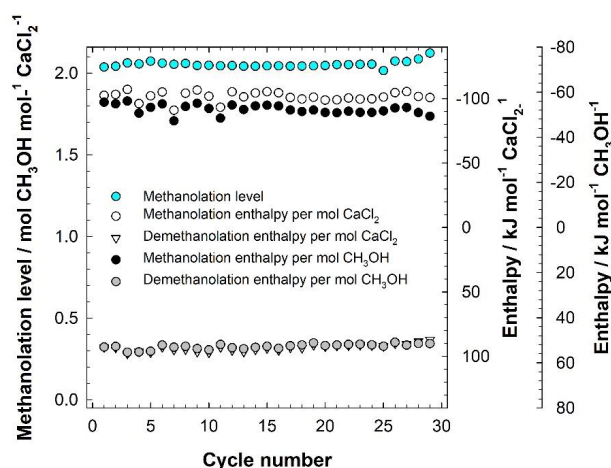


Figure 23. Molar enthalpy of methanolation and demethanolation for the composite material  $\text{CaCl}_2\text{-EV2}$  over thermal cycling in terms of the methanolation level.

### 3.4 Energy analysis of different $\text{CaCl}_2$ -based adsorbents and $\text{CH}_3\text{OH}$ as adsorbate

The assessment of the life-cycle performance of the chemical and composite adsorbents is indispensable for upscaling. Therefore, cyclic methanolation/demethanolation tests were conducted. The number of cycles varied from sixteen to twenty-nine. The chemical adsorbent



CaCl<sub>2</sub> and the composite adsorbents CaCl<sub>2</sub>-BC and CaCl<sub>2</sub>-EV2 exhibited good CH<sub>3</sub>OH adsorption abilities, as plotted in Figure 24. The CH<sub>3</sub>OH loading increased with increasing CaCl<sub>2</sub> content. The highest average CH<sub>3</sub>OH uptake ( $0.57 \pm 0.01$ ) g g<sup>-1</sup> was gained with single CaCl<sub>2</sub>, the lowest was yielded with CaCl<sub>2</sub>-EV2 ( $0.41 \pm 0.00$ ) g g<sup>-1</sup>, which possessed a CaCl<sub>2</sub> content of 69% (Table 8). For the specific enthalpies and energy storage densities of the working pairs CaCl<sub>2</sub>-CH<sub>3</sub>OH and CaCl<sub>2</sub>-BC-CH<sub>3</sub>OH, notable standard deviations were calculated. During the last methanolation runs a decelerated CH<sub>3</sub>OH diffusion, which was caused by an insufficient reactive gas flow, resulted in a shift in the baseline and underestimation of the heat of reaction by integration of the DSC peak area (Figure 24). The specific reaction enthalpies referred to the dry sample mass averaged ( $838 \pm 111$ ) kJ kg<sup>-1</sup> for pure CaCl<sub>2</sub>, ( $681 \pm 57$ ) kJ kg<sup>-1</sup> for CaCl<sub>2</sub>-BC, and ( $631 \pm 23$ ) kJ kg<sup>-1</sup> for CaCl<sub>2</sub>-EV2. The corresponding gravimetric energy densities of the methanolated adsorbents reached values between ( $540 \pm 74$ ) kJ kg<sup>-1</sup> and ( $455 \pm 17$ ) kJ kg<sup>-1</sup> (Table 8) and were much higher than that achieved with the working pairs CaCl<sub>2</sub>-C<sub>2</sub>H<sub>5</sub>OH, CaCl<sub>2</sub>-ZnCl<sub>2</sub>-C<sub>2</sub>H<sub>5</sub>OH, CaCl<sub>2</sub>-ZnCl<sub>2</sub>-C<sub>2</sub>H<sub>5</sub>OH, and CaCl<sub>2</sub>-ENG-C<sub>2</sub>H<sub>5</sub>OH (Table 7). Results show that CH<sub>3</sub>OH is a better working fluid than C<sub>2</sub>H<sub>5</sub>OH with respect to energy storage efficiency.

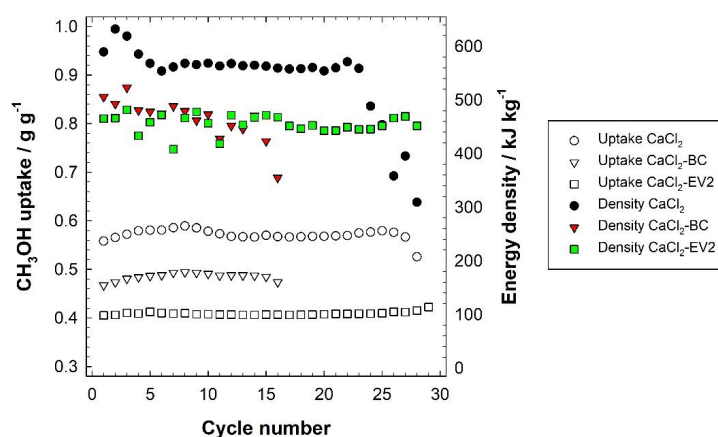


Figure 24. The energy storage density of the working pairs CaCl<sub>2</sub>-CH<sub>3</sub>OH, CaCl<sub>2</sub>-BC-CH<sub>3</sub>OH, and CaCl<sub>2</sub>-EV-CH<sub>3</sub>OH over multi-cyclic methanolation/demethanolation reactions. The sorbate uptake was normalized to the dry mass of the chemical and compound adsorbent tested.

For a hybrid adsorption heating and cooling system, the sufficient cooling power of the adsorbent material is also of pivotal importance. As shown in Figure 25, the cooling output was constant over cycling. The average specific cooling power decreased with a reduction in the CaCl<sub>2</sub> content in the following sequence: CaCl<sub>2</sub> ( $220 \pm 5$ ) W kg<sup>-1</sup>, CaCl<sub>2</sub>-BC ( $203 \pm 4$ ) W kg<sup>-1</sup>, and CaCl<sub>2</sub>-EV2 ( $153 \pm 3$ ) W kg<sup>-1</sup>. The greatest specific cooling power maximum of ( $443 \pm 33$ ) W kg<sup>-1</sup> for the composite CaCl<sub>2</sub>-EV2 was due to smaller sample mass and larger pore volume. A decline in the reaction rate resulted in a drop in the maximum specific cooling power for CaCl<sub>2</sub>-EV2. The other materials experienced also a decrease in the cooling power over cycling because of CH<sub>3</sub>OH

pressure losses inside the system. Regarding the coefficient of performance an inverse behavior was observed (Figure 25).

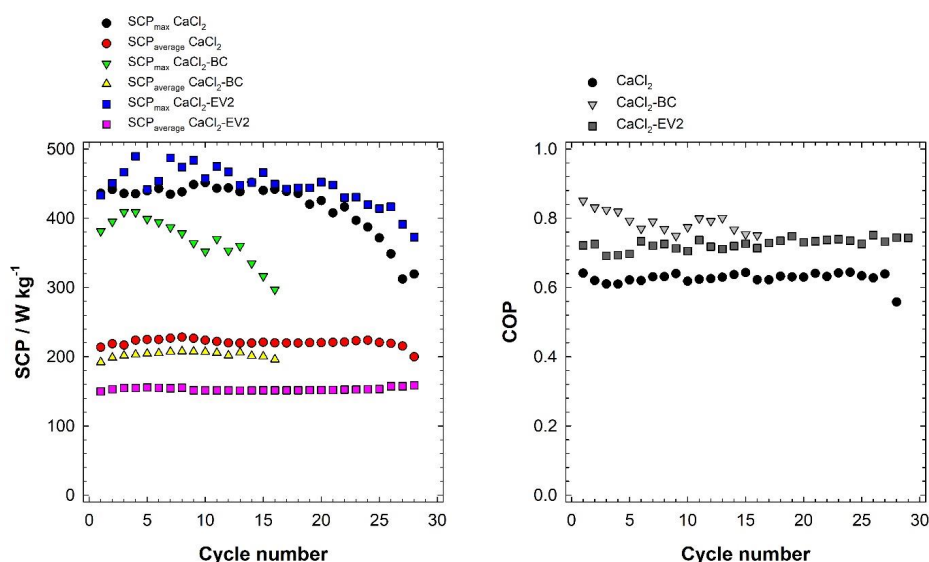


Figure 25. Adsorption cooling characteristics of pure  $\text{CaCl}_2$  and the composite materials  $\text{CaCl}_2\text{-BC}$  and  $\text{CaCl}_2\text{-EV2}$  versus the cycle number. The maximum specific cooling power (left) was obtained at the highest mass gain rate, whereas the average specific cooling power is associated to the total  $\text{CH}_3\text{OH}$  uptake. The reaction time varied from 40 min to 50 min.

The highest COP was attained with the adsorbent containing biochar, which was averaged to  $0.79 \pm 0.03$ , followed by  $\text{CaCl}_2\text{-EV2}$  with  $0.73 \pm 0.02$  (Table 8). This trend is attributed to differences in the demethanolation enthalpies. The demethanolation enthalpy decreased sequentially from  $\text{CaCl}_2$  to  $\text{CaCl}_2\text{-EV2}$  to  $\text{CaCl}_2\text{-BC}$ .

Table 8. Energy storage and cooling performance specifications of materials reacting with  $\text{CH}_3\text{OH}$  as sorbate. Measurements were carried out at a  $\text{CH}_3\text{OH}$  vapor pressures of 6.8 kPa, which corresponds to an evaporation temperature of 8.5 °C, at 25 °C. The materials were regenerated at a maximum desorption temperature of 150 °C. The SCP was averaged over the total  $\text{CH}_3\text{OH}$  uptake.

Material	Methanol uptake ( $\text{g g}^{-1}$ )	$\Delta_r h$ ( $\text{kJ kg}^{-1}$ )	E ( $\text{kJ kg}^{-1}$ )	$\text{SCP}_{\text{max}}$ ( $\text{W kg}^{-1}$ )	$\text{SCP}_{\text{average}}$ ( $\text{W kg}^{-1}$ )	COP (-)	Number of cycles
$\text{CaCl}_2$	$0.57 \pm 0.01$	$838 \pm 111$	$540 \pm 74$	$419 \pm 38$	$220 \pm 5$	$0.63 \pm 0.02$	28
$\text{CaCl}_2\text{-BC}$	$0.48 \pm 0.01$	$681 \pm 57$	$464 \pm 39$	$369 \pm 32$	$203 \pm 4$	$0.79 \pm 0.03$	16
$\text{CaCl}_2\text{-EV2}$	$0.41 \pm 0.00$	$631 \pm 23$	$455 \pm 17$	$443 \pm 33$	$153 \pm 3$	$0.73 \pm 0.02$	29

The incorporation of  $\text{CaCl}_2$  into porous and in particular carbonaceous host matrices aimed at improving thermal conductivity, permeability, and stability. Results suggest that expanded graphite and biochar had minimal effects on the overall adsorbent characteristics. During the

cycling test, structural changes, which were specifically noticed for single  $\text{CaCl}_2$  and  $\text{CaCl}_2\text{-EV2}$ , influenced the  $\text{CH}_3\text{OH}$  diffusion and thermal transfer of the materials studied. The observed limitations in mass and heat transfer could be reduced by optimizing the total  $\text{CaCl}_2$  content and applying alternative supports with hierarchical pore structures and defined shapes for example produced by extrusion that are not subjected to changes in geometry.

## 4 Conclusion

Dispersion of  $\text{CaCl}_2$  within the support matrices clinoptilolite, binder-free zeolite 13X, expanded graphite, biochar, and expanded vermiculite influenced  $\text{C}_2\text{H}_5\text{OH}$  and  $\text{CH}_3\text{OH}$  adsorption behavior as well as heat and cold storage performance. Thermal and kinetic properties strongly were dependent on nature and pore size of the support and total  $\text{CaCl}_2$  content of the composite adsorbent. Chemical adsorption was considered the primary adsorption process. Composite adsorbents with high  $\text{CaCl}_2$  loading exhibited good adsorption abilities and thermal efficiencies, but were prone to uncontrolled overstoichiometric adsorbate uptake and deliquescence under isothermal ethanolation and methanolation conditions. Heat and mass transfer constraints were anticipated to a small degree. The composite material  $\text{CaCl}_2\text{-Z13X}$  exhibited the best kinetic characteristics, but required charging temperatures higher than  $180\text{ }^\circ\text{C}$  to be completely regenerated. The uptake and release of  $\text{C}_2\text{H}_5\text{OH}$  by  $\text{CaCl}_2$ ,  $\text{CaCl}_2\text{-ZNC}$ , and  $\text{CaCl}_2\text{-ENG}$  proceeded in several non-integer steps and were associated with slow reaction kinetics under the conditions studied. Vermiculite supported  $\text{CaCl}_2$  showed an accelerated methanolation reaction which resulted in a narrow methanolation/demethanolation hysteresis and cyclically stable performance. Results imply that  $\text{CH}_3\text{OH}$  is a suitable adsorbate in combination with chemical and composite adsorbents for heating and cooling applications, owing to its sufficient kinetics and intrinsic energy. Variations in the conversion rates resulting from structural deterioration were observed over cycling, in particular for single  $\text{CaCl}_2$ ,  $\text{CaCl}_2\text{-ZNC}$ ,  $\text{CaCl}_2\text{-ENG}$ , and  $\text{CaCl}_2\text{-EV2}$ .

## Acknowledgements

This work was supported by the Federal Ministry for Economic Affairs and Energy and the Federal Ministry of Education and Research.

## References

- [1] Neupert U, Euting T, Kretschmer T, Notthoff C, Ruhlig K, Weimert B. *Energiespeicher: technische Grundlagen und energiewirtschaftliches Potenzial*. Stuttgart: Fraunhofer IRB Verlag; 2009.
- [2] Bundesministerium für Energie und Wirtschaft. *Energiedaten: Gesamtausgabe 2017*. <https://www.bmwi.de/Redaktion/DE/Artikel/Energie/energiedaten-gesamtausgabe.html> (accessed January 19, 2017).
- [3] Juhlich K. *Climate change 28/2016: CO2 emission factors for fossil fuels*. 2016.
- [4] Carling RW, Wondolowski AT, Macmillan DC. Enthalpy of formation of  $\text{CaCl}_2\cdot 2\text{CH}_3\text{OH}$  and  $\text{CaCl}_2\cdot 2\text{C}_2\text{H}_5\text{OH}$  by solution calorimetry. *J Chem Thermodyn* 1982;14:125–31.

- doi:10.1016/0021-9614(82)90024-6.
- [5] Iyimen-Schwarz Z, Lechner MD. Energiespeicherung durch chemische Reaktionen. I. DSC-Messungen zur quantitativen Verfolgung der Enthalpieänderungen von Speicherstoffen für die Hin- und Rückreaktion. *Thermochim Acta* 1983;68:349–61. doi:10.1016/0040-6031(83)80237-8.
- [6] Hirata Y, Fujioka K. Thermophysical properties and heat transfer characteristics of CaCl<sub>2</sub> heat pump reactor associated with structural change of reactive salts. V Minsk Int Semin “Heat Pipes, Heat Pumps, Refrig 2003;2:287–98.
- [7] Fujioka K, Kato S-I, Fujiki S, Hirata Y. Variations of molar volume and heat capacity of reactive solids of CaCl<sub>2</sub> used for chemical heat pumps. *J Chem Eng Japan* 1996;29:858–64. doi:10.1252/jcej.29.858.
- [8] Offenhartz PO, Brown FC, Mar RW, Carling RW. A heat pump and thermal storage system for solar heating and cooling based on the reaction of calcium chloride and methanol vapor. *J Sol Energy Eng* 1980;102:59–65.
- [9] Offenhartz PO. Solar heating and cooling with the CaCl<sub>2</sub>-CH<sub>3</sub>OH chemical heat pump. Proc. DOE Heat Pump Contract. Progr. Integr. Meet. June 2-4, 1981, Mc Lean, Virginia, USA: 1982, p. 75–8.
- [10] Linder M. Using thermochemical reactions in thermal energy storage systems. In: Cabeza LF, editor. *Adv. Therm. energy storage Syst. Methods Appl.* 1st ed., Woodhead Publishing; 2014, p. 357–74. doi:https://doi.org/10.1533/9781782420965.3.357.
- [11] Fujioka K, Hatanaka K, Hirata Y. Composite reactants of calcium chloride combined with functional carbon materials for chemical heat pumps. *Appl Therm Eng* 2008;28:304–10. doi:10.1016/j.applthermaleng.2006.02.032.
- [12] Gordeeva LG, Grekova A, Krieger TA, Aristov YI. Composites “binary salts in porous matrix” for adsorption heat transformation. *Appl Therm Eng* 2013;50:1633–8. doi:10.1016/j.applthermaleng.2011.07.040.
- [13] Gordeeva LG, Aristov YI. Composite sorbent of methanol “LiCl in mesoporous silica gel” for adsorption cooling: Dynamic optimization. *Energy* 2011;36:1273–9. doi:10.1016/j.energy.2010.11.016.
- [14] Gordeeva LG, Freni A, Restuccia G, Aristov YI. Influence of characteristics of methanol sorbents “salts in mesoporous silica” on the performance of adsorptive air conditioning cycle. *Ind Eng Chem Res* 2007;46:2747–52. doi:10.1021/ie060666n.
- [15] Gordeeva LG, Freni A, Krieger TA, Restuccia G, Aristov YI. Composites “lithium halides in silica gel pores”: Methanol sorption equilibrium. *Microporous Mesoporous Mater* 2008;112:254–61. doi:10.1016/j.micromeso.2007.09.040.
- [16] Maggio G, Gordeeva LG, Freni A, Aristov YI, Santori G, Polonara F, et al. Simulation of a solid sorption ice-maker based on the novel composite sorbent “lithium chloride in silica gel pores.” *Appl Therm Eng* 2009;29:1714–20. doi:10.1016/j.applthermaleng.2008.07.026.
- [17] Gong LX, Wang RZ, Xia ZZ, Lu ZS. Experimental study on an adsorption chiller employing lithium chloride in silica gel and methanol. *Int J Refrig* 2012;35:1950–7. doi:10.1016/j.ijrefrig.2012.06.013.
- [18] Lu ZS, Wang RZ. Study of the new composite adsorbent of salt LiCl/silica gel-methanol used in an innovative adsorption cooling machine driven by low temperature heat source. *Renew Energy* 2014;63:445–51. doi:10.1016/j.renene.2013.10.010.
- [19] Gordeeva LG, Grekova AD, Krieger TA, Aristov YI. Adsorption properties of composite materials (LiCl + LiBr)/silica. *Microporous Mesoporous Mater* 2009;126:262–7. doi:10.1016/j.micromeso.2009.06.015.

- [20] Grekova A, Gordeeva LG, Aristov YI. Composite sorbents “Li/Ca halogenides inside multi-wall carbon nano-tubes” for thermal energy storage. *Sol Energy Mater Sol Cells* 2016;155:176–83. doi:10.1016/j.solmat.2016.06.006.
- [21] Gordeeva LG, Aristov YI. Novel sorbents of ethanol “salt confined to porous matrix” for adsorptive cooling. *Energy* 2010;35:2703–8. doi:10.1016/j.energy.2009.04.001.
- [22] Gordeeva LG, Frazzica A, Sapienza A, Aristov YI, Freni A. Adsorption cooling utilizing the “LiBr/silica – ethanol” working pair: Dynamic optimization of the adsorber/heat exchanger unit. *Energy* 2014;75:390–9. doi:10.1016/j.energy.2014.07.088.
- [23] Brancato V, Frazzica A, Sapienza A, Gordeeva LG, Freni A. Ethanol adsorption onto carbonaceous and composite adsorbents for adsorptive cooling system. *Energy* 2015;84:177–85. doi:10.1016/j.energy.2015.02.077.
- [24] Grekova AD., Girkov IS., Nikulin V V., Tokarev MM, Gordeeva LG, Aristov YI. New composite sorbents of water and methanol “salt in anodic alumina”: Evaluation for adsorption heat transformation. *Energy* 2016;106:231–9. doi:10.1016/j.energy.2016.03.050.
- [25] Aristov YI, Gordeeva LG, Pankratiev YD, Plyasova LM, Bikova I V., Freni A, et al. Sorption equilibrium of methanol on new composite sorbents “CaCl<sub>2</sub>/silica gel.” *Adsorption* 2007;13:121–7. doi:10.1007/s10450-007-9012-x.
- [26] Gordeeva LG, Freni A, Aristov YI, Restuccia G. Composite sorbent of methanol “lithium chloride in mesoporous silica gel” for adsorption cooling machines: Performance and stability evaluation. *Ind Eng Chem Res* 2009;48:6197–202. doi:10.1021/ie8016303.
- [27] Patnaik P. *Handbook of inorganic chemicals*. vol. 529. McGraw-Hill New York; 2003.
- [28] Lowell S, Shields JE, Thomas MA, Thommes M. *Characterization of porous solids and powders: Surface area, pore size and density*. Springer Netherlands; 2004.
- [29] Kleiber M, Joh R, Span R. VDI heat atlas. In: VDI-Gesellschaft Verfahrenstechnik und Chemieingenieurwesen., editor. VDI heat atlas. 2nd ed., Berlin, Heidelberg: Springer; 2010, p. 301–418.
- [30] Wongsuwan W, Kumar S, Neveu P, Meunier F. A review of chemical heat pump technology and applications. *Appl Therm Eng* 2001;21:1489–519. doi:https://doi.org/10.1016/S1359-4311(01)00022-9.
- [31] Cacciola G, Giordano N. Chemical processes for energy storage and transmission. *Appl Energy* 1986;25:315–37. doi:https://doi.org/10.1016/0306-2619(86)90032-2.
- [32] Mar RW, Carling RW. The calcium chloride—ethanol system. *Thermochim Acta* 1981;45:213–7. doi:https://doi.org/10.1016/0040-6031(81)80147-5.
- [33] Iyimen-Schwarz Z. *Energiespeicherung durch chemische Reaktionen*. Universität Osnabrück, 1984.
- [34] Becker R, Hartwig H, Köppe H, Vanecek H, Velić P, Warncke R, et al. *Gmelin Handbuch der Anorganischen Chemie*. Berlin, Heidelberg: Springer; 1978. doi:10.1007/978-3-662-06224-1.
- [35] Korhammer K, Apel C, Osterland T, Ruck WKL. Reaction of calcium chloride and magnesium chloride and their mixed salts with ethanol for thermal energy storage. *Energy Procedia*, vol. 91, 2016, p. 161–71. doi:10.1016/j.egypro.2016.06.194.
- [36] Korhammer K, Mihály J, Bálint S, Trif L, Vass Á, Tompos A, et al. Reversible formation of alcohol solvates and their potential use for heat storage. *Submitt to J Therm Anal Calorim* 2018.
- [37] Knowlton GD, White TR, Mckague HL. Thermal study of types of water associated with clinoptilolite. *Clays Clay Miner* 1981;29:403–11. doi:10.1346/CCMN.1981.0290510.
- [38] Dunne SR. *Industrial Gas Phase Adsorptive Separations*. In: Kulprathipanja S, editor.

- Zeolites Ind. Sep. Catal., Wiley-Blackwell; 2010, p. 273–305. doi:10.1002/9783527629565.ch9.
- [39] Jänchen J, Schumann K, Thrun E, Brandt A, Unger B, Hellwig U. Preparation, hydrothermal stability and thermal adsorption storage properties of binderless zeolite beads. *Int J Low-Carbon Technol* 2012;7:275–9. doi:10.1093/ijlct/cts037.
- [40] Jänchen J, Ackermann D, Weiler E, Stach H, Brösicke W. Calorimetric investigation on zeolites,  $\text{AlPO}_4$ 's and  $\text{CaCl}_2$  impregnated attapulgite for thermochemical storage of heat. *Thermochim Acta* 2005;434:37–41. doi:10.1016/j.tca.2005.01.009.
- [41] Jänchen J, Ackermann D, Stach H, Brösicke W. Studies of the water adsorption on zeolites and modified mesoporous materials for seasonal storage of solar heat. *Sol Energy* 2004;76:339–44. doi:10.1016/j.solener.2003.07.036.
- [42] Jänchen J, Stach H. Adsorption properties of porous materials for solar thermal energy storage and heat pump applications. *Energy Procedia* 2012;30:289–93. doi:10.1016/j.egypro.2012.11.034.
- [43] Alexopoulos K, Lee MS, Liu Y, Zhi Y, Liu Y, Reyniers MF, et al. Anharmonicity and confinement in zeolites: Structure, spectroscopy, and adsorption free energy of ethanol in H-ZSM-5. *J Phys Chem C* 2016;120:7172–82. doi:10.1021/acs.jpcc.6b00923.
- [44] Piccini GM, Alessio M, Sauer J. Ab initio study of methanol and ethanol adsorption on Brønsted sites in zeolite H-MFI. *Phys Chem Chem Phys* 2018. doi:10.1039/C8CP03632B.
- [45] Tian B, Jin ZQ, Wang LW, Wang RZ. Permeability and thermal conductivity of compact chemical and physical adsorbents with expanded natural graphite as host matrix. *Int J Heat Mass Transf* 2012;55:4453–9. doi:https://doi.org/10.1016/j.ijheatmasstransfer.2012.04.016.
- [46] Galwey AK, Brown ME. Thermal decomposition of ionic solids. 1st ed. Elsevier Science; 1999.
- [47] Herzog TH, Jänchen J. Adsorption properties of modified zeolites for operating range enhancement of adsorption heat pumps through the use of organic adsorptive agents. *Energy Procedia* 2016;91:155–60. doi:10.1016/j.egypro.2016.06.192.
- [48] Cui Q, Tao G, Chen H, Guo X, Yao H. Environmentally benign working pairs for adsorption refrigeration. *Energy* 2005;30:261–71. doi:10.1016/j.energy.2004.05.005.
- [49] Blume H-P, Brümmer GW, Horn R, Kandeler E, Kögel-Knabner I, Kretzschmar R, et al. Scheffer/Schachtschabel: Lehrbuch der Bodenkunde. 16th ed. Berlin, Heidelberg: Springer-Verlag; 2010. doi:10.1007/978-3-662-49960-3.



# A. Final energy consumption statistics

Figure A.1 shows the final energy consumption of major energy-end-use sectors subdivided into several applications. According to Federal Ministry of Economic Affairs and Energy statistics, heat energy accounted for 89.0% of the domestic sector final energy consumption in 2015. Room heating and hot water production dominated with 68.6% and 14.4%, respectively [4]. In the industrial sector, the consumption of heat energy amounted to 73.0%. In contrary, the level of energy consumed by air conditioning systems and utilized on process cooling was relatively low.

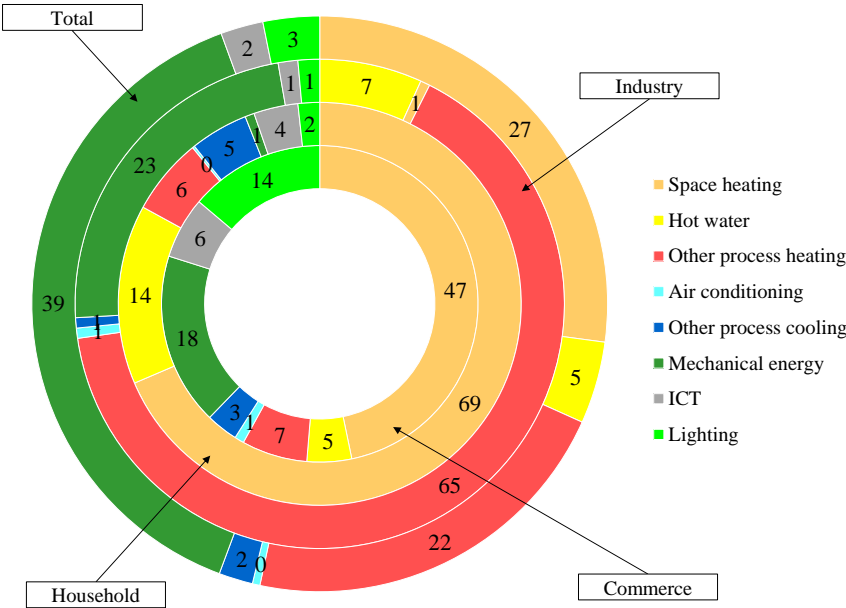


Figure A.1.: Percentage energy consumption by final user and application for domestic, industrial and commercial sectors in Germany in 2015. Data extracted from [4].





## **B. Selective literature review on composite materials**

Table B.1.: Representative overview of literature data on the working pair composite adsorbent-ethanol as TCMs for low grade heating and cooling applications.

Author	Year	Reference	Study type	Scale	Application	System type	Salt	Host matrix	Pore size	Synthesis method
Gordeeva & Aristov	2010	[194]	Experimental	Grain	Ice-making, air conditioning		LiBr	Carbon Sibunit	Mesopore	Dry impregnation
Gordeeva & Aristov	2010	[194]	Experimental	Grain	Ice-making, air conditioning		LiCl	Activated carbon fiber	Mesopore	Dry impregnation
Gordeeva & Aristov	2010	[194]	Experimental	Grain	Ice-making, air conditioning		SrCl <sub>2</sub>	Alumina	Mesopore	Dry impregnation
Gordeeva et al.	2014	[195]	Experimental	Laboratory	Cooling		LiBr	Silica gel KSK	Mesopore	Dry impregnation
Brancato et al.	2015	[196]	Experimental	Grain	Cooling, air conditioning		LiBr	Silica gel KSK	Mesopore	Dry impregnation
Gordeeva & Aristov	2010	[194]	Experimental	Grain	Ice-making, air conditioning		CaBr <sub>2</sub>	Silica gel	Mesopore	Dry impregnation
Gordeeva & Aristov	2010	[194]	Experimental	Grain	Ice-making, air conditioning		CaCl <sub>2</sub>	Silica gel	Mesopore	Dry impregnation
Gordeeva & Aristov	2010	[194]	Experimental	Grain	Ice-making, air conditioning		Ca(NO <sub>3</sub> ) <sub>2</sub>	Silica gel	Mesopore	Dry impregnation
Gordeeva & Aristov	2010	[194]	Experimental	Grain	Ice-making, air conditioning		CuSO <sub>4</sub>	Silica gel	Mesopore	Dry impregnation
Gordeeva & Aristov	2010	[194]	Experimental	Grain	Ice-making, air conditioning		LiBr	Silica gel	Mesopore	Dry impregnation
Gordeeva & Aristov	2010	[194]	Experimental	Grain	Ice-making, air conditioning		LiCl	Silica gel	Mesopore	Dry impregnation
Gordeeva & Aristov	2010	[194]	Experimental	Grain	Ice-making, air conditioning		Mg(NO <sub>3</sub> ) <sub>2</sub>	Silica gel	Mesopore	Dry impregnation
Gordeeva & Aristov	2010	[194]	Experimental	Grain	Ice-making, air conditioning		MgSO <sub>4</sub>	Silica gel	Mesopore	Dry impregnation
Gordeeva & Aristov	2010	[194]	Experimental	Grain	Ice-making, air conditioning		NiBr <sub>2</sub>	Silica gel	Mesopore	Dry impregnation

Table B.2.: Representative overview of literature data on the working pair composite adsorbent-methanol as TCMs for low grade heating and cooling applications.

Author	Year	Reference	Study type	Scale	Application	System type	Salt	Host matrix	Pore size	Synthesis method
Fujioka et al.	2008	[130]	Experimental	Grain	Cooling, air conditioning		CaCl <sub>2</sub>	Activated carbon fiber		Wet impregnation
Grekova et al.	2016	[191]	Experimental	Grain	Heat storage		LiBr	Carbon nanotube	Mesopore	Wet impregnation
Grekova et al.	2016	[191]	Experimental	Grain	Heat storage		LiCl	Carbon nanotube	Mesopore	Wet impregnation
Fujioka et al.	2008	[130]	Experimental	Grain	Cooling, air conditioning		CaCl <sub>2</sub>	Expanded graphite		Wet impregnation
Grekova et al.	2016	[197]	Experimental	Grain	Heat transformation		LiCl	Anodic alumina	Mesopore	Vacuum impregnation
Aristov et al.	2007	[198]	Experimental	Grain	Heat storage, cooling		CaCl <sub>2</sub>	Silica gel KSK	Mesopore	Impregnation
Gordeeva et al.	2009	[199]	Experimental	Grain / Lab	Cooling		LiCl	Silica gel KSK	Mesopore	Dry impregnation
Gordeeva et al.	2011	[200]	Experimental	Laboratory	Cooling		LiCl	Silica gel KSK	Mesopore	Dry impregnation
Gordeeva et al.	2007	[201]	Experimental	Grain	Cooling		BaCl <sub>2</sub>	Silica gel	Mesopore	Impregnation
Gordeeva et al.	2007	[201]	Experimental	Grain	Cooling		CaBr <sub>2</sub>	Silica gel	Mesopore	Impregnation
Gordeeva et al.	2007	[201]	Experimental	Grain	Cooling		CaCl <sub>2</sub>	Silica gel	Micropore	Impregnation
Gordeeva et al.	2007	[201]	Experimental	Grain	Cooling		CaCl <sub>2</sub>	Silica gel	Mesopore	Impregnation
Aristov et al.	2007	[198]	Experimental	Grain	Heat storage, cooling		CaCl <sub>2</sub>	Silica gel	Mesopore	Impregnation
Gordeeva et al.	2013	[162]	Experimental	Grain	Cooling, air conditioning		CaCl <sub>2</sub> -CaBr <sub>2</sub>	Silica gel	Mesopore	Impregnation
Gordeeva et al.	2007	[201]	Experimental	Grain	Cooling		Ca(NO <sub>3</sub> ) <sub>2</sub>	Silica gel	Mesopore	Impregnation
Gordeeva et al.	2007	[201]	Experimental	Grain	Cooling		CoCl <sub>2</sub>	Silica gel	Mesopore	Impregnation
Gordeeva et al.	2007	[201]	Experimental	Grain	Cooling		CuCl <sub>2</sub>	Silica gel	Mesopore	Impregnation
Gordeeva et al.	2007	[201]	Experimental	Grain	Cooling		LiBr	Silica gel	Mesopore	Impregnation
Gordeeva et al.	2008	[202]	Experimental	Grain	Cooling		LiBr	Silica gel	Mesopore	Impregnation
Gordeeva et al.	2007	[201]	Experimental	Grain	Cooling		LiCl	Silica gel	Micropore	Impregnation
Gordeeva et al.	2007	[201]	Experimental	Grain	Cooling		LiCl	Silica gel	Mesopore	Impregnation
Gordeeva et al.	2008	[202]	Experimental	Grain	Cooling		LiCl	Silica gel	Mesopore	Impregnation
Maggio	2009	[203]	Numerical	Laboratory	Ice-making		LiCl	Silica gel	Mesopore	Impregnation
Gong et al.	2012	[204]	Experimental	Laboratory	Cooling	Closed	LiCl	Silica gel	Mesopore	Impregnation
Lu et al.	2014	[205]	Experimental	Laboratory	Cooling	Closed	LiCl	Silica gel	Mesopore	Dry impregnation
Gordeeva et al.	2009	[165]	Experimental	Grain	Heat storage, cooling		LiCl-LiBr	Silica gel	Mesopore	Dry impregnation
Gordeeva et al.	2007	[201]	Experimental	Grain	Cooling		MgBr <sub>2</sub>	Silica gel	Mesopore	Impregnation
Gordeeva et al.	2007	[201]	Experimental	Grain	Cooling		MgCl <sub>2</sub>	Silica gel	Mesopore	Impregnation
Gordeeva et al.	2007	[201]	Experimental	Grain	Cooling		MnCl <sub>2</sub>	Silica gel	Mesopore	Impregnation
Gordeeva et al.	2007	[201]	Experimental	Grain	Cooling		NiBr <sub>2</sub>	Silica gel	Mesopore	Impregnation
Gordeeva et al.	2013	[162]	Experimental	Grain	Cooling, air conditioning		LiCl-LiBr	Expanded vermiculite	Macropore	Impregnation

Table B.3.: Representative overview of literature data on the working pair composite adsorbent-water as TCMs for low grade heating and cooling applications.

Author	Year	Reference	Study type	Scale	Application	System type	Salt	Host matrix	Pore size	Synthesis method
Zondag et al.	2010	[234]	Experimental	Laboratory	Heat storage, heating	Open	MgCl <sub>2</sub>	Cellulose		Impregnation
de Boer et al.	2004	[235]	Experimental	Prototype	Heating, cooling	Closed	Na <sub>2</sub> S	Cellulose		Impregnation
Aristov et al.	2000	[138]	Experimental	Grain	Heat storage		CaCl <sub>2</sub>	Carbon Sibunit		Impregnation
Linnow et al.	2014	[236]	Experimental	Grain	Heat storage		MgSO <sub>4</sub>	Carbon	Mesopore	Wet impregnation
Casey et al.	2014	[71]	Experimental	Grain	Heat storage	Open	CaCl <sub>2</sub>	Activated carbon	Micropore	Dry impregnation
Casey et al.	2015	[152]	Experimental	Laboratory	Heat storage	Open	CaCl <sub>2</sub>	Activated carbon	Micropore	Dry impregnation
Liu et al.	2004	[135]	Experimental	Grain	Heat storage		CaCl <sub>2</sub>	Activated carbon	Micropore	Wet impregnation
Okada et al.	2010	[186]	Experimental		Air conditioning		CaCl <sub>2</sub>	Activated carbon		Dry impregnation
Posern & Osburg	2017	[187]	Experimental	Laboratory	Heat storage	Open	MgSO <sub>4</sub>	Activated carbon		Wet impregnation
Posern & Osburg	2017	[187]	Experimental	Laboratory	Heat storage	Open	SrBr <sub>2</sub>	Activated carbon		Wet impregnation
Wang et al.	2016	[158]	Experimental	Grain	Air-to water system		CaCl <sub>2</sub>	Activated carbon fiber	Micropore	Wet impregnation
Ye et al.	2014	[188]	Experimental	Grain	Cooling	Closed	CaCl <sub>2</sub>	Activated carbon fiber	Micro-macro	Wet impregnation
Tso & Chao	2012	[189]	Experimental	Grain	Cooling		CaCl <sub>2</sub>	Activated carbon-silica	Micropore	Wet impregnation
Grekova et al.	2016	[191]	Experimental	Grain	Heat storage		CaCl <sub>2</sub>	Carbon nanotube	Mesopore	Wet impregnation
Grekova et al.	2016	[191]	Experimental	Grain	Heat storage		LiCl	Carbon nanotube	Mesopore	Wet impregnation
Zhang et al.	2015	[192]	Experimental	Grain	Heat storage		CaCl <sub>2</sub>	Carbon nanotube	Micropore	Mixing
Fujioka & Suzuki	2013	[190]	Experimental	Grain	Heat pump		CaCl <sub>2</sub>	Expanded graphite		Wet impregnation
Mauran et al.	2008	[85]	Experimental	Prototype	Heating, cooling	Closed	SrBr <sub>2</sub>	Expanded graphite		Impregnation
Kumita et al.	2013	[237]	Experimental	Grain	Heat pump		CaCl <sub>2</sub>	Anodized aluminum	Mesopore	Wet impregnation
Suwa et al.	2014	[238]	Experimental	Grain	Cooling		CaCl <sub>2</sub>	Anodized aluminum	Meso-macro	Wet impregnation
Aristov et al.	2000	[138]	Experimental	Grain	Heat storage		CaCl <sub>2</sub>	Alumina		Impregnation
Davoud & Aristov	2003	[141]	Experimental	Grain	Heat pump, cooling		CaCl <sub>2</sub>	Alumina	Mesopore	Impregnation
Tanashev et al.	2013	[131]	Experimental	Grain	Heat transformation		CaCl <sub>2</sub>	Alumina	Mesopore	Impregnation
Grekova et al.	2016	[197]	Experimental	Grain	Heat transformation		CaCl <sub>2</sub>	Anodic alumina	Mesopore	Vacuum impregnation
Jabbari-Hichri et al.	2014	[239]	Experimental	Grain	Heat storage		CaCl <sub>2</sub>	Silica-alumina	Mesopore	Dry impregnation
Linnow et al.	2014	[236]	Experimental	Grain	Heat storage		MgSO <sub>4</sub>	Glass	Mesopore	Wet impregnation
Posern & Kaps	2009	[206]	Experimental	Grain	Heat storage		MgSO <sub>4</sub>	Glass		Impregnation
Posern & Kaps	2009	[206]	Experimental	Grain	Heat storage		MgSO <sub>4</sub> -CaCl <sub>2</sub>	Glass		Impregnation
Posern & Kaps	2009	[206]	Experimental	Grain	Heat storage		MgSO <sub>4</sub> -LiCl	Glass		Impregnation
Liu et al.	2004	[135]	Experimental	Grain	Heat storage		CaCl <sub>2</sub>	Silica gel FSM16	Mesopore	Wet impregnation
Zhang & Qui	2007	[136]	Experimental	Grain	Cooling		CaCl <sub>2</sub>	Silica gel MSG	Macropore	Dry impregnation
Aristov et al.	1996	[133]	Experimental	Grain	Heat storage		CaCl <sub>2</sub>	Silica gel KSK	Mesopore	Dry impregnation
Aristov et al.	2002	[137]	Experimental	Grain	Heat storage		CaCl <sub>2</sub>	Silica gel KSK	Mesopore	Dry impregnation
Aristov et al.	2000	[138]	Experimental	Grain	Heat storage		CaCl <sub>2</sub>	Silica gel KSK	Mesopore	Dry impregnation
Aristov et al.	2006	[139]	Experimental	Grain	Heat storage		CaCl <sub>2</sub>	Silica gel KSK	Mesopore	Dry impregnation
Aristov et al.	2006	[140]	Experimental	Grain	Heat storage		CaCl <sub>2</sub>	Silica gel KSK	Mesopore	Dry impregnation
Davoud & Aristov	2003	[141]	Experimental	Grain	Heat pump, cooling		CaCl <sub>2</sub>	Silica gel KSK	Mesopore	Dry impregnation
Okunev et al.	2008	[142]	Numerical	Laboratory	Cooling		CaCl <sub>2</sub>	Silica gel KSK	Mesopore	Dry impregnation
Freni et al.	2007	[143]	Experimental	Laboratory	Cooling		CaCl <sub>2</sub>	Silica gel KSK	Mesopore	Dry impregnation
Restuccia et al.	2004	[144]	Exp-num	Laboratory	Cooling		CaCl <sub>2</sub>	Silica gel KSK	Mesopore	Dry impregnation
Tanashev et al.	2013	[131]	Experimental	Grain	Heat transformation		CaCl <sub>2</sub>	Silica gel KSK	Mesopore	Dry impregnation
Tokarev & Airstov	1997	[145]	Experimental	Grain	Heat storage		CaCl <sub>2</sub>	Silica gel KSK	Mesopore	Dry impregnation
Levitskij et al.	1996	[146]	Experimental	Grain	Cooling, air conditioning	Open	CaCl <sub>2</sub>	Silica gel KSK	Mesopore	Wet impregnation
Tanasehev & Aristov	2000	[147]	Experimental	Grain	Heat pump, cooling		CaCl <sub>2</sub>	Silica gel KSK	Mesopore	Impregnation
Gordeeva et al.	2006	[148]	Experimental	Grain	Heat pump, air conditioning		CaCl <sub>2</sub>	Silica gel KSK	Mesopore	Dry impregnation
Gordeeva et al.	2006	[148]	Experimental	Grain	Heat pump, air conditioning		CuSO <sub>4</sub>	Silica gel KSK	Mesopore	Dry impregnation
Gordeeva et al.	1998	[149]	Experimental	Grain	Cooling, air conditioning		LiBr	Silica gel KSK	Mesopore	Dry impregnation

Table B.3.: Summary and analysis of literature data on the working pair composite adsorbent-water as TCMs for low-grade thermal energy storage applications.

(continued)

Author	Year	Reference	Study type	Scale	Application	System type	Salt	Host matrix	Pore size	Synthesis method
Aristov et al.	2000	[138]	Experimental	Grain	Heat storage		LiBr	Silica gel KSK	Mesopore	Impregnation
Aristov et al.	2002	[137]	Experimental	Grain	Heat storage		LiBr	Silica gel KSK	Mesopore	Dry impregnation
Tanashev et al.	2013	[131]	Experimental	Grain	Heat transformation		LiBr	Silica gel KSK	Mesopore	Impregnation
Aristov et al.	2012	[150]	Experimental	Laboratory	Cooling		LiNO <sub>3</sub>	Silica gel KSK	Mesopore	Dry impregnation
Aristov et al.	2000	[138]	Experimental	Grain	Heat storage		MgCl <sub>2</sub>	Silica gel KSK	Mesopore	Impregnation
Tanashev et al.	2013	[131]	Experimental	Grain	Heat transformation		MgCl <sub>2</sub>	Silica gel KSK	Mesopore	Impregnation
Gordeeva et al.	2006	[148]	Experimental	Grain	Heat pump, air conditioning		MgSO <sub>4</sub>	Silica gel KSK	Mesopore	Dry impregnation
Gordeeva et al.	2006	[148]	Experimental	Grain	Heat pump, air conditioning		Na <sub>2</sub> SO <sub>4</sub>	Silica gel KSK	Mesopore	Dry impregnation
Aristov et al.	1996	[134]	Experimental	Grain	Heat storage		CaCl <sub>2</sub>	Silica gel KSM	Micropore	Dry impregnation
Aristov et al.	2000	[138]	Experimental	Grain	Heat storage		CaCl <sub>2</sub>	Silica gel KSM	Micropore	Dry impregnation
Aristov et al.	2002	[137]	Experimental	Grain	Heat storage		CaCl <sub>2</sub>	Silica gel KSM	Micropore	Dry impregnation
Tokarev & Airstov	1997	[145]	Experimental	Grain	Heat storage		CaCl <sub>2</sub>	Silica gel KSM	Micropore	Dry impregnation
Aristov et al.	2000	[138]	Experimental	Grain	Heat storage		LiBr	Silica gel KSM	Micropore	Impregnation
Ponomarenko et al.	2010	[151]	Experimental	Grain	Heat storage		CaCl <sub>2</sub>	Silica gel SBA-15	Mesopore	Wet impregnation
Casey et al.	2014	[71]	Experimental	Grain	Heat storage	Open	CaCl <sub>2</sub>	Silica gel	Micropore	Dry impregnation
Casey et al.	2015	[152]	Experimental	Laboratory	Heat storage	Open	CaCl <sub>2</sub>	Silica gel	Micropore	Dry impregnation
Cortes et al.	2012	[153]	Experimental	Grain	Cooling, air conditioning		CaCl <sub>2</sub>	Silica gel	Mesopore	Dry impregnation
Daou et al.	2006	[154]	Exp-num	Grain	Cooling, air conditioning		CaCl <sub>2</sub>	Silica gel	Micropore	Wet impregnation
Daou et al.	2007	[155]	Experimental	Laboratory	Cooling		CaCl <sub>2</sub>	Silica gel	Micropore	Wet impregnation
Liu & Wang	2003	[156]	Experimental	Grain	Heating, cooling		CaCl <sub>2</sub>	Silica gel	Macropore	Wet impregnation
Ristić et al.	2011	[157]	Experimental	Grain	Heat storage		CaCl <sub>2</sub>	Silica gel	Mesopore	Wet impregnation
Wang et al.	2016	[158]	Experimental	Grain	Air-to water system		CaCl <sub>2</sub>	Silica gel	Mesopore	Wet impregnation
Wu et al.	2007	[159]	Experimental	Grain / lab	Heat storage	Open	CaCl <sub>2</sub>	Silica gel	Mesopore	Wet impregnation
Wu et al.	2009	[160]	Numerical	Laboratory	Heat storage	Open	CaCl <sub>2</sub>	Silica gel	Mesopore	Wet impregnation
Zhu et al.	2006	[161]	Experimental	Grain / lab	Heat storage	Open	CaCl <sub>2</sub>	Silica gel	Mesopore	Wet impregnation
Gordeeva et al.	2013	[162]	Experimental	Grain	Cooling, air conditioning		CaCl <sub>2</sub> -CaBr <sub>2</sub>	Silica gel	Mesopore	Impregnation
Cortes et al.	2012	[153]	Experimental	Grain	Cooling, air conditioning		LiBr	Silica gel		Dry impregnation
Gong et al.	2010	[163]	Experimental	Grain	Cooling	Closed	LiCl	Silica gel	Mesopore	Impregnation
Gong et al.	2011	[164]	Experimental	Laboratory	Cooling	Closed	LiCl	Silica gel	Mesopore	Impregnation
Gordeeva et al.	2009	[165]	Experimental	Grain	Heat storage, cooling		LiCl-LiBr	Silica gel	Mesopore	Dry impregnation
Cortes et al.	2012	[153]	Experimental	Grain	Cooling, air conditioning		MgCl <sub>2</sub>	Silica gel	Mesopore	Dry impregnation
Jarimi et al.	2017	[166]	Experimental	Grain	Heat storage	Open	KCOOH	Silica gel		Impregnation
Mrowiec-Bialoń et al.	1997	[167]	Experimental	Grain	Heat storage / transformation		CaCl <sub>2</sub>	Silica xerogel	Mesopore	Sol-gel method
Mrowiec-Bialoń et al.	1999	[168]	Experimental	Grain	Heat storage / transformation		LiBr	Silica aerogel	Mesopore	Sol-gel method
Aristov et al.	2000	[138]	Experimental	Grain	Heat storage		CaCl <sub>2</sub>	Aerogel		Impregnation
Aristov et al.	2000	[138]	Experimental	Grain	Heat storage		LiBr	Aerogel		Impregnation
Jänchen et al.	2004	[18]	Experimental	Grain	Heat storage, heating	Closed	CaCl <sub>2</sub>	Aluminosilicate	Mesopore	Impregnation
Jänchen et al.	2004	[18]	Experimental	Laboratory	Heat storage, heating	Closed	CaCl <sub>2</sub>	Aluminosilicate	Mesopore	Impregnation
Ristić et al.	2012	[183]	Experimental	Grain	Heat storage		CaCl <sub>2</sub>	Iron silicate FeKIL2	Mesopore	Wet impregnation
Ristić & Henninger	2014	[184]	Experimental	Grain	Heat storage		CaCl <sub>2</sub>	Disordered iron silicate	Mesopore	Wet impregnation
Ristić & Henninger	2014	[184]	Experimental	Grain	Dehumidification		CaCl <sub>2</sub>	Ordered silicate	Mesopore	Wet impregnation
Tokarev et al.	2002	[185]	Experimental	Grain	Heating, Cooling		CaCl <sub>2</sub>	MCM-41	Mesopore	Dry impregnation
Liu et al.	2013	[169]	Experimental	Grain	Heat storage	Open	CaCl <sub>2</sub>	Wakkanai siliceous shale	Mesopore	Wet impregnation
Liu et al.	2015	[170]	Experimental	Grain	Heat storage	Open	CaCl <sub>2</sub>	Wakkanai siliceous shale	Mesopore	Wet impregnation
Liu et al.	2015	[170]	Experimental	Grain	Heat storage	Open	LiCl	Wakkanai siliceous shale	Mesopore	Wet impregnation
Mette	2014	[171]	Exp-num	Grain / lab	Heat storage, heating	Open	CaCl <sub>2</sub>	Clay	Micro-macro	Wet impregnation
Mette	2014	[171]	Exp-num	Grain / lab	Heat storage, heating	Open	MgSO <sub>4</sub>	Clay	Micro-macro	Wet impregnation
Jänchen et al.	2005	[31]	Experimental	Grain	Heat storage		CaCl <sub>2</sub>	Attapulgit	Mesopore	Impregnation

(continued)

Table B.3.: Summary and analysis of literature data on the working pair composite adsorbent-water as TCMs for low-grade thermal energy storage applications.

Author	Year	Reference	Study type	Scale	Application	System type	Salt	Host matrix	Pore size	Synthesis method
Lass-Seyoum et al.	2012	[172]	Experimental	Laboratory	Heat storage	Closed	CaCl <sub>2</sub>	Attapulgite		
Posern & Kaps	2010	[173]	Experimental	Grain	Heat storage		MgSO <sub>4</sub>	Attapulgite	Micropore	Impregnation
Posern & Kaps	2010	[173]	Experimental	Grain	Heat storage		MgSO <sub>4</sub> -MgCl <sub>2</sub>	Attapulgite	Micropore	Impregnation
Lass-Seyoum et al.	2012	[172]	Experimental	Laboratory	Heat storage	Closed	CaCl <sub>2</sub>	Poolkohl		
Tretiak & Abdallah	2009	[174]	Experimental	Laboratory	Cooling		CaCl <sub>2</sub>	Kaolin clay-vermiculite		Wet impregnation
Aristov et al.	2000	[175]	Experimental	Grain	Heat storage		CaCl <sub>2</sub>	Expanded vermiculite	Meso-macro	Impregnation
Casey et al.	2014	[71]	Experimental	Grain	Heat storage	Open	CaCl <sub>2</sub>	Vermiculite	Macropore	Dry impregnation
Casey et al.	2015	[152]	Experimental	Laboratory	Heat storage	Open	CaCl <sub>2</sub>	Vermiculite	Macropore	Dry impregnation
Casey et al.	2017	[176]	Experimental	Laboratory	Heat storage	Open	CaCl <sub>2</sub>	Vermiculite	Macropore	Dry impregnation
Jarimi et al.	2017	[166]	Experimental	Grain	Heat storage	Open	CaCl <sub>2</sub>	Vermiculite	Macropore	Impregnation
Jarimi et al.	2017	[166]	Experimental	Grain	Heat storage	Open	CaCl <sub>2</sub> -LiCl	Vermiculite	Macropore	Impregnation
Casey et al.	2017	[176]	Experimental	Laboratory	Heat storage	Open	CaCl <sub>2</sub> -LiNO <sub>3</sub>	Vermiculite	Macropore	Dry impregnation
Casey et al.	2014	[71]	Experimental	Grain	Heat storage	Open	Ca(NO <sub>3</sub> ) <sub>2</sub>	Vermiculite	Macropore	Dry impregnation
Casey et al.	2015	[152]	Experimental	Laboratory	Heat storage	Open	Ca(NO <sub>3</sub> ) <sub>2</sub>	Vermiculite	Macropore	Dry impregnation
Casey et al.	2014	[71]	Experimental	Grain	Heat storage	Open	LiBr	Vermiculite	Macropore	Dry impregnation
Casey et al.	2015	[152]	Experimental	Laboratory	Heat storage	Open	LiBr	Vermiculite	Macropore	Dry impregnation
Jarimi et al.	2017	[166]	Experimental	Grain	Heat storage	Open	LiCl	Vermiculite	Macropore	Impregnation
Zhang et al.	2016	[177]	Experimental	Grain	Heat storage	Closed	LiCl	Expanded vermiculite	Macropore	Wet impregnation
Casey et al.	2014	[71]	Experimental	Grain	Heat storage	Open	LiNO <sub>3</sub>	Vermiculite	Macropore	Dry impregnation
Casey et al.	2015	[152]	Experimental	Laboratory	Heat storage	Open	LiNO <sub>3</sub>	Vermiculite	Macropore	Dry impregnation
Sapienza et al.	2012	[178]	Experimental	Laboratory	Heat storage		LiNO <sub>3</sub>	Expanded vermiculite	Micropore	Impregnation
Jarimi et al.	2017	[166]	Experimental	Grain	Heat storage	Open	MgCl <sub>2</sub>	Vermiculite	Macropore	Impregnation
Casey et al.	2014	[71]	Experimental	Grain	Heat storage	Open	MgSO <sub>4</sub>	Vermiculite	Macropore	Dry impregnation
Casey et al.	2015	[152]	Experimental	Laboratory	Heat storage	Open	MgSO <sub>4</sub>	Vermiculite	Macropore	Dry impregnation
Jarimi et al.	2017	[166]	Experimental	Grain	Heat storage	Open	MgSO <sub>4</sub>	Vermiculite	Macropore	Impregnation
Jarimi et al.	2017	[166]	Experimental	Grain	Heat storage	Open	MgSO <sub>4</sub> -CaCl <sub>2</sub>	Vermiculite	Macropore	Impregnation
Jarimi et al.	2017	[166]	Experimental	Grain	Heat storage	Open	MgSO <sub>4</sub> -MgCl <sub>2</sub>	Vermiculite	Macropore	Impregnation
Casey et al.	2014	[71]	Experimental	Grain	Heat storage	Open	CaCl <sub>2</sub>	Zeolite 13X	Micropore	Dry impregnation
Casey et al.	2015	[152]	Experimental	Laboratory	Heat storage	Open	CaCl <sub>2</sub>	Zeolite 13X	Micropore	Dry impregnation
Chan et al.	2012	[179]	Exp-num	Laboratory	Cooling		CaCl <sub>2</sub>	Zeolite 13X	Micropore	Wet impregnation
Cortes et al.	2012	[153]	Experimental	Grain	Cooling, air conditioning		CaCl <sub>2</sub>	Zeolite 13X	Micropore	Dry impregnation
Mette	2014	[171]	Exp-num	Grain / lab	Heat storage, heating	Open	CaCl <sub>2</sub>	Zeolite 13X binder-free	Micro-macro	Wet impregnation
Nonnen et al.	2016	[180]	Experimental	Laboratory	Heat storage	Open	CaCl <sub>2</sub>	Zeolite 13X Ca-X		Wet impregnation
Whiting et al.	2014	[181]	Experimental	Grain	Heat storage		MgCl <sub>2</sub>	Zeolite 13X	Micropore	Impregnation
Whiting et al.	2014	[181]	Experimental	Grain	Heat storage		MgCl <sub>2</sub>	Zeolite mordenite	Micropore	Impregnation
Whiting et al.	2014	[181]	Experimental	Grain	Heat storage		MgCl <sub>2</sub>	Zeolite Faujasite Na	Micropore	Impregnation
Whiting et al.	2014	[181]	Experimental	Grain	Heat storage		MgCl <sub>2</sub>	Zeolite Faujasite H	Micropore	Impregnation
Hongois et al.	2011	[120]	Experimental	Grain / lab	Heat storage, heating	Open	MgSO <sub>4</sub>	Zeolite 13X	Micropore	Wet impregnation
Mette	2014	[171]	Exp-num	Grain / lab	Heat storage, heating	Open	MgSO <sub>4</sub>	Zeolite 13X	Micro-macro	Wet impregnation
Whiting et al.	2013	[182]	Experimental	Grain	Heat storage		MgSO <sub>4</sub>	Zeolite 13X	Micropore	Impregnation
Whiting et al.	2014	[182]	Experimental	Grain	Heat storage		MgSO <sub>4</sub>	Zeolite Faujasite Na	Micropore	Impregnation
Whiting et al.	2014	[182]	Experimental	Grain	Heat storage		MgSO <sub>4</sub>	Zeolite Faujasite H	Micropore	Impregnation
Whiting et al.	2014	[182]	Experimental	Grain	Heat storage		MgSO <sub>4</sub>	Zeolite mordenite	Micropore	Impregnation
Permyakova et al.	2017	[193]	Experimental	Grain	Heat storage		CaCl <sub>2</sub>	Metal-organic framework		Encapsulation

## C. List of materials and devices used in this study

Table C.1.: List of chemical substances used.

ID	Substance	Formula	Supplier	Grade	CAS-No.
C1	Calcium chloride	CaCl <sub>2</sub>	AppliChem	≥ 97%	10043-52-4
C2	Calcium chloride	CaCl <sub>2</sub>	Merck	p.A.	10043-52-4
C3	Calcium chloride hexahydrate	CaCl <sub>2</sub> · 6 H <sub>2</sub> O	AppliChem	p.A.	7774-34-7
C4	Potassium chloride	KCl	Roth	Ph.Eur.	7447-40-7
C5	Magnesium chloride	MgCl <sub>2</sub>	Roth	≥ 98.5	7786-30-3
C6	Ethanol	C <sub>2</sub> H <sub>5</sub> OH	Merck	≥ 99.9%	64-17-5
C7	Methanol	CH <sub>3</sub> OH	Merck	p.A.	67-56-1

Table C.2.: Information on physical and chemical properties of the pure reagents included in the safety data sheet.

ID	C1	C2	C3	C4	C5	C6	C7
State	Solid	Solid	Solid	Solid	Solid	Liquid	Liquid
Appearance	Powder	Powder	Powder	Powder	Powder	-	-
pH	7-11	8-10 <sup>1 2</sup>	-	5.5-8.0 <sup>1 3</sup>	5.0-6.5 <sup>1 4</sup>	7.0 <sup>1 5 6</sup>	-
<i>T<sub>m</sub></i> (°C)	770-782	772	29.92	772	708	-114.5	-98
<i>T<sub>b</sub></i> (°C)	>1600	-	-	1413 <sup>6</sup>	1412 <sup>6</sup>	78.3 <sup>6</sup>	64.5 <sup>6</sup>
<i>ρ<sub>s</sub></i> (g cm <sup>-3</sup> )	2.15 <sup>1</sup>	2.15 <sup>1</sup>	1.71 <sup>1</sup>	1.98 <sup>1</sup>	2.32 <sup>1</sup>	0.790-0.793 <sup>1</sup>	0.792 <sup>1</sup>
<i>ρ</i> (kg m <sup>-1</sup> )	700-900	-	-	1000	-	-	-
<i>p</i> (hPa)	-	-	-	-	-	59 <sup>1</sup>	128 <sup>1</sup>
<i>M</i> (g mol <sup>-1</sup> )	110.98	110.98	219.09	74.56	95.22	46.07	32.04
Water solubility (g L <sup>-1</sup> )	745 <sup>1</sup>	740 <sup>1</sup>	5360 <sup>1</sup>	347 <sup>1</sup>	542 <sup>1</sup>	Soluble	Soluble
Water content (%)	-	-	-	-	-	≤ 0.01	0.003

<sup>1</sup> Reference temperature: 20 °C

<sup>2</sup> 100 g L<sup>-1</sup>

<sup>3</sup> 50 g L<sup>-1</sup>

<sup>4</sup> 25 g L<sup>-1</sup>

<sup>5</sup> 10 g L<sup>-1</sup>

<sup>6</sup> Reference pressure: 1013 hPa



Table C.3.: List of host materials used.

Material	ID	Supplier	Appearance	$D$ (mm)	$d_{pore}$ (nm)	$V_{pore}$ ( $\text{cm}^3 \text{g}^{-1}$ )	$\rho_s$ ( $\text{kg m}^{-3}$ )	$\rho_b$ ( $\text{kg m}^{-3}$ )	$\rho_a$ ( $\text{g m}^{-2}$ )	$S_{BET}$ ( $\text{m}^2 \text{g}^{-1}$ )	$\lambda$ ( $\text{W m}^{-1} \text{K}^{-1}$ )	$T_m$ ( $^{\circ}\text{C}$ )	pH (-)
Silica gel	SG	Roth	Grains	1.0-3.0	Meso	-	-	400- 900	-	750	-	>550	4.0- 8.0
Expanded vermiculite	EV	Deutsche Vermiculite	Grains	0.0-1.0	Macro	-	-	120- 130	-	5.42	0.07	1315	7.0
Expanded vermiculite	EV2	Deutsche Vermiculite	Grains	2.0-6.0	Macro	-	-	100- 105	-	4.04	0.07	1315	7.0
Expanded natural graphite compacted	ENG	SGL Carbon Group	Pellets	-	Meso	-	-	50	750	-	-	-	-
Expanded natural graphite powder	ENGP	SGL Carbon Group	Powder	-	Meso	-	-	100	-	20	-	-	-
Activated carbon foam	ACF	Blücher	Foam	-	Micro- Meso	-	-	-	4600	-	-	-	-
Binder-free zeolite	Z13X	Chemiewerk Bad Köstritz	Beads	2.5-3.5	Micro	-	-	0.62- 0.7	-	-	-	-	-
Zeolite natural clinoptilolite	ZNC	Zeolith Umwelttechnik	Powder	0.0-0.5	Micro	-	-	-	-	-	-	-	-
Biochar	BC	Bioenergy Concept	Grains	0.0-2.0	-	-	-	-	-	-	-	-	-

## Appendix C. List of materials and devices used in this study

Table C.4.: List of composite adsorbents synthesized.

Sample ID	Host matrix	Salt	Method	w (wt%)	Paper
SG-CaCl <sub>2</sub>	SG	CaCl <sub>2</sub>	Wet impregnation	32	I
EV-CaCl <sub>2</sub>	EV	CaCl <sub>2</sub>	Wet impregnation	22	I
CaCl <sub>2</sub> -ACF-VI	ACF	CaCl <sub>2</sub>	Vacuum impregnation	31	II, III
CaCl <sub>2</sub> -MSH-ACF-VI	ACF	Molten CaCl <sub>2</sub>	Vacuum impregnation	58	II, III
CaCl <sub>2</sub> -ENG-VI	ENG	CaCl <sub>2</sub>	Vacuum impregnation	87	II, III
CaCl <sub>2</sub> -MSH-ENG-VI	ENG	Molten CaCl <sub>2</sub>	Vacuum impregnation	90	II, III
CaCl <sub>2</sub> -ENGP-S-4	ENGP	CaCl <sub>2</sub>	Wet impregnation	87	II, III
CaCl <sub>2</sub> -ENGP-S-2	ENGP	CaCl <sub>2</sub>	Wet impregnation	66	II, III
CaCl <sub>2</sub> -ENGP-S-1	ENGP	CaCl <sub>2</sub>	Wet impregnation	51	II, III
CaCl <sub>2</sub> -ENG	ENG	CaCl <sub>2</sub>	Vacuum impregnation	64	VIII
CaCl <sub>2</sub> -Z13X	Z13X	CaCl <sub>2</sub>	Wet impregnation	16	VIII
CaCl <sub>2</sub> -ZNC	ZNC	CaCl <sub>2</sub>	Wet impregnation	30	VIII
CaCl <sub>2</sub> -BC	BC	CaCl <sub>2</sub>	Wet impregnation	83	VIII
CaCl <sub>2</sub> -EV2	EV2	CaCl <sub>2</sub>	Vacuum impregnation	69	VIII

Table C.5.: List of devices.

Device	Manufacturer
TGA/DSC 1	Mettler Toledo
TGA/DSC gas controller GC 200	Mettler Toledo
STARe software version 11.00a	Mettler Toledo
Alumina crucible 70 $\mu$ L	Mettler Toledo
Ministat	Huber
Ultrasonic bath Sonorex Super 10P	Bandeln
USB-Hygrometer PCE-HT71	Datalogs
Ultrapure water system Ultra Clear UV	SG Wasseraufbereitung
ICP-OES Optima 3000	Perkin Elmer
Autosampler AS 90 für ICP-OES	Perkin Elmer
BET Autosorb iQ MP	Quantachrome
Quantachrome NovaWin	Quantachrome Instruments
Bio-Rad FT-Raman spectrometer	Digilab
LABSYS evo thermal analyzer	Setaram
Aluminum crucible 100 $\mu$ L	Setaram
Aluminum lid with 700 micron hole	Setaram
AKTS Calisto Processing, version 1.41	Setaram
Vacuum OmniStar™ gas analysis system	Pfeiffer
PW 3710 based PW 1050 Bragg-Brentano parafocusing goniometer	Philips
HTK2000 high temperature oven chamber	Anton-Paar
PDF-4 (2010) database	ICDD
Aldrich® AtmosBag	Sigma-Aldrich



## D. Supplementary data on paper II and paper III

The composite materials presented in **paper II** and **paper III** were examined in supplementary cyclic tests employing simultaneous TGA/DSC. The cyclic test consisted of five consecutive isothermal hydration and dynamic dehydration runs. Samples of 10 mg were placed in 70  $\mu\text{L}$  alumina crucibles and hydrated at a  $\text{H}_2\text{O}$  vapor pressure of 20 mbar at 30  $^\circ\text{C}$  for 60 min after 15 min of stabilization. The  $\text{H}_2\text{O}$  vapor pressure was generated by humidifying a flowing  $\text{N}_2$  gas stream of 125  $\text{mL min}^{-1}$ . Prior to dehydration, the samples were stabilized at 30  $^\circ\text{C}$  for stability determination. Dehydration was carried out by heating the samples to 200  $^\circ\text{C}$  with constant heating rates of 3  $\text{K min}^{-1}$  in controlled dry  $\text{N}_2$  gas atmosphere. The samples were finally cooled down to the initial temperature with temperature ramp rates of  $-10 \text{ K min}^{-1}$ .  $\text{H}_2\text{O}$  uptake and release were calculated from the change in mass of the specimen recorded by TGA as a function of time. Specific gravimetric energy densities were obtained by integration of the peak area between the DSC signal and the baseline. Measurement data were baseline-corrected and processed with the STARe software 11.00a from Mettler Toledo.

The results plotted in Figure D.1 show the stable cycling performance of the different composite adsorbents.  $\text{CaCl}_2$  confined to ENG, denoted  $\text{CaCl}_2\text{-ENG-VI}$  and containing 87%  $\text{CaCl}_2$ , performed best in terms of  $\text{H}_2\text{O}$  adsorption/desorption and corresponding energy storage density. A tiny melting peak was observed in the first dehydration run, but apparently had no negative effect on the  $\text{H}_2\text{O}$  uptake. The dehydration of the compound adsorbent  $\text{CaCl}_2\text{-MSH-ENG-VI}$  with a  $\text{CaCl}_2$  content of 90% was accompanied by a phase change event resulting in lower amount of  $\text{H}_2\text{O}$  exchanged by one gram of dry composite material and reduced energy density when compared to the hydration process. The better  $\text{H}_2\text{O}$  adsorption/desorption ability of the  $\text{CaCl}_2\text{-MSH-ACF-VI}$  composite is attributed to the higher  $\text{CaCl}_2$  loading in comparison to that of the  $\text{CaCl}_2\text{-ACF-VI}$ . Since only 31% and 58% of  $\text{CaCl}_2$  were impregnated into  $\text{CaCl}_2\text{-ACF-VI}$  and  $\text{CaCl}_2\text{-MSH-ACF-VI}$ , the ACF-based composites displayed low overall adsorption performance. No melting occurred in  $\text{CaCl}_2\text{-ACF-VI}$  and  $\text{CaCl}_2\text{-MSH-ACF-VI}$ . Discrepancies between the values of  $\text{H}_2\text{O}$  uptake and release appear to arise from  $\text{H}_2\text{O}$  desorption during the stabilization period.

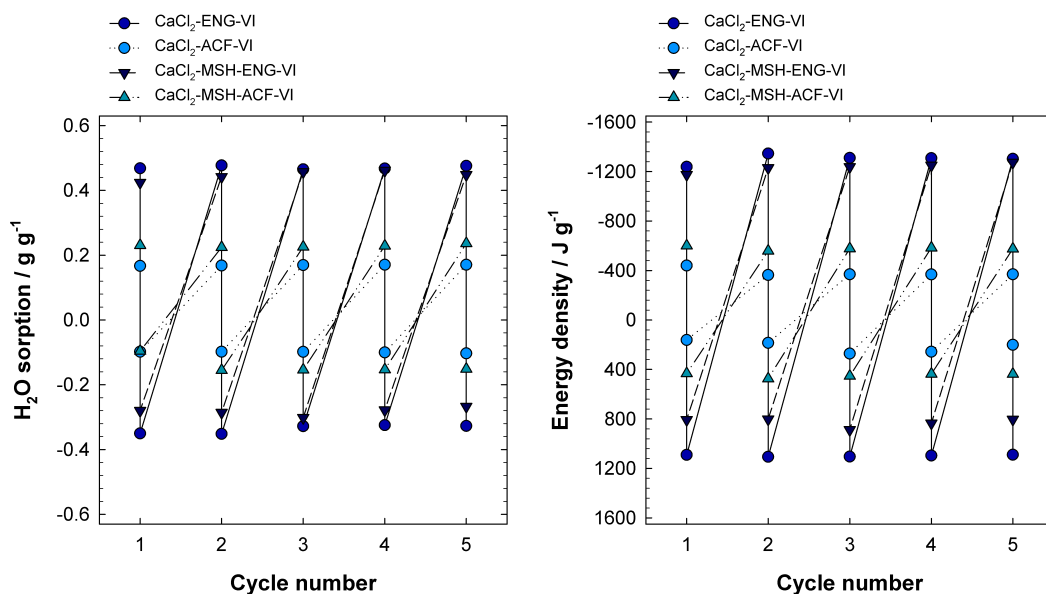


Figure D.1.: Water uptake and release (left) and energy density (right) over five successive hydration/dehydration cycles of the composite adsorbents synthesized by impregnation. Values are referred to the dry weight of the composite adsorbent.

Onset temperatures ( $T_{\text{onset}}$ ) and peak temperatures ( $T_{\text{peak}}$ ) of the dehydration reactions of all composite adsorbents tested did not change significantly over cycling, as shown in Table D.1. The dissociation of the ENG supported CaCl<sub>2</sub> samples proceeded in two indistinct stages, whereas the ACF supported CaCl<sub>2</sub> samples decomposed in one single step. The melting points observed coincided well with the melting point of CaCl<sub>2</sub>·4H<sub>2</sub>O, according to literature data [240].

Table D.1.: Onset temperature ( $T_{\text{onset}}$ ) and peak temperature ( $T_{\text{peak}}$ ) of the dehydration reaction of the composite adsorbents studied in respect of the dehydration step and cycle number.

Cycle number	Melting		Step 1		Step 2	
	$T_{\text{onset}}$ °C	$T_{\text{peak}}$ °C	$T_{\text{onset}}$ °C	$T_{\text{peak}}$ °C	$T_{\text{onset}}$ °C	$T_{\text{peak}}$ °C
<b>CaCl<sub>2</sub>-ENG-VI</b>						
1	40	42	89	114	105	130
2	-	-	81	114	100	132
3	-	-	78	113	103	133
4	-	-	79	113	102	132
5	-	-	85	113	103	132
<b>CaCl<sub>2</sub>-ACF-VI</b>						
1	-	-	82	100	-	-
2	-	-	48	98	-	-
3	-	-	66	98	-	-
4	-	-	59	98	-	-
5	-	-	84	98	-	-
<b>CaCl<sub>2</sub>-MSH-ENG-VI</b>						
1	40	42	49	111	102	121
2	40	42	44	112	98	120
3	40	42	48	101	101	121
4	40	42	70	109	100	121
5	40	42	44	109	97	120
<b>CaCl<sub>2</sub>-MSH-ACF-VI</b>						
1	-	-	32	131	-	-
2	-	-	53	122	-	-
3	-	-	41	116	-	-
4	-	-	32	120	-	-
5	-	-	32	114	-	-

The calculated H<sub>2</sub>O uptake/release and associated energy storage density values slightly differed from the results given in **paper II** and **paper III**, due to differences in the measurement procedure.



## E. Supplementary data on paper IV

In this chapter, results on the thermal cyclability and heating rate dependence of the deethanolation reaction of the reaction pairs studied in **paper IV**, namely  $\text{CaCl}_2\text{-C}_2\text{H}_5\text{OH}$ ,  $\text{MgCl}_2\text{-C}_2\text{H}_5\text{OH}$ , and  $\text{CaCl}_2\text{-MgCl}_2\text{-C}_2\text{H}_5\text{OH}$ , are outlined in detail. The enthalpies of reaction were derived from manual integration of the baseline-corrected DSC peaks. For the reaction pair  $\text{CaCl}_2\text{-C}_2\text{H}_5\text{OH}$ , a kinetic analysis was executed besides an energy analysis. The reaction rates for the ethanolation and deethanolation reaction were calculated at a given point of time over the progress of the reactions. The reactivity between  $\text{CaCl}_2$  and  $\text{C}_2\text{H}_5\text{OH}$  was low in the first few cycles (Figure E.2). Predrying at elevated temperatures caused a structural collapse of the bulk material and impeded the accessibility of  $\text{C}_2\text{H}_5\text{OH}$  molecules so that the overall ethanolation level successively increased from about 0.7 to about 1.5 during the first ethanolation/deethanolation reaction cycles, as shown in Figure E.1. The corresponding ethanolation and deethanolation enthalpies followed the same pattern; they reached constant values with continuous cycling (Figure E.1). However, the normalized ethanolation and deethanolation enthalpies increased over the first cycles, before attaining stable values.

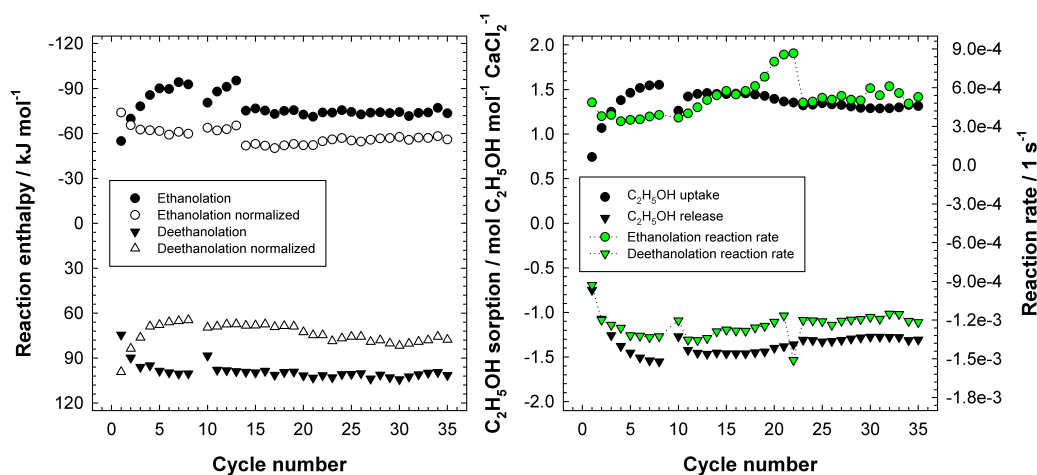


Figure E.1.: Changes in molar reaction enthalpy (left),  $\text{C}_2\text{H}_5\text{OH}$  sorption (right) and maximum reaction rate (right) of  $\text{CaCl}_2$  ethanulates over thermal cycling.



Regarding the speed of the ethanolation reaction, a slight decrease was observed at the beginning of the cycle test. Despite only small changes in the  $C_2H_5OH$  uptake, the ethanolation reaction rate greatly increased continuously up to the 22<sup>nd</sup> cycle. After a sharp drop, the ethanolation rates fluctuated around a constant value, which was similar to the value of the 1<sup>st</sup> cycle. This observation is attributed to the slightly lower level of ethanolation when compared with that of the previous cycles. The total maximum deethanolation rate was also reached in the 22<sup>nd</sup> cycle. Since the deethanolation reactions were performed under dynamic conditions, the overall deethanolation reaction rates are around twice as high as the ethanolation reaction rates. The ethanolation of  $CaCl_2$  is characterized by a single reaction peak at low degrees of conversion; the maximum reaction rate was attained within seconds (Figure E.1). The reaction rate finally decreased as the ethanolation reaction progressed. The deethanolation reaction described a completely different scheme (Figure E.3). The  $C_2H_5OH$  was released in three indistinct stages; the highest deethanolation reaction rate was measured in the first step. The stepwise desorption is the result of changes in the local temperature and  $C_2H_5OH$  pressure inside and above the material. The size of the  $C_2H_5OH$  molecule and the  $C_2H_5OH$  concentration inside the material also contribute to a slow diffusion.

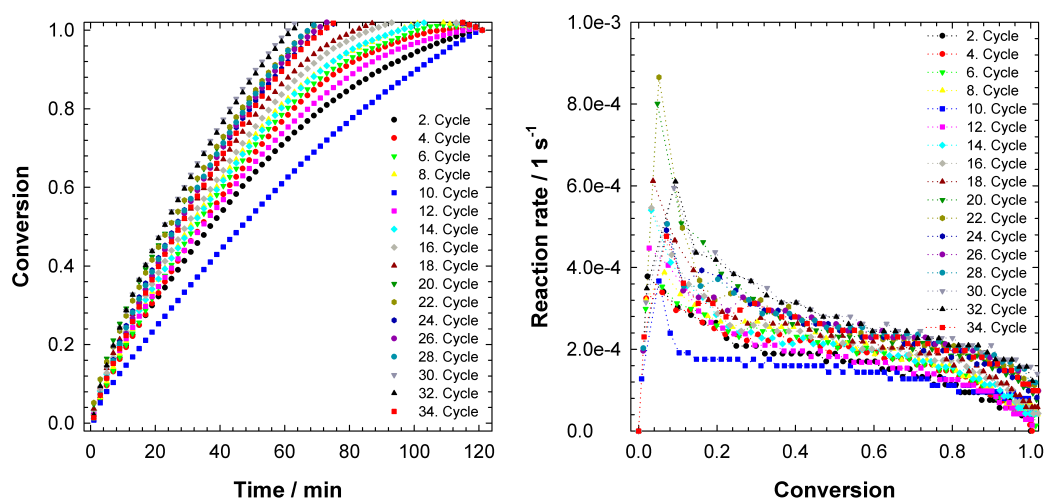


Figure E.2.: Changes in conversion (left) and reaction rate (right) of the ethanolation reaction of  $CaCl_2$  over multi-cyclic ethanolation/deethanolation runs.

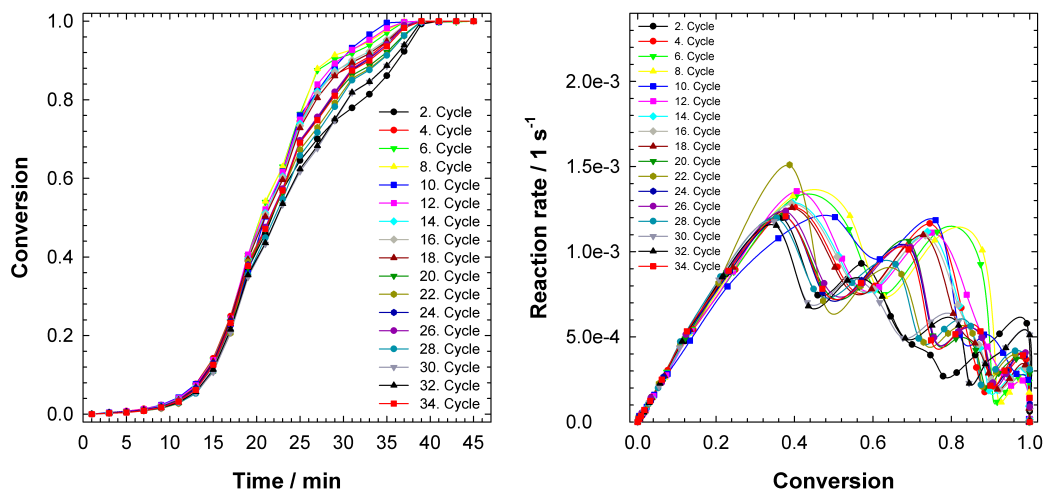


Figure E.3.: Changes in conversion (left) and reaction rate (right) of the deethanolation reaction of  $\text{CaCl}_2$  over multi-cyclic ethanolation/deethanolation.

Hygrothermal cycling apparently induced changes in the microstructure of the pure  $\text{CaCl}_2$  sample, due to periodic mechanical and thermal stress. The ethanolated  $\text{CaCl}_2$  occupies more volume than the  $\text{CaCl}_2$  anhydride. During ethanolation and deethanolation, a  $\text{C}_2\text{H}_5\text{OH}$  vapor pressure gradient is assumed to be established and the absorption and evolution of heat in conjunction with the low total thermal conductivity of the material produces a temperature distribution across the material. In conclusion, cycle stability is given in terms of energy storage, but variations of the structural properties affect the speed of the ethanolation and deethanolation reaction and alter the cycleability of the reaction pair  $\text{CaCl}_2\text{-C}_2\text{H}_5\text{OH}$ .

Thermal cycling of the reaction pair  $\text{MgCl}_2\text{-C}_2\text{H}_5\text{OH}$  was not reproducible, as depicted in Figure E.4. The material irreversibly decomposed over cycling resulting in a decline in the  $\text{C}_2\text{H}_5\text{OH}$  uptake with increasing number of operation cycles. The reaction enthalpies for ethanolation and deethanolation normalized to one mole of  $\text{C}_2\text{H}_5\text{OH}$  gradually increased with consecutive ethanolation/deethanolation cycles connoting the presence of multiple reactions.

As shown in Figure E.5, the addition of 2 parts of  $\text{CaCl}_2$  to one part of  $\text{MgCl}_2$  improved the cycle stability of  $\text{MgCl}_2$ . The stable thermal behavior and cycling performance makes the binary salt mixture a good candidate material for heat storage applications. With respect to the reaction kinetics, there is no apparent improvement, since the demethanolation reaction rate (Figure E.8) is similar to that of pure  $\text{CaCl}_2$  (Figure E.6). The existence of side reactions was not investigated for this material and cannot be excluded at present.

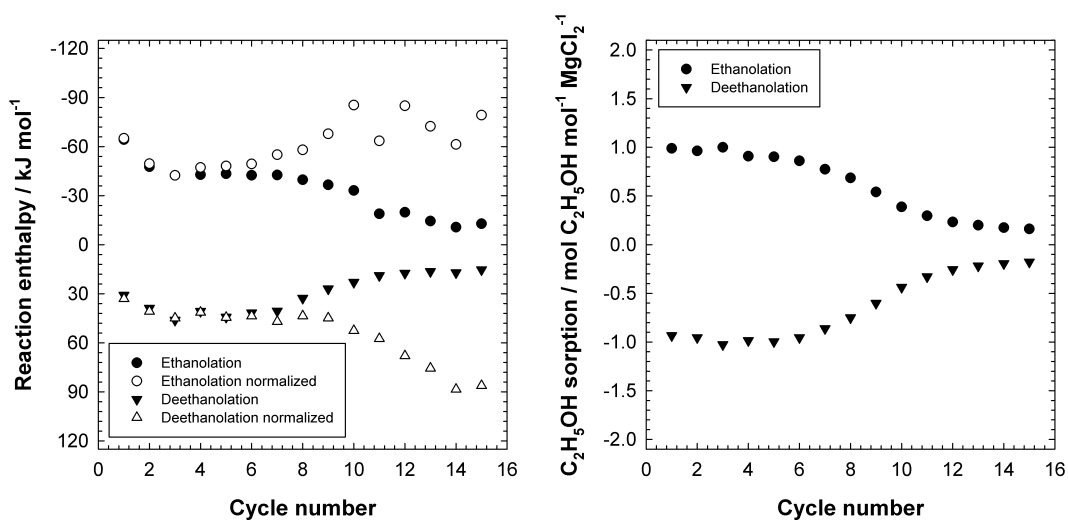


Figure E.4: Changes in molar reaction enthalpy (left) and  $\text{C}_2\text{H}_5\text{OH}$  uptake and release (right) of  $\text{MgCl}_2$  ethanولات over thermal cycling.

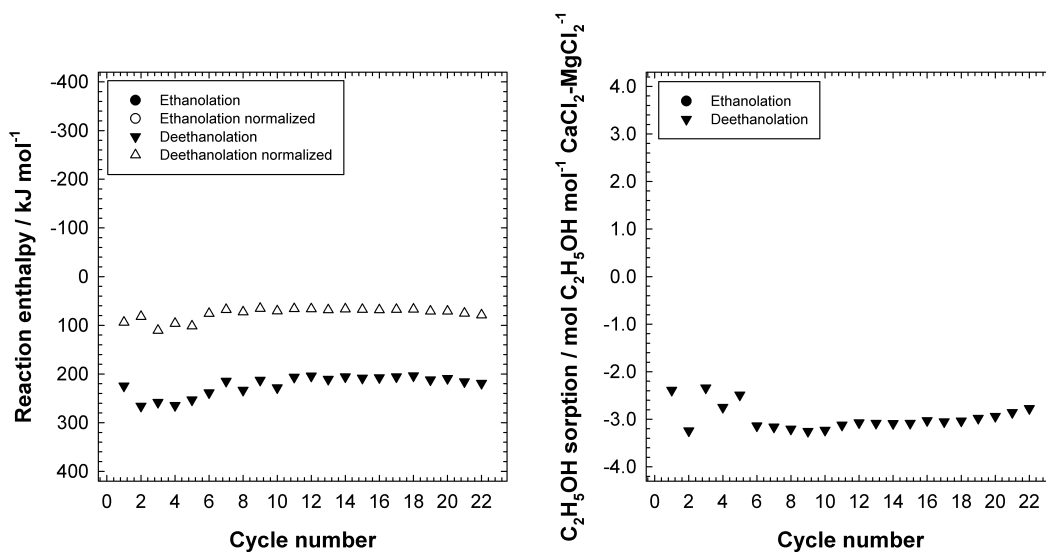


Figure E.5: Changes in molar reaction enthalpy (left) and  $\text{C}_2\text{H}_5\text{OH}$  uptake and release (right) of the binary salt mixture  $\text{CaCl}_2\text{-MgCl}_2$  over thermal cycling. The physical mixture was prepared by mixing anhydrous  $\text{CaCl}_2$  and anhydrous  $\text{MgCl}_2$  in the molar ratio of 2:1.

In general, several factors influence the rate of a reaction. One of the most important factors is the temperature applied to the system. In this study, the deethanolation reactions were carried out under dynamic conditions. To evaluate the impact of the heating rate on the deethanolation reaction rate, TGA/DSC measurements with different heating rates ( $1 \text{ K min}^{-1}$ ,  $5 \text{ K min}^{-1}$ , and  $10 \text{ K min}^{-1}$ ) were conducted. A shift of the deethanolation peak temperature towards higher values as well as a lift in the reaction rate with an increase in the heating rate occurred for all reaction pairs investigated, as illustrated in Figure E.6 to Figure E.8. The material has more time to reach a specific temperature at low heating rates and consequently the reaction is completed at lower temperatures. For real applications concerning reactor design aspects, the temperature and associated heating rate dependence of the materials have to be taken into account.

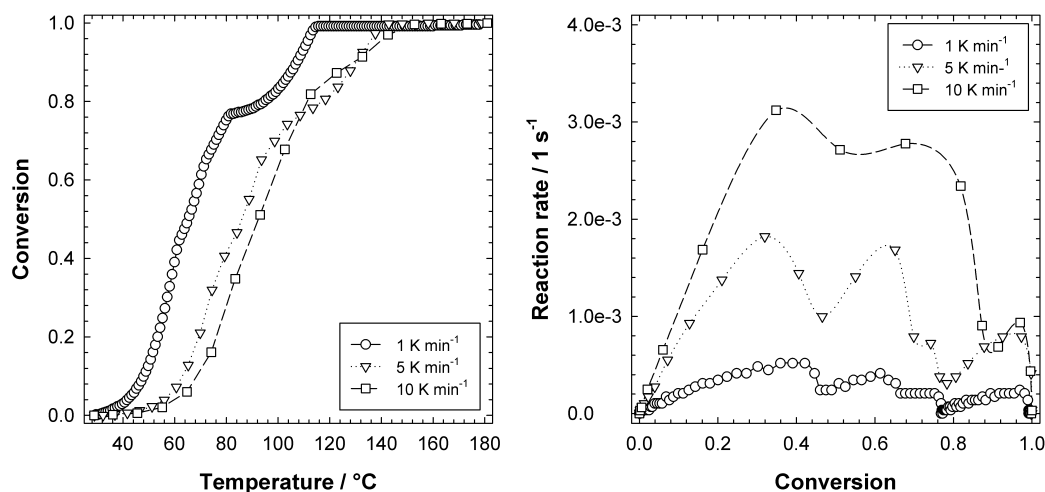


Figure E.6.: Heating rate dependence of the deethanolation temperature (left) and reaction rate (right) of the deethanolation reaction of ethanolated  $\text{CaCl}_2$ .

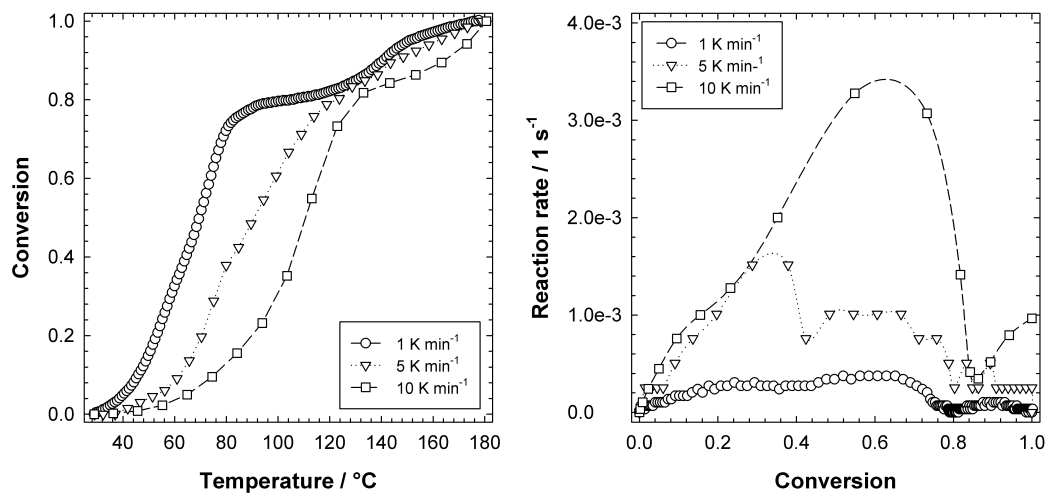


Figure E.7.: Heating rate dependence of the deethanolation temperature (left) and reaction rate (right) of the deethanolation reaction of ethanolated MgCl<sub>2</sub>.

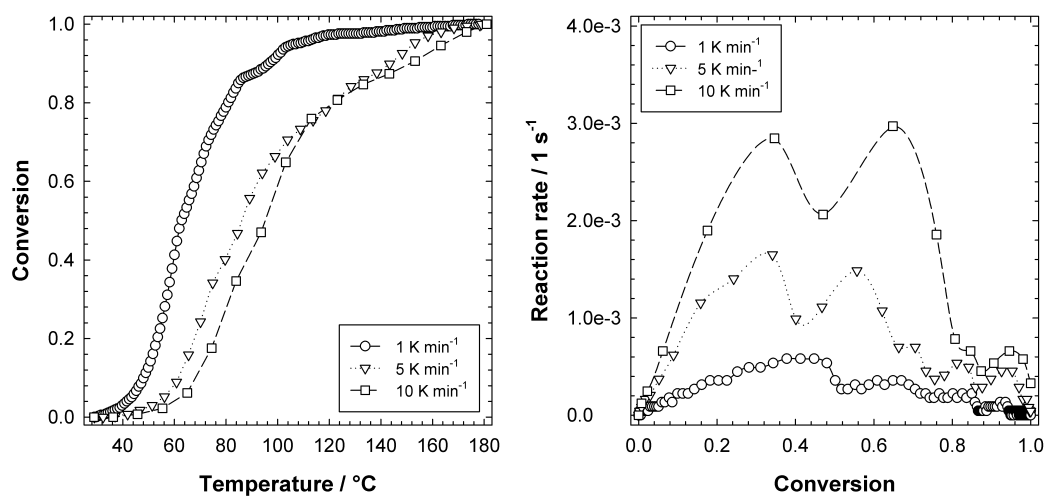


Figure E.8.: Heating rate dependence of the deethanolation temperature (left) and reaction rate (right) of the deethanolation reaction of ethanolated CaCl<sub>2</sub>-MgCl<sub>2</sub> binary salt pair with a mixing ratio of 2:1.

# Bibliography

- [1] European Commission. Press release. Clean energy for all Europeans – Unlocking Europe’s growth potential, 2016.
- [2] T. A. Friedrich. Häppchenweise Energiezukunft. *VDI-nachrichten*, Ausgabe 49, 2016.
- [3] U. Neupert, T. Euting, T. Kretschmer, C. Notthoff, K. Ruhlig, and B. Weimert. *Energiespeicher: technische Grundlagen und energiewirtschaftliches Potenzial*. Fraunhofer IRB Verlag, Stuttgart, 2009.
- [4] Bundesministerium für Energie und Wirtschaft. *Energiedaten: Gesamtausgabe*, 2017.
- [5] E. O. Ataer. Storage of thermal energy, in energy storage systems. In *Encyclopedia of Life support systems (EOLSS), developed under the auspices of the UNESCO*. Eolss Publishers, Oxford, 2006.
- [6] E. Morofsky. History of thermal energy storage. In H. Ö. Paksoy, editor, *Thermal energy storage for sustainable energy consumption: Fundamentals, case studies and design. NATO science series (Mathematics, Physics and Chemistry)*, pages 3–22. Springer, Dordrecht, 2007.
- [7] P. Pinel, C. A. Cruickshank, I. Beausoleil-Morrison, and A. Wills. A review of available methods for seasonal storage of solar thermal energy in residential applications. *Renewable and Sustainable Energy Reviews*, 15(7):3341–3359, 2011.
- [8] A. Gil, M. Medrano, I. Martorell, A. Lázaro, P. Dolado, B. Zalba, and L. F. Cabeza. State of the art on high temperature thermal energy storage for power generation. Part 1—Concepts, materials and modellization. *Renewable and Sustainable Energy Reviews*, 14(1):31–55, 2010.
- [9] L. F. Cabeza, A. Castell, C. Barreneche, A. De Gracia, and A. I. Fernández. Materials used as PCM in thermal energy storage in buildings: A review. *Renewable and Sustainable Energy Reviews*, 15(3):1675–1695, 2011.

- 
- [10] P. Tatsidjodoung, N. Le Pierrès, and L. Luo. A review of potential materials for thermal energy storage in building applications. *Renewable and Sustainable Energy Reviews*, 18:327–349, 2013.
- [11] Y. Kato. Chemical energy conversion technologies for efficient energy use. In H. Ö. Paksoy, editor, *Thermal energy storage for sustainable energy consumption: Fundamentals, case studies and design. NATO science series (Mathematics, Physics and Chemistry)*, pages 377–391. Springer, Dordrecht, 2007.
- [12] A. Sharma, V. V. Tyagi, C. R. Chen, and D. Buddhi. Review on thermal energy storage with phase change materials and applications. *Renewable and Sustainable Energy Reviews*, 13(2):318–345, 2009.
- [13] H. P. Garg, S. C. Mullick, and A. K. Bhargava. Chemical energy storage. In *Solar thermal energy storage*, pages 292–427. Springer Netherlands, Dordrecht, 1985.
- [14] P. Gantenbein. Sorption storage unit with zeolite (silicagel) / water. In C. Bales, editor, *Laboratory tests of chemical reactions and prototype sorption storage units: Report B4 of substask B*, pages 8–15. IEA SHC Task 32, 2008.
- [15] D. Jaehnig. Solid sorption storage system (MODESTORE). In C. Bales, editor, *Laboratory tests of chemical reactions and prototype sorption storage units: Report B4 of substask B*, pages 16–22. IEA SHC Task 32, 2008.
- [16] E. P. Ng and S. Mintova. Nanoporous materials with enhanced hydrophilicity and high water sorption capacity. *Microporous and Mesoporous Materials*, 114(1-3):1–26, 2008.
- [17] B. B. Saha, A. Akisawa, and T. Kashiwagi. Silica gel water advanced adsorption refrigeration cycle. *Energy*, 22(4):437–447, 1997.
- [18] J. Jänchen, D. Ackermann, H. Stach, and W. Brösicke. Studies of the water adsorption on zeolites and modified mesoporous materials for seasonal storage of solar heat. *Solar Energy*, 76(1-3):339–344, 2004.
- [19] T. Núñez, W. Mittelbach, and H. M. Henning. Development of an adsorption chiller and heat pump for domestic heating and air-conditioning applications. *Applied Thermal Engineering*, 27(13):2205–2212, 2007.
- [20] A. Akahira, K. C. A. Alam, Y. Hamamoto, A. Akisawa, and T. Kashiwagi. Mass recovery four-bed adsorption refrigeration cycle with energy cascading. *Applied Thermal Engineering*, 25(11-12):1764–1778, 2005.

- [21] D. C. Wang, J. Y. Wu, Z. Z. Xia, H. Zhai, R. Z. Wang, and W. D. Dou. Study of a novel silica gel-water adsorption chiller. Part II. Experimental study. *International Journal of Refrigeration*, 28:1084–1091, 2005.
- [22] G. Z. Yang, Z. Z. Xia, R. Z. Wang, D. Keletigui, D. C. Wang, Z. H. Dong, and X. Yang. Research on a compact adsorption room air conditioner. *Energy Conversion and Management*, 47(15-16):2167–2177, 2006.
- [23] R. J. H. Grisel, S. F. Smeding, and R. de Boer. Waste heat driven silica gel/water adsorption cooling in trigeneration. *Applied Thermal Engineering*, 30(8-9):1039–1046, 2010.
- [24] W. S. Chang, C. C. Wang, and C. C. Shieh. Experimental study of a solid adsorption cooling system using flat-tube heat exchangers as adsorption bed. *Applied Thermal Engineering*, 27(13):2195–2199, 2007.
- [25] W. S. Chang, C. C. Wang, and C. C. Shieh. Design and performance of a solar-powered heating and cooling system using silica gel/water adsorption chiller. *Applied Thermal Engineering*, 29(10):2100–2105, 2009.
- [26] K. Oertel and M. Fischer. Adsorption cooling system for cold storage using methanol/silicagel. *Applied Thermal Engineering*, 18(9-10):773–786, 1998.
- [27] A. Hauer. Adsorption systems for TES—Design and demonstration projects. In H. Ö. Paksoy, editor, *Thermal energy storage for sustainable energy consumption*, pages 409–427. Springer Netherlands, Dordrecht, 234th edition, 2007.
- [28] Z. Lu, R. Wang, and Z. Xia. Experimental analysis of an adsorption air conditioning with micro-porous silica gel-water. *Applied Thermal Engineering*, 50(1):1015–1020, 2013.
- [29] A. Ristić, N. Z. Logar, S. K. Henninger, and V. Kaučič. The performance of small-pore microporous aluminophosphates in low-temperature solar energy storage: The structure-property relationship. *Advanced Functional Materials*, 22(9):1952–1957, 2012.
- [30] J. Jänchen and H. Stach. Adsorption properties of porous materials for solar thermal energy storage and heat pump applications. *Energy Procedia*, 30:289–293, 2012.
- [31] J. Jänchen, D. Ackermann, E. Weiler, H. Stach, and W. Brösicke. Calorimetric investigation on zeolites,  $\text{AlPO}_4$ 's and  $\text{CaCl}_2$  impregnated attapulgite for thermochemical storage of heat. *Thermochimica Acta*, 434(1-2):37–41, 2005.



- [32] P. L. Llewellyn, F. Schüth, Y. Grillet, F. Rouquerol, J. Rouquerol, and K. K. Unger. Water sorption on mesoporous aluminosilicate MCM-41. *Langmuir*, 11(2):574–577, 1995.
- [33] R. Lang, M. Roth, M. Stricker, and T. Westerfeld. Development of a modular zeolite-water heat pump. *Heat and Mass Transfer*, 35:229–234, 1999.
- [34] Q. Cui, G. Tao, H. Chen, X. Guo, and H. Yao. Environmentally benign working pairs for adsorption refrigeration. *Energy*, 30(2-4 SPEC. ISS.):261–271, 2005.
- [35] F. Poyelle, J.-J. Guilleminot, and F. Meunier. Experimental tests and predictive model of an adsorptive air conditioning unit. *Industrial & Engineering Chemistry Research*, 38(1):298–309, 1999.
- [36] G. Restuccia, A. Freni, F. Russo, and S. Vasta. Experimental investigation of a solid adsorption chiller based on a heat exchanger coated with hydrophobic zeolite. *Applied Thermal Engineering*, 25(10):1419–1428, 2005.
- [37] B. Mette, H. Kerskes, H. Drück, and H. Müller-Steinhagen. New highly efficient regeneration process for thermochemical energy storage. *Applied Energy*, 109:352–359, 2013.
- [38] R. Weber, S. Asenbeck, and H. Kerskes. Entwicklung eines kombinierten Warmwasser-Sorptionswärmespeichers für thermische Solaranlagen. Technical report, Institut für Thermodynamik und Wärmetechnik, Universität Stuttgart, Stuttgart, 2013.
- [39] I. Solmuş, C. Yamali, Bi. Kaftanoğlu, D. Baker, and A. Çağlar. Adsorption properties of a natural zeolite-water pair for use in adsorption cooling cycles. *Applied Energy*, 87(6):2062–2067, 2010.
- [40] L. Z. Zhang. Design and testing of an automobile waste heat adsorption cooling system. *Applied Thermal Engineering*, 20(1):103–114, 2000.
- [41] S. Jiangzhou, R. Z. Wang, Y. Z. Lu, Y. X. Xu, and J. Y. Wu. Experimental investigations on adsorption air-conditioner used in internal-combustion locomotive driver-cabin. *Applied Thermal Engineering*, 22(10):1153–1162, 2002.
- [42] L. Bonaccorsi, E. Proverbio, A. Freni, and G. Restuccia. In situ growth of zeolites on metal foamed supports for adsorption heat pumps. *Journal of Chemical Engineering of Japan*, 40(13):1307–1312, 2007.
- [43] B. B. Saha, I. I. El-Sharkawy, T. Miyazaki, S. Koyama, S. K. Henninger, A. Herbst, and C. Janiak. Ethanol adsorption onto metal organic framework: Theory and experiments. *Energy*, 79:363–370, 2015.

- [44] A. Khutia, H. U. Rammelberg, T. Schmidt, S. Henninger, and C. Janiak. Water sorption cycle measurements on functionalized MIL-101Cr for heat transformation application. *Chemistry of Materials*, 25(5):790–798, 2013.
- [45] C. Janiak and S. K. Henninger. Porous coordination polymers as novel sorption materials for heat transformation processes. *Chimia*, 67(6):419–24, 2013.
- [46] A. Rezk, R. AL-Dadah, S. Mahmoud, and A. Elsayed. Investigation of ethanol/metal organic frameworks for low temperature adsorption cooling applications. *Applied Energy*, 112:1025–1031, 2013.
- [47] F. Jeremias, D. Fröhlich, C. Janiak, and S. K. Henninger. Water and methanol adsorption on MOFs for cycling heat transformation processes. *New Journal of Chemistry*, 38(5):1846–1852, 2014.
- [48] B. T. Nguyen, H. L. Nguyen, T. C. Nguyen, K. E. Cordova, and H. Furukawa. High methanol uptake capacity in two new series of metal-organic frameworks: Promising materials for adsorption-driven heat pump applications. *Chemistry of Materials*, 28(17):6243–6249, 2016.
- [49] J. Ehrenmann, S. K. Henninger, and C. Janiak. Water adsorption characteristics of MIL-101 for heat-transformation applications of MOFs. *European Journal of Inorganic Chemistry*, 2011(4):471–474, 2011.
- [50] E. Passos, F. Meunier, and J. C. Gianola. Thermodynamic performance improvement of an intermittent solar-powered refrigeration cycle using adsorption of methanol on activated carbon. *Journal of Heat Recovery Systems*, 6(3):259–264, 1986.
- [51] T. F. Qu, R. Z. Wang, and W. Wang. Study on heat and mass recovery in adsorption refrigeration cycles. *Applied Thermal Engineering*, 21(4):439–452, 2001.
- [52] R. E. Critoph. Towards a one tonne per day solar ice maker. *Renewable Energy*, 9(1-4):626–631, 1996.
- [53] R. E. Critoph. Multiple bed regenerative adsorption cycle using the monolithic carbon–ammonia pair. *Applied Thermal Engineering*, 22:667–677, 2002.
- [54] L. W. Wang, J. Y. Wu, R. Z. Wang, Y. X. Xu, and S. G. Wang. Experimental study of a solidified activated carbon-methanol adsorption ice maker. *Applied Thermal Engineering*, 23(12):1453–1462, 2003.
- [55] D. C. Wang and J. Y. Wu. Influence of intermittent heat source on adsorption ice maker using waste heat. *Energy Conversion and Management*, 46(6):985–998, 2005.

- [56] I. I. El-Sharkawy, K. Kuwahara, B. B. Saha, S. Koyama, and K. C. Ng. Experimental investigation of activated carbon fibers/ethanol pairs for adsorption cooling system application. *Applied Thermal Engineering*, 26(8-9):859–865, 2006.
- [57] I. I. El-Sharkawy, M. Hassan, B. B. Saha, S. Koyama, and M. M. Nasr. Study on adsorption of methanol onto carbon based adsorbents. *International Journal of Refrigeration*, 32(7):1579–1586, 2009.
- [58] A. Al Mers, A. Azzabakh, A. Mimet, and H. El Kalkha. Optimal design study of cylindrical finned reactor for solar adsorption cooling machine working with activated carbon-ammonia pair. *Applied Thermal Engineering*, 26(16):1866–1875, 2006.
- [59] Z. Tamainot-Telto and R. E. Critoph. Monolithic carbon for sorption refrigeration and heat pump applications. *Applied Thermal Engineering*, 21(1):37–52, 2001.
- [60] H. S. Kil, T. Kim, K. Hata, K. Ideta, T. Ohba, H. Kanoh, I. Mochida, S. H. Yoon, and J. Miyawaki. Influence of surface functionalities on ethanol adsorption characteristics in activated carbons for adsorption heat pumps. *Applied Thermal Engineering*, 72(2):160–165, 2014.
- [61] V. Brancato, L. G. Gordeeva, A. Sapienza, A. Freni, and A. Frazzica. Dynamics study of ethanol adsorption on microporous activated carbon for adsorptive cooling applications. *Applied Thermal Engineering*, 105:28–38, 2016.
- [62] K. E. N'Tsoukpoe, N. Le Pierrès, and L. Luo. Experimentation of a LiBr-H<sub>2</sub>O absorption process for long-term solar thermal storage: Prototype design and first results. *Energy*, 53:179–198, 2013.
- [63] C. Bales. TCA heat pump and storage unit ClimateWell 10. In C. Bales, editor, *Laboratory tests of chemical reactions and prototype sorption storage units: Report B4 of substask B*, pages 3–7. IEA SHC Task 32, 2008.
- [64] R. Weber and V. Dorer. Long-term heat storage with NaOH. *Vacuum*, 82(7):708–716, 2008.
- [65] S. Lourdudoss and H. Stymne. An energy storing absorption heat pump process. *International Journal of Energy Research*, 11(2):263–274, 1987.
- [66] J. A. Quinnell, J. H. Davidson, and J. Burch. Liquid calcium chloride solar storage: Concept and analysis. *Journal of Solar Energy Engineering*, 133(1):11010–11018, 2011.
- [67] L. G. Gordeeva and Y. I. Aristov. Dynamic study of methanol adsorption on activated carbon ACM-35.4 for enhancing the specific cooling power of adsorptive chillers. *Applied Energy*, 117:127–133, 2014.

- [68] H. Kerskes, F. Bertsch, B. Mette, A. Wörner, and F. Schaube. Thermochemische Energiespeicher. *Chemie-Ingenieur-Technik*, 83(11):2014–2026, 2011.
- [69] M. Linder. Using thermochemical reactions in thermal energy storage systems. In L. F. Cabeza, editor, *Advances in thermal energy storage systems: Methods and applications*, pages 357–374. Woodhead Publishing, 1st edition, 2014.
- [70] G. Wettermark. Thermochemical energy storage. In B. Kilkış and S. Kakaç, editors, *Energy storage systems. NATO ASI series (series E: Applied sciences)*, pages 673–681. Springer Netherlands, Dordrecht, 1989.
- [71] S. P. Casey, J. Elvins, S. Riffat, and A. Robinson. Salt impregnated desiccant matrices for ‘open’ thermochemical energy storage—Selection, synthesis and characterisation of candidate materials. *Energy and Buildings*, 84:412–425, 2014.
- [72] A. H. Abedin and M. A. Rosen. Closed and open thermochemical energy storage: Energy- and exergy-based comparisons. *Energy*, 41(1):83–92, 2012.
- [73] J. Cot-Gores, A. Castell, and L. F. Cabeza. Thermochemical energy storage and conversion: A-state-of-the-art review of the experimental research under practical conditions. *Renewable and Sustainable Energy Reviews*, 16(7):5207–5224, 2012.
- [74] P. Gao, X. F. Zhang, L. W. Wang, R. Z. Wang, D. P. Li, Z. W. Liang, and A. F. Cai. Study on  $\text{MnCl}_2/\text{CaCl}_2\text{-NH}_3$  two-stage solid sorption freezing cycle for refrigerated trucks at low engine load in summer. *Energy Conversion and Management*, 109:1–9, 2016.
- [75] Z. Iyimen-Schwarz and M. D. Lechner. Energiespeicherung durch chemische Reaktionen. I. DSC-Messungen zur quantitativen Verfolgung der Enthalpieänderungen von Speicherstoffen für die Hin- und Rückreaktion. *Thermochimica Acta*, 68(2-3):349–361, 1983.
- [76] V. M. van Essen, H. A. Zondag, J. Cot Gores, L. P. J. Bleijendaal, M. Bakker, R. Schuitema, W. G. J. van Helden, Z. He, and C. C. M. Rindt. Characterization of  $\text{MgSO}_4$  hydrate for thermochemical seasonal heat storage. *Journal of Solar Energy Engineering*, 131(4):41014–41017, 2009.
- [77] V. M. van Essen, J. Cot Gores, L. P. J. Bleijendaal, H. A. Zondag, R. Schuitema, M. Bakker, and W. G. J. van Helden. Characterization of salt hydrates for compact seasonal thermochemical storage. In *Proceedings of the 3rd International Conference on Energy Sustainability (ASME 2009)*, volume 2, pages 825–830, San Francisco, USA, 2009.

- [78] H. Kerskes, F. Bertsch, S. Asenbeck, and B. Mette. Abschlussbericht CWS - Chemische Wärmespeicherung mittels reversibler Feststoff-Gasreaktionen, Teilvorhaben Niedertemperatur-Wärmespeicherung; BMWI Verbundprojekt, Förderkennzeichen 0327468B. Technical report, Institut für Technische Thermodynamik des Deutschen Zentrums für Luft- und Raumfahrt, Stuttgart, 2012.
- [79] K. E. N'Tsoukpoe, T. Schmidt, H. U. Rammelberg, B. A. Watts, and Wolfgang K. L. Ruck. A systematic multi-step screening of numerous salt hydrates for low temperature thermochemical energy storage. *Applied Energy*, 124:1–16, 2014.
- [80] B. Michel, N. Mazet, S. Mauran, D. Stitou, and J. Xu. Thermochemical process for seasonal storage of solar energy: Characterization and modeling of a high density reactive bed. *Energy*, 47(1):553–563, 2012.
- [81] B. Michel, N. Mazet, and P. Neveu. Experimental investigation of an innovative thermochemical process operating with a hydrate salt and moist air for thermal storage of solar energy: Global performance. *Applied Energy*, 129:177–186, 2014.
- [82] C. J. Ferchaud, H. A. Zondag, A. Rubino, and R. de Boer. Seasonal sorption heat storage – Research on thermochemical materials and storage performance. In *Proceedings of Heat Power Cycle 2012*, pages 1–7, Alkmaar, the Netherlands, 2012.
- [83] F. Bertsch, B. Mette, S. Asenbeck, H. Kerskes, and H. Müller-Steinhagen. Low temperature chemical heat storage – An investigation of hydration reactions. In *Effstock 2009*, pages 1–8, Stockholm, 2009.
- [84] R. de Boer, W. G. Haije, and J. B. J. Veldhuis. Determination of structural, thermodynamic and phase properties in the  $\text{Na}_2\text{S}-\text{H}_2\text{O}$  system for application in a chemical heat pump. *Thermochimica Acta*, 395(1-2):3–19, 2002.
- [85] S. Mauran, H. Lahmidi, and V. Goetz. Solar heating and cooling by a thermochemical process. First experiments of a prototype storing 60 kWh by a solid/gas reaction. *Solar Energy*, 82(7):623–636, 2008.
- [86] M. Richter, M. Bouché, and M. Linder. Heat transformation based on  $\text{CaCl}_2/\text{H}_2\text{O}$  – Part A: Closed operation principle. *Applied Thermal Engineering*, 102:615–621, 2016.
- [87] M. Richter, E.-M. Habermann, E. Siebecke, and M. Linder. A systematic screening of salt hydrates as materials for a thermochemical heat transformer. *Thermochimica Acta*, 659:136–150, 2018.
- [88] J. Andersson, M. Azoulay, and J. de Pablo. Chemical heat pumping—A rapid experimental procedure for investigating the suitability of salt hydrates under dynamic conditions. *International Journal of Energy Research*, 12(1):137–145, 1988.

- [89] T. Esaki, M. Yasuda, and N. Kobayashi. Experimental evaluation of the heat output/input and coefficient of performance characteristics of a chemical heat pump in the heat upgrading cycle of  $\text{CaCl}_2$  hydration. *Energy Conversion and Management*, 150:365–374, 2017.
- [90] R. W. Carling. Dissociation pressures and enthalpies of reaction in  $\text{MgCl}_2 \cdot n\text{H}_2\text{O}$  and  $\text{CaCl}_2 \cdot n\text{NH}_3$ . *The Journal of Chemical Thermodynamics*, 13(6):503–512, 1981.
- [91] K. Linnow, M. Niermann, D. Bonatz, K. Posern, and M. Steiger. Experimental studies of the mechanism and kinetics of hydration reactions. *Energy Procedia*, 48:394–404, 2014.
- [92] P. A. J. Donkers, L. Pel, and O. C. G. Adan. Experimental studies for the cyclability of salt hydrates for thermochemical heat storage. *Journal of Energy Storage*, 5:25–32, 2016.
- [93] A. Fopah Lele, F. Kuznik, O. Opel, and Wolfgang K. L. Ruck. Performance analysis of a thermochemical based heat storage as an addition to cogeneration systems. *Energy Conversion and Management*, 106:1327–1344, 2015.
- [94] O. Opel, H. U. Rammelberg, M. Gérard, and W. Ruck. Thermochemical storage materials research - TGA/DSC-hydration studies. In *Proceedings of the International Conference for Sustainable Energy Storage (IC-SES)*, Belfast, 2011.
- [95] K. Posern and C. Kaps. Humidity controlled calorimetric investigation of the hydration of  $\text{MgSO}_4$  hydrates. *Journal of Thermal Analysis and Calorimetry*, 92(3):905–909, 2008.
- [96] H. U. Rammelberg, T. Schmidt, and W. Ruck. Hydration and dehydration of salt hydrates and hydroxides for thermal energy storage – Kinetics and energy release. *Energy Procedia*, 30:362–369, 2012.
- [97] H. Ogura, M. Haguro, Y. Shibata, and Y. Otsubo. Reaction characteristics of  $\text{CaSO}_4/\text{CaSO}_4 \cdot 1/2\text{H}_2\text{O}$  reversible reaction for chemical heat pump. *Journal of Chemical Engineering of Japan*, 40(13):1252–1256, 2007.
- [98] J.-H. Lee, H. Ogura, and S. Sato. Reaction control of  $\text{CaSO}_4$  during hydration/dehydration repetition for chemical heat pump system. *Applied Thermal Engineering*, 63(1):192–199, 2014.
- [99] G. Balasubramanian, M. Ghommem, M. R. Hajj, W. P. Wong, J. A. Tomlin, and I. K. Puri. Modeling of thermochemical energy storage by salt hydrates. *International Journal of Heat and Mass Transfer*, 53(25):5700–5706, 2010.

- 
- [100] H. Zondag, B. Kikkert, S. Smeding, R. de Boer, and M. Bakker. Prototype thermochemical heat storage with open reactor system. *Applied Energy*, 109:360–365, 2013.
- [101] S. Lan, H. Zondag, A. van Steenhoven, and C. Rindt. Kinetic study of the dehydration reaction of lithium sulfate monohydrate crystals using microscopy and modeling. *Thermochimica Acta*, 621:44–55, 2015.
- [102] M. Roelands, R. Cuypers, K. D. Kruit, H. Oversloot, A. J. de Jong, W. Duvalois, L. van Vliet, and C. Hoegaerts. Preparation & characterization of sodium sulfide hydrates for application in thermochemical storage systems. *Energy Procedia*, 70(0):257–266, 2015.
- [103] A. J. de Jong, L. van Vliet, C. Hoegaerts, M. Roelands, and R. Cuypers. Thermochemical heat storage – From reaction storage density to system storage density. *Energy Procedia*, 91(0):128–137, 2016.
- [104] C. Rivera, I. Pilatowsky, E. Méndez, and W. Rivera. Experimental study of a thermochemical refrigerator using the barium chloride–ammonia reaction. *International Journal of Hydrogen Energy*, 32(15):3154–3158, 2007.
- [105] T. X. Li, R. Z. Wang, and L. W. Wang. High-efficient thermochemical sorption refrigeration driven by low-grade thermal energy. *Chinese Science Bulletin*, 54(6):885–905, 2009.
- [106] F. A. Jaeger, M. T. Howerton, S. E. Podlaseck, J. E. Mayers, D. G. Beshore, and W. R. Haas. Development of ammoniated salts: Thermochemical energy storage systems. Phase IB. Technical Report February–September 1977, Martin Marietta Corporation, Denver, 1978.
- [107] E. R. T. Bevers, H. A. J. Oonk, W. G. Haije, and P. J. van Ekeren. Investigation of thermodynamic properties of magnesium chloride amines by HPDSC and TG. *Journal of Thermal Analysis and Calorimetry*, 90(3):923–929, 2007.
- [108] V. Goetz and A. Marty. A model for reversible solid-gas reactions submitted to temperature and pressure constraints: Simulation of the rate of reaction in solid-gas reactor used as chemical heat pump. *Chemical Engineering Science*, 47(17-18):4445–4454, 1992.
- [109] Y. Hirata and K. Fujioka. Thermophysical properties and heat transfer characteristics of  $\text{CaCl}_2$  heat pump reactor associated with structural change of reactive salts. *V Minsk International Seminar "Heat Pipes, Heat Pumps, Refrigerators"*, 2:287–298, 2003.

- [110] K. Fujioka, S.-I. Kato, S. Fujiki, and Y. Hirata. Variations of molar volume and heat capacity of reactive solids of  $\text{CaCl}_2$  used for chemical heat pumps. *Journal of Chemical Engineering of Japan*, 29(5):858–864, 1996.
- [111] S. Lourdudoss, T. Schuler, and W. Raldow. Determination of the heat capacity of calcium chloride octa- and tetraammines. *Inorganica Chimica Acta*, 54:L31–L33, 1981.
- [112] A. Marty. Etude par microcalorimétrie de la réactivité de deux ammoniacates de chlorure de manganèse. *Journal of Thermal Analysis and Calorimetry*, 37(3):479–498, 1991.
- [113] T. X. Li, R. Z. Wang, R. G. Oliveira, and L. W. Wang. Performance analysis of an innovative multimode, multisalt and multieffect chemisorption refrigeration system. *AIChE Journal*, 53(12):3222–3230, 2007.
- [114] T. X. Li, R. Z. Wang, L. W. Wang, and Z. S. Lu. Experimental investigation of an innovative dual-mode chemisorption refrigeration system based on multifunction heat pipes. *International Journal of Refrigeration*, 31(6):1104–1112, 2008.
- [115] P. Neveu and J. Castaing. Solid-gas chemical heat pumps: Field of application and performance of the internal heat of reaction recovery process. *Heat Recovery Systems and CHP*, 13(3):233–251, 1993.
- [116] R. W. Carling, A. T. Wondolowski, and D. C. Macmillan. Enthalpy of formation of  $\text{CaCl}_2 \cdot 2\text{CH}_3\text{OH}$  and  $\text{CaCl}_2 \cdot 2\text{C}_2\text{H}_5\text{OH}$  by solution calorimetry. *The Journal of Chemical Thermodynamics*, 14(2):125–131, 1982.
- [117] Z. Iyimen-Schwarz. *Energiespeicherung durch chemische Reaktionen*. Dissertation, Universität Osnabrück, 1984.
- [118] P. O'D. Offenhartz, F. C. Brown, R. W. Mar, and R. W. Carling. A heat pump and thermal storage system for solar heating and cooling based on the reaction of calcium chloride and methanol vapor. *Journal of Solar Energy Engineering*, 102(1):59–65, 1980.
- [119] P. O'D. Offenhartz. Solar heating and cooling with the  $\text{CaCl}_2\text{-CH}_3\text{OH}$  chemical heat pump. In *Proceedings of the DOE Heat Pump Contractors' Program Integration Meeting, June 2-4, 1981*, pages 75–78, Mc Lean, Virginia, USA, 1982.
- [120] S. Hongois, F. Kuznik, P. Stevens, and J.-J. Roux. Development and characterisation of a new  $\text{MgSO}_4$ -zeolite composite for long-term thermal energy storage. *Solar Energy Materials and Solar Cells*, 95(7):1831–1837, 2011.



- [121] C. Vaccarino, A. Barbaccia, F. Frusteri, G. Galli, and G. Maisano. A low-temperature heat storage system utilizing mixtures of magnesium salt hydrates and ammonium nitrate. *Journal of Solar Energy Engineering*, 107(1):54–57, 1985.
- [122] H. U. Rammelberg, M. Myrau, T. Schmidt, and W. K. Ruck. An optimization of salt hydrates for thermochemical heat storage. In *Innovative Materials for Processes in Energy Systems*, volume 3, pages 550–555, Fukuoka, 2013.
- [123] H. U. Rammelberg, T. Osterland, B. Priehs, O. Opel, and Wolfgang K. L. Ruck. Thermochemical heat storage materials – Performance of mixed salt hydrates. *Solar Energy*, 136:571–589, 2016.
- [124] A. D. Pathak, S. V. Nedeia, H. A. Zondag, C. C. M. Rindt, and D. M. J. Smeulders. A DFT based equilibrium study of a chemical mixture Tachyhydrite and their lower hydrates for long term heat storage. *Journal of Physics: Conference Series*, 745(3):32003, 2016.
- [125] A. D. Pathak, I. C. Tranca, S. V. Nedeia, H. A. Zondag, C. C. M. Rindt, and D. M. J. Smeulders. A first-principles study of chemical mixtures of  $\text{CaCl}_2$  and  $\text{MgCl}_2$  hydrates for optimized seasonal heat storage. *The Journal of Physical Chemistry*, 121(38):20576–20590, 2017.
- [126] S. Mauran, P. Prades, and F. L’Haridon. Heat and mass transfer in consolidated reacting beds for thermochemical systems. *Heat Recovery Systems and CHP*, 13(4):315–319, 1993.
- [127] Y. I. Aristov, G. Restuccia, G. Cacciola, and M. M. Tokarev. Selective water sorbents for multiple applications, 7. Heat conductivity of  $\text{CaCl}_2$ - $\text{SiO}_2$  composites. *Reaction Kinetics and Catalysis Letters*, 65(2):277–284, 1998.
- [128] J. H. Han, K.-H. Lee, and H. Kim. Effective thermal conductivity of graphite–metallic salt complex for chemical heat pumps. *Journal of Thermophysics and Heat Transfer*, 13(4):481–488, 1999.
- [129] K. Wang, J. Y. Wu, R. Z. Wang, and L. W. Wang. Effective thermal conductivity of expanded graphite– $\text{CaCl}_2$  composite adsorbent for chemical adsorption chillers. *Energy Conversion and Management*, 47(13-14):1902–1912, 2006.
- [130] K. Fujioka, K. Hatanaka, and Y. Hirata. Composite reactants of calcium chloride combined with functional carbon materials for chemical heat pumps. *Applied Thermal Engineering*, 28(4):304–310, 2008.
- [131] Y. Y. Tanashev, A. V. Krainov, and Y. I. Aristov. Thermal conductivity of composite sorbents "salt in porous matrix" for heat storage and transformation. *Applied Thermal Engineering*, 61(2):401–407, 2013.

- [132] L. G. Gordeeva and Y. I. Aristov. Composites 'salt inside porous matrix' for adsorption heat transformation: A current state-of-the-art and new trends. *International Journal of Low-Carbon Technologies*, 7(4):288–302, 2012.
- [133] Y. I. Aristov, M. M. Tokarev, G. Cacciola, and G. Restuccia. Selective water sorbents for multiple applications, 1.  $\text{CaCl}_2$  confined in mesopores of silica gel: Sorption properties. *Reaction Kinetics and Catalysis Letters*, 59(2):325–333, 1996.
- [134] Yu. I. Aristov, M. M. Tokarev, G. Restuccia, and G. Cacciola. Selective water sorbents for multiple applications, 2.  $\text{CaCl}_2$  confined in micropores of silica gel: Sorption properties. *Reaction Kinetics and Catalysis Letters*, 59(2):335–342, 1996.
- [135] C. Y. Liu, K. Morofuji, K. Tamura, and K.-I. Aika. Water sorption of  $\text{CaCl}_2$ -containing materials as heat storage media. *Chemistry Letters*, 33(3):292–293, 2004.
- [136] X. J. Zhang and L. M. Qiu. Moisture transport and adsorption on silica gel-calcium chloride composite adsorbents. *Energy Conversion and Management*, 48(1):320–326, 2007.
- [137] Y. I. Aristov, G. Restuccia, G. Cacciola, and V. N. Parmon. A family of new working materials for solid sorption air conditioning systems. *Applied Thermal Engineering*, 22(2):191–204, 2002.
- [138] Y. I. Aristov, G. Restuccia, M. M. Tokarev, and G. Cacciola. Selective water sorbents for multiple applications, 10. Energy storage ability. *Reaction Kinetics and Catalysis Letters*, 69(2):345–353, 2000.
- [139] Y. I. Aristov, I. S. Glaznev, L. G. Gordeeva, I. V. Koptug, L. Y. U. Ilyina, J. Kärger, C. Krause, and B. Dawoud. Dynamics of water sorption on composites " $\text{CaCl}_2$  in silica": Single grain, granulated bed, consolidated layer. In W. C. Conner and J. Fraissard, editors, *Fluid Transport in Nanoporous Materials*, pages 553–565, Dordrecht, 2006. Springer Netherlands.
- [140] Y. I. Aristov, I. S. Glaznev, A. Freni, and G. Restuccia. Kinetics of water sorption on SWS-1L (calcium chloride confined to mesoporous silica gel): Influence of grain size and temperature. *Chemical Engineering Science*, 61(5):1453–1458, 2006.
- [141] B. Dawoud and Y. I. Aristov. Experimental study on the kinetics of water vapor sorption on selective water sorbents, silica gel and alumina under typical operating conditions of sorption heat pumps. *International Journal of Heat and Mass Transfer*, 46(2):273–281, 2003.
- [142] B. N. Okunev, A. P. Gromov, L. I. Heifets, and Y. I. Aristov. A new methodology of studying the dynamics of water sorption/desorption under real operating

- conditions of adsorption heat pumps: Modelling of coupled heat and mass transfer in a single adsorbent grain. *International Journal of Heat and Mass Transfer*, 51(1-2):246–252, 2008.
- [143] A. Freni, F. Russo, S. Vasta, M. Tokarev, Y. I. Aristov, and G. Restuccia. An advanced solid sorption chiller using SWS-1L. *Applied Thermal Engineering*, 27(13):2200–2204, 2007.
- [144] G. Restuccia, A. Freni, S. Vasta, and Y. I. Aristov. Selective water sorbent for solid sorption chiller: Experimental results and modelling. *International Journal of Refrigeration*, 27(3):284–293, 2004.
- [145] M. M. Tokarev and Y. I. Aristov. Selective water sorbents for multiple applications, 4.  $\text{CaCl}_2$  confined in silica gel pores: Sorption/desorption kinetics. *Reaction Kinetics and Catalysis Letters*, 62(1):143–150, 1997.
- [146] E. A. Levitskij, Y. I. Aristov, M. M. Tokarev, and V. N. Parmon. "Chemical Heat Accumulators": A new approach to accumulating low potential heat. *Solar Energy Materials and Solar Cells*, 44(3):219–235, 1996.
- [147] Y. Y. Tanashev and Y. I. Aristov. Thermal conductivity of a silica gel + calcium chloride system: The effect of adsorbed water. *Journal of Engineering Physics and Thermophysics*, 73(5):876–883, 2000.
- [148] L. G. Gordeeva, I. S. Glaznev, E. V. Savchenko, V. V. Malakhov, and Y. I. Aristov. Impact of phase composition on water adsorption on inorganic hybrids "salt/silica". *Journal of Colloid and Interface Science*, 301(2):685–691, 2006.
- [149] L. G. Gordeeva, G. Restuccia, G. Cacciola, and Y. I. Aristov. Selective water sorbents for multiple applications, 5.  $\text{LiBr}$  confined in mesopores of silica gel: Sorption properties. *Reaction Kinetics and Catalysis Letters*, 63(1):81–88, 1998.
- [150] Y. I. Aristov, A. Sapienza, D. S. Ovoshchnikov, A. Freni, and G. Restuccia. Reallocation of adsorption and desorption times for optimisation of cooling cycles. *International Journal of Refrigeration*, 35(3):525–531, 2012.
- [151] I. V. Ponomarenko, I. S. Glaznev, A. V. Gubar, Y. I. Aristov, and S. D. Kirik. Synthesis and water sorption properties of a new composite " $\text{CaCl}_2$  confined into SBA-15 pores". *Microporous and Mesoporous Materials*, 129(1-2):243–250, 2010.
- [152] S. P. Casey, D. Aydin, S. Riffat, and J. Elvins. Salt impregnated desiccant matrices for 'open' thermochemical energy storage—Hygrothermal cyclic behaviour and energetic analysis by physical experimentation. *Energy and Buildings*, 92:128–139, 2015.

- [153] F. B. Cortés, F. Chejne, F. Carrasco-Marín, A. F. Pérez-Cadenas, and C. Moreno-Castilla. Water sorption on silica- and zeolite-supported hygroscopic salts for cooling system applications. *Energy Conversion and Management*, 53(1):219–223, 2012.
- [154] K. Daou, R. Z. Wang, and Z. Z. Xia. Development of a new synthesized adsorbent for refrigeration and air conditioning applications. *Applied Thermal Engineering*, 26(1):56–65, 2006.
- [155] K. Daou, R. Z. Wang, Z. Z. Xia, and G. Z. Yang. Experimental comparison of the sorption and refrigerating performances of a  $\text{CaCl}_2$  impregnated composite adsorbent and those of the host silica gel. *International Journal of Refrigeration*, 30(1):68–75, 2007.
- [156] Y. Liu and R. Wang. Pore structure of new composite adsorbent  $\text{SiO}_2 \cdot x\text{H}_2\text{O} \cdot y\text{CaCl}_2$  with high uptake of water from air. *Science in China Series E: Technological Sciences*, 46(5):551–559, 2003.
- [157] A. Ristić, S. K. Henninger, and V. Kaučič. Investigations on new water sorbent for heat storage. In *Proceedings of the International Conference for Sustainable Energy Storage (IC-SES)*, Belfast, 2011.
- [158] J. Y. Wang, R. Z. Wang, and L. W. Wang. Water vapor sorption performance of ACF- $\text{CaCl}_2$  and silica gel- $\text{CaCl}_2$  composite adsorbents. *Applied Thermal Engineering*, 100:893–901, 2016.
- [159] H. Wu, S. Wang, and D. Zhu. Effects of impregnating variables on dynamic sorption characteristics and storage properties of composite sorbent for solar heat storage. *Solar Energy*, 81(7):864–871, 2007.
- [160] H. Wu, S. Wang, D. Zhu, and Y. Ding. Numerical analysis and evaluation of an open-type thermal storage system using composite sorbents. *International Journal of Heat and Mass Transfer*, 52(21-22):5262–5265, 2009.
- [161] D. Zhu, H. Wu, and S. Wang. Experimental study on composite silica gel supported  $\text{CaCl}_2$  sorbent for low grade heat storage. *International Journal of Thermal Sciences*, 45(8):804–813, 2006.
- [162] L. G. Gordeeva, A. Grekova, T. A. Krieger, and Y. I. Aristov. Composites "binary salts in porous matrix" for adsorption heat transformation. *Applied Thermal Engineering*, 50(2):1633–1638, 2013.
- [163] L. X. Gong, R. Z. Wang, Z. Z. Xia, and C. J. Chen. Adsorption equilibrium of water on a composite adsorbent employing lithium chloride in silica gel. *Journal of Chemical and Engineering Data*, 55(8):2920–2923, 2010.

- [164] L. X. Gong, R. Z. Wang, Z. Z. Xia, and C. J. Chen. Design and performance prediction of a new generation adsorption chiller using composite adsorbent. *Energy Conversion and Management*, 52(6):2345–2350, 2011.
- [165] L. G. Gordeeva, A. D. Grekova, T. A. Krieger, and Y. I. Aristov. Adsorption properties of composite materials (LiCl + LiBr)/silica. *Microporous and Mesoporous Materials*, 126(3):262–267, 2009.
- [166] H. Jarimi, A. Devrim, Y. Zhang, Y. Ding, O. Ramadan, X. Chen, A. Dodo, Z. Utlu, and S. Riffat. Materials characterization of innovative composite materials for solar-driven thermochemical heat storage (THS) suitable for building application. *International Journal of Low-Carbon Technologies*, 13(1):30–42, 2017.
- [167] J. Mrowiec-Białoń, A. B. Jarzebski, A. I. Lachowski, J. J. Malinowski, and Y. I. Aristov. Effective inorganic hybrid adsorbents of water vapor by the sol–gel method. *Chemistry of Materials*, 9:2486–2490, 1997.
- [168] J. Mrowiec-Białoń, A. I. Lachowski, A. B. Jarzebski, L. G. Gordeeva, and Y. I. Aristov. SiO<sub>2</sub>–LiBr nanocomposite sol–gel adsorbents of water vapor: Preparation and properties. *Journal of Colloid and Interface Science*, 218(2):500–503, 1999.
- [169] H. Liu, K. Nagano, D. Sugiyama, J. Togawa, and M. Nakamura. Honeycomb filters made from mesoporous composite material for an open sorption thermal energy storage system to store low-temperature industrial waste heat. *International Journal of Heat and Mass Transfer*, 65:471–480, 2013.
- [170] H. Liu, K. Nagano, and J. Togawa. A composite material made of mesoporous siliceous shale impregnated with lithium chloride for an open sorption thermal energy storage system. *Solar Energy*, 111:186–200, 2015.
- [171] B. Mette. *Experimentelle und numerische Untersuchungen zur Reaktionsführung thermochemischer Energiespeicher*. Dissertation, Universität Stuttgart, 2014.
- [172] A. Lass-Seyoum, M. Blicher, D. Borozdenko, T. Friedrich, and T. Langhof. Transfer of laboratory results on closed sorption thermo-chemical energy storage to a large-scale technical system. *Energy Procedia*, 30:310–320, 2012.
- [173] K. Posern and C. Kaps. Calorimetric studies of thermochemical heat storage materials based on mixtures of MgSO<sub>4</sub> and MgCl<sub>2</sub>. *Thermochimica Acta*, 502(1-2):73–76, 2010.
- [174] C. S. Tretiak and N. B. Abdallah. Sorption and desorption characteristics of a packed bed of clay–CaCl<sub>2</sub> desiccant particles. *Solar Energy*, 83(10):1861–1870, 2009.

- [175] Y. I. Aristov, G. Restuccia, M. M. Tokarev, H.-D. Buerger, and A. Freni. Selective water sorbents for multiple applications. 11.  $\text{CaCl}_2$  confined to expanded vermiculite. *Reaction Kinetics and Catalysis Letters*, 71(2):377–384, 2000.
- [176] S. P. Casey, D. Aydin, J. Elvins, and S. Riffat. Salt impregnated desiccant matrices for ‘open’ thermochemical energy conversion and storage — Improving energy density utilisation through hydrodynamic & thermodynamic reactor design. *Energy Conversion and Management*, 142:426–440, 2017.
- [177] Y. Zhang, R. Wang, T. Li, and Y. Zhao. Thermochemical characterizations of novel vermiculite-LiCl composite sorbents for low-temperature heat storage. *Energies*, 9(10), 2016.
- [178] A. Sapienza, I. S. Glaznev, S. Santamaria, A. Freni, and Y. I. Aristov. Adsorption chilling driven by low temperature heat: New adsorbent and cycle optimization. *Applied Thermal Engineering*, 32(1):141–146, 2012.
- [179] K. C. Chan, C. Y. H. Chao, G. N. Sze-To, and K. S. Hui. Performance predictions for a new zeolite 13X/ $\text{CaCl}_2$  composite adsorbent for adsorption cooling systems. *International Journal of Heat and Mass Transfer*, 55(11-12):3214–3224, 2012.
- [180] T. Nonnen, S. Beckert, K. Gleichmann, A. Brandt, B. Unger, H. Kerskes, B. Mette, S. Bonk, T. Badenhop, F. Salg, and R. Gläser. A Thermochemical long-term heat storage system based on a salt/zeolite composite. *Chemical Engineering & Technology*, 39(12):2427–2434, 2016.
- [181] G. T. Whiting, D. Grondin, D. Stosic, S. Bennici, and A. Auroux. Zeolite- $\text{MgCl}_2$  composites as potential long-term heat storage materials: Influence of zeolite properties on heats of water sorption. *Solar Energy Materials and Solar Cells*, 128:289–295, 2014.
- [182] G. T. Whiting, D. Grondin, S. Bennici, and A. Auroux. Heats of water sorption studies on zeolite- $\text{MgSO}_4$  composites as potential thermochemical heat storage materials. *Solar Energy Materials and Solar Cells*, 112:112–119, 2013.
- [183] A. Ristić, D. Maučec, S. K. Henninger, and V. Kaučič. New two-component water sorbent  $\text{CaCl}_2\text{-FeKIL}_2$  for solar thermal energy storage. *Microporous and Mesoporous Materials*, 164:266–272, 2012.
- [184] A. Ristić and S. K. Henninger. Sorption composite materials for solar thermal energy storage. *Energy Procedia*, 48:977–981, 2014.
- [185] M. M. Tokarev, L. G. Gordeeva, V. Romannikov, I. S. Glaznev, and Y. I. Aristov. New composite sorbent  $\text{CaCl}_2$  in mesopores for sorption cooling/heating. *International Journal of Thermal Sciences*, 41(5):470–474, 2002.

- [186] K. Okada, M. Nakanome, Y. Kameshima, T. Isobe, and A. Nakajima. Water vapor adsorption of  $\text{CaCl}_2$ -impregnated activated carbon. *Materials Research Bulletin*, 45(11):1549–1553, 2010.
- [187] K. Posern and A. Osburg. Determination of the heat storage performance of thermochemical heat storage materials based on  $\text{SrCl}_2$  and  $\text{MgSO}_4$ . *Journal of Thermal Analysis and Calorimetry*, pages 1–5, 2017.
- [188] H. Ye, Z. Yuan, S. Li, and L. Zhang. Activated carbon fiber cloth and  $\text{CaCl}_2$  composite sorbents for a water vapor sorption cooling system. *Applied Thermal Engineering*, 61(2):690–696, 2013.
- [189] C. Y. Tso and C. Y. H. Chao. Activated carbon, silica-gel and calcium chloride composite adsorbents for energy efficient solar adsorption cooling and dehumidification systems. *International Journal of Refrigeration*, 35(6):1626–1638, 2012.
- [190] K. Fujioka and H. Suzuki. Thermophysical properties and reaction rate of composite reactant of calcium chloride and expanded graphite. *Applied Thermal Engineering*, 50(2):1627–1632, 2013.
- [191] A. Grekova, L. G. Gordeeva, and Y. I. Aristov. Composite sorbents "Li/Ca halogenides inside multi-wall carbon nano-tubes" for thermal energy storage. *Solar Energy Materials and Solar Cells*, 155(August):176–183, 2016.
- [192] H. Zhang, Y. Yuan, F. Yang, N. Zhang, and X. Cao. Inorganic composite adsorbent  $\text{CaCl}_2/\text{MWNT}$  for water vapor adsorption. *RSC Advances*, 5(48):38630–38639, 2015.
- [193] A. Permyakova, S. Wang, E. Courbon, F. Nouar, N. Heymans, P. D'Ans, N. Barrier, P. Billefont, G. De Weireld, N. Steunou, M. Frere, and C. Serre. Design of salt-metal organic framework composites for seasonal heat storage applications. *Journal of Materials Chemistry A*, 5(25):12889–12898, 2017.
- [194] L. G. Gordeeva and Y. I. Aristov. Novel sorbents of ethanol "salt confined to porous matrix" for adsorptive cooling. *Energy*, 35(6):2703–2708, 2010.
- [195] L. G. Gordeeva, A. Frazzica, A. Sapienza, Y. I. Aristov, and A. Freni. Adsorption cooling utilizing the "LiBr/silica – ethanol" working pair: Dynamic optimization of the adsorber/heat exchanger unit. *Energy*, 75:390–399, 2014.
- [196] V. Brancato, A. Frazzica, A. Sapienza, L. G. Gordeeva, and A. Freni. Ethanol adsorption onto carbonaceous and composite adsorbents for adsorptive cooling system. *Energy*, 84:177–185, 2015.

- [197] A. D. Grekova, I. S. Girnuk, V. V. Nikulin, M. M. Tokarev, L. G. Gordeeva, and Y. I. Aristov. New composite sorbents of water and methanol "salt in anodic alumina": Evaluation for adsorption heat transformation. *Energy*, 106:231–239, 2016.
- [198] Y. I. Aristov, L. G. Gordeeva, Y. D. Pankratiev, L. M. Plyasova, I. V. Bikova, A. Freni, and G. Restuccia. Sorption equilibrium of methanol on new composite sorbents "CaCl<sub>2</sub>/silica gel". *Adsorption*, 13(2):121–127, 2007.
- [199] L. G. Gordeeva, A. Freni, Y. I. Aristov, and G. Restuccia. Composite sorbent of methanol "lithium chloride in mesoporous silica gel" for adsorption cooling machines: Performance and stability evaluation. *Industrial & Engineering Chemistry Research*, 48(13):6197–6202, 2009.
- [200] L. G. Gordeeva and Y. I. Aristov. Composite sorbent of methanol "LiCl in mesoporous silica gel" for adsorption cooling: Dynamic optimization. *Energy*, 36(2):1273–1279, 2011.
- [201] L. G. Gordeeva, A. Freni, G. Restuccia, and Y. I. Aristov. Influence of characteristics of methanol sorbents "salts in mesoporous silica" on the performance of adsorptive air conditioning cycle. *Industrial & Engineering Chemistry Research*, 46(9):2747–2752, 2007.
- [202] L. G. Gordeeva, A. Freni, T. A. Krieger, G. Restuccia, and Y. I. Aristov. Composites "lithium halides in silica gel pores": Methanol sorption equilibrium. *Microporous and Mesoporous Materials*, 112(1-3):254–261, 2008.
- [203] G. Maggio, L. G. Gordeeva, A. Freni, Y. I. Aristov, G. Santori, F. Polonara, and G. Restuccia. Simulation of a solid sorption ice-maker based on the novel composite sorbent "lithium chloride in silica gel pores". *Applied Thermal Engineering*, 29(8-9):1714–1720, 2009.
- [204] L. X. Gong, R. Z. Wang, Z. Z. Xia, and Z. S. Lu. Experimental study on an adsorption chiller employing lithium chloride in silica gel and methanol. *International Journal of Refrigeration*, 35(7):1950–1957, 2012.
- [205] Z. S. Lu and R. Z. Wang. Study of the new composite adsorbent of salt LiCl/silica gel-methanol used in an innovative adsorption cooling machine driven by low temperature heat source. *Renewable Energy*, 63:445–451, 2014.
- [206] K. Posern and C. Kaps. Influences of salt hydrate mixtures and pore sizes on the sorption heat of composite TES materials. In *Proceedings of the 11th International Conference on Thermal Energy Storage (Effstock 2009)*, Stockholm, 2009.



- [207] International Energy Agency. Technology roadmap: Energy storage. Technical report, IEA, Paris, 2014.
- [208] H.W. Bakhuis Roozeboom. Experimentelle und theoretische Studien über die Gleichgewichtsbedingungen zwischen festen und flüssigen Verbindungen von Wasser mit Salzen, besonders mit dem Chlorcalcium. *Zeitschrift für Physikalische Chemie*, 4, 1889.
- [209] E. M. Collins and A. W. C. Menzies. A comparative method for measuring aqueous vapor and dissociation pressures with some of its applications. *The Journal of Physical Chemistry*, 40(3):379–397, 1935.
- [210] A. Lannung. Dampfdruckmessungen des Systems Calciumchlorid–Wasser. *Zeitschrift für anorganische und allgemeine Chemie*, 228(1):1–18, 1936.
- [211] É. Buzágh-Gere, S. Gál, and J. Simon. Untersuchung von Dehydratationsvorgängen. I. Die Dehydratisierung von Erdalkalihalogenuid-Hydraten in ihrer eigenen Gasatmosphäre. *Zeitschrift für anorganische und allgemeine Chemie*, 400(1):37–44, 1973.
- [212] É. Buzágh-Gere, J. Sztatisz, and S. Gál. Investigation of dehydration process, II. Processes preceding dehydration of alkaline earth halides. *Journal of Thermal Analysis*, 10(1):89–98, 1976.
- [213] V. B. Parker, D. D. Wagman, and W. H. Evan. *NBS technical note 270-6: Selected values of thermodynamic properties*. U.S. Government Printing Office, Washington, 1971.
- [214] G. Wehner. Über die basischen Chloride des Magnesiums. *Zeitschrift für anorganische und allgemeine Chemie*, 272(1-4):201–210, 1953.
- [215] D. Petzold and R. Naumann. Thermoanalytische Untersuchungen zur Zersetzung von  $\text{MgCl}_2 \cdot 6\text{H}_2\text{O}$  unter quasiisobaren Bedingungen. *Journal of Thermal Analysis*, 19(1):25–34, 1980.
- [216] T.-J. Gardner and G. L. Messing. Magnesium salt decomposition and morphological development during evaporative decomposition of solutions. *Thermochimica Acta*, 78(1):17–27, 1984.
- [217] K. Sugimoto, R. E. Dinnebier, and J. C. Hanson. Structures of three dehydration products of bischofite from in situ synchrotron powder diffraction data ( $\text{MgCl}_2 \cdot n\text{H}_2\text{O}$ ;  $n = 1, 2, 4$ ). *Acta Crystallographica Section B*, 63(2):235–242, 2007.

- [218] K. Heide and H. J. Eichhorn. Die thermische Zersetzung des  $\text{MgCl}_2 \cdot 6\text{H}_2\text{O}$  unter dynamischen Bedingungen — Ein Beitrag zur kinetischen Analyse nichtisothermer Festkörperreaktionen. *Journal of Thermal Analysis*, 7(2):397–409, 1975.
- [219] A. K. Galwey and G. M. Laverty. The thermal decomposition of magnesium chloride dihydrate. *Thermochimica Acta*, 138(1):115–127, 1989.
- [220] Q.-Z. Huang, G.-M. Lu, J. Wang, and J.-G. Yu. Mechanism and kinetics of thermal decomposition of  $\text{MgCl}_2 \cdot 6\text{H}_2\text{O}$ . *Metallurgical and Materials Transactions B*, 41(5):1059–1066, 2010.
- [221] B. Smeets, E. Iype, S. V. Nedea, H. A. Zondag, and C. C. M. Rindt. A DFT based equilibrium study on the hydrolysis and the dehydration reactions of  $\text{MgCl}_2$  hydrates. *The Journal of Chemical Physics*, 139(12):124312, 2013.
- [222] J. C. J. Bart and W. Roovers. Magnesium chloride—ethanol adducts. *Journal of Materials Science*, 30(11):2809–2820, 1995.
- [223] S. Lowell, J. E. Shields, M.A. Thomas, and M. Thommes. *Characterization of porous solids and powders: Surface area, pore size and density*. Springer Netherlands, 2004.
- [224] J. Haber, J. H. Block, and B. Delmon. Manual of methods and procedures for catalyst characterization (technical report). *Pure and Applied Chemistry*, 67(8-9):1257–1306, 1995.
- [225] R. W. Mar and R. W. Carling. The calcium chloride—ethanol system. *Thermochimica Acta*, 45(2):213–217, 1981.
- [226] Y. I. Aristov, L. G. Gordeeva, Y. D. Pankratiev, L. M. Plyasova, I. V. Bikova, A. Freni, and G. Restuccia. Sorption equilibrium of methanol on new composite sorbents “ $\text{CaCl}_2/\text{silica}$  gel”. *Adsorption*, 13(2):121–127, 2007.
- [227] A. K. Galwey and M. E. Brown. *Thermal decomposition of ionic solids*. Elsevier Science, 1st edition, 1999.
- [228] L. J. Olmer and M. L. Quinet. No Title. *Bulletin de la Société Chimique de France*, [5](1):1579–1584, 1934.
- [229] H. J. Kandiner. *Magnesium : Teil B - Lieferung 1. Verbindungen bis Magnesium und Jod*. Mg. Magnesium (System-Nr. 27). Springer-Verlag, Berlin, Heidelberg, 8th edition, 1963.
- [230] E. Lloyd, C. B. Brown, D. G. R. Bonnell, and W. J. Jones. XC.-Equilibrium between alcohols and salts. Part II. *Journal of the Chemical Society*, pages 658–666, 1928.

- [231] B. Tian, Z. Q. Jin, L. W. Wang, and R. Z. Wang. Permeability and thermal conductivity of compact chemical and physical adsorbents with expanded natural graphite as host matrix. *International Journal of Heat and Mass Transfer*, 55(15):4453–4459, 2012.
- [232] H.-P. Blume, G. W. Brümmer, R. Horn, E. Kandeler, I. Kögel-Knabner, R. Kretzschmar, K. Stahr, and B.-M. Wilke. *Scheffer/Schachtschabel: Lehrbuch der Bodenkunde*. Springer-Verlag, Berlin, Heidelberg, 16th edition, 2010.
- [233] N. Wegscheider. *Synthesis and characterization of salt porous-carrier composites for a thermochemical battery*. Bachelor thesis, University of Lüneburg, 2013.
- [234] H. A. Zondag, V. M. van Essen, L. P. J. Bleijendaal, B. W. J. Kikkert, and M. Bakker. Application of  $\text{MgCl}_2 \cdot 6\text{H}_2\text{O}$  for thermochemical seasonal solar heat storage. In *Proceedings of the 5th International Renewable Energy Storage Conference (IRES 2010)*, Berlin, Germany, 2010.
- [235] R. de Boer, W. G. Haije, J. B. J. Veldhuis, and S. F. Smeding. Solid-sorption cooling with integrated thermal storage: The SWEAT prototype. In *Proceedings of the 3rd International Conference on Heat Powerd Cycles (HPC 2004)*, Larnaca, Cyprus, 2004.
- [236] K. Linnow, K. Posern, T. Talreja, M. Niermann, C. Kaps, and M. Steiger. Calorimetric investigation of magnesium sulfate hydration in porous materials. In *Proceedings of the ISES EuroSun 2014 Conference*, pages 1394–1400, Aix-les-Bains, 2014.
- [237] M. Kumita, M. Meiwa, K. Watanabe, and A. Kodama. Preparation of calcium chloride-anodized aluminum composite for water vapor sorption. *Applied Thermal Engineering*, 50(2):1564–1569, 2013.
- [238] Y. Suwa, M. Kumita, H. Komori, A. Kodama, and Y. Otani. Impregnation of calcium chloride into alumina thin film prepared by oxalic acid anodizing. *Journal of Chemical Engineering of Japan*, 47(7):602–607, 2014.
- [239] A. Jabbari-Hichri, S. Bennici, and A. Auroux. Water sorption heats on silica-alumina-based composites for interseasonal heat storage. *Journal of Thermal Analysis and Calorimetry*, 118(2):1111–1118, 2014.
- [240] P. Patnaik. *Handbook of inorganic chemicals*, volume 529. McGraw-Hill New York, 2003.

# Acknowledgements

First and foremost, I want to express my sincere gratitude to my supervisor Prof. Wolfgang Ruck who granted me the privilege to pursue my doctoral degree at the Leuphana University of Lüneburg. I am grateful for the valuable support and constant encouragement he has provided during my PhD study. He gave me the intellectual freedom to explore the wide field of thermal energy storage.

I am deeply indebted to my supervisors and mentors Prof. Oliver Opel and Prof. Thomas Osterland for offering me the opportunity to work on different research projects and to participate in renowned conferences disseminating my research findings and sharing the latest insights with the scientific community. They have created a collaborative and inspiring working environment, which has been highly conducive for my professional and personal development. I am profoundly appreciative for their generous advice, guidance, and constructive feedback.

This PhD thesis contains work that has been carried out in close cooperation with the Renewable Energy Research Group at the Institute of Materials and Environmental Chemistry at the Research Center for Natural Sciences of the Hungarian Academy of Sciences. I am much obliged to *Ádám, András, Emília, Judith, László, and Szabolcs* for the fruitful collaboration and the vital exchange of our expertise. My cordial thanks go to *Ádám, Dorottya, Emília, Gábor, Zoltán, and Zsuzsanna* who have made my visiting research stay at the MTA TTK a truly delightful and memorable one.

My colleagues and PhD fellows *Amanda, Armand, Christina, Holger, Karsten, Marlies, and Mona*, deserve special mention for brightening my days with stimulating scientific discussions, refreshing coffee breaks and amusing film nights. I am also very thankful to my bachelor student *Nina* whom I have had the pleasure to supervise. She patiently assisted with preparation of dozens of composite samples and processing of collected TGA/DSC data.

At this point, I would like to take the opportunity to thank the co-authors of the papers included in this cumulative doctoral thesis and all reviewers for their kind support and insightful comments.

This PhD research would not have been possible without funding through the European Regional Development Fund, the federal state of Lower Saxony, the Federal Ministry of Education and Research, and the Federal Ministry for Economic Affairs and Energy. I moreover gratefully acknowledge the Fund for Young Researchers for worldwide conference participations received from the Leuphana University of Lüneburg.

I also warmly thank all my flatmates and international friends, with whom I have enjoyed merry moments, witty board games, adventurous trips, and intensive bouldering sessions. I particularly thank Felix whose patience and companionship have been invaluable. Finally, I owe my parents and my sister Vanessa my most heartfelt debt of gratitude for their continuous inspiration and moral support.

# Curriculum vitae

## BERUFSERFAHRUNG

---

<b>Leuphana Universität Lüneburg</b> <i>Wissenschaftliche Mitarbeiterin</i>	<b>Lüneburg</b> 2012-2017
Projekte	
<ul style="list-style-type: none"><li>• Entwicklung einer Chemisorptionskälteanlage mit erhöhter Speicher- und Lastmanagementfähigkeit (BMW ZIM KF)</li><li>• Reversible Reaktionen anorganischer Salze mit Alkoholen zur Wärmespeicherung (BMBF)</li><li>• Innovations-Inkubator Teilmaßnahme 2.1: Existenzgründungsprojekte (NBank/EFRE)</li><li>• Innovations-Inkubator Teilmaßnahme 1.1: Kompetenztandem Thermische Batterie (NBank/EFRE)</li></ul>	
<b>ETEP Umweltberatung – Estudos Tecnicos e Projetos Etep Ltda.</b> <i>IAESTE-Fachpraktikum im Bereich Abwasserbehandlung</i>	<b>São Paulo</b> 2009
<b>Karlsruher Institut für Technologie (KIT)</b> <i>Studentische Hilfskraft</i>	<b>Karlsruhe</b> 2007-2009

## LEHRERFAHRUNG

---

<b>Leuphana Universität Lüneburg</b> <i>Betreuung von Bachelorarbeiten und studentischen Hilfskräften</i>	<b>Lüneburg</b> 2012-2017
<b>Karlsruher Institut für Technologie (KIT)</b> <i>Betreuung Grundlagenpraktikum</i>	<b>Karlsruhe</b> 2008

## STIPENDIEN

---

<b>Leuphana Universität Lüneburg</b> Nachwuchsförderfonds	<b>Lüneburg</b> 2015-2016
--	------------------------------

**AUSBILDUNG**

---

<b>Leuphana Universität Lüneburg</b>	<b>Lüneburg</b>
<i>Promotion zur Doktorin der Naturwissenschaften (Dr. rer. nat)</i>	2018
Nachhaltigkeitsforschung Energie	
Thema: Development and characterization of thermochemical materials based on salt hydrates and salt alcoholates	
<b>Karlsruher Institut für Technologie (KIT)</b>	<b>Karlsruhe</b>
<i>Diplomstudium Chemieingenieurwesen (Dipl.-Ing.)</i>	2011
Diplomarbeit: Entwicklung von dezentralen Filtersystemen zur Verbesserung der Wasserqualität in Gunung Kidul, Indonesien, unter Einbeziehung lokaler natürlicher Ressourcen	
Schwerpunkte: Wassertechnologie, Lebensmittelverfahrenstechnik	
<b>Aventinus-Gymnasium Burghausen</b>	<b>Burghausen</b>
<i>Abitur</i>	2004

**GUTACHTERTÄTIGKEITEN**

---

Applied Energy, Energy and Buildings, Energy Conversion and Management, Heat Transfer Engineering, International Conference on Applied Energy

## AKADEMISCHE ERFOLGE

---

### Veröffentlichungen in Zeitschriften

- 2019 Korhammer K, Mihály J, Bálint S, Trif L, Vass Á, Tompos A, et al. Reversible formation of alcohol solvates and their potential use for heat storage. *Journal of Thermal Analysis and Calorimetry* 2019;138:11–33.
- 2018 Korhammer K, Opel O, Ruck WKL. Energy storage and adsorption cooling efficiency of novel composite adsorbents. To be submitted to *Thermochimica Acta*.
- 2018 Korhammer K, Neumann K, Opel O, Ruck WKL. Thermodynamic and kinetic study of  $\text{CaCl}_2\text{-CH}_3\text{OH}$  adducts for solid sorption refrigeration by TGA/DSC. *Applied Energy* 2018;230:1255–78.
- 2017 Korhammer K, Neumann K, Opel O, Ruck WKL. Micro-scale thermodynamic and kinetic analysis of a calcium chloride methanol system for process cooling. *Energy Procedia* 2017;105:4363–9.
- 2016 Korhammer K, Apel C, Osterland T, Ruck WKL. Reaction of calcium chloride and magnesium chloride and their mixed salts with ethanol for thermal energy storage. *Energy Procedia* 2016;91:161–71.
- 2016 Korhammer K, Druske M-M, Fopah-Lele A, Rammelberg HU, Wegscheider N, Opel O, et al. Sorption and thermal characterization of composite materials based on chlorides for thermal energy storage. *Applied Energy* 2016;162:1462–72.
- 2015 N'Tsoukpoe KE, Rammelberg HU, Lele AF, Korhammer K, Watts BA, Schmidt T, et al. A review on the use of calcium chloride in applied thermal engineering. *Appl Therm Eng* 2015;75:513–31.
- 2014 Druske M-M, Fopah-Lele A, Korhammer K, Rammelberg HU, Wegscheider N, Ruck W, et al. Developed materials for thermal energy storage: Synthesis and characterization. *Energy Procedia* 2014;61:96–9.



**Konferenzbeiträge**

- 2016 Vass Á, Korhammer K, Mihály J, Trif L, Tompos A, Tálás E. Kalcium klorid-, magnézium klorid – alkohol rendszerek alkalmazása hőtárolásra szolgáló reverzibilis szolvát képzési reakciókban. In: Bohner B, Ádám A, Timár Z, Ziegenheim S, editors. XXXIX Kémiai Előadói Napok Konferencia helye, ideje: Szeged, Magyarország, 2016.10.17-2016.10.19, Szeged: 2016, p. 141–5.
- 2016 Korhammer K, Rammelberg HU, Opel O, Ruck WKL. High-capacity storage and power management for industrial cold energy at  $-20^{\circ}\text{C}$  by developing a thermochemical refrigeration machine. Proceedings of the 10th International Renewable Energy Storage Conference (IRES 2016), Düsseldorf, Germany: EUROSOLAR; 2016.
- 2016 Druske M, Rammelberg HU, Neumann K, Korhammer K, Opel O, Ruck WKL. Mixed salts in thermochemical heat storage applications. Proceedings of the 10th International Renewable Energy Storage Conference (IRES 2016), Düsseldorf, Germany: EUROSOLAR; 2016.
- 2013 Fopah Lele A, Korhammer K, Wegscheider N, Rammelberg HU, Osterland T, Ruck W. Thermal conductivity measurement of salt hydrate as porous material using calorimetric (DSC) method. 8th World Conference on Experimental Heat Transfer, Fluid Mechanics and Thermodynamics (ExHFT), Lisboa, Portugal: A. Faria - Edicao Electronica Lda.; 2013.
- 2012 Korhammer K, Rammelberg HU, N'Tsoukpoe KE, Schmidt T, Ruck WKL. Characterization and improvement of heat storage material applications. Proceedings of the 7th International Renewable Energy Storage Conference and Exhibition (IRES 2012), Berlin, Germany: EUROSOLAR; 2012, p. 1870.
- 2012 Osterland T, Rammelberg HU, N'Tsoukpoe K, Rönnebeck T, Fopah Lele A, Belz K, et al. Conception of a heat storage system for household applications. Proceedings of the 7th International Renewable Energy Storage Conference and Exhibition (IRES 2012), Berlin, Germany: EUROSOLAR; 2012, p. 429–32.

**Teilnahme an Konferenzen und Fachtagungen**

- 2017 2nd German-Czech R&D Conference, January 11-12, 2017, Fraunhofer Institute for Integrated Systems and Device Technology IISB, Erlangen, Germany.
- 2016 8th International Conference on Applied Energy (ICAE 2016), October 8-11, 2016, Beijing, China. Oral presentation.
- 2016 Mini-conference on biomass, waste and renewable energy, June 6, 2016, Research Center for Natural Sciences HAS, Budapest, Hungary. Oral and poster presentation.
- 2016 International Energy Agency – Solar Heating and Cooling/ Energy Conservation through Energy Storage Programme (IEA-SHC/ECES): 2nd Task/Annex definition meeting, September 15-16, 2016, TU Vienna, Vienna, Austria.
- 2016 10th International Renewable Energy Storage Conference (IRES 2016), March 15-17, 2016, Düsseldorf, Germany. Oral and poster presentation.
- 2015 4th International Conference on Solar Heating and Cooling for Buildings and Industry (SHC 2015), December 2-4, 2015, Istanbul, Turkey. Oral presentation.
- 2015 International Energy Agency – Energy Conservation through Energy Storage Programme (IEA-ECES), Annex 30: 1st Workshop, October 29-30, 2015, KTH Royal Institute of Technology, Stockholm, Sweden.
- 2015 International Energy Agency – Solar Heating and Cooling/ Energy Conservation through Energy Storage Programme (IEA-SHC/ECES), Task 42/Annex 29: 14th Experts meeting, October 5-7, 2015, University of Zaragoza, Zaragoza, Spain.
- 2014 6th International Conference on Applied Energy (ICAE 2014), May 30 - June 2, 2014, Taipei, Taiwan. Oral presentation.
- 2012 7th International Renewable Energy Storage Conference and Exhibition (IRES 2012), November 12-14, 2012, Berlin, Germany. Poster presentation.



# Declaration of authorship

Ich versichere, dass Ich die eingereichte Dissertation "Development and characterization of thermochemical materials based on salt hydrates and salt alcoholates" selbständig und ohne unerlaubte Hilfsmittel verfasst habe. Anderer als der von mir angegebenen Hilfsmittel und Schriften habe ich mich nicht bedient. Alle wörtlich oder sinngemäß den Schriften anderer Autorinnen oder Autoren entnommenen Stellen habe ich kenntlich gemacht.

Hiermit erkläre ich, dass die Abhandlung in der gegenwärtigen oder einer anderen Fassung noch keinem anderen Fachbereich vorgelegen hat. Den Inhalt der Dissertation habe ich noch nicht im Rahmen einer Diplom- oder anderen Prüfungsarbeit verwendet.

Hamburg, November 2018

Kathrin Korhammer



